

University of Messina



*Department of Biomedical, Dental, Morphological
and Functional Imaging Sciences
(BIOMORF)*

PhD School in

Translational Molecular Medicine and Surgery

XXXV cycle

MED/10

PhD Thesis

***RNA-binding proteins: novel mediators of inflammation and
accelerated aging in Chronic Obstructive Pulmonary Disease***

Coordinator

Ch. Prof. Gaetano Caramori

Tutor

Ch. Prof. Gaetano Caramori

Co-tutor

Ch. Prof.ssa Cristiana Stellato

PhD Student

Ilaria Salvato

505497

2021/2022

Index

Abstract	1
Part 1. Introduction	4
1. RNA-Binding Proteins (RBPs) and their Role in Post-Transcriptional Gene Regulation (PTGR)	5
1.1. Definition of PTGR, main mechanisms and molecular determinants	5
1.2. General role of PTGR in homeostasis and disease	8
1.3. Focus on RBPs as mediators of PTGR	11
1.3.1. RBPs binding modes of interaction with mRNAs	12
1.3.2. Regulatory elements modulating RBP:transcript association: sequences and post-translational modification of target mRNAs	16
1.3.3. Main RBPs with functions on control of mRNA turnover and translation	21
1.3.4. Post-translational modifications of RBPs: major determinants of function	29
1.4. Crosstalk between PTGR regulatory factors: non-coding RNAs (ncRNAs) and RBPs	32
2. RBPs: role in disease	35
2.1. RBPs in Cancer	35
2.2. Chronic Obstructive Pulmonary Disease (COPD): RBPs as molecular pathogenic link with in oxidative stress and inflammation	38
2.3. Main pathogenetic mechanisms in COPD: potential involvement of RBPs	40
2.3.1. Genetics and Epigenetics	40
2.3.2. Accelerated aging	45
2.3.3. Chronic inflammation	49
2.3.4. Spreading inflammation and aging phenotype through extracellular vesicles: role in COPD	53
2.4. Overview of diagnostic approaches and management of COPD patients: unmet needs	56
2.5. RBPs in COPD: current status	59
2.6. Targeting RBPs and their functions in COPD: is there a role?	62
2.6.1. RNA-targeting strategies	62
2.6.2. Protein-targeting strategies	63
References Part 1	67

Part 2. PhD Research plan	93
1. General Aim and Specific Study of the PhD project	94
1.1. Specific study: Characterization of the RNA-binding protein AUF-1 in airway epithelial inflammatory responses	95
2. Final considerations: Study limitations and Future direction	144
2.1. Study limitations	144
2.2. Future direction	145
References Part 2	159

Abstract

Background. RNA-binding proteins (RBPs) play a key role in post-transcriptional gene regulation (PTGR) of genes involved in numerous biological processes. These proteins act through the binding to specific cis-elements present in their RNA targets and by forming, with other regulatory factors, dynamic ribonucleoprotein complexes (RNPs) that ultimately determine the fate of different type of RNAs. There are several families of RBPs classified according to the type of RNA target that they bind. Multiple studies in the last decade have established that aberrant expression and function of RBPs participate to cancer pathogenesis by altering the stability and translation of genes involved in many mechanism of neoplastic transformation. Many of the cancer-related pathways for which PTGR mediated by RBPs has been established are also critically involved in chronic inflammation; to this end, many important basic and preclinical studies and gene ablation animal models indicate that RBPs are critically involved also in inflammatory responses and immunity. In contrast to the growing number of studies on the role of RBPs in human cancer, translational studies based on chronic inflammatory disease are still scarce. In particular, one of these studies demonstrated the loss of AU-rich element factor 1 (AUF-1) in airway epithelium of patients with stable chronic obstructive pulmonary disease (COPD) and in cytokine-and cigarette smoke-challenged human epithelial cells, along with a global downregulation of RBPs expression.

Aim. The thesis aimed at identifying the role of AUF-1 as determinant of increased inflammation and accelerated cellular senescence in COPD pathogenesis, and understanding the mechanisms mediating cytokine-induced AUF-1 loss. On these bases, our long-term aim is to explore RBP therapeutic targeting, for which we plan to develop dedicated experimental models.

Results. Using an RNA immunoprecipitation and sequencing (RIP-Seq) approach, we identified AUF-1 targets in the airway epithelial cell line BEAS-2B and identified specific interacting sequences in targeted transcripts. *In vitro* validation of AUF-1 association to selected transcripts was performed by biotin pulldown, while the levels of AUF-1 targets were evaluated by qRT-PCR, revealing a differential alteration by partial or near-total loss of AUF-1. Cytomix-induced decreased levels of AUF-1 protein were associated with accelerated cell senescence readouts of lysosomal damage, cell cycle arrest and secretion of senescence-associated secretory phenotype (SASP) factors. Interestingly, AUF-1 protein was detected into extracellular vesicles (EVs), suggesting a mechanism of loss of intracellular protein. Finally, AUF-1 targets were also identified in the human SASP proteome atlas and as differentially expressed genes in transcriptomic databases of HSAEC and lung tissue samples from stable COPD patients.

Conclusions. The studies performed in this thesis suggested that AUF-1 may play a pathogenic role in COPD by altering post-transcriptional control of epithelial gene expression, thus contributing to increased airway inflammation, also through EVs-related functions. Overall, the identification of

these changes can be used to infer putative pathogenetic roles of RBPs and identify novel disease-related regulatory networks, that will be further investigated with dedicated experimental models.

Part 1.
Introduction

1. RNA-Binding Proteins (RBPs) and their Role in Post-Transcriptional Gene Regulation (PTGR)

1.1. Definition of PTGR, main mechanisms and molecular determinants

The regulation of gene expression is a critical process of cell biology.

Inherited genes carry the genetic instructions that regulate all cellular activities, but they only partially define the functions of cells. It is necessary that each cell activates a precise and regulated pattern of gene expression in order to gain specific characteristics that determine its behaviour and allow to respond to environmental signals.

The first and highly regulated process of gene regulation is the transcription, but it represents only the tip of the iceberg of the complex events required to produce a mature mRNA fully competent for the translation. The result of transcription of coding genes is a primary transcript, called precursor messenger RNA (pre-mRNA), that undergoes extensive modifications before its transport from the nucleus to the cytoplasm, where the translation takes place [1]. These processing steps are in turn finely regulated, providing an additional level of control of gene expression. In addition, coding and non-coding RNAs can be biochemically modified via methylation, pseudouridylation, or by editing, altering RNA coding sequences, localization, stability and translational efficiency [2] (**Figure 1**).

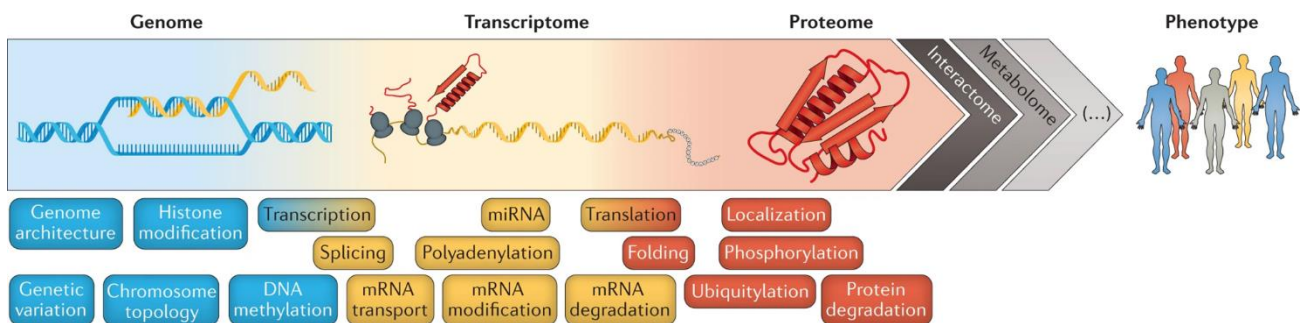


Figure 1. Overview of regulatory steps of gene expression. The flow of events that converts the information carried by a gene into a functional protein undergoes to a multi-step control, connecting the phenotype to the genotype. The cell is able to control protein production through: the modulation of gene transcription (**transcriptional control**; blue boxes); the control of splicing, modifications and localization of RNA molecules (**post-transcriptional control**; yellow boxes); the sorting of mRNAs to translate and the function-specific modification of proteins (**translational and post-translational control**; red boxes) [3].

The complexity of transcription makes this process inefficient to arrest or reprogramme once it has started. Therefore, there are numerous post-transcriptional events that determine specific expression patterns in gene expression, dispelling the direct correlation between mRNA and protein levels.

The transcriptional control is integrated with post-transcriptional regulatory mechanisms that, through coordinated signalling, regulate RNA turnover and translation rates in all basic homeostatic process like cell cycle, proliferation, stress responses as well as in disease process. Post-transcriptional gene regulation (PTGR) is mediated by protein factors, mainly represented by RNA-binding proteins (RBPs) and noncoding RNAs (ncRNA), including microRNAs (miRNAs) and long non-coding RNAs (lncRNAs). These trans-acting factors associate with mRNAs, by creating dynamic ribonucleoprotein complexes (RNPs), thanks to their ability to recognize specific mRNA sequences and/or establish conformational interactions. Through these complex actions, they influence every step of the life cycle of mRNAs, including pre-mRNA splicing, cytoplasmic translocation and translation of mature mRNAs [4] (**Figure 2**). Moreover, RBPs and miRNAs can regulate the same mRNA by cooperating or competing for a regulatory outcome [5]. A single miRNA and RBP can also target multiple mRNAs, and combinations of miRNAs and RBPs probably coordinate the outcomes of post-transcriptional gene expression [6].

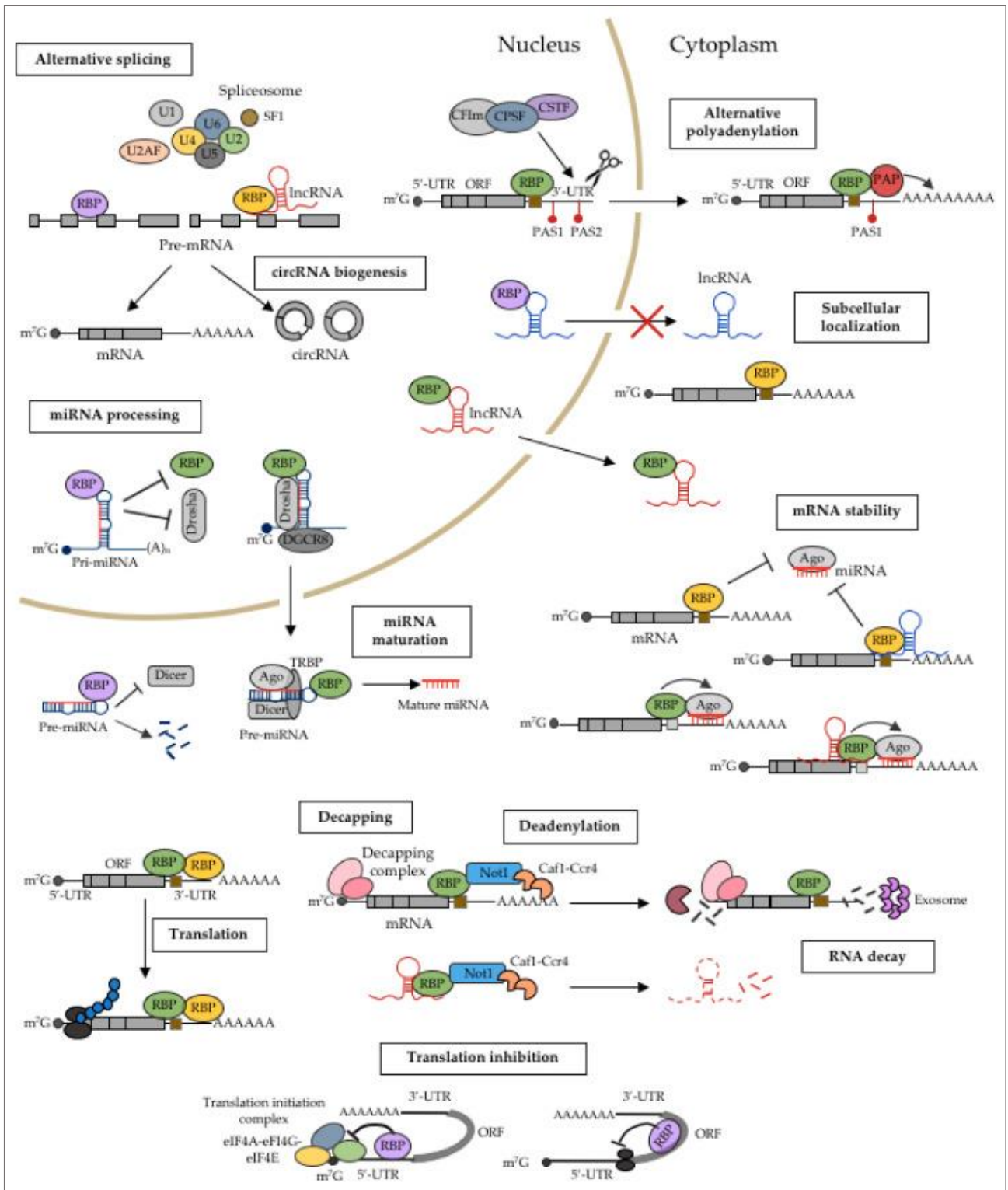


Figure 2. Post-transcriptional regulation of gene expression. RBPs associate with mRNAs after their transcription, by forming ribonucleoprotein complexes with other RBPs and regulatory molecules, like microRNAs (miRNAs). RBPs regulate all post-transcriptional stages of the mRNA life cycle, from pre-mRNA splicing and maturation in the nucleus, to transport in the cytoplasm of mature transcripts. In the cytoplasm, they bind to functional mature transcripts to regulate their stability and translation. Other RBPs also associate with non-coding RNAs, such as miRNAs and long noncoding RNAs (lncRNAs), regulating their life cycle [7].

1.2. General role of PTGR in homeostasis and disease

Specific PTGR programs allow eukaryotic cells to regulate physiological function. These mechanisms represent post-transcriptional checkpoints that control mRNA splicing, mRNA localization, mRNA stability and protein translation, but they have also important roles in pathological conditions, such as inflammation and cancer.

Post-transcriptional control of mRNA splicing. This mechanism assume a central role in maintaining quiescent status in immune cells. For example, upon bacterial challenge, almost one-fifth of the genes expressed in human dendritic cells undergo alternative splicing. Alternatively processed transcripts of toll-like receptor pathways generate numerous variants of receptors, adaptors and signalling molecules, that in turn have extensive effects on signal transduction [8]. Post-transcriptional regulation by alternative polyadenylation allows the generation of alternative 3'-untranslated region (UTR) isoforms. Greater length of 3'UTRs increases the number of miRNAs and/or RBPs binding sites, thus regulating the protein expression, or even functional diversity. For example, higher expression of longer 3'UTR isoforms was demonstrated in in both human and murine quiescent T cells compared to activated T cells [9].

Subcellular localization of mRNA. The active transport of transcripts, through mRNA-proteins complexes, determines their specific subcellular localization. As an example, in polarized cells like neurons, transcripts localization has important physiological implications. Synaptic plasticity and long-term memory formation, as well as local translocation in axons, are strongly influenced by RNA transport and consequent local protein synthesis. Long-distance mRNAs transport relays on large granules containing RBPs, ribosomes and translation factors, in a microtubule-dependent manner [10,11]. Examples of localized neuronal mRNAs are the transcripts coding for microtubule-associated protein 2 (MAP2), the α -subunit of a calmodulin-dependent protein kinase (α CaMKII), brain-derived neurotrophic factor (BDNF), and activity-regulated cytoskeletal-related (Arc) [12]. It has been shown that mRNAs localized in dendrites undergo a local translocation upon synaptic inputs induced by electroconvulsive shock [13].

Control of mRNA half-life. The balance between RNA synthesis and degradation, dynamically regulated during cell life, determines steady-state mRNA levels. Transcripts encoding transcription factors have a relatively short life, in contrast to transcripts encoding metabolic proteins that have longer half-life [12]. The regulation of mRNAs stability is a crucial process in inflammatory and immunogenic responses, that is finely regulated by RBPs.

For example, mouse models lacking tristetruprolin (TTP) and AU-rich element binding factor 1 (AUF-1), the two main RBPs that enhances mRNA decay of inflammatory mediators, clearly indicate their relevance as endogenous ‘brakes’ for inflammatory responses. Mouse model knock-out for the RBP AUF-1 shows, in different experimental settings, a complex phenotype with both overexpressed inflammatory process and accelerated aging (**Figure 3**). Decreased AUF-1 levels and activity induced accelerated aging as a result of influence both on transcriptional and post-transcriptional mechanisms: in fact, AUF-1 can act as transcription factor, upregulating transcription of the telomerase reverse transcriptase (TERT) mRNA and as RBP, promoting the decay of the cyclin-dependent kinase inhibitors p21^{WAP/CIP1}, contrasting senescence-induced cell cycle arrest [14].

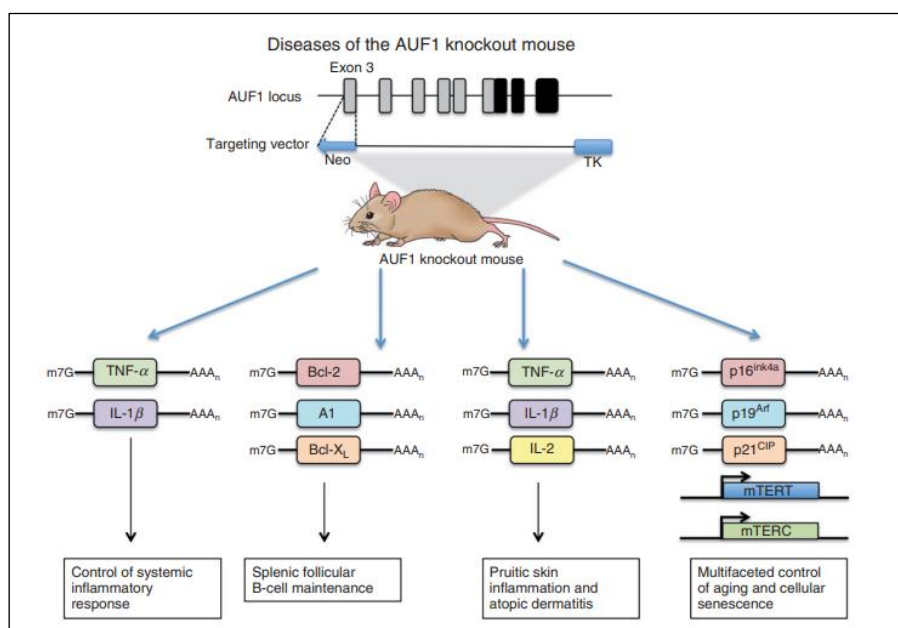


Figure 3. AUF-1 knockout mouse model displays multiple abnormalities. The AUF-1 knockout mouse was generated by homologous recombination in mouse embryonic stem cells by targeting the RNA-binding motif containing the third exon of AUF-1, allowing for disruption of the remainder of the reading frame. Loss of AUF-1 results in dysregulation of multiple mRNA targets and transcription of select genes leading to specific phenotypes observed in the AUF-1 knockout mouse. Abbreviations: Neo, neomycin-resistant cassette; TK, thymidine kinase cassette; filled box, coding region; open box, noncoding region [14].

Moreover, mice *AUF-1*^{-/-} model are highly susceptible to endotoxin-induced septic shock with increased mortality due to an overexpressed inflammatory response, mediated by the lack of AUF-1-mediated degradation of and tumor necrosis factor (TNF)- α and interleukin (IL)-1 β mRNA [15].

Autoantibodies against AUF-1 were detected in 33% of systemic lupus erythematosus patients, 20% of patients with rheumatoid arthritis, 17% of patients with mixed connective tissue disorders and below 10% of patients with other related rheumatic diseases [16].

In Japanese people affected by rheumatoid arthritis, a single nucleotide polymorphism (SNP) in the promoter region of TTP, which impairs its transcriptional activity, has been shown to be associated with disease duration and the response time to anti-TNF antibody therapy [17]. Another SNP located in the coding region of TTP gene is significantly associated with the risk of rheumatoid arthritis in African-American patients [18].

Chronic activation and cytoplasmic localization of human antigen R (HuR) are implicated in several inflammatory diseases including vascular inflammation and atherosclerosis [19,20], pancreatitis [21] and cachexia [22]. HuR is also a mediator of rheumatoid arthritis, by stabilizing the transcripts and consequently increasing the expression of TNF- α and cyclooxygenase (COX)-2, both involved in osteocartilage destruction [23,24].

Regulation of mRNA translation. The differential recruitment of mRNAs to ribosomes results in a lack of correlation between the relative amounts of mRNA and the amount of the synthesized protein. Translation of most mRNAs is controlled by proteins acting as translation factors, regulatory elements for repression or increase in translation rates. Phosphorylation of eukaryotic initiation factor (eIF)-2 α reduces the amount of active initiation complexes, leading to a rapid reduction of translation. The availability of eIF4E, member of the initiation complex, is controlled by 4E-binding proteins (4E-BP) that displace eIF4G from eIF4E, and thus inhibit association of the small ribosomal subunit with them RNA (**Figure 4**). There is also an mRNA-specific control of translational regulation mediated by RBPs and miRNAs, by which translation of defined groups of mRNAs is modulated without affecting general protein biosynthesis. For instance, the enzyme aconitase is able to regulate iron-dependent translation initiation through binding to a stem-loop structure in the 5'UTR of transcripts involved in iron metabolism [12]. A differential regulation of mRNAs due to different degree of translational inhibition was associated to duration and severity of hypoxic condition. In prostate cancer cells a selective pattern of mRNAs associated with hypoxic polysomes and some of them were translationally enriched [25]. Murine naïve T cells contain pre-existing mRNA of glycolytic enzymes, whose translation begin only upon T-cell receptor (TCR) activation. Similarly, in human naïve and central memory T cells the translation of preformed mRNA of metabolic enzymes that are involved in glycolysis and fatty acid synthesis, but also mRNAs encoding for the early activation markers cluster of differentiation (CD)-69 or CD40L, is repressed in the absence of TCR stimulation [9].

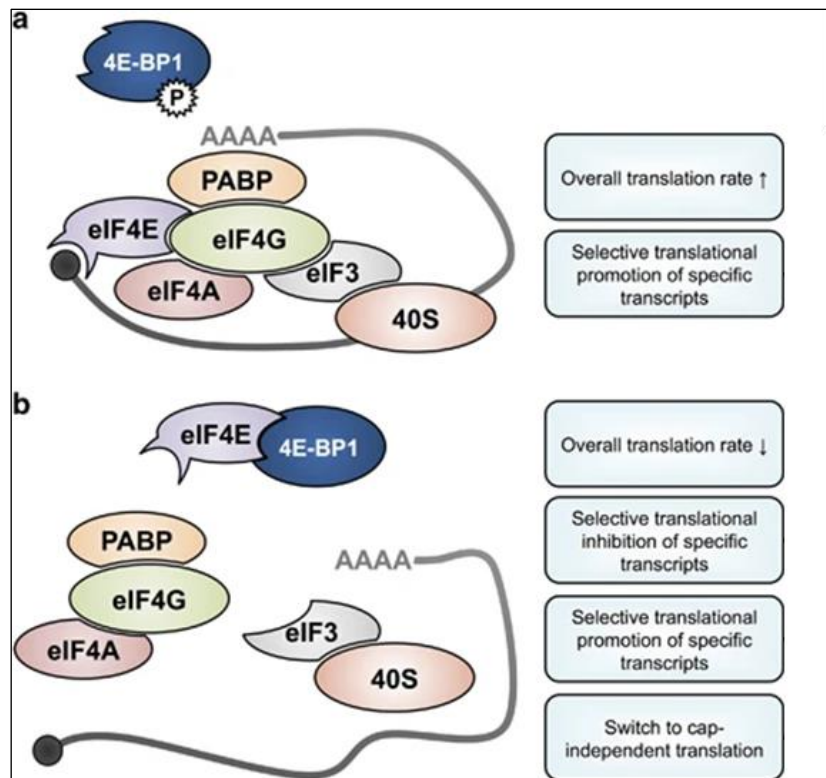


Figure 4. Schematic illustration of 4E-BP1 regulating eIF4F assembly and its impact on translation rates. A. Phosphorylated 4E-binding proteins (4E-BP)-1 is not able to bind eukaryotic initiation factor (eIF)-4E and to prohibit the eIF4F formation, resulting in an increase of overall translation rate and specific translation of transcripts. **B.** Non-phosphorylated 4E-BP1 binds eIF4E, prohibits eIF4F formation and thus leads to a decrease in overall translation rate and a decrease in specific translation of transcripts [26].

1.3. Focus on RBPs as mediators of PTGR

RBPs are a large group of over 2000 proteins that heterogeneously bind and regulate RNAs. They have been classified in several databases.

Gerstberger et al. presented a manually curated census of 1542 RBPs that interact with all known classes of RNAs, evaluating their evolutionary conservation, their abundance and their tissue-specific expression, grouped into mRNA-binding, pre-rRNA-binding, tRNA-binding, small nuclear RNA (snRNA)-binding, small nucleolar RNA (snoRNA)-binding proteins and ncRNA-binding category (**Figure 5**). In total, about 50% of RBPs are thought to have direct or indirect effects on the intracellular fate of mRNAs, and, therefore, on post-transcriptional regulation of gene expression [27]. This census identified RBPs based on binding domains, but there are also RBPs acting with different binding modes (**Figure 6**). A definition on presence or absence of binding domains describes “canonical” and “non-canonical” RBPs binding modes.

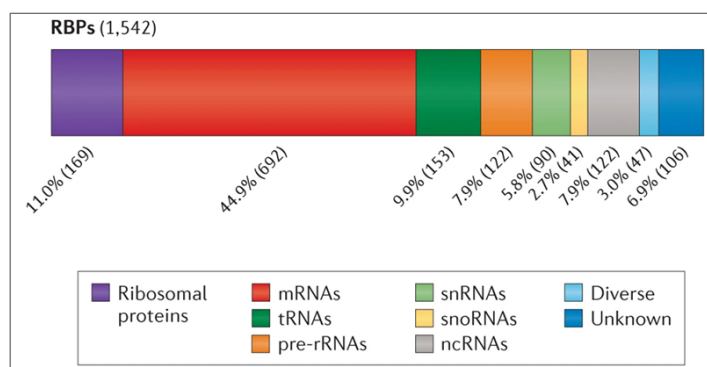


Figure 5. RBPs classification according to targeted RNA species. RBPs can be grouped by their respective targets: ribosomal proteins, mRNA, tRNA, pre-ribosomal RNA, small nuclear RNA (snRNA), small nucleolar RNA (snoRNA), noncoding RNA (ncRNA). For some RBPs the target is not yet known or they can bind to diverse targets [27].

A unified resource of 1350 human RBPs is curated in the RBP Expression and Disease Dynamics database (READ DB) In this non-redundant database RBPs are reported with their tissue-wide RNA and protein expression levels, evolutionary conservation, disease associations, protein–protein interactions, microRNA predictions, their known RNA recognition sequence motifs as well as predicted binding targets and associated functional themes [28].

Neelamraju et al. conducted a meta-analysis of a catalogue of 1344 human RBPs studying their domain architecture, protein structural disorder, tissue wide expression, evolutionary conservation and their role in the disease context. Analysis of the extent of conservation of RBPs revealed that RBPs are preserved across majority of the species studied here suggestive of a wider conservation of post-transcriptional processes. Moreover, they showed that several RBPs, including those conserved, are highly unstructured, indicating the importance of their disorder in the formation and maintenance of RNPs [29].

1.3.1. RBPs binding modes of interaction with mRNAs

The functional activity of conventional RBPs is defined by their modular structure, composed by the repetition of multiple domains. Most of RBPs contain one or more canonical RNA-binding domains (RBDs), typically composed of 60-100 aminoacids, that coordinate the sequence-specific association between RBPs and their target RNAs. However, recent proteome-wide approaches further uncovered a number of highly conserved “unconventional” RBPs lacking the canonical RBDs but actively involved in mRNA life cycle (**Figure 6**).

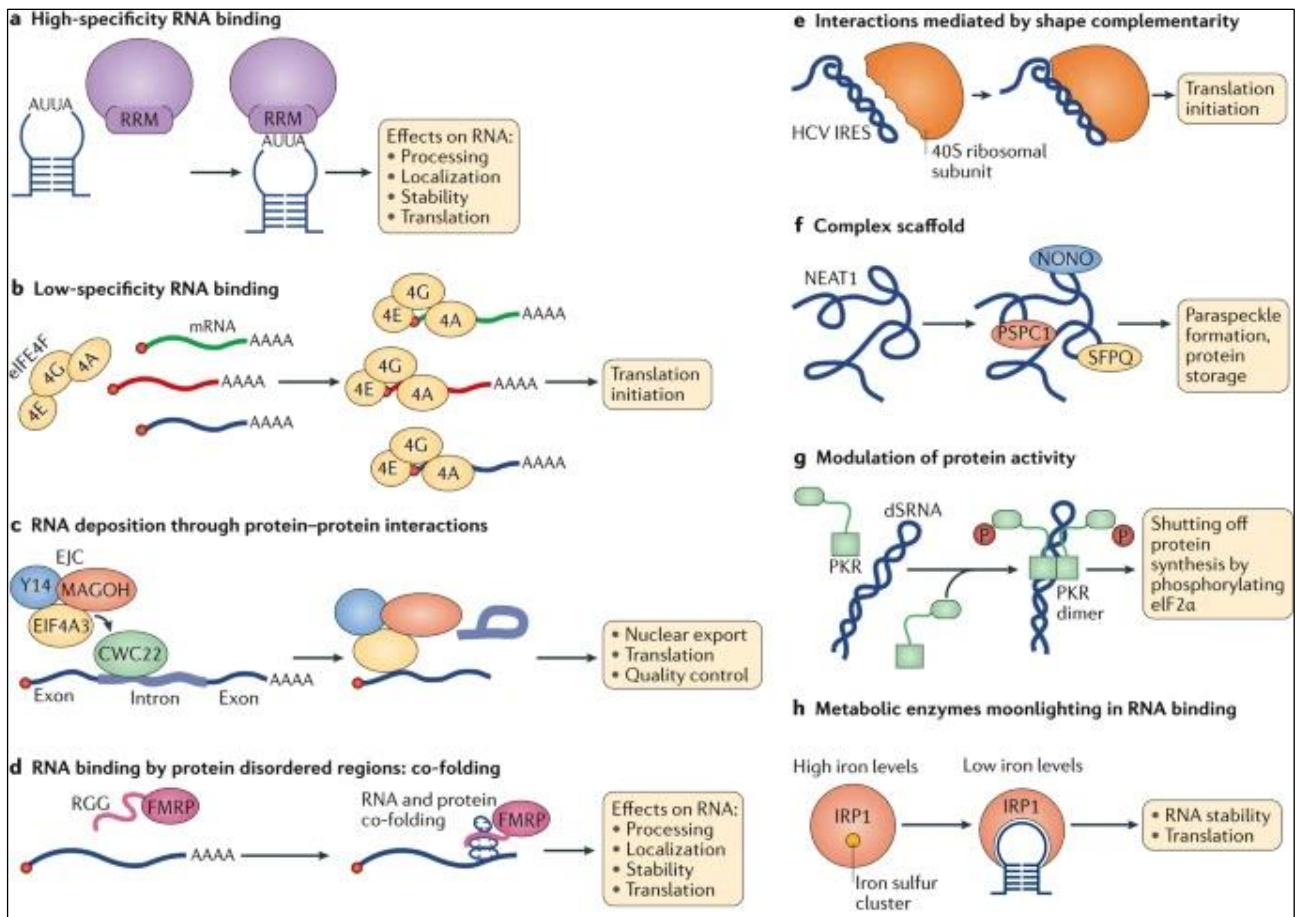


Figure 6. Modes of RNA binding. **A.** An RNA-binding protein (RBP) harbouring a classic RNA-binding domain such as the RNA recognition motif (RRM) can interact with high specificity with an RNA sequence in the context of a stem-loop. **B.** The eukaryotic translation initiation factor 4F (eIF4F) complex is composed of the cap-binding proteins eIF4E (4E) and eIF4G (4G) and the helicase eIF4A (4A). This complex associates with capped RNA in a sequence-independent manner to enable translation initiation. **C.** The exon junction complex (EJC) is deposited non-selectively on nascent transcripts by its interaction with the splicing factor CWC22 (complexed with CEF1 22) about 20 nucleotides upstream of the exon-exon junction, immediately following intron removal. **D.** The intrinsically disordered Arg-Gly-Gly (RGG) repeat motif of fragile X mental retardation protein (FMRP) co-folds with its target RNA, forming a tight electrostatic and shape-complementation-driven interaction. **E.** The internal ribosome entry site (IRES) of hepatitis C virus (HCV) interacts directly with the ribosome through a complex interaction mode that involves shape complementarity between the IRES and the 40S ribosome subunit. **F.** The long non-coding RNA nuclear enriched abundant transcript 1 (NEAT1) sequesters the RBPs non-POU domain-containing octamer-binding protein (NONO), paraspeckle component 1 (PSPC1) and splicing factor, proline- and glutamine-rich (SFPQ) to form paraspeckles. **G.** Interferon-induced, double-stranded RNA-activated protein kinase (PKR) binds to double-stranded RNA (dsRNA) derived from viral replication. Binding RNA promotes PKR dimerization, autophosphorylation and activation. Active PKR phosphorylates eIF2 α to block protein synthesis in infected cells. **H.** Iron-regulatory protein 1 (IRP1) associates with an iron-sulfur cluster to catalyse the interconversion between citrate and isocitrate. In conditions of low iron levels, the iron-sulfur cluster is no longer synthesized and IRP1 binds mRNAs that encode cellular factors involved in iron homeostasis, thereby regulating their fate. eIF4A3, eukaryotic initiation factor 4A-III; MAGOH, protein mago nashi homolog; Y14, RBP Y14 [30].

Canonical RBDs. The extreme heterogeneity of RBDs makes their classification very difficult (**Table 1**). Generally, canonical RBDs bind to short sequences of single-strand RNA, but they can also recognize sequences of secondary structured RNAs. Moreover, the interaction can involve a single protein-RNA element or, as it more often happens, it engages multiple RBPs and RNA molecules. The association between RBPs and RNA is also driven by the co-existence of multiple binding domains, along with onset of additional chemical interactions (hydrogen bonds, stacking interactions, weaker interactions) that further enhance the specificity of the interaction. Moreover, some RBDs can mediate protein-protein interactions [31-33].

Table 1. Main RNA binding domain in RBPs.

Domain	Description
RRM	RNA recognition motif, single-strand RNA (ssRNA)-binding
RG/RGG	RG/RGG box repeats are arginine glycine rich low complexity regions, may bind RNA or act as protein-protein interaction domains in shuttling
DEAD	DEAD and DEAH box helicase motif, unwinds RNA (and DNA)
zf-CCCH	Zinc finger motif type C-x8-C-x5-C-x3-H, ssRNA-binding
KH	KH-homology domain, ssRNA-binding
GTP_EFTU, GTP_EFTU_D2, GTP_EFTU_D3	GTP-elongation factor family, proteins usually consist of 3 structural domains, 2 oligonucleotide binding domains (D2 and D3) and a GTP-binding domain
dsrm	Double-stranded RNA binding motif
zf-CCHC	Zinc knuckle, C-x2-C-x4-H-x4-C, ssRNA-binding
LSM	Like Sm domain is found in snRNP complexes, bind A/U rich regions
OB_NTP_bind	Oligonucleotide/oligosaccharide-binding (OB)-fold, found in DEAD-box helicases in association with HA2 domain, regulates helicase activity through RNA binding
HA2	Helicase-associated domain, found in RNA helicases
G-patch	G-patch domain, ~48 amino acids with 6 conserved glycines, found in RBPs
IBN_N	Importin-beta N-terminal domain, RNA transport or RBP transport proteins
SAP	(SAF-A/B, Acinus and PIAS) motif, RNA/DNA-binding domain
TUDOR	Tudor domain, found in Tudor proteins, Tudor proteins are in complexes with RBPs
RnaseA	RNase A domain, ssRNA endonuclease
zf-C2H2_jaz	JAZ dsRNA-binding protein zinc-fingers, dsRNA-binding
MMR_HSR1	50S ribosome-binding GTPase domain, found in RBPs

KOW	KOW (Kyprides, Ouzounis, Woese) motif, found in a variety of ribosomal proteins
RNase_T	RNase T ssRNA exonuclease domain
MIF4G	MIF4G (Middle domain of eukaryotic initiation factor 4G (eIF4G)), RNA- (and DNA-) binding
zf-RanBP	RNA-binding Ran-binding-protein-like zinc finger
NTF2	Nuclear transport factor 2 (NTF2) domain, found in RNA export factors
PAZ	Piwi Argonaut and Zwiile (PAZ) domain, posttranscriptional silencing domain, binds siRNAs
RBM1CTR	C-terminal region found in hnRNPs
PAM2	PABP-interacting motif PAM2, found in RBPs
Xpo1	exportin 1 domain, RNA transport or RBP transport proteins
S1	S1 ssRNA-binding domain
HGTP_anticodon	Anticodon binding domain, found in aminoacyl-tRNA synthetases
tRNA-synt_2b	tRNA synthetase class II core domain (G, H, P, S and T), core catalytic domain of tRNA synthetases
Piwi	Piwi domain (P-element induced wimpy testis), posttranscriptional silencing domain, dsRNA guide hydrolysis of ssRNA
CSD	cold-shock domain, ssRNA/ssDNA binding
Ribosomal_L7Ae	domain found in ribosomal proteins L7Ae/L30e/S12e/Gadd45
RNase_Zc3h12a	ssRNA endonuclease domain found in Zc3h12a proteins, member of the NYN domain family
Anticodon_1	tRNA anticodon-binding domain, found in tRNA synthetases
R3H	R3H domain, R-x3-H conserved core, binds ssRNA/ssDNA

The most common RBDs is the RNA Recognition Motif (RRM). It is a small domain of 90 aminoacids and structurally composed by two α -helices against an antiparallel β -sheet. The interaction with RNA engages few nucleotides (about 2-8) through several stacking interactions and hydrogen bonds [33]. Multiple copies of RRMs are often consecutively combined in order to create a larger and more specific binding interface that recognizes a longer sequence.

K homology (KH) domains form a three-layer β sheet packed against three α helices. Based on their topology, they are classified into type I ($\beta\alpha\alpha\beta\beta\alpha$) and type II ($\alpha\beta\beta\alpha\alpha\beta$) subfamilies. Unlike RRM, there are no aromatic aminoacids in the chemical structure and the recognition takes place through chemical bonds, such as shape complementarity, electrostatic interactions and hydrogen bonding [34].

The third most common RBDs are double-stranded RNA-binding motifs (dsRBMs). They specifically interact with double-stranded RNA. dsRBDs often appear as tandem repeats or in combination with other functional RBDs. The domain is made up of an antiparallel β -sheet flanked by α -helices on one face. Although the dsRBMs have common structural characteristics, the chemical models are different and determine a different specificity for the different RNAs, such as inner rings, bulges or helices containing, misalignments, stem rings. For this reason they are involved in multiple functions such as RNP localization, RNA interference, RNA processing, RNA localization, RNA editing and translational control [35,36].

Zinc-finger domains are characterized by the presence of a coordinated Zn^{2+} ion. Zinc finger motifs that interact with RNA include C2H2, CCHC, CCCH and CCCC, where C and H refer to the


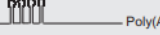

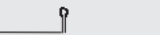

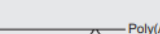
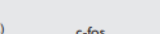

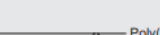
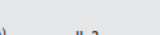
interspersed cysteine (C) and histidine (H) residues that coordinate the zinc atom. CCHC motifs recognize stem loop elements in RNA structure, while CCCH and CCCC subtypes generally recognize three nucleotides repetition [37].

Non-canonical RBDs. The unconventional RBPs containing non-canonical RBD are characterized by unfolded and flexible regions of the protein that lack any defined tertiary structure under native conditions, defined intrinsically disordered regions (IDRs). These regions present repeated motif rich of glycine, serine and arginine that mediate RNA binding. Interactions mediated by unconventional RBPs promote protein-RNA co-folding, interaction by shape complementary, scaffolding protein–RNA complexes or altering the activity of the bound protein [32]. Unconventional RBPs include metabolic enzymes, such as 3-hydroxyacyl-CoA dehydrogenase type 2 (HSD17B10), regulators of alternative splicing, the E3 ubiquitin and ISG15 ligase TRIM25 and others [30] (**Figure 5**).

1.3.2. Regulatory elements modulating RBP:transcript association: sequences and post-translational modification of target mRNAs

Regulatory cis-acting sequences, located in the 3'UTRs and 5'UTRs and, less often, in the coding sequence of the transcripts act as binding sites for RBPs whose interaction determines their fate, controlling the stability and/or translation of targeted mRNAs. They have been initially defined untranslated sequence elements for regulation (USERS) [6] (**Table 2**).

Table 2. Main cis-elements mediating mRNA stability and example of transcript bearing the element [38].

Determinant	Location	Description	Example
AU-rich element (ARE) ²¹ Class I (dispersed AUUUA)	3' UTR	<u>AUUUA-(N)₈₉-AUUUA-(N)₁₇-AUUUUAAGAUUUA</u>	c-myc
Class II (tandem AUUUA)		<u>AAUAUUUAUUUAUUUAUUUAUUUUA</u>	GM-CSF
Class III (U-rich, non-AUUUA)		<u>AUCCUGCCAGUGUGUUUGUAAUUA</u>	c-jun
Iron response element (IRE) ⁸	3' UTR	5' UTR  3' UTR  Poly(A)	Transferrin receptor
Histone stem-loop ²²	3' UTR	5' UTR  3' UTR 	Histone
Coding region determinant (CRD) ²³	Coding	5' UTR  CRD  3' UTR  Poly(A) ARE	c-fos
Jun kinase response element (JRE) ²⁴	5' UTR	5' UTR  JRE  3' UTR  Poly(A) ARE	IL-2

The most conserved and well-characterized RBP binding sequence is the adenosine/uridine-rich elements, called AU-rich elements (AREs). Generally, AREs contain AUUUA pentamers within a U-rich region spanning from 40 to 150 nucleotides [39] (**Table 3**).

Table 3. Classification of Adenylate-uridylate-rich elements as described by [40].

Group	Motif	Representative transcripts
I	WAUUUAW with U-rich region	c-fos, c-myc
IIA	AUUUUAUUUUAUUUUAUUUA	GM-CSF, TNF- α
IIB	AUUUUAUUUUAUUUUA	IFN- α
IIC	WAUUUUAUUUUAUUAW	COX-2, IL-2, VEGF
IID	WWAUUUUAUUUAWW	FGF2
IIE	WWWWAUUUUAUUUWW	u-PA receptor
III	U-rich region, non-AUUUA	c-jun

GM-CSF: granulocyte macrophage-colony stimulating factor; TNF: tumour necrosis factor; IFN: interferon; COX: cyclooxygenase; IL: interleukin; VEGF: vascular endothelial growth factor; FGF: fibroblast growth factor; u-Pa: urokinase plasminogen activator. *: proposed classification by Wilusz *et al.*

The presence of an ARE sequence regulates mRNA turnover. These sequences are specifically recognized by a subgroup of RBPs defined ARE-binding proteins (ARE-BPs) [41] (**Table 4**). Those proteins may also recognize other sequences [42].

Table 4. RBPs containing canonical RNA-binding domains (RBDs) classified according to their effect on target mRNAs. [Based on [43-50].

RBPs official name	Alternative names	RBDs
mRNA destabilization		
ZFP36	TTP	CCCH tandem zinc-finger
ZFP36L1	ERF1 BRF1 BERG36	2 C ₃ H tandem zinc-finger
HNRNPD	AUF1	2 RRM _s
HNRNPA1	HNRPA1	2 RRM _s
KHSRP	KSRP FUBP2 FBP2	4 KH domains
mRNA stabilization		
ELAVL1	HuR	3 RRM _s
ELAVL2	HuB HELN1	
ELAVL3	HuC PLE21	
ELAVL4	HuD PNEM	

Pre-mRNA processing		
HNRNPA2B1		2 RRM
Repression of translation		
TIA1		3 RRM
TIAL1	TIAR TCBP	3 RRM

Several RBPs associating with ARE sequences of gene transcripts involved in these processes mediate mRNA destabilization, such as TTP, AUF-1 and KH-type splicing regulatory protein (KSRP), while others, HuR have a stabilizing effect [51,52]. A group of ARE-binding proteins, including T-cell-restricted intracellular antigen-1 (TIA-1) and T-cell internal antigen-1 related protein (TIAR), induce translational silencing of targeted transcripts [53]. By binding to ARE-bearing transcripts induced by a specific response, RBPs coordinately regulate PTGR for multiple transcripts that are also functionally related [6].

Another USER is composed of guanosine/uridine-rich sequences, defined as GU-rich element (GRE). The GREs are classified into five clusters according to GUUUG pentamers in the 3'UTR of mRNA. Transcripts containing GRE are involved in multiple cell functions, such as cell growth and activation and regulation of apoptosis, but also in inflammatory responses, including c-Jun, Jun-b and TNF-receptor-1B [54]. The first RBP to be characterized as GRE-BP was CUG-repeat binding protein 1 (CUGBP1), a member of the CUGBP and Embryonic Lethal abnormal vision-like Factor (CELF) family of RBPs [55].

Moreover, many RBPs are able to bind to other sequences, such as guanosine/cytosine-rich motif for AUF-1 [42] and also to a defined subset of primary RNAs by recognizing low-complexity motifs composed of just one or two nucleotides. Specific binding is not only mediated by linear sequence motifs, but also by other structural features of RNAs, such as RNA secondary structure and base compositional context. Moreover, the presence of RBD type is correlated to a preferential recognition of structural mRNA elements. For example, RBPs with zinc finger domains tend to bind structured motifs, while RBPs with KH domains prefer to recognize large hairpin loops. In addition, some RBPs can bind to multiple distinct motifs [56,57].

Epitranscriptome. Several reversible biochemical modifications of mRNAs, collectively known as “epitranscriptome”, modulate all aspects of RNA metabolism during physiological and pathological processes, by triggering changes in RNA structure which modulate the accessibility of RBPs to RNA [58] (**Figure 7**).

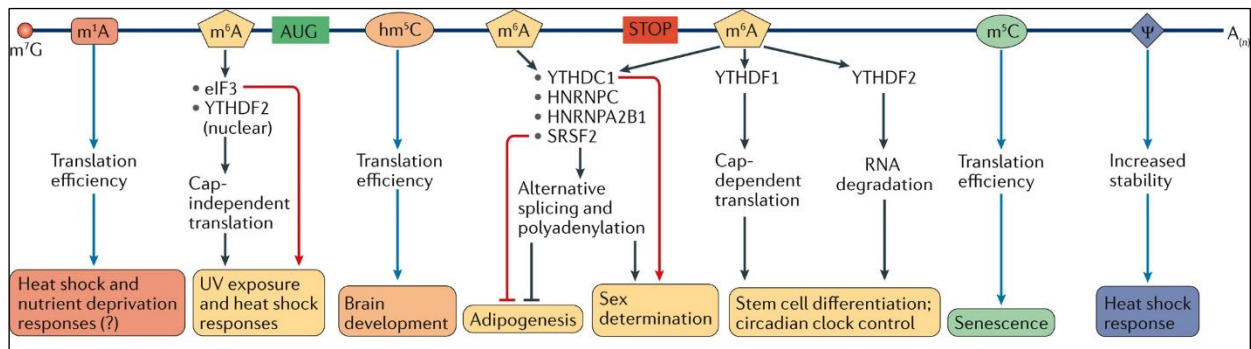


Figure 7. mRNA modifications and their established biological functions. The levels of N1-methyladenosine (m¹A) are altered by nutrient deprivation or heat shock, which indicates a possible role in directing cellular responses during these conditions. N6-methyladenosine (m⁶A) in 5' untranslated regions (5' UTRs) facilitates cap-independent translation through interactions with the eukaryotic translation initiation factor 3 (eIF3) complex in response to heat shock or UV exposure. YTH domain-containing family protein 2 (YTHDF2) protects 5' UTR m⁶A from demethylation. In coding sequences, 5-hydroxymethylcytosine (hm⁵C) increases translation efficiency via an unknown mechanism; hm⁵C levels are highest in the brain. m⁶A in coding regions affects RNA processing by modulating the binding of YTH domain-containing protein 1 (YTHDC1), heterogeneous nuclear ribonucleoprotein C (HNRNPC), HNRNPA2B1 and serine/arginine-rich splicing factor 2 (SRSF2). m⁶A in 3' UTRs also affects RNA processing via the aforementioned readers, as well as cap-dependent translation via YTHDF1 and RNA degradation via YTHDF2. Regulation of mRNA stability by m⁶A is crucial for stem cell differentiation and circadian clock control. 5-Methylcytosine (m⁵C) is linked to the translational control of senescence-related genes. Pseudouridine (Ψ) in 3' UTRs has been shown to increase the stability of modified transcripts during heat shock [59].

The methylation of adenosine in RNA molecules (N⁶-adenosine methylation or m⁶A) is the most prevalent among post-translational RNA modification (**Figure 8**); this modification is present in 0.1–0.4% of all cellular adenosines, accounting for ~50% of all methylated ribonucleotides [60].

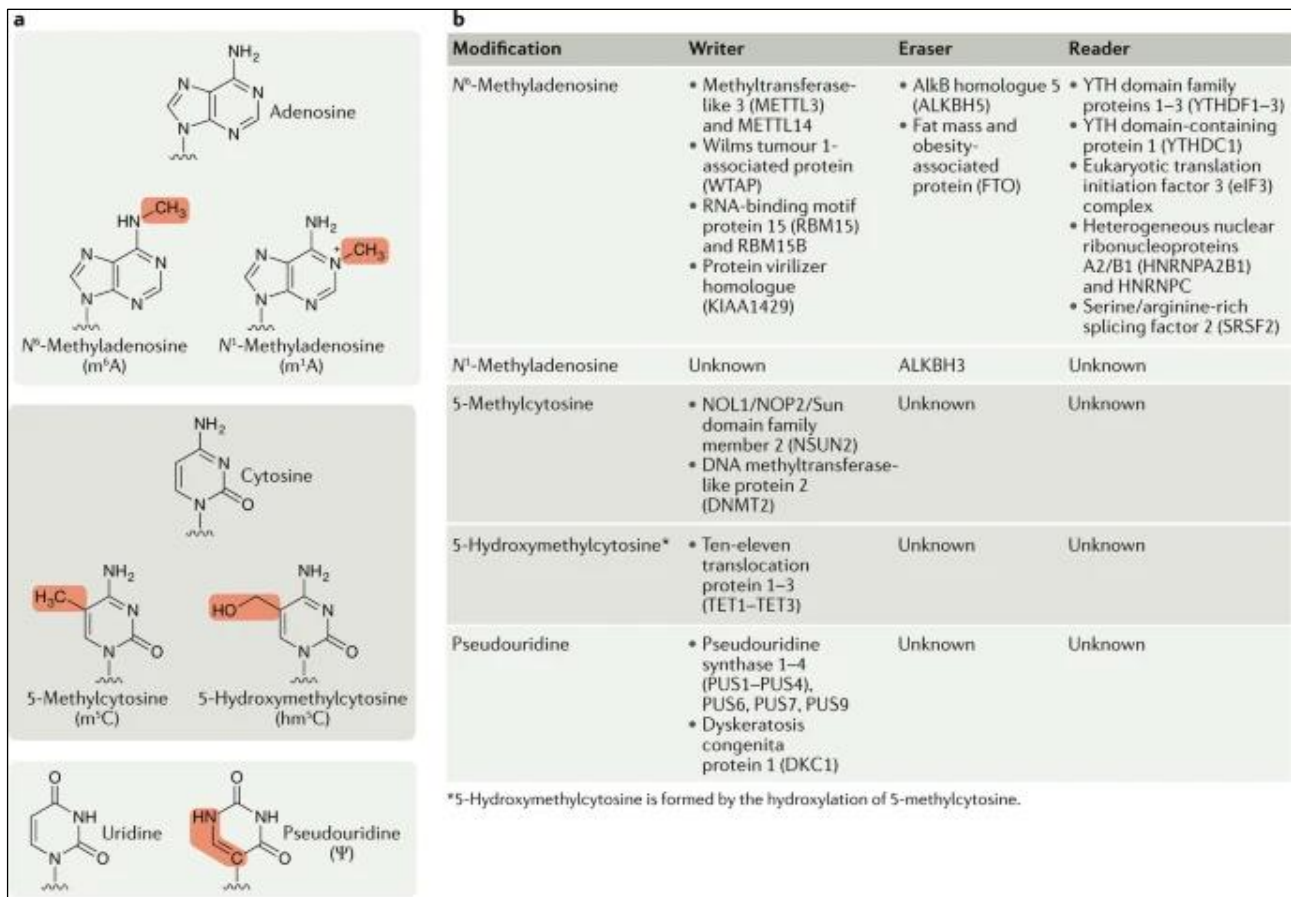


Figure 8. RNA modifications and their writers, erasers and readers. A. Chemical structures of unmodified and modified RNA bases. **B.** The writers, readers and erasers of RNA modifications [59].

Adenosine methylation occurs predominantly in two consensus sequence motifs: G m⁶A C (~70%) and A m⁶A C (~30%). The m⁶A are mostly localized in highly conserved regions: long internal exons, locations upstream of stop codons, and the 3'UTR of mRNA. m⁶A is mediated by special RNPs (i.e., methyltransferases, demethyltransferases) called writers, erasers and readers as they can respectively install, remove or recognize this modification [61,62] (**Figure 9**). Through recognition and binding of reader RBPs, this modification can influence cellular processes, such as mRNA stability and translation, splicing, miRNA biogenesis, X-chromosome inactivation, in homeostatic and disease conditions [63,64].

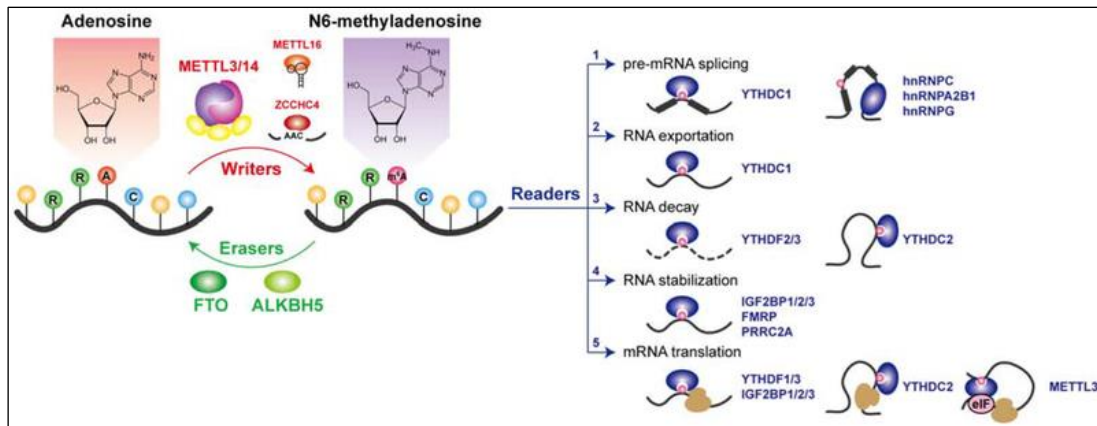


Figure 9. The m⁶A methylation machinery and the biological functions of m⁶A. The methyltransferase complex (writers), composed by methyltransferase-like (METTL)-3/METTL14 heterodimer, adds the m⁶A modification on mRNAs. METTL16 catalyzes m⁶A formation in U6 small nuclear RNA (snRNA) and some structured RNAs, while ZCCHC4 is responsible for deposition of m⁶A on rRNA. RNA demethylases (erasers) fat mass and obesity-associated protein (FTO) and AlkB family member 5 (ALKBH5) remove the RNA m⁶A modification. The biological functions of m⁶A modification are achieved by specific recognition and binding by RBPs (readers), which affects RNA fate by regulating RNA splicing, export, decay, stabilization, and translation [61].

In mouse T cells the deletion of m⁶A ‘writer’ protein METTL3 disrupts T cell homeostasis and differentiation: naïve T cells deficient for METTL3 failed to undergo homeostatic expansion and mRNAs of suppressors of cytokine signalling (SOCS) family genes encoding signal transducer and activator of transcription (STAT)-signalling inhibitory proteins, SOCS1 and SOCS3. Cytokine inducible SH2 containing protein (CISH) showed slower mRNA decay, as a consequence of failed adenosine methylation. Moreover, m⁶A plays important roles for inducible degradation of SOCS mRNAs in response to IL-7 signalling in order to reprogram naïve T cells for proliferation and differentiation [65].

The reversible RNA methylation regulates essential features of cancer cells. In glioblastoma, METTL3 or METTL14 induces changes in mRNA m⁶A levels, altering mRNA expression of oncogenes, such as a disintegrin and metalloproteinase (ADAM)-19. In human lung adenocarcinoma, METTL3 promotes translation of epidermal growth factor receptor (EGFR), whose mRNA is affected by m⁶A in the last exon [66].

1.3.3. Main RBPs with functions on control of mRNA turnover and translation

Highly relevant to PTGR regulation in lung disease context, genes involved in immune responses, inflammation and carcinogenesis are highly enriched for RBP binding sequences, especially AREs (**Table 5**). The specificity of PTGR is provided by the combination of multiple elements – structural features of RBPs and related binding sequences, co-expression of regulatory molecules, signalling-

induced post-translational modification changes in RNP composition and binding affinity, and so on - ultimately regulate protein expression by stabilizing or degrading target mRNAs, and modulating translation rates. In general terms, HuR acts as a positive regulator of mRNA stability and translation, TTP has been described as promoter of mRNA decay of their targets, while TIAR and TIA-1 regulate translation of targeted transcripts. More complex is the multifunctional profile of AUF-1 [42].

Table 5. Short list of AU-rich elements (ARE)-RBP and their functional effect on mRNA target stability and translational efficiency of genes relevant in inflammatory responses. Based on [67].

ARE-BPs	mRNA stability		Protein expression			
	Increase	Decrease	Translational efficiency		Abundance	
			Increase	Decrease	Up-regulated	Down-regulated
AUF-1	c-myc c-fos PTH GM-CSF TNF- α	c-myc c-fos p21 Cyclin D1 GM-CSF IL-3				GM-CSF IL-3
HuR	c-fos MyoD		p53	TNF- α	p21	TNF- α
	p21 Cyclin A Cyclin B1 Cyclin D1			COX-2	Cyclin A	
	GM-CSF TNF- α COX-2 IL-3 VEGF Myogenin				Cyclin B1 NOS II/iNOS GM-CSF COX-2	
					VEGF p53	
HelN1	TNF- α NF-M		NF-M GLUT1		NF-M GLUT1	
HuD	GAP-43				GAP-43	
TTP		c-fos GM-CSF TNF- α COX-2 IL-2 IL-3				GM-CSF TNF- α IL-2 IL-3
BRF1		TNF- α IL-3				GM-CSF IL-3
TIA1				TNF- α COX2		TNF- α COX2
KSRP		c-fos				NOS II/iNOS
		TNF- α IL-2 c-jun				
CUG-BP2	COX-2			COX-2		COX-2
Nucleolin	BCL-2					

mRNA stabilization. HuR is the ubiquitously expressed member of the embryonic lethal abnormal vision (ELAV) family along with HuB (ELAVL2), HuC (ELAVL3), and HuD proteins that are primarily found in neurons, though their expression was also found in the serum of patients with encephalomyelitis, sensory neuronopathy, small cell lung cancer and paraneoplastic manifestations [68,69]. HuR contains three RRM, of which RRM1 and RRM2 are separated by a short linker of 7 aminoacid residues and bind with high affinity to AREs sequences, while RMM3 contributes to HuR interaction with target poly-(A) tails [44]. HuR mainly localizes in the nucleus but it can translocate to the cytoplasm upon cell activation by stressful stimuli (UV radiation, nutrient deprivation, cytokine stimulation), where it prevents the decay of mRNAs implicated in different pathologies, particularly cancer and inflammation. This translocation is mediated by the presence of the nucleocytoplasmic shuttling (HNS) sequence in HuR protein structure (**Figure 10**).

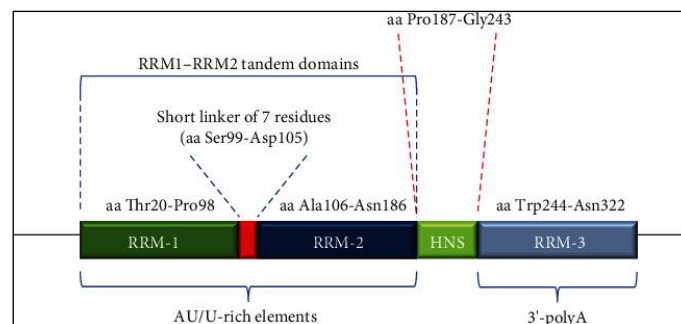


Figure 10. Schematic representation of HuR protein domains. The domains RRM1 and RRM2 are connected by a short linker of 7 residuals. RMM2 and RRM3 domains are spaced by the nucleocytoplasmic shuttling (HNS) sequence, which allows the protein to shuttle between the cytoplasm and the nucleus. RRM-1 and RRM-2 bind [70].

The mechanism of HuR-dependent mRNA stabilization is complex and not fully defined. Importantly, HuR prevents mRNA decay protecting the body of the message from degradation by competitive binding to sites shared with mRNA-destabilizing RBPs [71] and interfering with miRNA [52].

Overexpression of HuR increases the mRNA stability of several cell cycle regulators, such as cyclin A1, cyclin B1, cyclin D1 and cyclin E1, thus contributing to cell proliferation [72-74].

In glioma cells, increased levels of HuR are associated to increased stability of COX-2, vascular-endothelial growth factor (VEGF) and c-myc mRNAs, while the inhibition of over-stabilization of HuR target mRNAs impairs the growth of glioma cells *in vitro* [75]. HuR also binds and stabilizes the mRNA of the negative regulator of adipogenesis, insulin-induced gene 1 (INSIG1), repressing

this process. The loss of HuR in adipose tissue significantly increase fat mass in mice, together with glucose intolerance and insulin resistance [76].

mRNA decay: TPA-induced sequence (TIS)-11 proteins: TTP and its family members. TTP, also known as zinc finger protein 36 homolog (ZFP36), is the prototypic member of the TPA-induced sequence (TIS)-11 family along with butyrate-response factor (BRF)-1 (also known as TIS11b and ZFP36L1) and BRF-2 (also known as TIS11d and ZFP36L2) [77]. The ZFP36 gene encodes a proline-rich zinc finger protein with three repetitions of the PPPP motif that determine its name. The protein contains two zinc finger domains that bind to ARE-mRNAs to promote their decay or translational repression [47,49] (**Figure 11**). TTP also self-regulates its mRNA through the link with its ARE in a negative feedback loop [78].

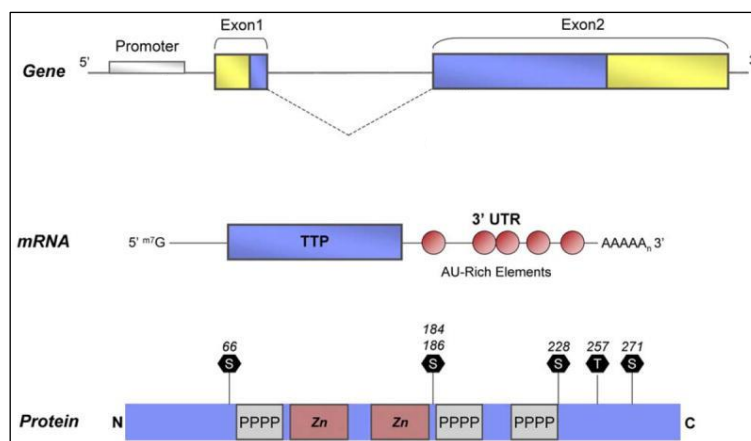


Figure 11. Schematic representation of TTP gene, mRNA, and protein. Human TTP gene consists of two exons and one intron. TTP mRNA contains ARE-motifs in the 3' UTR. TTP protein structure displays unique features including three tetra-proline (PPPP) repeats, two CCCH-type zinc (Zn) finger domains and several serine/threonine phosphorylation sites [77].

Another member of the TIS11 family is BRF-1, that is rapid induced in a cell type and stimulus-dependent manner [79].

The mechanism of action by which TIS11 members accelerate the degradation of mRNA is complex. TTP promotes the rapid decay of target mRNAs by directly binding to the ARE sequences. In particular, TIS11 members specifically bind the sequence UUAUUUAUU [80]. This binding depends on the integrity of the Cys3His residues of the two zinc-finger domains. Indeed, point mutations in either of the zinc-finger domains attenuated the binding with ARE-transcripts, resulting in increased stability of those mRNAs [81].

Once bound to ARE-containing transcripts, TTP mediates the decay by promoting their deadenylation through the recruitment of the carbon catabolite repression 4 (CCR4)–negative on TATA-less (NOT) deadenylase and the decapping protein (DCP)-1/DCP2-containing decapping complexes [82,83]. This event leaves the mRNA susceptible to rapid decay mediated by TIS11 family members via 5'-3' decay in processing (P)-bodies or 3'-5' decay mediated by complex of exonucleases known as the exosome [84,85].

Among the mRNA targeted by TTP there are several transcripts encoding key proteins in immune responses, such as TNF- α , IL-2, IL-3, IL-6, IL-10, interferon (IFN)- γ , granulocyte-macrophage colony-stimulating factor (GM-CSF) and COX-2. TTP also downregulates the stability of the mRNA encoding VEGF, assuming a potential role in tumor angiogenesis processes [86].

mRNA decay and multiple function of heterogeneous nuclear ribonucleoprotein (hnRNP)

family: AUF-1. The RBP AUF-1, also known as heterogeneous nuclear ribonucleoprotein (HNRNP)-D, belongs to a family of ubiquitously expressed HNRNPs. AUF-1 is expressed as four related isoforms derived from a common precursor mRNA by differential splicing of exons 2 and 7, referred as p37^{AUF-1}, p40^{AUF-1}, p42^{AUF-1}, and p45^{AUF-1}, based on their molecular weights. In particular, p37^{AUF-1} isoform lacks both exons 2 and 7, p40^{AUF-1} contains exon 2 but lacks exon 7, p42^{AUF-1} contains exon 7 but lacks exon 2, and p45^{AUF-1} contains the entire AUF-1 coding sequence [41]. All four AUF-1 isoforms contain conserved domains including two tandem RRM, of which the C-terminal of second RRM contain a glutamine-rich motif [43] (**Figure 12A**). Despite their common structure, the four isoforms show different binding affinity for their transcripts. In particular, p37^{AUF-1} and p42^{AUF-1} isoforms display threefold to fivefold higher affinity for AU-rich sequences than p40^{AUF-1} and p45^{AUF-1}. Another difference among AUF-1 isoforms is their subcellular localization that is mainly determined by the inclusion of exon 2 or 7. Indeed, p37^{AUF-1} and p40^{AUF-1}, that contain the nuclear import signal (NIS) in their C-terminal domain, shuttle efficiently between the nucleus and cytoplasm. The insertion of exon 7-encoded aminoacids in p42^{AUF-1} and p45^{AUF-1} isoforms disrupt the NIS, promoting their restriction to the nucleus [87-89] (**Figure 12B**).

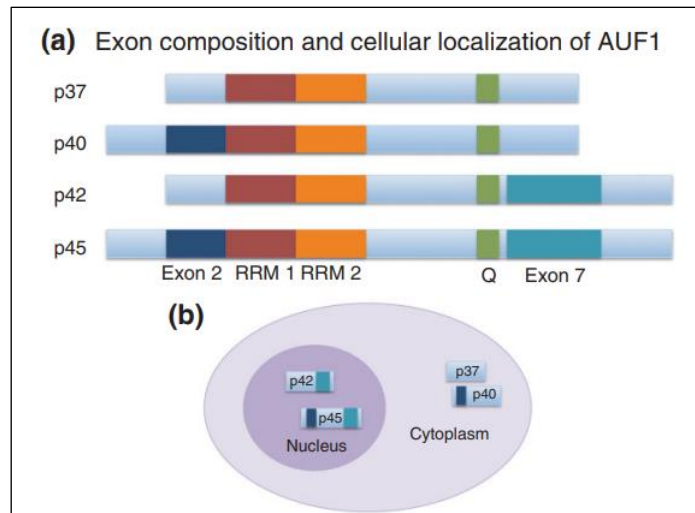


Figure 12. Domain organization and subcellular localization of AUF-1 isoforms. A. Domain organization of peptide sequences encoded by alternatively spliced exons 2 and 7. Glutamine-rich (Q-rich) for nucleocytoplasmic shuttling and RRM domains of proteins are also shown. **(b)** p37^{AUF-1} and p40^{AUF-1} isoforms are predominantly cytoplasmatic and shuttle more actively between the nucleus and cytoplasm compared with the larger p42^{AUF-1} and p45^{AUF-1} isoforms [14].

AUF-1 function is particularly complex, involving also transcriptional and translational regulatory roles (**Table 6**). AUF-1 has been shown to act as an ARE-mRNA decay factor and, occasionally, as an ARE-mRNA-stabilizing factor, although the consensus is that it primarily functions to promote rapid mRNA degradation [90]. The mRNA decay activity of AUF-1 appears to be principally mediated through the isoforms normally found in the cytoplasm (p37^{AUF-1} and p40^{AUF-1}) [91].

As most of RBPs, AUF-1 protein is not able to directly degrade RNAs by itself, but it recruits downstream components of the mRNA decay machinery. In particular, this process starts with AUF-1 oligomerization to ARE-containing transcripts. Then, cap-dependent translation initiation factors and molecular heat-shock chaperone proteins, including eIF4G, poly(A)-binding protein (PABP), heat shock protein (Hsp)-70 and Hsp27, are recruited, allowing the formation of a large multi-subunit complexes on ARE-containing transcripts, known as AUF-1- and signal transduction-regulated complex (ASTRC) [15,92]. ASTRC-mediated mRNA decay induces acceleration of 3'-deadenylation and the recruitment of the exosome complex, containing 3'-5' exoribonucleolytic and RNA helicase activities, to further accelerate degradation of the mRNA once deadenylation has been completed [93-95].

Table 6. Targets of AUF-1 activity [14].

Gene	Physiology	Mechanism of Action	Specific Isoform(s) Implicated
GRO α	Inflammation and cancer	Decay	
GM-CSF	Inflammation and cancer	Decay	p40 ^{AUF1}
IL-1 β	Inflammation	Decay	p40 ^{AUF1}
IL-10	Inflammation and cancer	Decay	p40 ^{AUF1}
IL-6	Inflammation and cancer	Decay	p37 ^{AUF1} and p42 ^{AUF1}
MCL1	Inflammation	Decay	p40 ^{AUF1} , p42 ^{AUF1} , and p45 ^{AUF1}
TNF- α	Inflammation and cancer	Decay	p40 ^{AUF1}
VEGF	Inflammation	Decay	
IL-2	Inflammation	Decay	
iNOS	Inflammation	Decay	p37 ^{AUF1} , p40 ^{AUF1} , p42 ^{AUF1} , and p45 ^{AUF1}
COX-2	Inflammation	Stability	p42 ^{AUF1}
CDKN2A	Cancer	Decay	
c-Myc	Cancer	Promotion of translation	
Cyclin D1	Cancer	Decay	p45 ^{AUF1}
Dicer1	Cancer	Decay	
E2F1	Cancer	Decay	
β -AR	Cardiac	Decay	p37 ^{AUF1}
B56 α	Cardiac	Decay	p37 ^{AUF1}
Kv4.3	Cardiac	Decay	
SERCA2A	Cardiac	Decay	
ENK	Neural development	Transcription	p37 ^{AUF1} , p40 ^{AUF1} , and p42 ^{AUF1}
HCV	Virus	Translation	
BCL2	Spleen development and inflammation	Decay and stability	p40 ^{AUF1} , p42 ^{AUF1} , and p45 ^{AUF1}
A1	Spleen development	Stability	
BCL	Spleen development	Stability	
p16 ^{Ink4}	Ageing	Decay	p37 ^{AUF1} and p40 ^{AUF1}
p21 ^{cip}	Ageing	Decay	p37 ^{AUF1} and p40 ^{AUF1}
p19 ^{ARF}	Ageing	Decay	p37 ^{AUF1} and p40 ^{AUF1}
TERT	Ageing and cancer	Transcription	p42 ^{AUF1} and p45 ^{AUF1}

A global analysis of AUF-1-bound targets and binding sites performed by photoactivatable ribonucleoside-enhanced cross-linking and immunoprecipitation (PAR CLIP) analysis revealed that AUF-1 recognizes also GRE sequences in mRNAs and noncoding RNAs. This interaction induces lower steady-state levels of the majority of AUF-1 target RNAs, promotes the translation of a different subset of target RNAs and enhances the steady-state levels of a subset of target mRNAs mostly encoding DNA-maintenance proteins [42]. Moreover, AUF-1 can act as transcription factor, as it was shown to be required for telomere maintenance via transcriptional activation of TERT gene and direct interaction with telomeric repeat sequences [96,97].

Translational control. The RBPs TIA-1 and TIAR are involved in translational regulation of targeted mRNAs. They share more than 80% of sequence homology. Their structure is composed of three N-terminal RRM motifs, that mediate binding to mRNA targets, and a C-terminal Q-rich prion-related domain (PRD), important for stress granules formation [45]. The RRM2 and RRM3 motifs both directly mediate the binding to the recognized target sequence: RRM3 improves overall binding affinity through its interaction with C-rich motifs while RRM2 guides protein-RNA interaction, through its affinity for pyrimidine-rich sequences. Both TIA-1 and TIAR are expressed as two isoforms with distinct functional properties on their targets. The inclusion/exclusion of an 11 aminoacid-long peptide at the beginning of RRM2 of TIA-1 forms TIA-1a and TIA-1b isoforms, respectively (**Figure 13**). Similarly for TIAR, inclusion/exclusion of a 17 aminoacids fragment within RRM1 discriminates TIARa from TIARb [98].

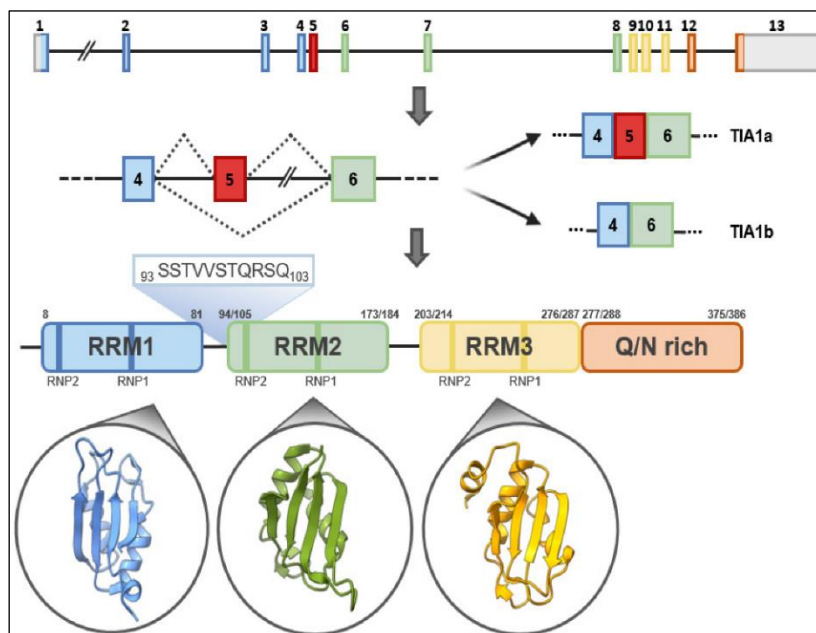


Figure 13. TIA-1 gene and protein structural details. Organization of exons and introns of TIA-1a and TIA-1b isoforms, generated by alternative splicing of exon 5. Both isoforms share three RRM domains and one C-terminal domain rich in asparagine and glutamine (Q/N-rich domain). The secondary-tertiary structures of each of the three RRM motifs are highlighted in the corresponding circles [99].

TIA-1 and TIAR exert the function of translational repressors mainly under stress conditions, including oxidative damage and hypoxia. They accumulate in the cytoplasm and associate with the 40S ribosomal subunit, forming inactive preinitiation complexes that will be aggregated into stress granules [100,101].

TIA-1 and TIAR can also act during the translation initiation phase to stop protein synthesis of upstream regulators. For example, during stress they can bind the terminal oligopyrimidine (TOP)

mRNA, which contains a 5' terminal oligopyrimidine tract (5'-TOP) that occurs mainly in transcripts coding for ribosomal proteins as well as for elongation factors (eIF1alpha and eIF2) which are not required in stress condition [102].

1.3.4. Post-translational modifications of RBPs: major determinants of function

The regulatory activity of RBPs on gene expression is dynamic and adapts to cell conditions continuously. Signals from intracellular and extracellular environment can lead to post-translational modifications (PTMs) of RBPs, that control several proprieties of RBPs, influencing their activity and localization, as well as the interaction with both target mRNAs and other proteins [103].

PTMs affecting RBPs are methylation, acetylation, ubiquitination, isomerization but the better characterized is phosphorylation (**Table 7**).

HuR. Phosphorylation events affecting HuR influence its function in different ways, by changing HuR protein stability, affinity for binding RNA, and subcellular localization. Phosphorylation of HuR by cell cycle-dependent kinase (CDK)-1 at Ser-202 in the hinge region inhibits HuR translocation in the cytoplasm, retaining it in the nucleus. In contrast, HuR phosphorylation on Thr-118 mediated by p38 MAPK lead to the accumulation of HuR in the cytoplasm. Checkpoint kinase 2 (CHK2)-mediated phosphorylation, instead, compromises HuR binding to target transcripts [104]. Methylation of HuR to Asp-271 by coactivator-associated arginine methyltransferase 1 (CARM1) and subsequent stabilization of TNF- α mRNA occurs in macrophages after lipopolysaccharides (LPS) treatment [52,105]. Moreover, HuR can be NEDDylated at lysine residues K283, K313 and K326, and, particularly, modifications at K313 and K326 are involved in HuR protein stability by increasing their nuclear localization [106].

Table 7. List of the main phosphorylation sites on RBPs [107].

RBP	Kinase	Phosphorylation site
TIS11	MK2	Ser52
TIS11	CAMK2	Ser52
TIS11	PKB	Ser248
TIS11	PKA	Ser197
TIS11	GSK3	Ser218
TIS11	ERK	Ser228
TIS11b	PKA/PKB	Ser54/92
TIS11b	mTOR	Ser334
TIS11d	PKB	Ser98
TIS11d	PKA/PKB	Ser28/98
TIS11d	mTOR	Ser57/73/416/464
KSRP	mTOR	Ser182, Ser185
KSRP	PKA	Ser481
Nucleolin	mTOR	Ser28/34/40/41/145/157/616, 189/403/212/460,Thr121
Roquin	ERK/MAPK	Ser770
Roquin	mTOR	Ser531/535
hnRNPK	CDK2	Ser284
hnRNPU	CK1	Ser187
hnRNPU	CAMK2	Ser247
hnRNPF	mTOR	Ser63
hnRNPA3	mTOR	Ser356/359/367
hnRNPA3	CK1	Ser359
hnRNPA3	PKA	Ser357
hnRNPAb	PKA	Ser260
AUF1	mTOR	Ser82/83, Thr177
hnRNPA2B1	mTOR	Ser245/247/266/272, Tyr254
hnRNPK	mTOR	Ser284/379
hnRNPC	mTOR	Ser229/232/241/268/306/313
hnRNPUL1	mTOR	Ser513
hnRNPUL1	CAMK2	Ser195
hnRNPA1	mTOR	Ser6/257
hnRNPA1	CDK1	Ser6
hnRNPH2	mTOR	Ser104
HuR	mTOR	Ser202
IMP2	mTOR	Ser102
IMP2	mTOR	Ser160/161/163

TTP. The RBP TTP presents several phosphorylation sites and it is highly phosphorylated *in vivo*, through the action of major kinase pathways, such as mitogen-activated protein kinases/ extracellular-signal-regulated kinase (MAPK/ERK), p38 mitogen-activated protein kinases (p38), c-Jun N-terminal kinases (JNK), glycogen synthase kinase (GSK)-3 β , protein kinase (PK)-A, PKB and PKC [108,109].

Coelho et al. demonstrated how the phosphorylation status of TTP regulates the expression of programmed death ligand 1 (PD-L1) in lung cancer cells (**Figure 14**). In non-cancerous cells the functionally active form of TTP, associated to a low phosphorylation status, binds to the 3'UTR of PD-L1 transcript, accelerating its mRNA degradation and thus decreasing its expression. The activation of oncogenic RAS pathway in tumor cells, including lung cancer cells, makes TTP highly phosphorylated which inhibits its function, leading to higher PD-L1 expression and occurrence of tumor immune resistance [110].

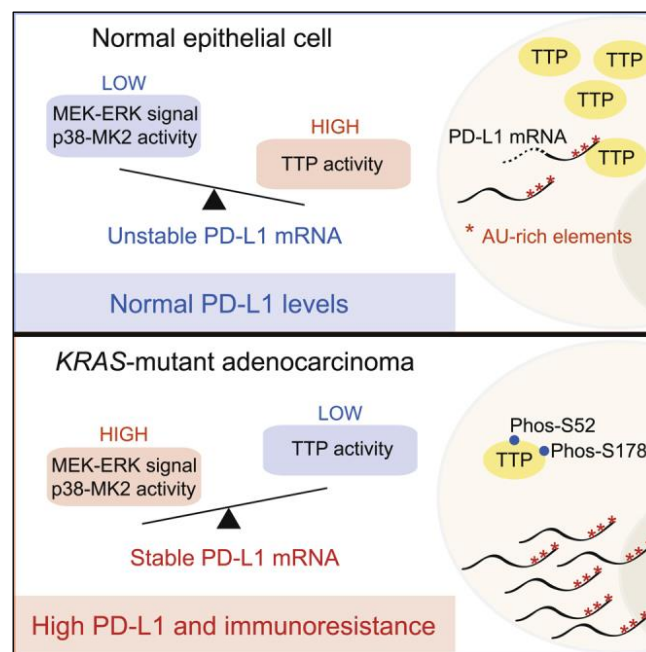


Figure 14. The role of TTP phosphorylation in regulating programmed death ligand 1 (PD-L1) expression in lung cancer cells. Oncogenic RAS signaling can upregulate tumor cell PD-L1 expression through a mechanism involving increases in PD-L1 mRNA stability via modulation of the AU-rich element-binding protein tristetraprolin (TTP). TTP negatively regulates PD-L1 expression through AU-rich elements in the 3' UTR of PD-L1 mRNA. MEK signaling downstream of RAS leads to phosphorylation and inhibition of TTP by the kinase MK2 [110].

AUF-1. Several but conflicting evidences do not clarify the role of AUF-1 phosphorylation. It has been reported that phosphorylation of AUF-1 isoform p40 at Ser83 and Ser87 is associated with destabilization of ARE-containing transcripts, while another group defined that hyperphosphorylation of AUF-1 by nucleophosmin-anaplastic lymphoma kinase (NPM-ALK) correlates with stabilization of several AUF-1 target mRNAs [41]. Both AUF-1 isoforms p37 and p34 can be selectively poly-ubiquitinated, determining AUF-1 degradation through proteasome pathway in a phosphor-HSP27 dependent manner [41].

1.4. Crosstalk between PTGR regulatory factors: non-coding RNAs (ncRNAs) and RBPs

Besides RBPs, another class of PTGR regulatory factors are ncRNAs, mainly represented by miRNAs and long ncRNAs (lncRNAs) (**Figure 2**).

Studies in macrophages have revealed important roles for lncRNAs in controlling inflammatory gene expression. They can mediate post-transcriptional mechanisms altering mRNA splicing, turnover or translation. Moreover, lncRNAs can act as miRNA sponges by preventing miRNA-mediated degradation of target mRNAs. For example, the lncRNA metastasis associated lung adenocarcinoma transcript 1 (MALAT1) controls alternative splicing of mRNA. Other lncRNAs can affect RBP Fox-1 homologue 2 (FOX2)-mediated pre-mRNA splicing. The lncRNA β -secretase 1 antisense transcript (BACE1-AS), whose levels are upregulated in Alzheimer patients, stabilizes its protein-coding sense transcript BACE1 by protecting it from RNase cleavage [8].

The PTGR pathways mediated by ncRNAs and RBP may collaborate or compete on specific mRNA substrates for a particular binding site on an mRNA, indicating important synergistic or antagonistic functions, respectively. Complex and diverse combinations of regulatory molecules (miRNA/RBP, RBP/RBP, miRNA/miRNA) (**Figure 15**) entail functional outcomes highly dependent from the biological context [5].

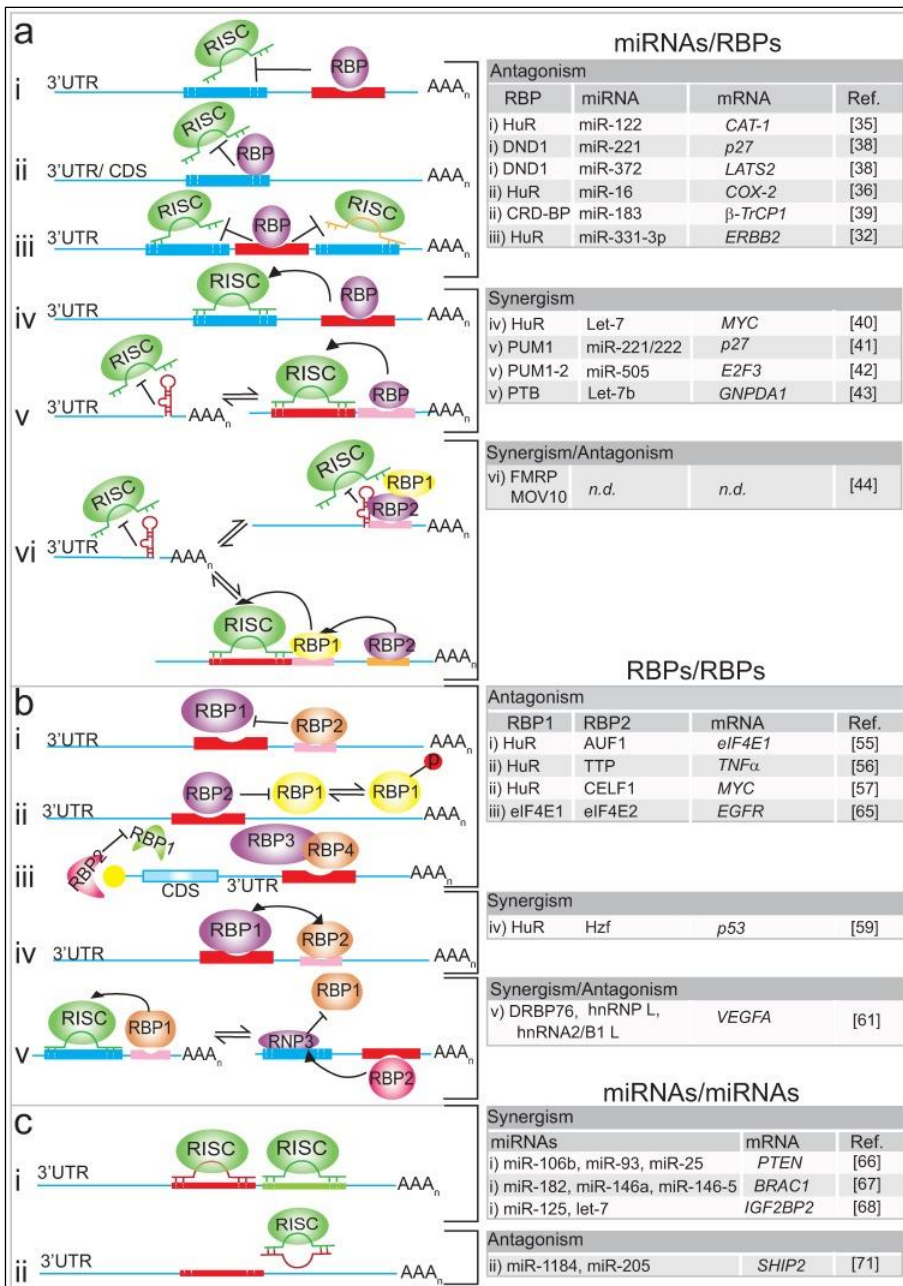


Figure 15. Crosstalk between miRNAs and RBPs. **A.** Interactions RBP/miRNA. Left upper panel: when in antagonism, the binding of the RBP to the transcript prevents the binding of the miRNAs. The RBP can bind the transcript next to the RISC binding site (i), overlap in 3'-UTRs or coding sequences (CDS) (ii), or in between sites (iii). Left middle panel: when in synergism, RBPs can promote the link between RISC and transcript (iv), modifying local RNA structures (v). Left lower panel: Different ways of interacting between RBPs can influence RISC activity in either synergistic or antagonistic manner (vi). **B.** Interactions RBP/RBP. Left upper panel: two RBPs can compete with each other for distinct binding sites (i) or for the same (ii). Furthermore, the translation initiation factors can also compete for a region in the cap end of the transcript (iii).

Left middle panel: The export of mature mRNA and protein synthesis can be promoted by a cooperative mechanism among RBPs (iv). Left lower panel: example of possible antagonistic or synergistic interaction of RBP on a target transcript (VEGF- α) (v). **C.** Interactions miRNA/miRNA. RISCs can also act synergistically or antagonistically. Left upper panel: as a result of synergism (i), a greater inhibition of the expression of the transcript is possible. Left lower panel: (ii) antagonistic interplay between RISC determine an increase of target expression [5].

Moreover, besides the RNA-RBPs and ncRNA-RBPs interactions mediated by the cis/trans recognitions, RBP-RBP dynamic interplay further give complexity to the regulatory mechanisms of common target mRNAs. In particular, the synergistic interaction between two RBPs with the same regulatory aim is known as cooperative model, in opposition to the competitive one, in which the antagonistic interaction leads to different regulatory outcome [111] (**Figure 16**).

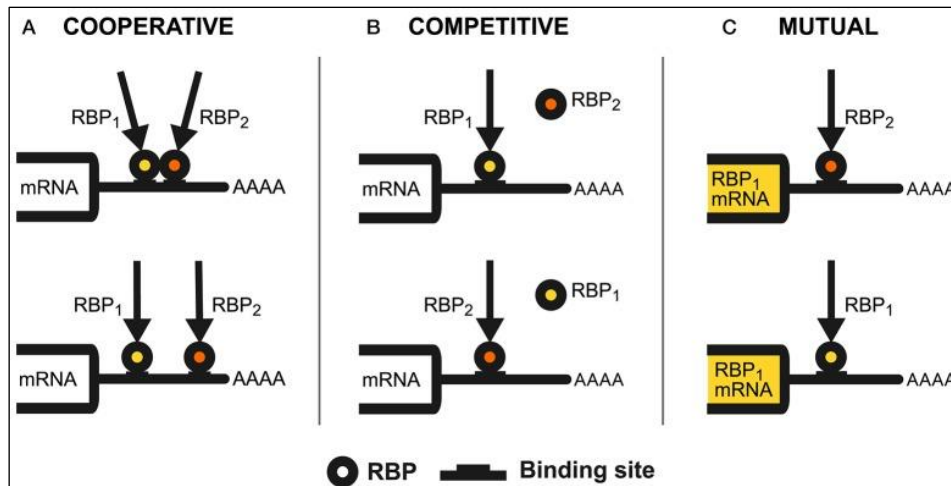


Figure 16. RBPs regulatory interplay models. Different patterns of regulatory interaction experimentally described between RBPs in a generic mRNA 3'-UTR as the interaction substrate. **A.** Cooperative interaction. Two RBPs can recognize binding sites on the target mRNA that can be close to each other, or distant but brought to proximity by the secondary structure of RNA. Two RBPs can also cooperate on distant sites without direct interaction between them. In this case (below) there is independent cooperation. **B.** Competitive interaction. Two RBPs compete for the superimposed binding on the same target mRNA. The regulation of the transcript is given by the balance between the two RBPs. **C.** Mutual interaction. Two RBPs control mutual expression, either to favor or limit expression [111].

2. RBPs: role in disease

The ability of RBPs to coordinate the complex networks of post-transcriptional events can impact many genes and signalling pathways. Alterations in RBPs expression and function are strongly associated to the onset and progression of many human diseases.

In the last years, the contribution of PTGR has been increasingly described in human cancer pathophysiology, while much less has been characterized regarding these mechanisms in chronic inflammatory diseases. RBPs have been studied in this field more recently, based on strong preclinical evidence implicating them in oxidative stress responses and inflammation, as discussed in paragraph 2.2.

RBPs role has been extensively characterized in neurodegenerative disorders, since they are characterized by high rate of mRNAs metabolism [112]. Moreover, many degenerative brain diseases are characterized by the deposition of toxic protein aggregates containing RBPs. The RBP fragile X mental retardation protein (FMRP) is encoded by FMR1 gene, susceptible to CGG triplet expansions in its 5'UTR, causing fragile X syndrome. FMRP has been proposed to regulate neuronal mRNAs by various mechanisms, including repression of translation elongation, transport of ribonucleoprotein particle granules towards synaptic terminals, where mRNAs are derepressed in a stimulus-dependent manner [113].

RBPs have also been found to critically regulate splicing during post-natal cardiac remodelling. Increased expression of the RBP HuR was observed in histological specimens of hyperplastic smooth muscle pathologies, including neointimal hyperplasia, neointimal proliferation and fibromuscular dysplasia [114]. Increased levels of AUF-1, instead, were detected in cardiac myocytes upon angiotensin II treatment, and they were associated to accelerated decay of the Kv4.3 mRNA, a potassium channel protein, contributing to cardiac hypertrophy [115].

2.1. RBPs in Cancer

Alterations of RBPs have been increasingly identified in human neoplastic diseases. Deregulation of RBPs expression and intracellular localization has the consequence the improper modulation of their target mRNAs and influence different stages of cancer development, such as cell proliferation, apoptosis, angiogenesis, senescence, epithelial mesenchymal transition (EMT), invasion and metastasis [112,116].

The RBP HuR, mainly characterized as functional antagonist of mRNA-decay promoting RBPs, is also widely described in the pathogenesis of cancers in colon, pancreas, brain, lung and others [52]. HuR localization in the cytoplasm of cancer cells is associated to the increased stabilization of important mediators of neoplastic transformation, such as the cationic aminoacid transporter 1

(CAT1) and COX-2, acting as a repressor for miRNA binding [5,117]. Overexpression and/or cytoplasmic localization of HuR is associated with lymph node metastatic disease in various cancers, including breast and lung cancers [118,119]. Moreover, HuR enhance the stability of mRNAs encoding for MMP-9, urokinase A (uPA) and uPA receptor (uPAR), that are involved in in extracellular matrix (ECM) degradation, thus affecting cell adhesion, invasion and metastasis [120-122].

The RBP TTP is an immediate-early response gene and it regulates mitotic signalling pathways in many cancer types while shares regulation of key inflammatory and stress response genes with other ARE-binding RBPs including HuR [123,124]. The interplay between these two RBPs can regulate the expression of common targets in an agonistic or antagonistic manner (**Figure 17**). Loss of TTP has been identified as pathogenic due to the ensuing stabilization, with increased translation, of multiple cancer hallmark genes: in particular, what is chiefly relevant for cancer pathogenesis is the loss of balance between levels of TTP and its functional antagonist HuR: loss of TTP is paralleled by increase of expression and activation of HuR [125,126]. HuR was found to be one of the most upregulated RBPs in small cell lung cancer (SCLC) and cytoplasmic levels of HuR has been shown associated with high tumor grade and poor survival rate in non-small cell lung cancer (NSCLC) [127,128]. In lung adenocarcinoma, TTP overexpression inhibits cell proliferation by inducing cell cycle arrest in the S phase and decreases the expression of autophagy-related transcripts, including Beclin1 and LC3II/I [129].

As an example, AUF-1 is also implicated in proliferation and invasiveness of breast cancer cells through aberrant regulation of several targets: suppression of the cyclin dependent kinase inhibitor (CDKN)-2A, increased secretion of stromal cell-derived factor 1 (SDF1) and matrix metalloproteinase (MMP)-2, and facilitation of the EMT [41].

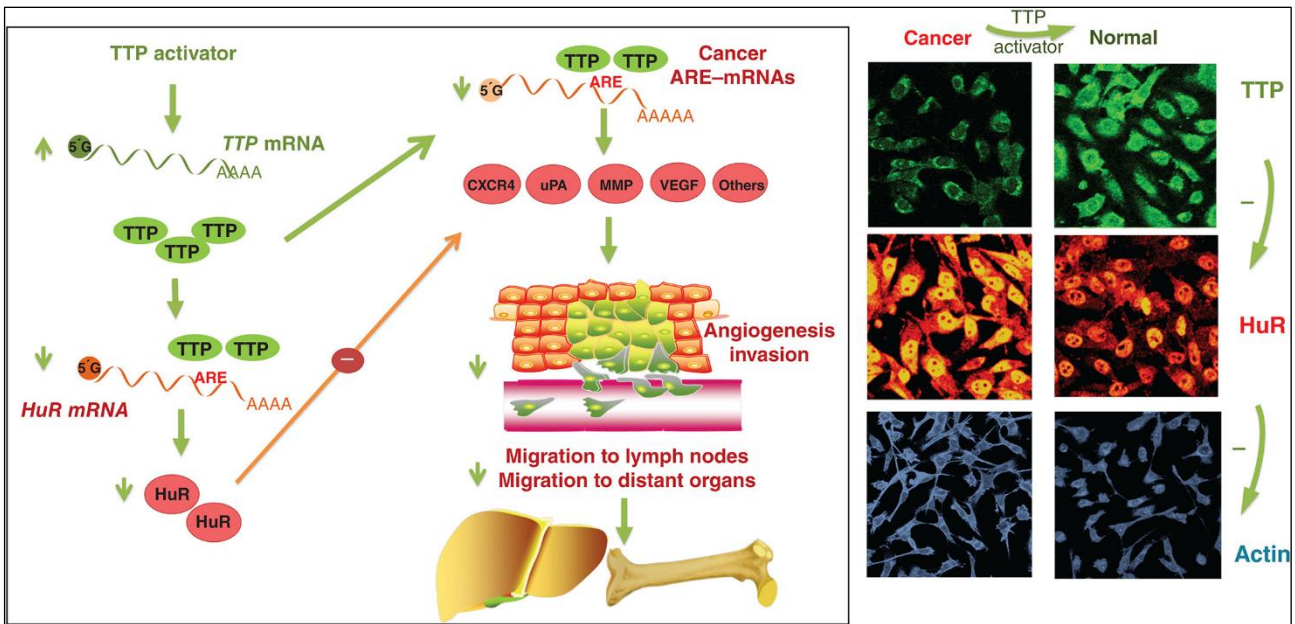


Figure 17. Graphical representation of potential modulation of the antagonistic effect between TTP and HuR. Through the use of a TTP activator, such as cell-permeable peptide-nucleic acid against miR-29a, TTP can act on HuR mRNA and induce a reduction in its expression while exerting mRNA-decaying effects on common targets. This combined effect determines a cascade of downstream events that leads to the modulation of several targets, previously stabilized by HuR, that promoted tumor progression and its metastasis. Right panel: changes in TTP and HuR expression levels are shown in both normal and tumor conditions through confocal microscopy. In blue the cytoskeletal polymerization of actin is shown [130].

It is now well accepted that tumor progression is critically sustained by inflammation. Since the early neoplastic transformation, the cells act as tumor promoters, producing an attractive environment for inflammatory cells that influence the whole tumour organ, regulating growth, migration and differentiation of all cell types in the tumour microenvironment. In the later stages of tumorigenic process, the inflammatory mechanisms favour neoplastic spread and metastasis [131].

Several key proteins that share common functions in inflammation and cancer process are coded by AU-rich mRNAs (**Table 8**).

In the context of lung pathology, lung cancer is importantly associated to chronic obstructive pulmonary disease (COPD). In particular, alteration of lung microenvironment - driven by aberrant signalling pathways, transcriptional regulation and epigenetic mechanisms - conducive for lung cancer are driven by oxidative stress-driven inflammation and accelerated cellular senescence featured in COPD [132-135], that will be discussed in following paragraphs.

Table 8. AU-rich elements in inflammation and cancer [136].

Symbol	Name	ARE ^a	Inflammation	Cancer
BCL2	B-cell CLL/lymphoma 2	III	Inflammatory response	Oncogenesis, apoptosis
CFOS	c-fos	III	Inflammatory response	Oncogenesis
CCND1	Cyclin D1	V		Oncogenesis, maintenance
CXCL-1	GRO- α	I	Chemotaxis	Oncogenesis, maintenance
ET2	Endothelin-2	IV	Chemotaxis, cell-cell signaling	Maintenance
EGF	Epidermal growth factor	V	Inflammatory response	Maintenance, angiogenesis, Invasion
EREG	Epiregulin	V	Cytokine response	Maintenance, angiogenesis
EGFR	EGF receptor	U-rich	Cytokine response	Cell growth, maintenance
FGF2	Fibroblastic growth factor 2	V	Chemotaxis	Cell growth, migration angiogenesis
CCL2	MCP-1	U-rich	Chemotaxis	Migration
CCL3	MIP-1 α	IV	Chemotaxis	Migration
CSF2	GM-CSF	I	Cytokine response	Hematopoiesis, maintenance
CXCL-1	(Melanoma growth stimulating activity, alpha), GRO- α	II	Inflammatory response, chemotaxis	Cell growth, maintenance
ELAVL1	HuR	III	Cytokine response	RNA-binding, cell growth angiogenesis, metastasis
F3	Tissue factor	IV	Coagulation	Invasion, angiogenesis
SLC2A1	Glucose transporter 1 (Glut1)	U-rich	Inflammatory response	Maintenance
HIFA	Hypoxia induced factor- α	III	Transcription, inflammatory response	Hypoxia response, angiogenesis
IL-1 β	Interleukin-1	II	Inflammatory response	Maintenance, metastasis
IL-6	Interleukin-6	IV	Inflammatory response	Cell growth, maintenance
IL8	Interleukin-8	III	Chemotaxis	Angiogenesis
LTA	Lymphotoxin	III	Inflammatory response	Oncogenesis
MMP13	Collagenase 3 (Matrix metalloproteinase-13)	V	Inflammatory response	Invasion, metastasis
NOS	Inducible nitric oxide synthase	V	Inflammatory response	DNA damage
PDGFB	Platelet-derived growth factor B	IV	Chemotaxis	Oncogenesis, maintenance
PFKB3	6-phosphofructo-2-kinase/fructose-2,6-bisphosphatase 3	III	–	Carbohydrate metabolism, maintenance
PLAU	Urokinase plasminogen activator (uPA)	IV	Inflammatory response, chemotaxis	Invasion, metastasis, angiogenesis
PLAUR	UPA receptor	V	Chemotaxis	Invasion, metastasis
PTGS2	Cyclooxygenase (COX-2)	III	Inflammation, motility	Angiogenesis
PTH1H	Parathyroid hormone-like hormone	V	Inflammation	Maintenance
SCL2A1	Glut1 receptor	V	Inflammatory response	Glycolysis, maintenance
SERPINE	Plasminogen inhibitor activator 2	V	Adhesion, coagulation	Invasion, metastasis
SELE	E-selectin	III	Leukocyte adhesion, migration	Migration, metastasis
TNF	Tumor necrosis factor α	III	Inflammation, cell-cell communication	Cell growth, maintenance
VCAM	Vascular cell adhesion molecule-1	III	Leukocyte rolling	Metastasis
VEGF	Vascular endothelial growth factor	IV	Chemotaxis	Hypoxia response, angiogenesis

2.2. Chronic Obstructive Pulmonary Disease (COPD): RBPs as molecular pathogenic link with in oxidative stress and inflammation

According to consensus definition [137], COPD is characterized by persistent respiratory symptoms (dyspnea, cough and/or sputum production) and progressive airflow limitation, due to airway and/or alveolar abnormalities, associated with enhanced chronic inflammatory response to noxious particles or gases; periods of acute worsening of respiratory symptoms (exacerbations) and coexistence with concomitant chronic diseases significantly impact the clinical course of COPD patients. COPD affects about 10% of population over 40 years of age and it represents the third leading cause of death worldwide, after ischemic heart disease and cancers [138], causing 3.23 million deaths in 2019 [139].

The economic burden of COPD is very high, driven by the costs of hospitalisation for acute exacerbations and the cost of long-term drug therapy [140]. The etiology of COPD is due to complex interactions between environmental factors and genetic background. The most significant environmental risk factor for COPD is long-term cigarette smoking. Cigarette smoke contains thousands of chemicals being antigenic, carcinogenic, cytotoxic and mutagenic inducing pathological changes in the respiratory tract. The gaseous phase contains short-lived volatile substances affecting the upper airways. The particulate or tar phase enters the lower respiratory tract and affects cells in the small airways and alveoli [141].

COPD diagnosis also represents an important independent risk factor for lung cancer development, especially for squamous-cell carcinoma (SCC) and SCLC histological subtypes: a history of COPD highly increases lung cancer risk and higher prevalence of lung cancer is observed in COPD patients compared to general population [142,143]. A recent study found 19 newly diagnosed cases of lung cancer in a population of 224 patients with stable COPD, over a median follow-up period of 4.58 years, representing an incidence of 1.85%/year [144].

The progressive chronic airflow limitation characterizing COPD is due to two major pathological processes: the remodelling and narrowing of small airways, and the destruction of the lung parenchyma with consequent loss of the alveolar attachments, resulting in pulmonary emphysema (**Figure 18**). These anatomical changes determine higher resistance to flow and closure of small airways at higher lung volumes during expiration, with consequent air trapping in the lung, leading to the characteristic hyperinflation of the lungs, associated to dyspnea and decrease exercise tolerance [145].

The following paragraphs will focus on the evidences collectively indicating the role of RBPs in the pathogenic mechanisms of COPD, in order to highlight their potential role as disease determinant/biomarker and therefore for prospective therapeutic targeting.

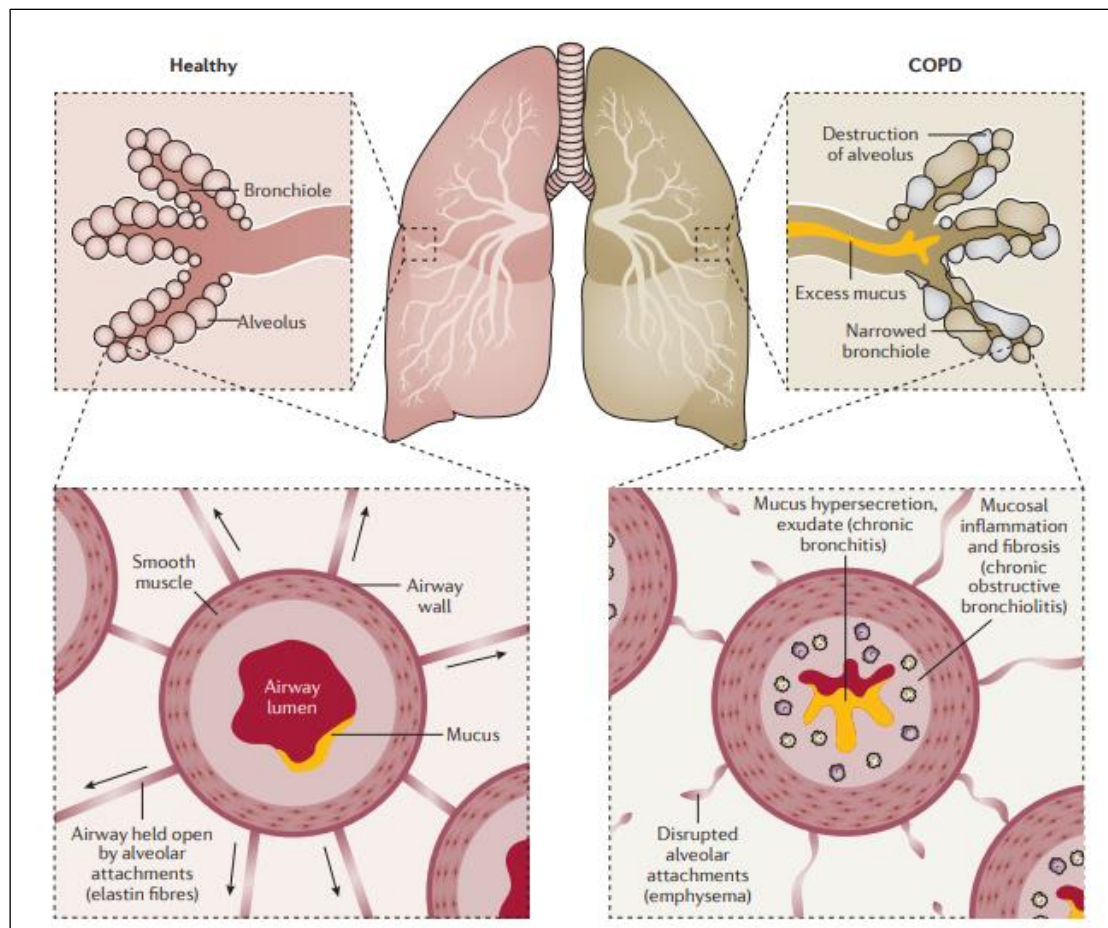


Figure 18. Airway obstruction in COPD. In healthy lungs, the small airways (bronchioles) are held open by alveolar wall attachments that contain elastin fibres. In COPD, the small airways are narrowed through thickening of the bronchiolar periphery wall by inflammation and fixed narrowing as a result of fibrosis, disruption of alveolar attachments as a result of emphysema and luminal occlusion by mucus and inflammatory exudate [146].

2.3. Main pathogenetic mechanisms in COPD: potential involvement of RBPs

2.3.1. Genetics and Epigenetics

The existence of a genetic predisposition for COPD has been pointed out by many genome-wide association studies (GWAS). Genetic-mapping studies have identified several SNPs in candidate genes associated with the disease.

Early genetic studies of familial linkage in COPD identified that mutations in the SERPINA1 gene, encoding for alpha-1 antitrypsin (AAT), resulted in severe AAT deficiency and accounted for ~1% of cases [147].

GWAS have been performed to identify associations between chromosomal regions and disease phenotypes in order to predict disease risk or susceptibility.

GWAS of lung function levels in general population cohorts have identified lung function genomic loci, including Hedgehog-interacting protein (HHIP) and family with sequence similarity 13 member A (FAM13A), associated with COPD susceptibility [148,149]. Moreover, another large GWAS and meta-analysis showed the association with moderate-to-severe or severe COPD susceptibility also for nicotinic acetylcholine receptor subunits alpha (CHRNA)-3/5, Ras and Rab interactor (RIN)-3, MMP3/MMP12 and TGF- β 2 loci [150]. The locus containing the genes for CHRNA3 and CHRNA5 was also described as a risk locus for the development of lung cancer in COPD patients [151,152]. In addition the rs1422795 SNP on the 5q33 locus, containing ADAM19 gene, confers susceptibility to both COPD and lung cancer [153].

Whole-exome sequencing has indicated a non-synonymous SNP in coiled-coil domain containing 38 (CCDC38) gene, which is implicated in ciliary function, in heavy smokers who do not develop COPD [154]. Since ciliary function abnormalities are known to be associated with both smoking and reduced mucociliary clearance in patients with COPD, it is possible that genetic factors can influence cilia function in bronchial epithelium and the extent of smoke damage.

Lamontagne and his group mapped COPD candidate causal genes by integrating GWAS and lung expression quantitative trait loci (eQTL) data [155]. They identified 12 novel candidate loci, including MROH1 on 8q24.3, SYCE1 on 10q26.3, ZDHHC21 on 9p22.3, CAMK2A on 5q32, DMPK on 19q13.32, PRR16 on 5q23.1, MYO15A on 17p11.2, TNFRSF10A on 8p21.3, BCO1 on 16q23.2 and HOXC6 on 12q13.13, BTN3A2 on 6p22.2 and TRBV30 on 7q34.

In addition to genetic alterations, epigenetic changes have also been reported to play an important role in the development of COPD. Epigenetic modifications influence gene expression without changes to the nucleotide sequence and they include DNA methylation, covalent histone modifications (histone acetylation, methylation, phosphorylation, ubiquitination and sulfonation), nucleosome remodelling.

DNA methylation is a dynamic process that controls gene silencing and nuclear architecture. De novo addition of a methyl residue to the 5' position of cytosine is controlled by DNA methyltransferase (DNMT)-1, while the methylation status is controlled by DNMT3a and DNMT3b [156]. DNA methylation varies between cell types and is associated with altered gene expression. Although CpG-rich regions (CpG islands) within the promoter region can regulate gene expression, the majority of the >16,000 differentially methylated regions (DMRs) in different cells/tissues are associated with alternative transcriptional start [157]. The first genome-wide epigenetic study of COPD patients identified 349 CpG sites that were significantly associated with the disease [158]. In the same study, they identified that DNA methylation was most likely attributed to hypomethylation of immune-modulatory genes, such as SERPINA1, leading to gene overexpression.

A genome-wide DNA methylation analysis identified suggestive genes with DNA methylation changes in COPD lung parenchymal tissues. In particular, the top differentially methylated CpG sites significantly hyper-methylated in COPD group compared with non-smokers included ANGPT1, PLD1, NFASC, ACTN4, RGS12, CAV1, PRKAG2, JARID2, HIPK2, and MECOM [159]. A genome-wide methylation landscape of DMRs associated with smoking revealed that smoking-related hyper-DMR genes and hypo-DMR genes were involved in synapse-related pathways and in immunosuppression. Moreover, correlation analysis of DMRs with their corresponding gene expression showed that genes affected by tobacco smoking were mostly related to immune system diseases [160].

The dynamic coiling of DNA around histones is controlled by the covalent and reversible addition of functional groups, mainly acetyl and methyl groups.

Acetylation of histones, determined by histone acetyl transferase proteins (HAT), promotes the access of transcription machinery to the promoter region, resulting in enhanced gene expression. Conversely, removing acetyl groups, mediated by histone deacetylases (HDACs), results in gene silencing [161]. Alterations to the activity of these enzymes can have a strong impact on gene expression.

The imbalance of histone acetylation and deacetylation alters the transcription of inflammatory genes, leading to changes of gene expression profile in smokers susceptible to COPD [162]. In peripheral lung, airway biopsies and alveolar macrophages of COPD patients there is an increase in the acetylation of histones associated with the promoter region of inflammatory genes, such as IL-8, that are regulated by nuclear factor kappa B (NF- κ B), and the degree of acetylation increases with disease severity [163].

HDAC2 is strongly susceptible to oxidants and free radicals action. Reduced expression levels and activity of HDAC2 were detected in the lungs of COPD patients [164,165]. Sirtuin (SIRT)-1 is another histone and protein deacetylase that specifically deacetylates histones H3 and H4 and non-histone proteins including transcription factors, co-activators and other signalling molecules [166]. SIRT1 expression has been demonstrated reduced in the lungs of smokers and patients with COPD [167].

Oxidative stress. Reactive oxygen species (ROS), including superoxide anion ($O_2^{\bullet-}$) and the hydroxyl radical ($\bullet OH$), are highly unstable species given the presence of unpaired electrons. They originate from both intracellular metabolism and exogenous sources. Exposure to elevated levels of ROS can overwhelm the antioxidant cell defences and cause severe damage to nucleic acids, proteins and lipids, leading to pathological processes, including neurodegenerative disorders, atherosclerosis, diabetes, and lung inflammatory diseases [168] (**Figure 19**). Moreover, ROS are also able to inhibit

mechanisms of DNA repair. As consequence, mutations that cause increased expression and function of oncogenes, and mutations that cause decreased expression and function of tumor suppressor genes ultimately leads to cancer [169].

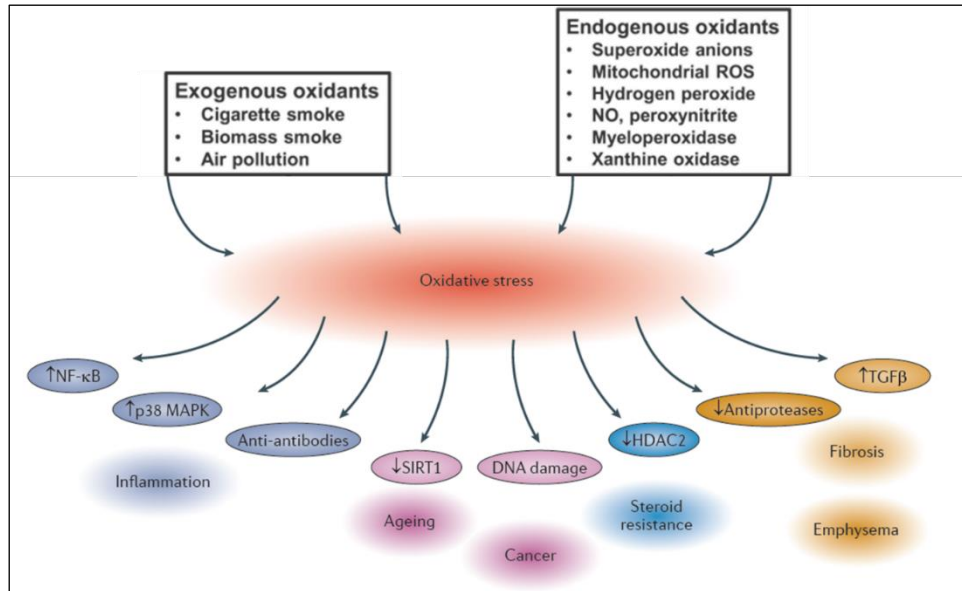


Figure 19. Increased oxidative stress and its consequences. Increased oxidative stress may be from exogenous oxidants and endogenous oxidants. Oxidative stress induces the activation of several mechanisms, including the proinflammatory transcription factor nuclear factor-KB (NF-kB), p38 mitogen-activate protein kinase (MAPK), generation of autoantibodies to carbonylated proteins, reduced expression of sirtuin (SIRT)-1, DNA damage, reduced histone deacetylase (HDAC)-2 expression, reduced activity of antiproteases and increased release of transforming growth factor (TGF)- β . Modified from [170,171].

Superoxide anions are produced mainly by NADPH oxidases (NOX) and are rapidly converted to more damaging ROS species, including the hydroxyl radical and hydrogen peroxide or peroxynitrite [172]. ROS generation may also result in the formation of reactive carbonyls, that lead to protein carbonylation, resulting in the so-called “carbonyl stress”. Moreover, hypochlorous acid produced by neutrophil-derived myeloperoxidase (MPO) lead to the formation of 3-chlorotyrosine.

The gene expression patterns activated upon oxidative stress and other damaging stimuli are finely regulated by post-transcriptional events. Several mRNAs regulated by ROS are targets of RBPs that positively or negatively alter their half-life and translational status (**Figure 20**).

Relevant to our study, AUF-1 associates with many mRNA regulated by oxidative stress. In particular, in response to treatment that triggers oxidative stress, including prostaglandin A2, UVC irradiation or LPS, AUF-1 lower the mRNA stability of cyclin D1, TNF- α , IL-1 β and COX-2 [168]. Many other ROS-regulated mRNAs are also modulated by TTP. In condition of oxidative stress triggered by high-glucose diets, animals showed elevated TTP levels in liver and skeletal muscle,

along with a reduction in TNF- α levels [173]. In addition, treatment with H₂O₂ has been shown to promote HuR translocation to the cytoplasm where it enhances HuR binding to p21^{WAP/CIP1} and MAPK phosphatase (MKP)-1 mRNAs, leading to their accumulation, while it reduces HuR interaction with the transcripts of SIRT1, cyclin A2 and cyclin B1 [168].

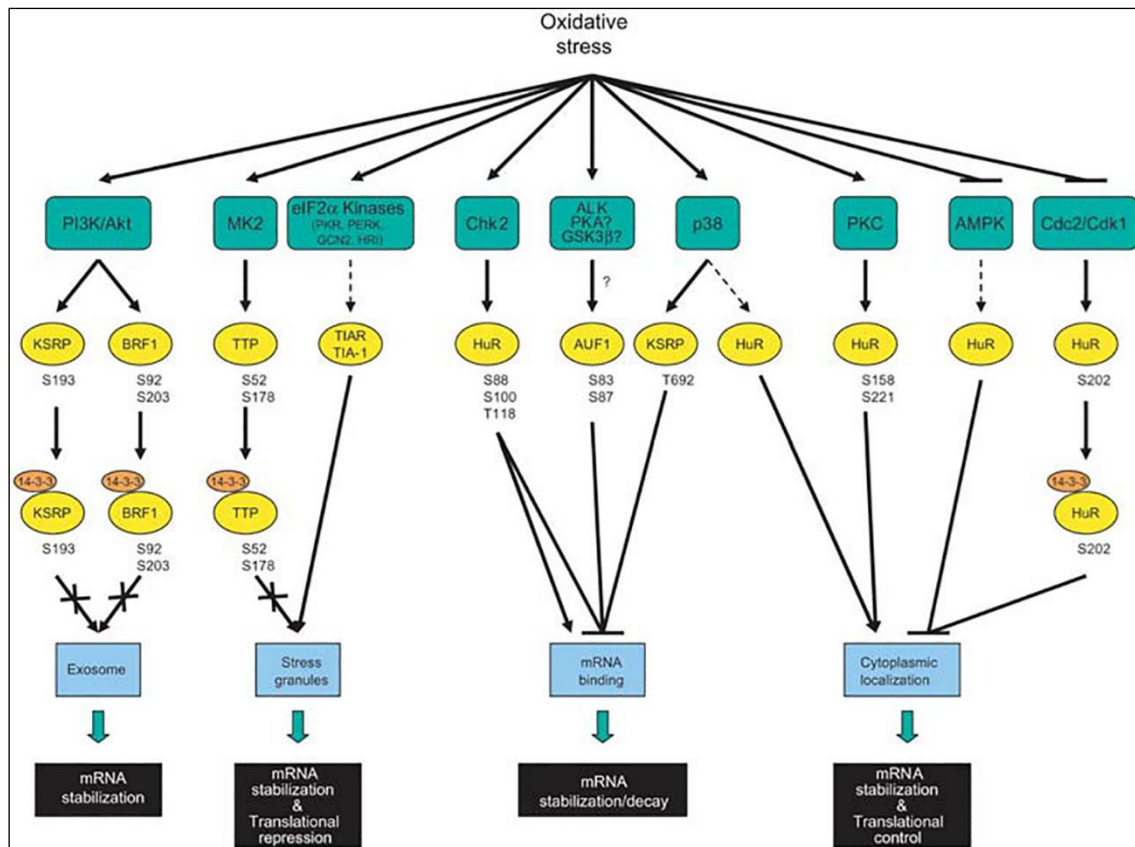


Figure 20. Post-transcriptional gene regulation by RBPs during oxidative stress. Green boxes: effector kinases in signaling cascades activated or repressed by oxidative stress. Yellow ovals: RBPs that are downstream of the effector kinases, either as direct phosphorylation substrates (solid arrow) or as indirect effectors (discontinuous arrow). ‘Phosphorylated residues (threonines and serines) are indicated below the oval and phosphorylation linked to association with 14–3–3 (orange) is shown. Blue squares: changes in subcellular localization, association with cellular compartments (SGs, exosome) or binding to target mRNAs following modification of RBPs by the signaling cascades. Black boxes: consequences of RBP modifications upon the expression and translation of the mRNA [168].

The respiratory system is an anatomical district constantly exposed to environmental oxidants.. In fact, oxidative stress plays a key role in the pathogenesis of COPD [174].

Increased oxidative stress has been demonstrated in lungs of COPD patients by measuring various markers of oxidative stress in the breath. Ethane, a volatile product of lipid peroxidation, is increased in exhaled breath of COPD patients and this is correlated with disease severity [175]. Chronic inhalation of cigarette smoke represents the most important source of exogenous oxidants. In addition,

several inflammatory and structural cells are source of endogenous oxidants in the lower airways of COPD patients, even in former smokers. Macrophages from COPD patients are activated and release multiple ROS as superoxide anions and hydrogen peroxide [176,177]. Moreover, carbonyl-modified proteins promote the generation of circulating autoantibodies responsible of lung injury and inflammation in severe COPD patients [178].

Significant increase of 8-hydroxy-2-deoxyguanosine (8-OH-dG), a marker of oxidant-induced DNA damage, was detected in peripheral lung of smokers with and without COPD [179]. The same research group demonstrated a selective decrease of Ku86 in the bronchiolar epithelium of patients with COPD and in a smoke-exposed mouse model susceptible to lung cancer. Ku86, together with Ku70, is part of DNA-binding regulatory subunits of the DNA-dependent protein kinase (DNA PK), initiating the repair of DNA double-strand breaks [180]. They also showed that oxidative stress, reproduced in primary human bronchial epithelial cells upon stimulation with hydrogen peroxide, is able to reduce Ku86 protein as observed in COPD patients, suggesting a contribution of DNA damage/repair imbalance to increased risk of lung carcinoma in COPD [179].

Many of the intracellular signalling pathways characterizing COPD pathogenesis are sensitive to oxidative stress. For example, NF- κ B is activated by oxidative stress and its expression is increased in airway epithelial cells and macrophages of COPD patients. Oxidative stress also activates TGF- β signalling pathways, involved in small airway fibrosis and increases the expression of MMP-9, a key enzyme involved in emphysema [176].

Direct contribution of PTGR in this context is however lacking despite to experimental evidences.

2.3.2. Accelerated aging

Aging has been defined as “the progressive decline of homoeostasis that occurs after the reproductive phase of life is complete, resulting in increased risk of disease or death” [181]. The limited number of divisions of a cell is determined by the exhaustion of programmed proliferative capacity, defined as intrinsic senescence. The exposure to oxidants is able to induce DNA damage that may result in cell cycle arrest, leading to the so-called stress-related senescence [182]. These senescent cells are metabolically active and acquire a senescence-associated secretory phenotype (SASP) characterized by the activation of pro-inflammatory pathways resulting in the secretion and release of several pro-inflammatory mediators such as cytokines, chemokines, proteins, growth factors, prostanoids and proteases, that altogether may affect other cells (**Figure 21**).

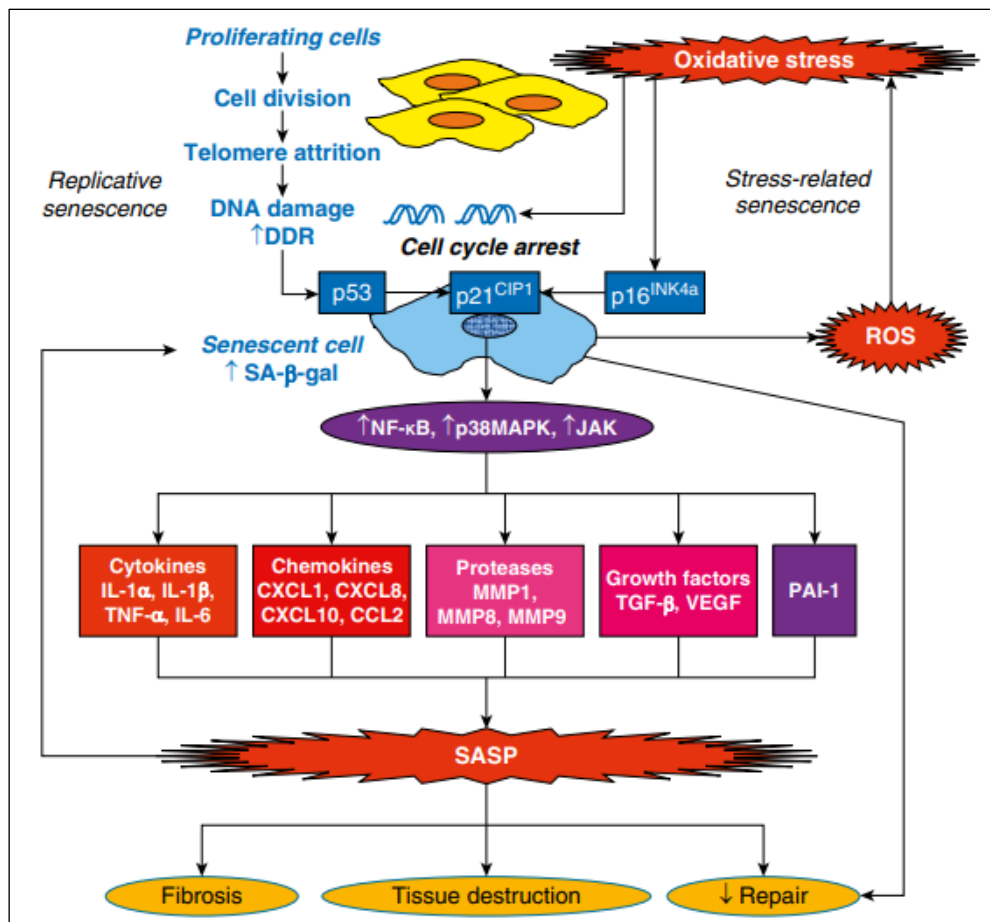


Figure 21. Main mechanisms and molecular mediators of cellular senescence. Cell division leads to progressive shortening of telomeres, and activates DNA damage response (DDR), which in turns activates p53 (replicative senescence). Cellular stresses, such as oxidative stress, may also cause DNA damage and activate p16^{INK4a} and the cyclin kinase inhibitor p21^{CIP1} (stress-related senescence), which induces cell cycle arrest. Senescent cells show activation of nuclear factor kappa B (NF-κB), p38 mitogen-activate protein kinase (MAPK) and Janus-activated kinase (JAK), resulting in the secretion of multiple inflammatory mediators known as the senescence-associated secretory phenotype (SASP), leading to including fibrosis and tissue destruction [183].

The SASP response is activated by p21^{CIP1}, which results in activation of MAPK and Janus-activated kinases (JAK), leading to the consequent activation of NF-κB and the secretion of proinflammatory cytokines, chemokines growth factors and other mediators, all increased in COPD. Moreover, senescent cells release ROS, which further drive the senescence process. Altogether, these events induce structural changes, including fibrosis and tissue destruction [183,184].

The SASP is also fundamental in the context of tumor biology, acting as both pro-tumorigenic and tumor-suppressive factors, and it may represent a pathogenic link between COPD and lung cancer (**Figure 22**). For example, the release of SASP-associated proteases induces the remodelling of extracellular matrix and tissue structure, promoting tumor cell invasion and metastasis [185]. Senescent fibroblasts acquiring SASP are able to induce EMT in adjacent cancerous epithelial cells

[186]. As counterpart, SASP can recruit immune cells, including CD4⁺ T cells, macrophages and natural killer (NK) cells, that suppress tumorigenesis [185].

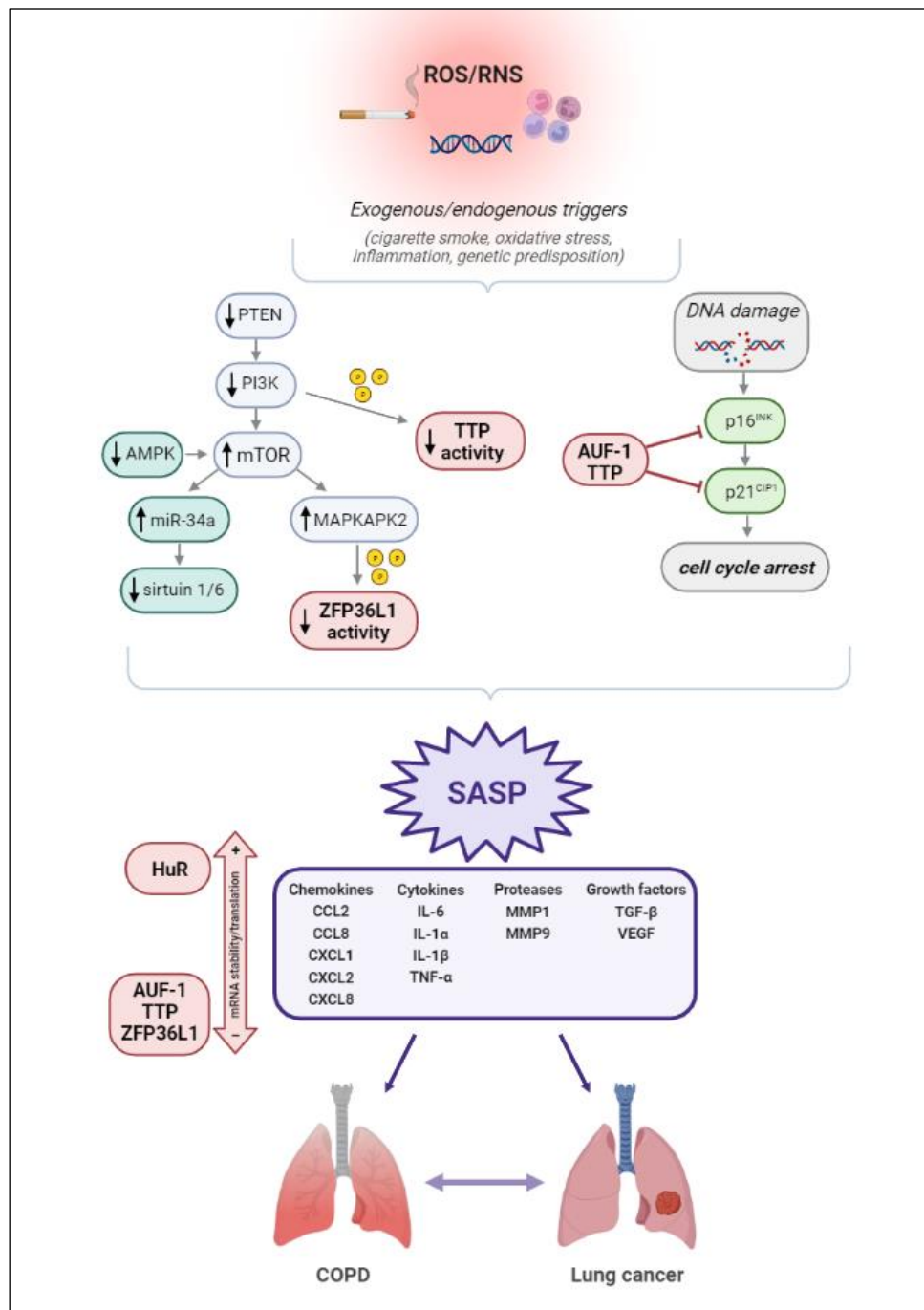


Figure 22. Involvement of RBPs in SASP linking COPD and lung cancer. Exogenous (cigarette smoke) and endogenous [reactive oxygen species (ROS)/ reactive nitrogen species (RNS), inflammation, genetic predisposition] factors trigger changes in cellular phenotypes regulated by transcriptional and post-transcriptional events, coordinated by stress-induced signalling pathways. Exemplary of post-transcriptional events, mechanistic target of rapamycin (mTOR) activation via phosphatidylinositol 3-kinase (PI3K) signalling leads to the inhibition of sirtuin-1 and sirtuin-6 through microRNA (miR)-34a upregulation, along with the downregulation of mRNA degrading activity of the RNA binding

protein (RBP) zinc finger protein 36-like 1 (ZFP36L1) via MAPKAPK2-mediated phosphorylation. PI3K signalling also acts as inhibitor of the RBP tristetraprolin (TTP). DNA damage induced by stress conditions results in cell cycle arrest as a consequence of the activation of cyclin-dependent kinase inhibitors p16^{INK} and p21^{CIP1}, negatively regulated by the RBPs AU-rich element binding factor 1 (AUF-1) and TTP. Upon these conditions, targeted cells acquire senescence-associated secretory phenotype (SASP) resulting in the secretion of multiple inflammatory cytokines, chemokines, proteins, growth factors vastly regulated by RBPs (short-listed in the figure), though complex changes in mRNA stability and translation. Among the RBPs characterized in these processes, human antigen R (HuR) has been reported to act globally as a positive regulator while AUF-1, TTP and ZFP36L1 generally decrease mRNA stability. AUF-1 has also regulatory roles in transcription. Dysregulation of SASP factors leads to the development of COPD and lung cancer [187].

The hallmarks of aging include telomere shortening, genomic instability, epigenetic alterations, loss of proteostasis, mitochondrial dysfunction, deregulated nutrient-sensing and stem cell exhaustion. All these features have been identified in the cells of COPD patients [182,188]. Telomere shortening was observed in circulating leukocytes derived from patients with COPD [189,190] and DNA damage associate to telomere was described in small airway epithelial cells of COPD patients [191]. Moreover, ROS reduce the expression and activity of SIRT1, that has protective effects against cellular senescence and aging, and it is reduced in the lungs of patients with COPD [192].

Aging cells accumulate damaged and misfolded proteins and the exposure to cigarette smoke may further lead to additional cellular leading to senescence. In bronchial and alveolar epithelial cell of COPD, autophagy can be both excessive or defective, resulting in cell death [182]. In addition, aging is also linked to alteration in mitochondrial metabolism, mainly resulting in abnormal ROS production [193].

The absence of TERT in mouse models results in replicative senescence of alveolar cells and low-grade lung inflammation [194]. TERT is regulated by the RBP AUF-1, as discussed in previous paragraphs [14]. The phosphoinositide-3-kinase (PI3K) - mechanistic target of rapamycin (mTOR) pathway is critical for cellular senescence and aging [195,196]. Both mTOR complex (mTORC)-1 and mTORC2, composing mTOR complex, are activated in lung cells from patients with COPD. Moreover, lung cell senescence has been demonstrated strongly associated with mTOR activity, since its inhibition improved replicative capacity and inhibited the SASP [197]. The signalling coordinated by mTOR was one of the pathways significantly affected by the changes in RBPs expression observed in COPD though an *in silico* analysis [198].

In particular, SASP factors are regulated by mTOR pathway in RBPs-dependent manner. Indeed, inhibition of mTOR inhibits SASP by specifically downregulating MAPKAPK2 (also known as MK2) translation. MAPKAPK2 specifically phosphorylates at Ser 54, Ser 92 and Ser 203 the RBP ZFP36L1, member of TTP zinc finger RBP family, inhibiting its binding to target mRNAs. Among the anti-inflammaging effects mediated by mTOR inhibition, downregulation of MAPKAPK2

decreases ZFP36L1 phosphorylation, a modification that blocks ZFP36L1 ability to degrade targeted SASP transcripts including IL-8, IL-1 β , MMP-3, MMP-10 and the cell cycle inhibitor CDKN1A mRNA [199]. In addition, PI3K signalling act as important functional inhibitor of the mRNA destabilizing activity of TTP, and a significant part of downstream targets of PI3K signalling is regulated at the level of mRNA stability [130,200].

2.3.3. Chronic inflammation

COPD is associated with a characteristic pattern of chronic inflammation that predominantly affects peripheral airways and lung parenchyma. The inflammatory network that characterizes COPD involves several immune cells such as neutrophils, alveolar macrophages, CD8⁺ T cytotoxic and CD4⁺ T lymphocytes, but also structural cells, including airway and alveolar epithelial cells, endothelial cells, and fibroblasts (**Figure 23**). Cigarette smoke and other irritants are able to activate surface macrophages and airway epithelial cells to release multiple chemotactic mediators, particularly chemokines, which attract circulating neutrophils, monocytes, and lymphocytes into the lungs [201]. In addition, the increase of innate lymphoid cells (ILCs) suggests that these cells contribute to induce and maintain pro-inflammatory status even after smoking cessation [202].

Once activated, epithelial cells and macrophages produce increased levels of pro-inflammatory mediators such as cytokines and chemokines, including IL-6, IL-8, IL-1 β , TNF- α , CCL-2 and others. Cigarette smoke also impairs mucus production from goblet cells and secretion of antioxidants, antiproteases and defensins, that are fundamental for defence of airways mediated by epithelial cells [203]. Alveolar macrophages also secrete elastolytic enzymes, including MMP-2, MMP-9, and MMP-12, cathepsins K, L, and S, but also CXCL9, CXCL10 and CXCL11 [204].

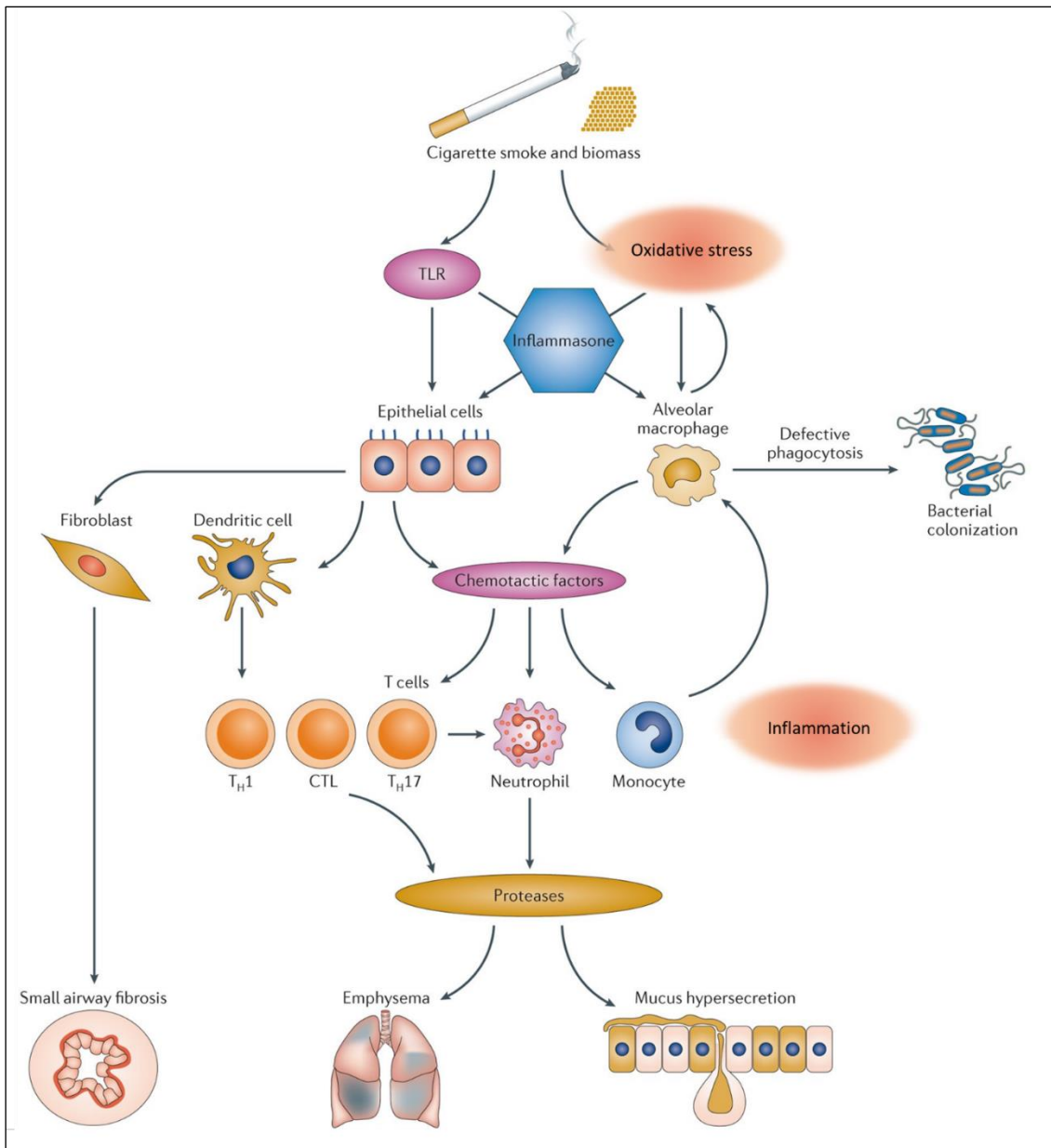


Figure 23. Inflammation in COPD. Cigarette smoke and other irritants activate macrophages and epithelial cells in the respiratory tract via the activation of toll-like receptors (TLRs) and oxidative stress to release multiple chemotactic factors, particularly chemokines. These chemotactic factors attract both innate and adaptive immune cells, leading to the release of multiple inflammatory mediators. Several cells, including epithelial cells, macrophages and neutrophils, also release proteases and fibrogenic mediators, which then break down connective tissue in the lung parenchyma, leading to emphysema, stimulate mucus hypersecretion, leading to chronic bronchitis, and activate fibroblasts, leading to small airway fibrosis [170].

Macrophage numbers are markedly increased in the airways, lung parenchyma, bronchoalveolar lavage (BAL) fluid and sputum of patients with COPD, and they secrete more inflammatory proteins compared to macrophages from normal smokers [201]. The release of these chemotactic factors lead to adhesion of neutrophils to endothelial cells and their following migration into the respiratory tract.

Neutrophils recruitment determines alveolar destruction through the secretion of serine proteases, including neutrophil elastase, cathepsin G, proteinase 3, as well as MMP8 and MMP9 [201,205]. Moreover, the number of CD4⁺ and CD8⁺ T lymphocytes dramatically increases in the lung parenchyma but also in the peripheral and central airways of patients with COPD [206], and they show increased expression of CXC receptor (CXCR)-3 [207]. Moreover, CD4⁺ Th17 cells secreting IL-17A and IL-22 are also increased in the airways of patients with COPD [208].

This chronically expressed inflammatory secretome alters the local microenvironment leading to structural cell activation and reinforcing a skewed Th1/Th17-driven inflammation. The end damage of such tissue dysfunction manifests as fibrosis, parenchymal loss and may lead to malignant transformation [183,188,209],

The regulation of the inflammatory mediators released by activated immune and structural cells, and involved in COPD pathogenesis are under the control of the proinflammatory transcription factor NF- κ B, which is activated in macrophages of COPD patients and upregulated in epithelium of smokers and COPD patients [210,211]. TNF- α is a potent activator of NF- κ B, and it may contribute to amplify the inflammatory response. Indeed, an increased concentration of TNF- α has been detected in induced sputum in patients with stable COPD, with a further increase during exacerbations. Moreover, TNF- α production from peripheral blood monocytes is also increased in patients with COPD and has been implicated in the cachexia and skeletal muscle apoptosis found in some patients with severe disease [201]. The pleiotropic cytokine IL-6 is also expressed in airway epithelium and is found increased in the sputum, exhaled breath, BAL fluid of patients with COPD, in particular following exacerbations, as well as in plasma, as important biomarkers of systemic inflammation [212-214].

The chemokine CCL2, a potent chemoattractant of monocyte, T-cells and mast cells, is overexpressed in airway epithelial cells, in the sputum and in the BAL fluid of patients with COPD [215-217]. IL-8 and other chemokines, including CXCL1 and CXCL5, are overexpressed in COPD patients [201].

The inflammatory process is finely regulated by dynamic and coordinated gene expression programmes, in which RBPs have a central role. RBPs are recognized mediators of post-transcriptional regulation of genes coding for inflammatory mediators, including the transcripts of IL-6, IL-8, IL-1 β , TNF- α , IFN- γ , TGF- β , VEGF, CXCL1, CXCL5, CXCL8, CCL2, CCL1 (**Table 9, Figure 21**), taking a key role in sustaining the accelerated, stress-induced premature cell senescence (SIPS) also defined as inflammaging [168,181,184]. In particular, both preclinical *in vitro* and *in vivo* studies showed that they are targeted by the RBPs HuR, TTP, and AUF-1 [218,219].

Table 9. SASP factors transcripts regulated by RBPs.

SASP factors	RBPs	Effect on mRNA	References
p21 ^{WAP/CIP1}	HuR	stabilization	[72]
	TTP	destabilization	[220,221]
	AUF-1		[72,96]
p16 ^{INK}	HuR	stabilization	[222,223]
	AUF-1	destabilization	[96,224]
IL-6	HuR	stabilization	[225-227]
	TTP	destabilization	[228-230]
	AUF-1		[88]
TNF- α	HuR	stabilization	[225,231]
	TTP	destabilization	[228,232]
	AUF-1		[15,233]
IL-1 α	HuR	stabilization	[234]
	TTP	destabilization	[235]
IL-1 β	TTP	destabilization	[235,236]
	AUF-1		[15,233]
CCL2	HuR	stabilization	[237]
	TTP	destabilization	[238]
	AUF-1		[233]
CCL8	HuR	stabilization	[237]
	TTP	destabilization	[239]
CXCL1	HuR	stabilization	[237]
	TTP	destabilization	[240,241]
CXCL2	HuR	stabilization	[237]
	TTP	destabilization	[240-242]
CXCL8	HuR	stabilization	[243,244]
	TTP	destabilization	[245,246]
MMP1	HuR	destabilization	[247,248]
MMP9	HuR	stabilization	[121]
	TTP	destabilization	[249]
	AUF-1		[250]
TGF- β	HuR	stabilization	[251]
VEGF	TTP	destabilization	[245,252]
	AUF-1		[253]
PAI	HuR	stabilization	[254]
	TTP	destabilization	[255]

Abbreviations: AUF-1: AU-rich element binding factor 1; CCL: C-C motif ligand; CXCL: C-X-C motif ligand; HuR: human antigen R; IL: interleukin; MMP: matrix metalloproteinase; PAI: plasminogen activator inhibitor; RBP: RNA

binding protein; SASP: Senescence-associated secretory phenotype; TGF: transforming growth factor; TNF: tumor necrosis factor; TTP: tristetraprolin; VEGF: vascular endothelial growth factor A.

2.3.4. Spreading inflammation and aging phenotype through extracellular vesicles: role in COPD

The growing knowledge on how lung microenvironment shapes homeostatic and pathological tissue responses is increasingly uncovering the role of EVs as mediators of intercellular communication and regulator of many fundamental biological processes, including inflammation and neoplastic transformation [256]. EVs are a group of membraned vesicles characterized by different size and origin. Microvesicles are the larger size class of EVs with a diameter of 50-500 nm and they are generated by budding of the plasma membrane. Exosomes are smaller EVs of 50-150 nm size originated in the lumen of multivesicular endosomes (MVEs) as intraluminal vesicles (ILVs) and secreted during the fusion of MVEs with the cell surface. Mechanisms of exosome biogenesis involve subunits of the endosomal sorting complex required for transport (ESCRT): ESCRT-III is required for the scission of the ILVs into the MVE lumen, while cargo clustering and membrane budding can occur by either ESCRT-dependent or ESCRT-independent mechanisms [257] (**Figure 24, Table 10**).

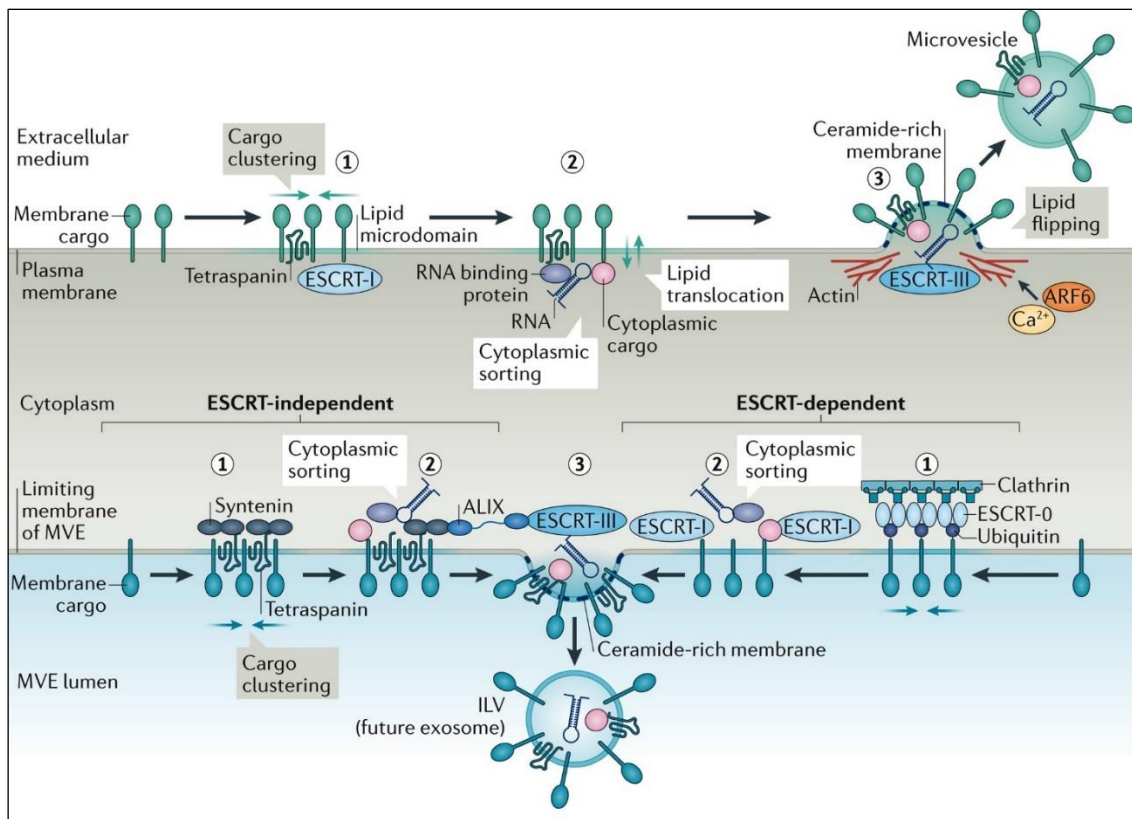


Figure 24. Mechanisms of biogenesis of EVs. Lipids and membrane-associated proteins are clustered in microdomains of the plasma membrane for microvesicles (top) and of the limiting membrane of the multivesicular endosome (MVE) for exosomes (bottom) (**step 1**). Soluble components, such as cytosolic proteins and RNA species, are recruited to be sorted in extracellular vesicles (EVs) (**step 2**). The clustered microdomains, together with additional machineries, promote membrane budding followed by a fission process either at the plasma membrane towards the extracellular medium or at the limiting membrane of the MVE towards the lumen of the MVE (**step 3**) [257].

Table 10. Characteristics of main extracellular vesicles [258].

Feature	Exosome	Apoptotic body	MV
Size	Homologous 30–100 nm	Heterogeneous 1–5 μ m	Heterogeneous 100–1000 nm
Markers	Membrane impermeable (PI negative) CD63, TSG101, Alix, flotillin	Membrane permeable (PI positive) Annexin V, DNA, histones	Membrane impermeable (PI negative) integrin, selectin, flotillin-2
Density	1.13–1.19 g/mL	1.16–1.28 g/mL	1.25–1.30 g/mL
Contents	Protein, lipid, different RNA species, and DNA	Cytosolic content (protein, RNAs, fragmented DNA) and cellular organelles	Protein, lipid, different RNA species, and DNA
Determinant of controlled contents	The cellular origin and physiological state of the cell	The cellular origin and stimuli	No direct correlation
Lipids	A major sorting of lipidic molecules from the parental cells (include BMP)	Characterized by phosphatidylserine externalization	The lipid contents are primarily derived from plasma membrane, and resemble the parental cells (without BMP)
Origin	Multivesicular bodies fusion with plasmatic membrane	Cellular debris, plasma membrane blebbing during cell apoptosis	Direct outward budding or blebbing from the plasma membrane
Mechanism of release	Constitutive or inducible, depending on the cell type of origin	Rho-associated kinase I and myosin ATPase activity	Relocation of phospholipids to the outer membrane, cytoskeleton rearrangements, generation of membrane curvature, and vesicle release
Detection methods	Electron microscopy, Western blot for exosome enriched markers	Flow cytometry, electron microscopy	Flow cytometry, electron microscopy
Isolation methods	Ultracentrifugation (100,000–200,000 \times g) filtration, density gradient Immunoprecipitation, Immune affinity capture and ExoQuick precipitation methods	Ultracentrifugation (10,000–20,000 \times g)	No standardized methods
Size determination and quantification	Dynamic light scattering Nanoparticle tracking analysis Surface plasmon resonance		

EVs derived from epithelial cell are considered to be major players in the EV-mediated communication in the lungs. Indeed, the enrichment of surface mucins suggests that EVs may have a role in homeostasis and immune defence, by allowing the interaction of EVs with inhaled materials or host cells [259,260].

Cellular stresses, including hypoxia, oxidative stress and irradiation, increase the secretions of EVs and modify their bioactive contents [261]. For example, increased level of ROS promote the sorting of Ephrin type-A receptor 2 (EphA2) into EVs in senescent cells [262]. EphA2 is a receptor tyrosine kinase that, upon activation, regulates migration, proliferation and differentiation of cells [263], thus its selective enrichment in senescent cell-derived EVs may represent a potential mechanism to spread the growth-promoting effect of senescent microenvironment and contribute to cancer progression. Moreover, the increased levels of miR-21 and miR-217 in EVs isolated from an *in vitro* model of endothelial replicative senescence mediates the inhibition of the epigenetic regulators DNMT1 and SIRT1 in recipient endothelial cells, inducing the acquisition of SASP, suggesting the role of EVs in spreading the premature senescence [264]. EVs derived from human bronchial epithelial cells exposed to cigarette smoke extract are enriched of miR-210 and its transfer to lung fibroblasts is able to inhibit ATG7 expression, one of the key regulators of the autophagy process, and induce myofibroblast differentiation, contributing to airway fibrotic remodelling characterizing COPD pathogenesis [265].

Elevated levels of circulating EVs in patients with COPD have been associated with markers of systemic inflammation including C-reactive protein (CRP), soluble tumour necrosis factor receptor-1 (sTNFR1) and IL-6 [266]. In EVs isolated from BAL of stable COPD patients, increased expression of miR-451a and miR-663a was found compared to EV from healthy subjects [267].

Besides the characterization of EVs-associated miRNA, recent evidences indicate that also RBPs can be sorted and carried into EVs released by immune and structural cells [268]. In this context, the release of EVs containing RBPs could be a mechanism for spreading inflammation and accelerated aging to nearby cells, by transferring RNAs critically involved in these biological processes or by acting on transcripts present in the recipient cell (**Figure 25**). For example, Statello et al. showed that a group of RBPs, mostly belonging to HNRNP family, are present in EVs in association with RNA molecules in form of ribonucleoprotein complexes, probably as a mechanism to keep them in a stable form during their shuttling into recipient cells [269].

A specific signature of EVs cargo can be predictive of the physiological or pathological state of the origin cell and indicate how they could alter biological processes in recipient cells. RBPs localized into EVs could be harnessed as new therapeutic strategies (e.g. drug delivery) or biomarkers for disease states, since their cargo reflects the physiology and microenvironment of the cells of origin.

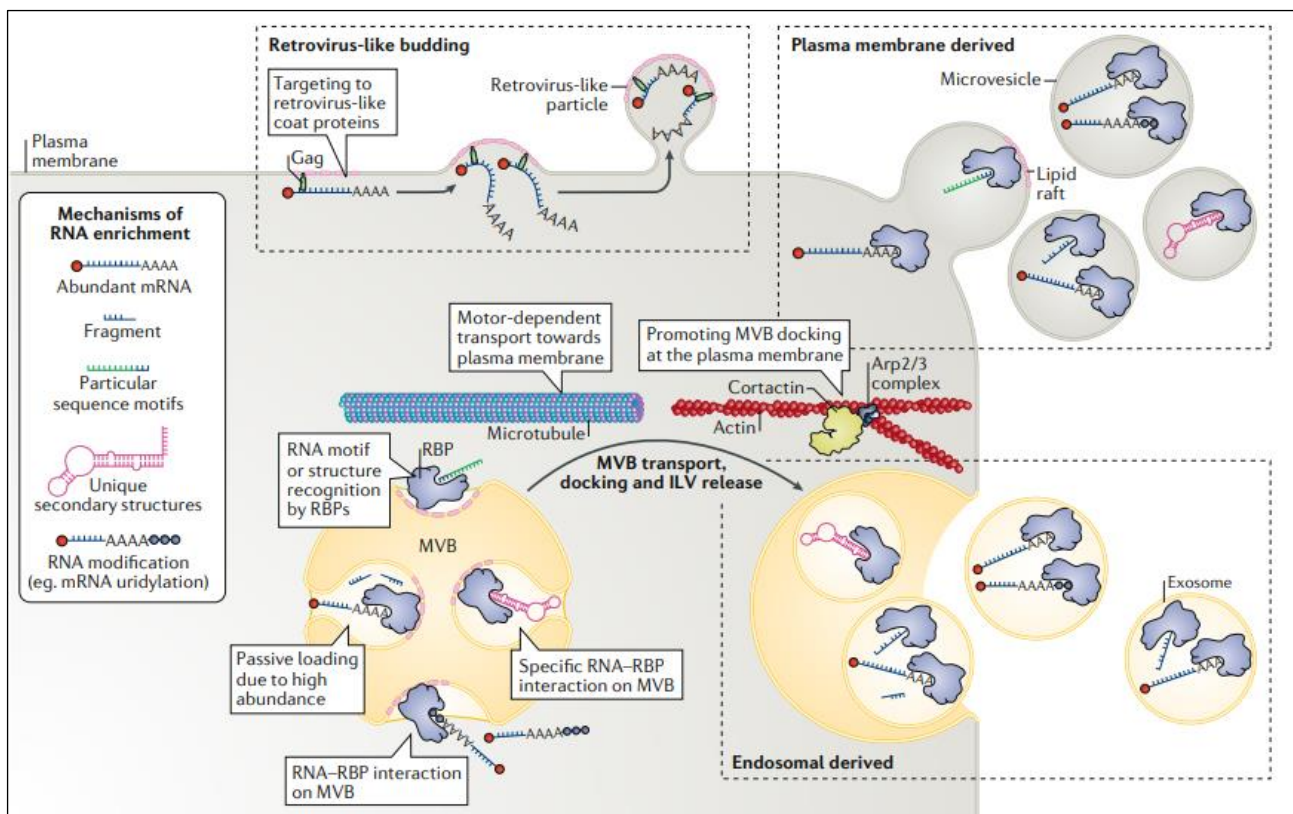


Figure 25. RNA packaging into EVs and their release into the extracellular space. RNAs can be targeted to the plasma membrane and released as microvesicles or as exosomes. Loading of RNA into extracellular vesicles (EVs) can occur via multiple routes: passively due to an abundance of the RNA in the cytosol; by recognition via a number of RNA-binding proteins (RBPs), such as Argonaute, annexin A2, major vault protein (MVP), heterogeneous nuclear ribonucleoproteins A2/B1 (HNRNPA2B1), YBX1, SYNCRIP and lupus La protein, that bind particular sequence motifs in the RNA or that recognize unique secondary RNA structures; and through specific modifications, such as uridylation. Packaging of RNA into EVs can also be promoted by its recognition by retroviral coat proteins such as Gag, which efficiently target RNAs they recognize to the plasma membrane, resulting in virus-like particle release [268].

2.4. Overview of diagnostic approaches and management of COPD patients: unmet needs

The diagnosis of COPD should be suspected in individuals with respiratory symptoms, such as cough, expectoration of sputum, shortness of breath upon exertion or lower respiratory tract infections occurring more frequently or lasting longer than expected (>2 weeks). The suspect should increase if the subjects also report risk factors for COPD, including exposure to cigarette smoke, environmental or occupational pollutants, the presence of a family history [146,270]. Unfortunately, COPD is frequently suspected at the time of a severe respiratory decompensation due to an acute exacerbation or following surgery, as a consequence of underestimation of symptoms. It is also noteworthy that

the diagnosis of COPD has to be considered even in relative young subjects presenting of those symptoms, since the smoking habit has increased in younger individuals [146].

The diagnosis of COPD is confirmed by spirometry, that allow the documentation of expiratory airflow limitation during a forced expiratory manoeuvre from total lung capacity to residual volume. The diagnosis of COPD is confirmed when the ratio of forced expiratory volume in 1 second (FEV_1)/forced vital capacity (FVC) is less than 0.7. Moreover, the spirometry test should be repeated after the administration of inhaled bronchodilators to distinguish the presence of irreversible airflow limitation of COPD from the large reversibility that characterizes airflow obstruction in patients with asthma [270]. The current Global Initiative for Chronic Obstructive Lung Disease (GOLD) scale classifies the severity of airflow obstruction as a percentage of normal FEV_1 as mild (GOLD1; FEV_1 of >80% of predicted normal), moderate (GOLD2; FEV_1 of 79–50% of predicted normal), severe (GOLD3; FEV_1 of 49–30% of predicted normal) and very severe (GOLD4; FEV_1 of <30% of predicted normal) [137].

Chest imaging techniques, including X-ray and high-resolution computer tomography, are important tools for the evaluation of patients suspected of having COPD. In particular, chest X-ray helps eliminate other diagnoses, such as interstitial lung diseases, congestive heart failure and most pulmonary infections, while computer tomography is used to control pulmonary emphysema and bronchial wall thickening [271].

Unfortunately, there are few clinically useful biomarkers that allow to follow disease severity or activity. Several soluble inflammatory mediators have been reported as biomarkers of COPD severity, mortality and hospitalization. Increases serum concentration of adiponectin, CRP, fibrinogen, leukocyte count, IL-6, IL-8, TNF- α and chitinase-3-like protein 1 (YKL-40) have been associated with COPD progression [272,273]. Sputum concentration of neutrophil elastase (NE), serine protease secreted by neutrophils, is elevated in bacterial infections in patients with COPD, while an increased concentration of sputum IL-6, IL-8 and MPO can predict the frequency of exacerbation [274,275] [. However, these biomarkers only marginally improve the prediction when used in addition to clinical variables [276].

Pilot studies using high-throughput technologies, including proteomics and metabolomics, are needed in order to identify novel biomarkers clinically applicable for COPD.

The management of stable COPD patients aims to reduce the exposure to harmful substances, relief of symptoms and reduce the risk of exacerbations (**Figure 26**).

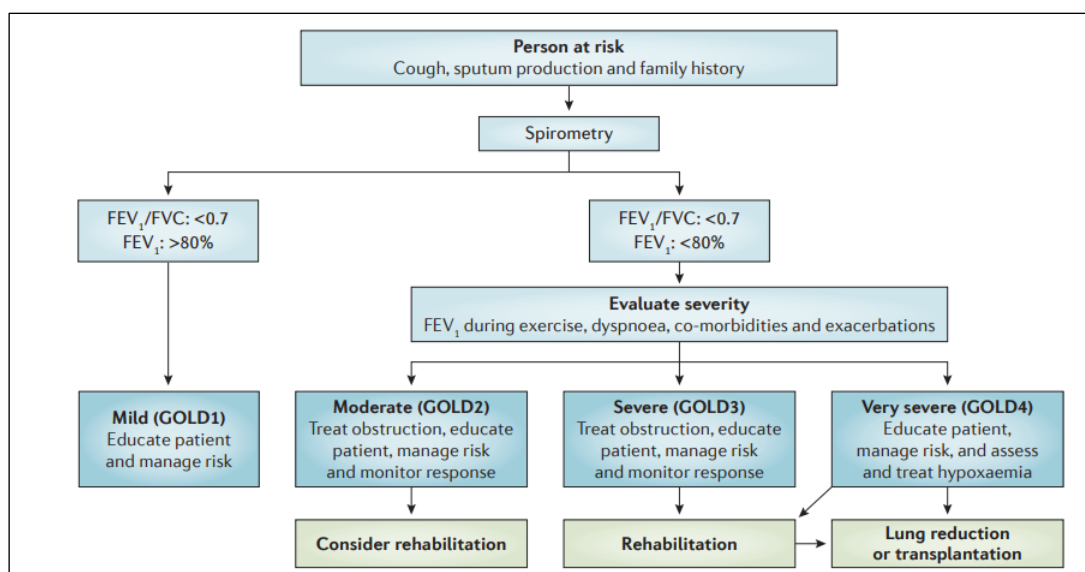


Figure 26. Algorithm for the diagnosis, staging and management programme for COPD. COPD, chronic obstructive pulmonary disease; FEV₁, forced expiratory volume in 1 second; FVC, forced vital capacity; GOLD, Global Initiative for Chronic Obstructive Lung Disease [146].

COPD patients are at higher risk for serious consequences derived from several vaccine-preventable diseases, determining include worsening of symptoms, hospitalizations, and even death. Annual vaccination against seasonal influenza is strongly recommended to all patients with stable COPD. There are some evidences on the efficacy of polyvalent pneumococcal vaccination in preventing exacerbations, pneumonia and mortality in COPD patients [277]. Moreover, the vaccination against the severe acute respiratory syndrome coronavirus 2 (SARS-CoV-2) is mandatory for COPD patients, since they show the worse disease outcomes [278].

The non-pharmacological treatments of pulmonary rehabilitation improves exercise capacity, reduces breathlessness, improves physical activity and psychological status [279,280].

The main pharmacological approach for the management of COPD symptoms is the treatment with bronchodilators. They alter airway smooth muscle tone and induce airways widening, improving expiratory flow. Bronchodilators include β_2 -adrenergic receptor agonists and muscarinic receptor antagonists. Muscarinic antagonists (anticholinergics) block M₃-receptors and, as consequence, reduce cholinergic tone, resulting in reduced airway resistance. They can be classified, according to duration of the effect, in short-acting muscarinic antagonist (SAMA), such as ipratropium bromide, and long-acting muscarinic antagonist (LAMA), such as tiotropium bromide or glycopyrronium bromide. The β_2 -agonists activate β_2 -receptors on airway smooth muscle, which functionally antagonize cholinergic tone and have the same bronchodilator effect as muscarinic antagonists. β_2 -agonists can be short-acting (SABA), such as salbutamol, or long-acting (LABA), such as salmeterol and indacaterol [146,177,270]. Several drug classes reduce the risk of exacerbations, including

inhaled corticosteroids (ICSs), macrolides, phosphodiesterase type 4 (PDE4) inhibitors and mucolytics. In patients with moderate to very severe COPD, ICS combined with LB is more effective compared to the single use in improving lung function, health status and reducing exacerbations [281]. However, ICSs are associated with an increased risk of pneumonia and osteoporosis [282,283]. Current therapies only treat some of the symptoms, and none of them is able to reverse the hallmark features of COPD. The increasing knowledge of mechanisms driving the disease has allowed to develop novel therapeutic approaches that aim to improve the existing classes of drugs and develop novel drugs, by targeting new pathways. Several clinical trials have investigated the improvement of existing classes of drugs, including glucocorticoids, β 2-agonists, PDE4 inhibitors and neutrophil elastase inhibitors. New drugs under development include dual-action muscarinic antagonists and β 2-agonists, kinase inhibitors, cytokine and chemokines modifiers, senolytics, anti-fibrotic compounds and compounds stimulating lung regeneration [284].

Moreover, omics-based approaches (genomic, transcriptomic, proteomic and metabolomic) are currently applied to promote a better understanding of COPD pathogenesis.

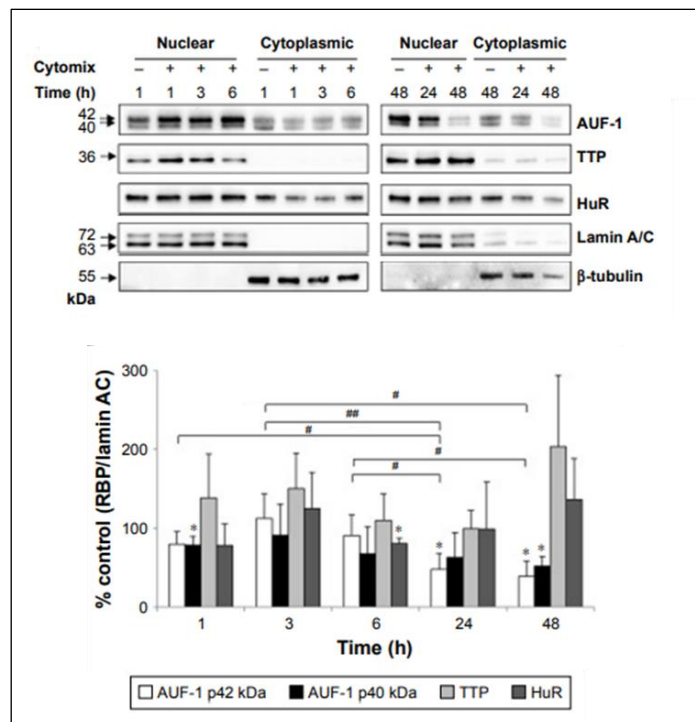
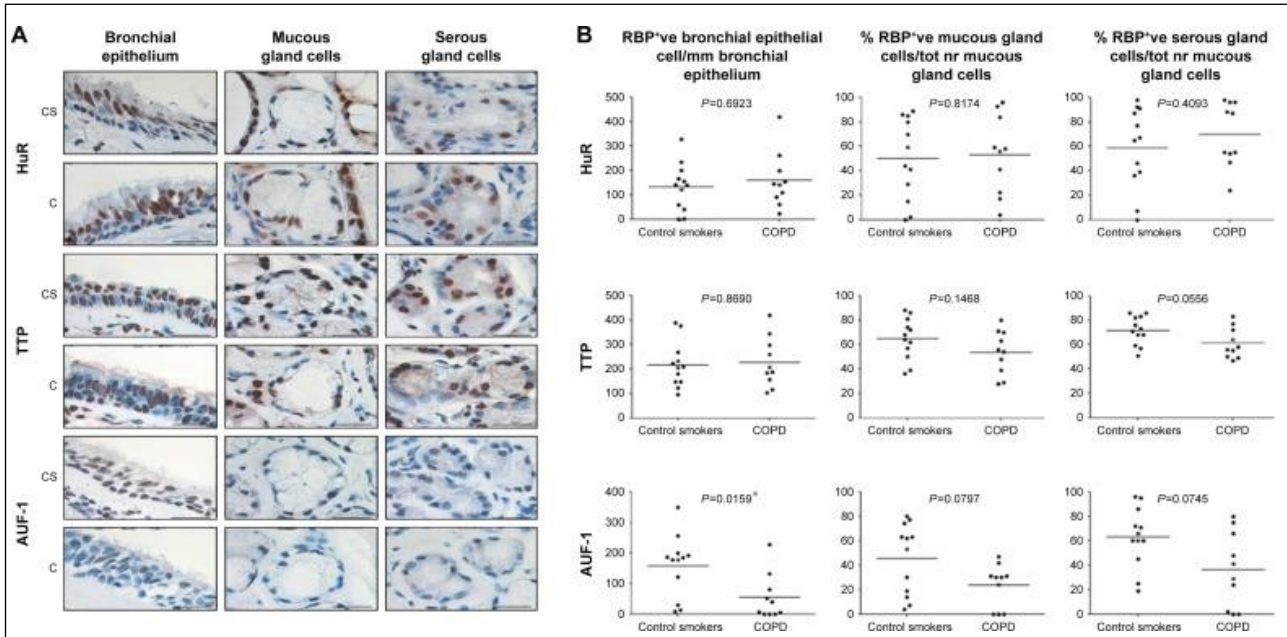
2.5. RBPs in COPD: current status

There are emerging evidences regarding the role of RBPs in the pathogenesis of chronic obstructive pulmonary disease (COPD), based on the strong preclinical evidence of HuR, TTP and AUF-1.

Recently, an immunohistochemical expression profile of RBPs in lower airway samples of stable COPD patients demonstrated decreased levels of AUF-1, but not of HuR and TTP, in bronchiolar epithelium compared to smokers with normal lung function [285] (**Figure 27**).

The same pattern was reproduced in human bronchial epithelial cells upon inflammatory stimulation and, additionally, increased levels of inflammatory mediators regulated by AUF-1 were detected in condition of AUF-1 loss [285] (**Figure 28**).

There are conflicting evidences regarding airway epithelial HuR expression in COPD, Baker et al. reported a significant reduction of HuR in peripheral lung samples from COPD patients and in mice exposed to cigarette smoke for 3 days, in contrast to the unchanged HuR levels detected by Ricciardi et al. [285,286]. In addition, another RBP, HNRNPC1/C2, part of the same protein family of AUF-1, was found significantly increased in COPD patients and in cigarette smoke-induced mouse model of COPD [287].



Furthermore, *in silico* analysis of bronchiolar epithelial cell transcriptome from COPD patients and matched smoker and non-smoker control subjects showed a global downregulation of RBPs expression; interestingly, several clusters of co-regulated RBPs were identified, revealing the potential for RBPs interplay and suggesting shared post-transcriptional regulation of biological pathways involved in COPD pathogenesis [198] (**Figure 29**).

Very few studies investigated AUF-1 in models of human lung inflammation. *In vitro*, cytosolic levels of AUF-1 increased significantly in primary airway epithelial cells infected with human rhinovirus, concomitant with a decreased expression of CXCL10 [288], while cigarette smoke-induced upregulation of CXCL8 was not AUF-1-dependent [244]. Recently, decreased levels of AUF-1 mRNA were found in BAL cells and peripheral blood mononuclear cells (PBMCs) of patients with sarcoidosis, another chronic inflammatory lung disease [289].

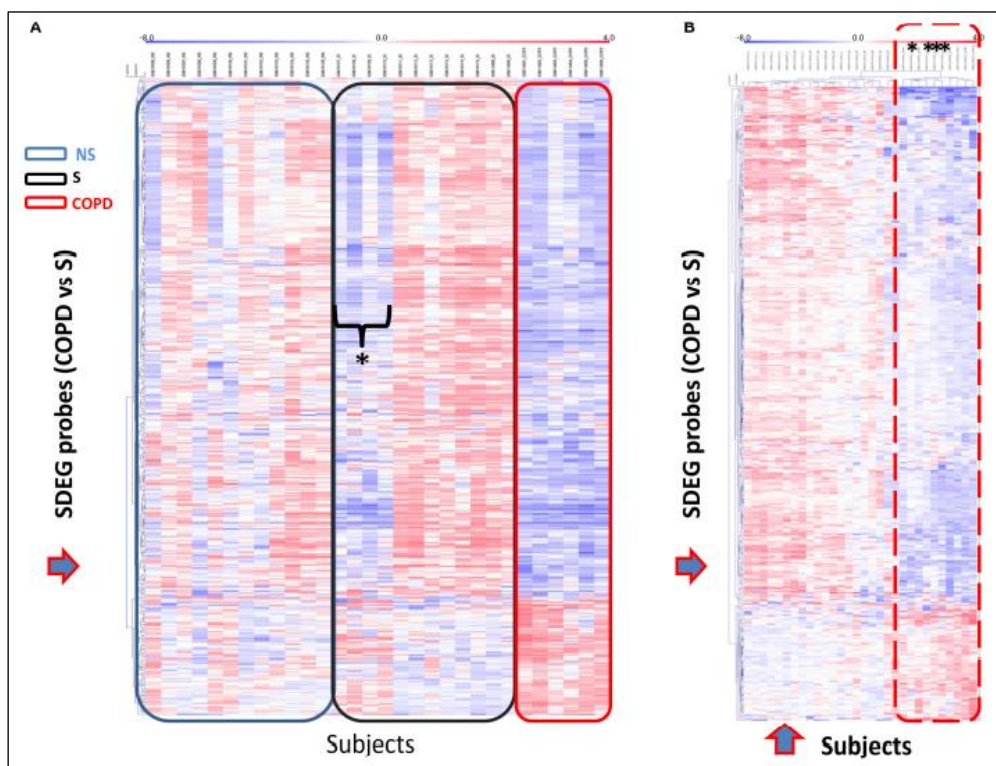


Figure 29. Unsupervised gene cluster analysis across the individual samples from GSE5058 dataset identifies selective global mRBPs repression in COPD patients shared by a subset of smoker controls. A. Unsupervised clustering analysis applied to (blue arrow) SDEG probe list identified in COPD/S (n = 409). Heatmap shows Significant FC/Differentially Expressed Genes (SDEG) probes' fluorescence intensity value (blue < 0, reduced: red > 0, increased). The data were normalized on the median and log2-transformed for relative fold changes. **B.** Unsupervised clustering analysis applied to both SDEG probe list and individual samples (blue arrows). Asterisks indicate the SDEG profiles of four smokers with normal al lung function (NLF), clustering with those of COPD patients indicated by the dotted line [198].

2.6. Targeting RBPs and their functions in COPD: is there a role?

The modulation of protein-RNA interactions has been considered a potential therapeutic target, that can be achieved with two main approaches: one acts on the RNA side by targeting the RNA molecules, while the other acts on the protein side (**Figure 30**).

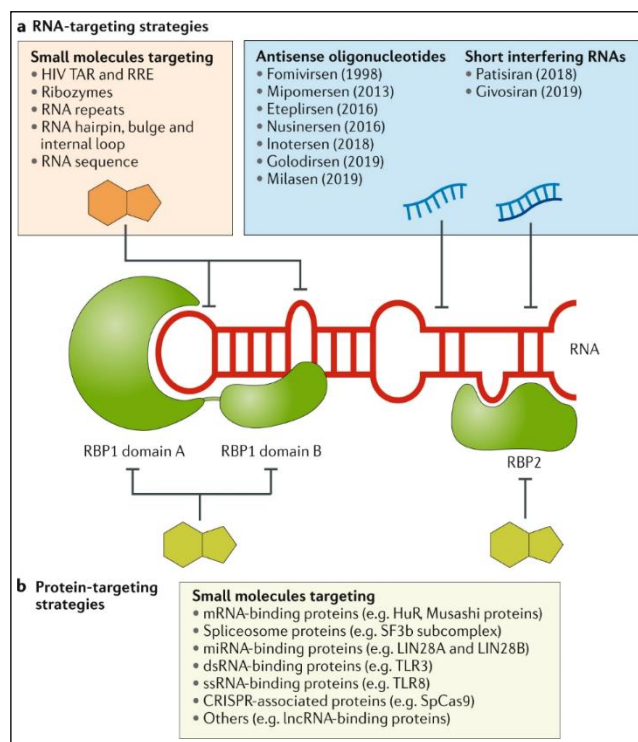


Figure 30. Approaches for targeting RNA-protein interaction. A. RNA-targeting strategies include small molecules that bind to RNA and nucleotide-based agents (antisense oligonucleotides and short interfering RNAs). The year of regulatory approval of the drug by the US Food and Drug Administration is indicated in parentheses. **B.** Protein-targeting strategies include small molecules and natural products that modulate the activity of RBPs [290].

2.6.1. RNA-targeting strategies

These approaches include nucleotide-based agents that target unstructured regions of RNA, as well as small molecules that bind directly to structured RNAs [291-293] (**Figure 30A**).

Two main classes of nucleotide-based agents, antisense oligonucleotides and short interfering RNAs, have been approved by the US Food and Drug Administration. In particular, the approval of Patisiran as the first short-interfering-RNA-based drug in 2018 and Givosiran in 2019 marked a new era for oligonucleotide-based strategies [290]. Similarly, the development of small molecules targeting RNA has rapidly progressed in the last years. A class of RNA-targeting small molecules bind to the CUG repeat or to other RNA repeats that are associated with trinucleotide repeat expansion disorders [294,295]. Other approaches include the use of molecules targeting directly secondary or tertiary

structural motifs of RNAs, such as hairpins, internal loops and precursor microRNA (pre-miRNA) [290].

2.6.2. Protein-targeting strategies

On the other side, RBPs targeting represents a therapeutic approach to inhibit their expression or function, and several inhibition strategies have been developed especially for targeting RBPs involved in cancer pathogenesis .

A number of small molecules and natural products that modulate RBPs have been identified, offering the advantage of good oral bioavailability and blood-brain barrier penetrance, as well as the possibility of systematic optimization to improve pharmacokinetics and potency [290] (**Figure 30B**). Small-molecules are able to inhibit RBPs function in multiple ways, from preventing the interaction with target RNAs to altering their enzymatic activity or inducing their degradation [296]. MS-444 was the first small molecular inhibitor developed to target HuR, interfering with its dimerization and, consequently, inhibiting its binding to target mRNAs [297] (**Figure 31**). Another small molecule targeting HuR is KH-3, that inhibits HuR–target mRNA interaction through competitively binding to HuR. Its action inhibits breast cancer cell growth and invasion *in vitro* and prevents lung metastasis [298].

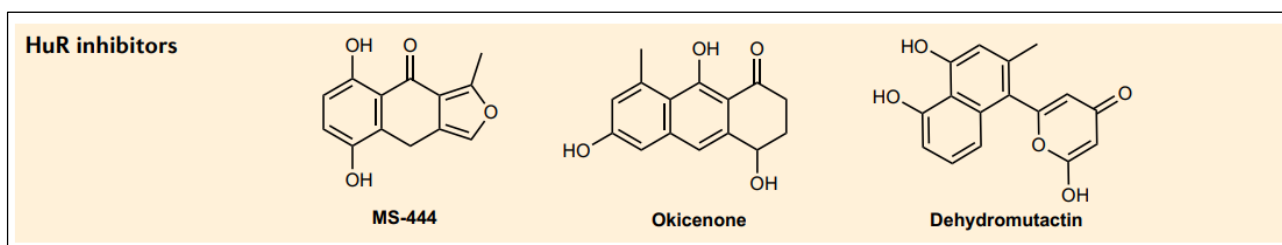


Figure 31. Small-molecules targeting HuR. Chemical structure of MS-444, okicenone and dehydromutactin that acts as inhibitor of HuR protein [290].

RK-33 was found to specifically bind to RNA helicase DDX3 and block its helicase activity [299]. The RBP Musashi protein is strongly inhibited by oleic acid, that prevent its interaction to target mRNA by binding to RRM1 protein domain and inducing conformational changes [300].

Natural or recombinant circular RNAs (circRNAs), an heterogeneous class of ncRNAs [Memczak S 2013], may be another therapeutic strategy, since their ability to sequester single or multiple RBPs and regulate their activity. For example, HuR is bound by circPABPN1 preventing its binding to poly(A)-binding protein 1 (PABPN1) mRNA, resulting in decreased PABPN1 translation [301] (**Figure 32**).

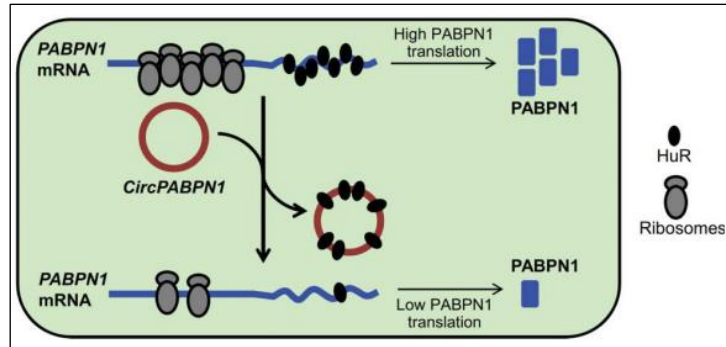


Figure 32. circPABPN1 suppresses PABPN1 translation. Proposed model whereby circPABPN1 sequesters HuR away from PABPN1 mRNA, in turn suppressing PABPN1 mRNA translation [301].

Attractive is the application of CRISPR/Cas9 system to directly target an RBP with multiple functional effect. For example, it could be possible to knockout an oncogenic RBP in cancer cells or modify the binding site in the target mRNA [296] (**Figure 33**).

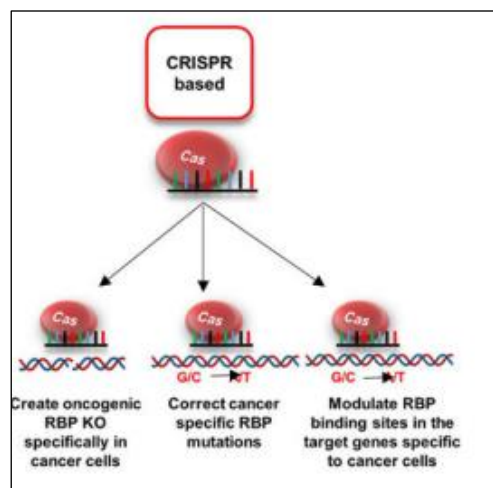


Figure 33. CRISPR-based strategy for cancer therapeutics. CRISPR-based approaches can be used to create oncogenic RBP knockout/knockin to correct cancer-specific mutation in RBP or RBP binding sites [296].

Several nanotechnology-based approaches, including liposomes and dendrimers, have been developed to selectively suppress RBPs in cells and tissues of interest with minimal or no toxicity to normal cells, thus offering immense potential for clinical application [302]. Nanoparticle delivery of small interfering RNA (siRNA) targeting RBPs is a promising approach. Inhibition of lung cancer cell proliferation was observed after HuR reduced expression achieved by delivering HuR-targeted siRNA into synthetic vesicles and this approach is also able to reduce the tumor burden in mouse models of lung cancer [303,304] (**Figure 34**). The natural analogues of these artificial nanocarriers are the extracellular vesicles (EVs), that are novel candidates for drug delivery systems with the advantages of high bioavailability and biocompatibility, ability to cross biological barriers and low

immunogenicity [305]. Importantly, EVs could be itself therapeutic targets since they carry multiple biological molecules, including RBPs, as it will be discussed in following paragraphs.

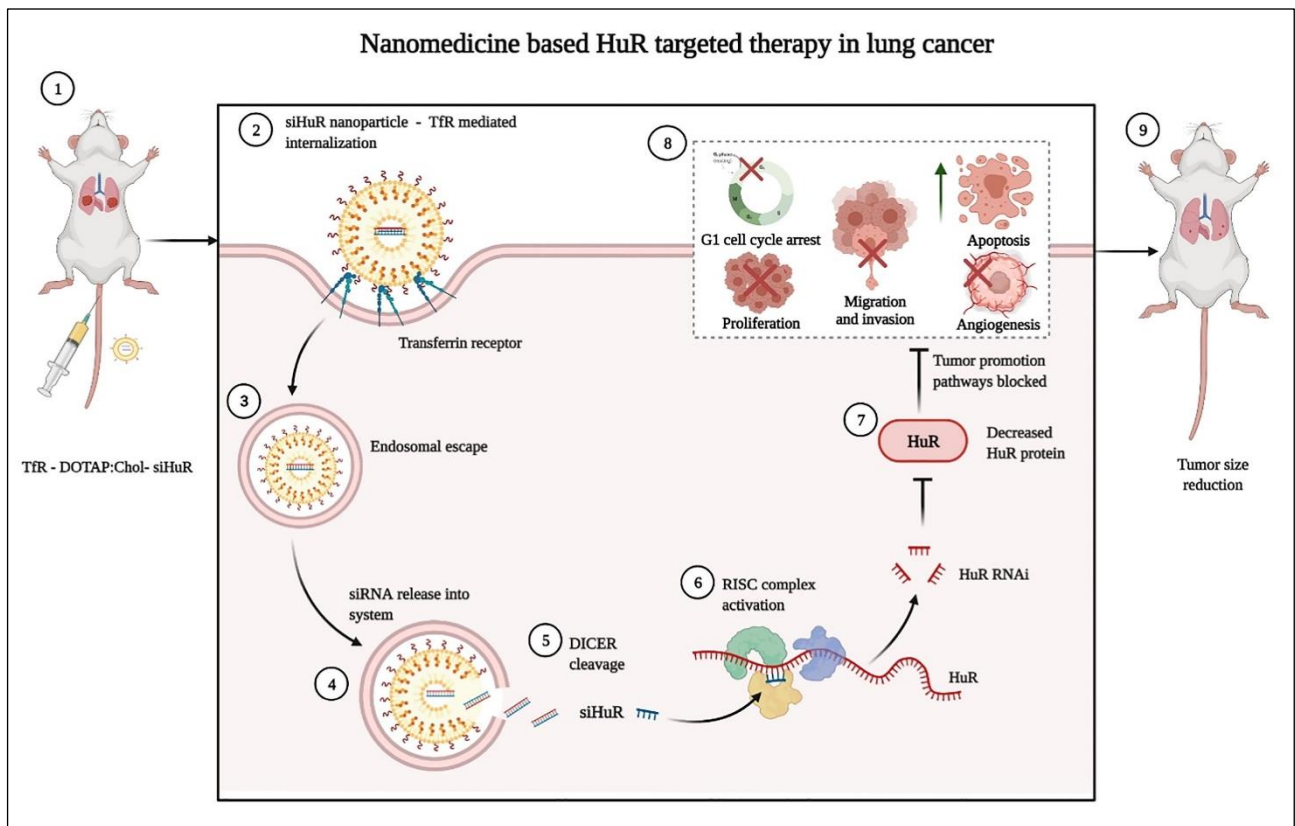


Figure 34. Schematic representation of nanomedicine-based HuR targeted therapy to reduce tumor growth in mouse models of lung cancer. Liposomal vesicles containing siRNA targeting HuR (siHuR) are internalized through the transferrin receptor (Tfr) exposed on lung cancer cells membrane. The RNA interference (RNAi) leads to decreased levels of HuR protein and the consequent blocking of tumor growth pathways [302,304].

Potential role of RBP-mediated control of pathogenic mechanisms of COPD can be inferred by pharmacological data. Aspirin is a widely used non-steroidal anti-inflammatory drug (NSAID) that acts not only by covalent modification of COX-2 enzyme but also through transcriptional regulation of immune-related genes [306]. Its use in COPD patients was associated decreased risk of developing lung carcinoma and decreased lung carcinoma-related mortality [307]. It is not known whether aspirin is able to interfere with RBP-mediated functions; to this end, HuR is a major positive regulator of COX-2 mRNA stability and this function has been experimentally targeted in colon cancer, where COX-2 is a key pathogenic factor [308]. Along the same lines, the anti-inflammatory effect of aged citrus peel (*chenpi*), commonly used in China as a dietary supplement for respiratory diseases, seems to prevent COPD through acting on PI3K-Akt-MAPK signalling pathway [309], opening to the hypothesis that this effect could affect downstream RBPs, regulated post-translationally through these

pathways. Systemic glucocorticoids *in vivo* induce the expression of TTP, indicating that post-transcriptional regulation is a major mechanism of the anti-inflammatory action of glucocorticoids [238]. Moreover, RBPs in modulating drugs response in COPD

The glucocorticoid receptor (GR) interacts with the RBP HNRNPU through its COOH terminal region and they colocalize into the nucleus [310]. Interestingly, it has been demonstrated that GR is able to act as an RBP, by associating with a subset of mRNAs carrying a guanosine-cytosine motif in their 5'UTR, including those for CCL2 and CCL7, and accelerating their decay [311]. Post-transcriptional control plays an important role also in the β 2-adrenergic receptor expression. The 3'UTR of β 2-adrenergic receptor mRNA contains a conserved ARE region bound by the RBPs TIAR and HuR, determining a suppression of protein synthesis of the receptor [312]. Moreover, the 3'UTR of β 1-adrenergic receptor is bound by AUF-1, HNRNPA1 and HuR [313,314].

References part 1

1. Cooper GM, Hausman RE. *The Cell: A Molecular Approach*. Sinauer Associates: Sunderland, MA.; 2013.
2. Chua BA, Van Der Werf I, Jamieson C, et al. Post-Transcriptional Regulation of Homeostatic, Stressed, and Malignant Stem Cells. *Cell Stem Cell*. 2020 Feb 6;26(2):138-159.
3. Buccitelli C, Selbach M. mRNAs, proteins and the emerging principles of gene expression control. *Nat Rev Genet*. 2020 Oct;21(10):630-644.
4. Glisovic T, Bachorik JL, Yong J, et al. RNA-binding proteins and post-transcriptional gene regulation. *FEBS Lett*. 2008 Jun 18;582(14):1977-86.
5. Iadevaia V, Gerber AP. Combinatorial Control of mRNA Fates by RNA-Binding Proteins and Non-Coding RNAs. *Biomolecules*. 2015 Sep 24;5(4):2207-22.
6. Keene JD. RNA regulons: coordination of post-transcriptional events. *Nat Rev Genet*. 2007 Jul;8(7):533-43.
7. Kang D, Lee Y, Lee JS. RNA-Binding Proteins in Cancer: Functional and Therapeutic Perspectives. *Cancers (Basel)*. 2020 Sep 21;12(9).
8. Carpenter S, Ricci EP, Mercier BC, et al. Post-transcriptional regulation of gene expression in innate immunity. *Nat Rev Immunol*. 2014 Jun;14(6):361-76.
9. Jurgens AP, Popović B, Wolkers MC. T cells at work: How post-transcriptional mechanisms control T cell homeostasis and activation. *Eur J Immunol*. 2021 Sep;51(9):2178-2187.
10. Kiebler MA, Bassell GJ. Neuronal RNA granules: movers and makers. *Neuron*. 2006 Sep 21;51(6):685-90.
11. Martin KC, Zukin RS. RNA trafficking and local protein synthesis in dendrites: an overview. *J Neurosci*. 2006 Jul 5;26(27):7131-4.
12. Halbeisen RE, Galgano A, Scherrer T, et al. Post-transcriptional gene regulation: from genome-wide studies to principles. *Cell Mol Life Sci*. 2008 Mar;65(5):798-813.
13. Matsumoto M, Setou M, Inokuchi K. Transcriptome analysis reveals the population of dendritic RNAs and their redistribution by neural activity. *Neurosci Res*. 2007 Mar;57(3):411-23.

14. Moore AE, Chenette DM, Larkin LC, et al. Physiological networks and disease functions of RNA-binding protein AUF1. *Wiley Interdiscip Rev RNA*. 2014 Jul-Aug;5(4):549-64.
15. Lu JY, Sadri N, Schneider RJ. Endotoxic shock in AUF1 knockout mice mediated by failure to degrade proinflammatory cytokine mRNAs. *Genes Dev*. 2006 Nov 15;20(22):3174-84.
16. Skriner K, Hueber W, Süleymanoglu E, et al. AUF1, the regulator of tumor necrosis factor alpha messenger RNA decay, is targeted by autoantibodies of patients with systemic rheumatic diseases. *Arthritis Rheum*. 2008 Feb;58(2):511-20.
17. Suzuki T, Tsutsumi A, Suzuki H, et al. Tristetraprolin (TTP) gene polymorphisms in patients with rheumatoid arthritis and healthy individuals. *Mod Rheumatol*. 2008;18(5):472-9.
18. Carrick DM, Chulada P, Donn R, et al. Genetic variations in ZFP36 and their possible relationship to autoimmune diseases. *J Autoimmun*. 2006 May;26(3):182-96.
19. Barton M, Meyer MR. HuR-ry Up: How Hydrogen Sulfide Protects Against Atherosclerosis. *Circulation*. 2019 Jan 2;139(1):115-118.
20. Fu X, Zhai S, Yuan J. Endothelial HuR deletion reduces the expression of proatherogenic molecules and attenuates atherosclerosis. *Int Immunopharmacol*. 2018 Dec;65:248-255.
21. Peng W, Furuuchi N, Aslanukova L, et al. Elevated HuR in Pancreas Promotes a Pancreatitis-Like Inflammatory Microenvironment That Facilitates Tumor Development. *Mol Cell Biol*. 2018 Feb 1;38(3).
22. Di Marco S, Mazroui R, Dallaire P, et al. NF-kappa B-mediated MyoD decay during muscle wasting requires nitric oxide synthase mRNA stabilization, HuR protein, and nitric oxide release. *Mol Cell Biol*. 2005 Aug;25(15):6533-45.
23. Sugihara M, Tsutsumi A, Suzuki E, et al. Effects of infliximab therapy on gene expression levels of tumor necrosis factor alpha, tristetraprolin, T cell intracellular antigen 1, and Hu antigen R in patients with rheumatoid arthritis. *Arthritis Rheum*. 2007 Jul;56(7):2160-9.
24. Suzuki E, Tsutsumi A, Sugihara M, et al. Expression of TNF-alpha, tristetraprolin, T-cell intracellular antigen-1 and Hu antigen R genes in synovium of patients with rheumatoid arthritis. *Int J Mol Med*. 2006 Aug;18(2):273-8.
25. Thomas JD, Johannes GJ. Identification of mRNAs that continue to associate with polysomes during hypoxia. *Rna*. 2007 Jul;13(7):1116-31.

26. Musa J, Orth MF, Dallmayer M, et al. Eukaryotic initiation factor 4E-binding protein 1 (4E-BP1): a master regulator of mRNA translation involved in tumorigenesis. *Oncogene*. 2016 Sep 8;35(36):4675-88.
27. Gerstberger S, Hafner M, Tuschl T. A census of human RNA-binding proteins. *Nat Rev Genet*. Vol. 15. England 2014. p. 829-45.
28. Hashemikhabir S, Neelamraju Y, Janga SC. Database of RNA binding protein expression and disease dynamics (READ DB). *Database (Oxford)*. 2015;2015:bav072.
29. Neelamraju Y, Hashemikhabir S, Janga SC. The human RBPome: from genes and proteins to human disease. *J Proteomics*. 2015 Sep 8;127(Pt A):61-70.
30. Hentze MW, Castello A, Schwarzl T, et al. A brave new world of RNA-binding proteins. *Nat Rev Mol Cell Biol*. 2018 May;19(5):327-341.
31. Ray D, Kazan H, Cook KB, et al. A compendium of RNA-binding motifs for decoding gene regulation. *Nature*. 2013 Jul 11;499(7457):172-7.
32. Coppin L, Leclerc J, Vincent A, et al. Messenger RNA Life-Cycle in Cancer Cells: Emerging Role of Conventional and Non-Conventional RNA-Binding Proteins? *Int J Mol Sci*. 2018 Feb 25;19(3).
33. Corley M, Burns MC, Yeo GW. How RNA-Binding Proteins Interact with RNA: Molecules and Mechanisms. *Mol Cell*. 2020 Apr 2;78(1):9-29.
34. Backe PH, Messias AC, Ravelli RB, et al. X-ray crystallographic and NMR studies of the third KH domain of hnRNP K in complex with single-stranded nucleic acids. *Structure*. 2005 Jul;13(7):1055-67.
35. Chang KY, Ramos A. The double-stranded RNA-binding motif, a versatile macromolecular docking platform. *Febs j*. 2005 May;272(9):2109-17.
36. Stefl R, Skrisovska L, Allain FH. RNA sequence- and shape-dependent recognition by proteins in the ribonucleoprotein particle. *EMBO Rep*. 2005 Jan;6(1):33-8.
37. Cléry A, Allen F. *From Structure to Function of RNA Binding Domains*. Landes Bioscience. 2011.
38. Raghavan A, Bohjanen PR. Microarray-based analyses of mRNA decay in the regulation of mammalian gene expression. *Brief Funct Genomic Proteomic*. 2004 Aug;3(2):112-24.

39. Chen CY, Shyu AB. AU-rich elements: characterization and importance in mRNA degradation. *Trends Biochem Sci.* 1995 Nov;20(11):465-70.
40. Wilusz CJ, Wilusz J. Bringing the role of mRNA decay in the control of gene expression into focus. *Trends Genet.* 2004 Oct;20(10):491-7.
41. White EJ, Brewer G, Wilson GM. Post-transcriptional control of gene expression by AUF1: mechanisms, physiological targets, and regulation. *Biochim Biophys Acta.* 2013 Jun-Jul;1829(6-7):680-8.
42. Yoon JH, De S, Srikantan S, et al. PAR-CLIP analysis uncovers AUF1 impact on target RNA fate and genome integrity. *Nat Commun.* 2014 Nov 4;5:5248.
43. Wagner BJ, DeMaria CT, Sun Y, et al. Structure and genomic organization of the human AUF1 gene: alternative pre-mRNA splicing generates four protein isoforms. *Genomics.* 1998 Mar 1;48(2):195-202.
44. Chen CY, Xu N, Shyu AB. Highly selective actions of HuR in antagonizing AU-rich element-mediated mRNA destabilization. *Mol Cell Biol.* 2002 Oct;22(20):7268-78.
45. Gilks N, Kedersha N, Ayodele M, et al. Stress granule assembly is mediated by prion-like aggregation of TIA-1. *Mol Biol Cell.* 2004 Dec;15(12):5383-98.
46. Khabar KS. The AU-rich transcriptome: more than interferons and cytokines, and its role in disease. *J Interferon Cytokine Res.* 2005 Jan;25(1):1-10.
47. Qi MY, Wang ZZ, Zhang Z, et al. AU-rich-element-dependent translation repression requires the cooperation of tristetraprolin and RCK/P54. *Mol Cell Biol.* 2012 Mar;32(5):913-28.
48. Wang I, Hennig J, Jagtap PK, et al. Structure, dynamics and RNA binding of the multi-domain splicing factor TIA-1. *Nucleic Acids Res.* 2014 May;42(9):5949-66.
49. Tao X, Gao G. Tristetraprolin Recruits Eukaryotic Initiation Factor 4E2 To Repress Translation of AU-Rich Element-Containing mRNAs. *Mol Cell Biol.* 2015 Nov;35(22):3921-32.
50. Waris S, García-Mauriño SM, Sivakumaran A, et al. TIA-1 RRM23 binding and recognition of target oligonucleotides. *Nucleic Acids Res.* 2017 May 5;45(8):4944-4957.
51. Raineri I, Wegmueller D, Gross B, et al. Roles of AUF1 isoforms, HuR and BRF1 in ARE-dependent mRNA turnover studied by RNA interference. *Nucleic Acids Res.* 2004;32(4):1279-88.

52. Srikantan S, Gorospe M. HuR function in disease. *Front Biosci (Landmark Ed)*. 2012 Jan 1;17(1):189-205.
53. Piecyk M, Wax S, Beck AR, et al. TIA-1 is a translational silencer that selectively regulates the expression of TNF-alpha. *Embo j*. 2000 Aug 1;19(15):4154-63.
54. Vlasova IA, Tahoe NM, Fan D, et al. Conserved GU-rich elements mediate mRNA decay by binding to CUG-binding protein 1. *Mol Cell*. 2008 Feb 1;29(2):263-70.
55. Rattenbacher B, Beisang D, Wiesner DL, et al. Analysis of CUGBP1 targets identifies GU-repeat sequences that mediate rapid mRNA decay. *Mol Cell Biol*. 2010 Aug;30(16):3970-80.
56. Dominguez D, Freese P, Alexis MS, et al. Sequence, Structure, and Context Preferences of Human RNA Binding Proteins. *Mol Cell*. 2018 Jun 7;70(5):854-867.e9.
57. Jolma A, Zhang J, Mondragón E, et al. Binding specificities of human RNA-binding proteins toward structured and linear RNA sequences. *Genome Res*. 2020 Jul;30(7):962-973.
58. Meyer KD, Saletore Y, Zumbo P, et al. Comprehensive analysis of mRNA methylation reveals enrichment in 3' UTRs and near stop codons. *Cell*. 2012 Jun 22;149(7):1635-46.
59. Lewis CJ, Pan T, Kalsotra A. RNA modifications and structures cooperate to guide RNA-protein interactions. *Nat Rev Mol Cell Biol*. 2017 Mar;18(3):202-210.
60. Zhang C, Fu J, Zhou Y. A Review in Research Progress Concerning m6A Methylation and Immunoregulation. *Front Immunol*. 2019;10:922.
61. Huang H, Weng H, Chen J. The Biogenesis and Precise Control of RNA m(6)A Methylation. *Trends Genet*. 2020 Jan;36(1):44-52.
62. Roundtree IA, Evans ME, Pan T, et al. Dynamic RNA Modifications in Gene Expression Regulation. *Cell*. 2017 Jun 15;169(7):1187-1200.
63. Roignant JY, Soller M. m(6)A in mRNA: An Ancient Mechanism for Fine-Tuning Gene Expression. *Trends Genet*. 2017 Jun;33(6):380-390.
64. Yang Y, Fan X, Mao M, et al. Extensive translation of circular RNAs driven by N(6)-methyladenosine. *Cell Res*. 2017 May;27(5):626-641.
65. Li HB, Tong J, Zhu S, et al. m(6)A mRNA methylation controls T cell homeostasis by targeting the IL-7/STAT5/SOCS pathways. *Nature*. 2017 Aug 17;548(7667):338-342.

66. Wang S, Sun C, Li J, et al. Roles of RNA methylation by means of N(6)-methyladenosine (m(6)A) in human cancers. *Cancer Lett.* 2017 Nov 1;408:112-120.
67. Barreau C, Paillard L, Osborne HB. AU-rich elements and associated factors: are there unifying principles? *Nucleic Acids Res.* 2005;33(22):7138-50.
68. Dalmau J, Furneaux HM, Cordon-Cardo C, et al. The expression of the Hu (paraneoplastic encephalomyelitis/sensory neuronopathy) antigen in human normal and tumor tissues. *Am J Pathol.* 1992 Oct;141(4):881-6.
69. Akamatsu W, Fujihara H, Mitsuhashi T, et al. The RNA-binding protein HuD regulates neuronal cell identity and maturation. *Proc Natl Acad Sci U S A.* 2005 Mar 22;102(12):4625-30.
70. Song X, Shi X, Li W, et al. The RNA-Binding Protein HuR in Digestive System Tumors. *Biomed Res Int.* 2020;2020:9656051.
71. Brennan CM, Steitz JA. HuR and mRNA stability. *Cell Mol Life Sci.* 2001 Feb;58(2):266-77.
72. Wang W, Furneaux H, Cheng H, et al. HuR regulates p21 mRNA stabilization by UV light. *Mol Cell Biol.* 2000 Feb;20(3):760-9.
73. Lal A, Mazan-Mamczarz K, Kawai T, et al. Concurrent versus individual binding of HuR and AUF1 to common labile target mRNAs. *Embo j.* 2004 Aug 4;23(15):3092-102.
74. Guo X, Hartley RS. HuR contributes to cyclin E1 deregulation in MCF-7 breast cancer cells. *Cancer Res.* 2006 Aug 15;66(16):7948-56.
75. Bolognani F, Gallani AI, Sokol L, et al. mRNA stability alterations mediated by HuR are necessary to sustain the fast growth of glioma cells. *J Neurooncol.* 2012 Feb;106(3):531-42.
76. Siang DTC, Lim YC, Kyaw AMM, et al. The RNA-binding protein HuR is a negative regulator in adipogenesis. *Nat Commun.* 2020 Jan 10;11(1):213.
77. Sanduja S, Blanco FF, Young LE, et al. The role of tristetraprolin in cancer and inflammation. *Front Biosci (Landmark Ed).* 2012 Jan 1;17(1):174-88.
78. Brooks SA, Connolly JE, Rigby WF. The role of mRNA turnover in the regulation of tristetraprolin expression: evidence for an extracellular signal-regulated kinase-specific, AU-rich element-dependent, autoregulatory pathway. *J Immunol.* 2004 Jun 15;172(12):7263-71.
79. Baou M, Jewell A, Murphy JJ. TIS11 family proteins and their roles in posttranscriptional gene regulation. *J Biomed Biotechnol.* 2009;2009:634520.

80. Brewer BY, Malicka J, Blackshear PJ, et al. RNA sequence elements required for high affinity binding by the zinc finger domain of tristetraprolin: conformational changes coupled to the bipartite nature of Au-rich mRNA-destabilizing motifs. *J Biol Chem.* 2004 Jul 2;279(27):27870-7.
81. Lai WS, Kennington EA, Blackshear PJ. Interactions of CCCH zinc finger proteins with mRNA: non-binding tristetraprolin mutants exert an inhibitory effect on degradation of AU-rich element-containing mRNAs. *J Biol Chem.* 2002 Mar 15;277(11):9606-13.
82. Collart MA. The Ccr4-Not complex is a key regulator of eukaryotic gene expression. *Wiley Interdiscip Rev RNA.* 2016 Jul;7(4):438-54.
83. Grudzien-Nogalska E, Kiledjian M. New insights into decapping enzymes and selective mRNA decay. *Wiley Interdiscip Rev RNA.* 2017 Jan;8(1).
84. Eulalio A, Behm-Ansmant I, Izaurralde E. P bodies: at the crossroads of post-transcriptional pathways. *Nat Rev Mol Cell Biol.* 2007 Jan;8(1):9-22.
85. Garneau NL, Wilusz J, Wilusz CJ. The highways and byways of mRNA decay. *Nat Rev Mol Cell Biol.* 2007 Feb;8(2):113-26.
86. Anderson P. Post-transcriptional regulons coordinate the initiation and resolution of inflammation. *Nat Rev Immunol.* 2010 Jan;10(1):24-35.
87. Ing NH, Massuto DA, Jaeger LA. Estradiol up-regulates AUF1p45 binding to stabilizing regions within the 3'-untranslated region of estrogen receptor alpha mRNA. *J Biol Chem.* 2008 Jan 18;283(3):1764-1772.
88. Paschoud S, Dogar AM, Kuntz C, et al. Destabilization of interleukin-6 mRNA requires a putative RNA stem-loop structure, an AU-rich element, and the RNA-binding protein AUF1. *Mol Cell Biol.* 2006 Nov;26(22):8228-41.
89. Xu N, Chen CY, Shyu AB. Versatile role for hnRNP D isoforms in the differential regulation of cytoplasmic mRNA turnover. *Mol Cell Biol.* 2001 Oct;21(20):6960-71.
90. von Roretz C, Di Marco S, Mazroui R, et al. Turnover of AU-rich-containing mRNAs during stress: a matter of survival. *Wiley Interdiscip Rev RNA.* 2011 May-Jun;2(3):336-47.
91. Sarkar B, Xi Q, He C, et al. Selective degradation of AU-rich mRNAs promoted by the p37 AUF1 protein isoform. *Mol Cell Biol.* 2003 Sep;23(18):6685-93.

92. Sinsimer KS, Gratacós FM, Knapinska AM, et al. Chaperone Hsp27, a novel subunit of AUF1 protein complexes, functions in AU-rich element-mediated mRNA decay. *Mol Cell Biol.* 2008 Sep;28(17):5223-37.
93. Chen CY, Gherzi R, Ong SE, et al. AU binding proteins recruit the exosome to degrade ARE-containing mRNAs. *Cell.* 2001 Nov 16;107(4):451-64.
94. Mukherjee D, Gao M, O'Connor JP, et al. The mammalian exosome mediates the efficient degradation of mRNAs that contain AU-rich elements. *Embo j.* 2002 Jan 15;21(1-2):165-74.
95. Goldstrohm AC, Wickens M. Multifunctional deadenylase complexes diversify mRNA control. *Nat Rev Mol Cell Biol.* Vol. 9. England 2008. p. 337-44.
96. Pont AR, Sadri N, Hsiao SJ, et al. mRNA decay factor AUF1 maintains normal aging, telomere maintenance, and suppression of senescence by activation of telomerase transcription. *Mol Cell.* 2012 Jul 13;47(1):5-15.
97. Enokizono Y, Konishi Y, Nagata K, et al. Structure of hnRNP D complexed with single-stranded telomere DNA and unfolding of the quadruplex by heterogeneous nuclear ribonucleoprotein D. *J Biol Chem.* 2005 May 13;280(19):18862-70.
98. Beck AR, Medley QG, O'Brien S, et al. Structure, tissue distribution and genomic organization of the murine RRM-type RNA binding proteins TIA-1 and TIAR. *Nucleic Acids Res.* 1996 Oct 1;24(19):3829-35.
99. Fernández-Gómez A, Izquierdo JM. The Multifunctional Faces of T-Cell Intracellular Antigen 1 in Health and Disease. *Int J Mol Sci.* 2022 Jan 26;23(3).
100. Kedersha N, Anderson P. Stress granules: sites of mRNA triage that regulate mRNA stability and translatability. *Biochem Soc Trans.* 2002 Nov;30(Pt 6):963-9.
101. Gottschald OR, Malec V, Krasteva G, et al. TIAR and TIA-1 mRNA-binding proteins co-aggregate under conditions of rapid oxygen decline and extreme hypoxia and suppress the HIF-1 α pathway. *J Mol Cell Biol.* 2010 Dec;2(6):345-56.
102. Damgaard CK, Lykke-Andersen J. Translational coregulation of 5'TOP mRNAs by TIA-1 and TIAR. *Genes Dev.* 2011 Oct 1;25(19):2057-68.
103. Lee EK. Post-translational modifications of RNA-binding proteins and their roles in RNA granules. *Curr Protein Pept Sci.* 2012 Jun;13(4):331-6.

104. Grammatikakis I, Abdelmohsen K, Gorospe M. Posttranslational control of HuR function. *Wiley Interdiscip Rev RNA*. 2017 Jan;8(1).
105. Li H, Park S, Kilburn B, et al. Lipopolysaccharide-induced methylation of HuR, an mRNA-stabilizing protein, by CARM1. Coactivator-associated arginine methyltransferase. *J Biol Chem*. 2002 Nov 22;277(47):44623-30.
106. Fernández-Ramos D, Martínez-Chantar ML. NEDDylation in liver cancer: The regulation of the RNA binding protein Hu antigen R. *Pancreatology*. 2015 Jul;15(4 Suppl):S49-54.
107. Venigalla RK, Turner M. RNA-binding proteins as a point of convergence of the PI3K and p38 MAPK pathways. *Front Immunol*. 2012;3:398.
108. Cao H, Deterding LJ, Blackshear PJ. Identification of a major phosphopeptide in human tristetraprolin by phosphopeptide mapping and mass spectrometry. *PLoS One*. 2014;9(7):e100977.
109. Cao H, Deterding LJ, Blackshear PJ. Phosphorylation site analysis of the anti-inflammatory and mRNA-destabilizing protein tristetraprolin. *Expert Rev Proteomics*. 2007 Dec;4(6):711-26.
110. Coelho MA, de Carné Trécesson S, Rana S, et al. Oncogenic RAS Signaling Promotes Tumor Immuno-resistance by Stabilizing PD-L1 mRNA. *Immunity*. 2017 Dec 19;47(6):1083-1099.e6.
111. Dassi E. Handshakes and Fights: The Regulatory Interplay of RNA-Binding Proteins. *Front Mol Biosci*. 2017;4:67.
112. Lukong KE, Chang KW, Khandjian EW, et al. RNA-binding proteins in human genetic disease. *Trends Genet*. 2008 Aug;24(8):416-25.
113. Gebauer F, Schwarzl T, Valcárcel J, et al. RNA-binding proteins in human genetic disease. *Nat Rev Genet*. 2021 Mar;22(3):185-198.
114. Pullmann R, Jr., Juhaszova M, López de Silanes I, et al. Enhanced proliferation of cultured human vascular smooth muscle cells linked to increased function of RNA-binding protein HuR. *J Biol Chem*. 2005 Jun 17;280(24):22819-26.
115. Zhou C, Vignere CZ, Levitan ES. AUF1 is upregulated by angiotensin II to destabilize cardiac Kv4.3 channel mRNA. *J Mol Cell Cardiol*. 2008 Dec;45(6):832-8.
116. Pereira B, Billaud M, Almeida R. RNA-Binding Proteins in Cancer: Old Players and New Actors. *Trends Cancer*. 2017 Jul;3(7):506-528.

117. Bhattacharyya SN, Habermacher R, Martine U, et al. Relief of microRNA-mediated translational repression in human cells subjected to stress. *Cell*. 2006 Jun 16;125(6):1111-24.
118. Luo NA, Qu YQ, Yang GD, et al. Post-transcriptional up-regulation of PDGF-C by HuR in advanced and stressed breast cancer. *Int J Mol Sci*. 2014 Nov 6;15(11):20306-20.
119. Lauriola L, Granone P, Ramella S, et al. Expression of the RNA-binding protein HuR and its clinical significance in human stage I and II lung adenocarcinoma. *Histol Histopathol*. 2012 May;27(5):617-26.
120. Huwiler A, Akool el S, Aschrafi A, et al. ATP potentiates interleukin-1 beta-induced MMP-9 expression in mesangial cells via recruitment of the ELAV protein HuR. *J Biol Chem*. 2003 Dec 19;278(51):51758-69.
121. Akool el S, Kleinert H, Hamada FM, et al. Nitric oxide increases the decay of matrix metalloproteinase 9 mRNA by inhibiting the expression of mRNA-stabilizing factor HuR. *Mol Cell Biol*. 2003 Jul;23(14):4901-16.
122. D'Alessio S, Blasi F. The urokinase receptor as an entertainer of signal transduction. *Front Biosci (Landmark Ed)*. 2009 Jan 1;14(12):4575-87.
123. Guo J, Wang H, Jiang S, et al. The Cross-talk between Tristetraprolin and Cytokines in Cancer. *Anticancer Agents Med Chem*. 2017 Nov 24;17(11):1477-1486.
124. Panganiban RP, Vonakis BM, Ishmael FT, et al. Coordinated post-transcriptional regulation of the chemokine system: messages from CCL2. *J Interferon Cytokine Res*. 2014 Apr;34(4):255-66.
125. Wang H, Ding N, Guo J, et al. Dysregulation of TTP and HuR plays an important role in cancers. *Tumour Biol*. 2016 Nov;37(11):14451-14461.
126. Young LE, Sanduja S, Bemis-Standoli K, et al. The mRNA binding proteins HuR and tristetraprolin regulate cyclooxygenase 2 expression during colon carcinogenesis. *Gastroenterology*. 2009 May;136(5):1669-79.
127. Lafzi A, Kazan H. Inferring RBP-Mediated Regulation in Lung Squamous Cell Carcinoma. *PLoS One*. 2016;11(5):e0155354.
128. Wang J, Wang B, Bi J, et al. Cytoplasmic HuR expression correlates with angiogenesis, lymphangiogenesis, and poor outcome in lung cancer. *Med Oncol*. 2011 Dec;28 Suppl 1:S577-85.

129. Dong F, Li C, Wang P, et al. The RNA binding protein tristetraprolin down-regulates autophagy in lung adenocarcinoma cells. *Exp Cell Res*. 2018 Jun 1;367(1):89-96.
130. Khabar KS. Hallmarks of cancer and AU-rich elements. *Wiley Interdiscip Rev RNA*. 2017 Jan;8(1).
131. Crusz SM, Balkwill FR. Inflammation and cancer: advances and new agents. *Nat Rev Clin Oncol*. 2015 Oct;12(10):584-96.
132. Barnes PJ, Adcock IM. Chronic obstructive pulmonary disease and lung cancer: a lethal association. *Am J Respir Crit Care Med*. Vol. 184. United States 2011. p. 866-7.
133. Durham AL, Adcock IM. The relationship between COPD and lung cancer. *Lung Cancer*. 2015 Nov;90(2):121-7.
134. Nucera F, Mumby S, Paudel KR, et al. Role of oxidative stress in the pathogenesis of COPD. *Minerva Med*. 2022 Feb 10.
135. Barreiro E, Fermoselle C, Mateu-Jimenez M, et al. Oxidative stress and inflammation in the normal airways and blood of patients with lung cancer and COPD. *Free Radic Biol Med*. 2013 Dec;65:859-871.
136. Khabar KS. Post-transcriptional control during chronic inflammation and cancer: a focus on AU-rich elements. *Cell Mol Life Sci*. 2010 Sep;67(17):2937-55.
137. www.goldcopd.org.
138. Prevalence and attributable health burden of chronic respiratory diseases, 1990-2017: a systematic analysis for the Global Burden of Disease Study 2017. *Lancet Respir Med*. 2020 Jun;8(6):585-596.
139. www.who.int
140. Iheanacho I, Zhang S, King D, et al. Economic Burden of Chronic Obstructive Pulmonary Disease (COPD): A Systematic Literature Review. *Int J Chron Obstruct Pulmon Dis*. 2020;15:439-460.
141. Obernolte H, Niehof M, Braubach P, et al. Cigarette smoke alters inflammatory genes and the extracellular matrix - investigations on viable sections of peripheral human lungs. *Cell Tissue Res*. 2022 Feb;387(2):249-260.

142. Ahn SV, Lee E, Park B, et al. Cancer development in patients with COPD: a retrospective analysis of the National Health Insurance Service-National Sample Cohort in Korea. *BMC Pulm Med.* 2020 Jun 15;20(1):170.
143. Ang L, Ghosh P, Seow WJ. Association between previous lung diseases and lung cancer risk: a systematic review and meta-analysis. *Carcinogenesis.* 2021 Dec 31;42(12):1461-1474.
144. Machida H, Inoue S, Shibata Y, et al. The Incidence and Risk Analysis of Lung Cancer Development in Patients with Chronic Obstructive Pulmonary Disease: Possible Effectiveness of Annual CT-Screening. *Int J Chron Obstruct Pulmon Dis.* 2021;16:739-749.
145. Caramori G, Casolari P, Barczyk A, et al. COPD immunopathology. *Semin Immunopathol.* 2016 Jul;38(4):497-515.
146. Barnes PJ, Burney PG, Silverman EK, et al. Chronic obstructive pulmonary disease. *Nat Rev Dis Primers.* 2015 Dec 3;1:15076.
147. Silverman EK, Sandhaus RA. Clinical practice. Alpha1-antitrypsin deficiency. *N Engl J Med.* 2009 Jun 25;360(26):2749-57.
148. Hancock DB, Eijgelsheim M, Wilk JB, et al. Meta-analyses of genome-wide association studies identify multiple loci associated with pulmonary function. *Nat Genet.* 2010 Jan;42(1):45-52.
149. Repapi E, Sayers I, Wain LV, et al. Genome-wide association study identifies five loci associated with lung function. *Nat Genet.* 2010 Jan;42(1):36-44.
150. Cho MH, McDonald ML, Zhou X, et al. Risk loci for chronic obstructive pulmonary disease: a genome-wide association study and meta-analysis. *Lancet Respir Med.* 2014 Mar;2(3):214-25.
151. Hung RJ, McKay JD, Gaborieau V, et al. A susceptibility locus for lung cancer maps to nicotinic acetylcholine receptor subunit genes on 15q25. *Nature.* 2008 Apr 3;452(7187):633-7.
152. Pillai SG, Ge D, Zhu G, et al. A genome-wide association study in chronic obstructive pulmonary disease (COPD): identification of two major susceptibility loci. *PLoS Genet.* 2009 Mar;5(3):e1000421.
153. Young RP, Hopkins RJ, Whittington CF, et al. Individual and cumulative effects of GWAS susceptibility loci in lung cancer: associations after sub-phenotyping for COPD. *PLoS One.* 2011 Feb 3;6(2):e16476.

154. Wain LV, Sayers I, Soler Artigas M, et al. Whole exome re-sequencing implicates *CCDC38* and cilia structure and function in resistance to smoking related airflow obstruction. *PLoS Genet.* 2014 May;10(5):e1004314.
155. Lamontagne M, Bérubé JC, Obeidat M, et al. Leveraging lung tissue transcriptome to uncover candidate causal genes in COPD genetic associations. *Hum Mol Genet.* 2018 May 15;27(10):1819-1829.
156. Esteller M. Epigenetics in cancer. *N Engl J Med.* 2008 Mar 13;358(11):1148-59.
157. Duruisseaux M, Esteller M. Lung cancer epigenetics: From knowledge to applications. *Semin Cancer Biol.* 2018 Aug;51:116-128.
158. Qiu W, Baccarelli A, Carey VJ, et al. Variable DNA methylation is associated with chronic obstructive pulmonary disease and lung function. *Am J Respir Crit Care Med.* 2012 Feb 15;185(4):373-81.
159. Sundar IK, Yin Q, Baier BS, et al. DNA methylation profiling in peripheral lung tissues of smokers and patients with COPD. *Clin Epigenetics.* 2017;9:38.
160. Mao Y, Huang P, Wang Y, et al. Genome-wide methylation and expression analyses reveal the epigenetic landscape of immune-related diseases for tobacco smoking. *Clin Epigenetics.* 2021 Dec 9;13(1):215.
161. Peserico A, Simone C. Physical and functional HAT/HDAC interplay regulates protein acetylation balance. *J Biomed Biotechnol.* 2011;2011:371832.
162. Szulakowski P, Crowther AJ, Jiménez LA, et al. The effect of smoking on the transcriptional regulation of lung inflammation in patients with chronic obstructive pulmonary disease. *Am J Respir Crit Care Med.* 2006 Jul 1;174(1):41-50.
163. Ito K, Ito M, Elliott WM, et al. Decreased histone deacetylase activity in chronic obstructive pulmonary disease. *N Engl J Med.* 2005 May 12;352(19):1967-76.
164. Barnes PJ. Role of HDAC2 in the pathophysiology of COPD. *Annu Rev Physiol.* 2009;71:451-64.
165. Ito K, Lim S, Caramori G, et al. Cigarette smoking reduces histone deacetylase 2 expression, enhances cytokine expression, and inhibits glucocorticoid actions in alveolar macrophages. *Faseb j.* 2001 Apr;15(6):1110-2.

166. Rajendrasozhan S, Yao H, Rahman I. Current perspectives on role of chromatin modifications and deacetylases in lung inflammation in COPD. *Copd*. 2009 Aug;6(4):291-7.
167. Rajendrasozhan S, Yang SR, Kinnula VL, et al. SIRT1, an antiinflammatory and antiaging protein, is decreased in lungs of patients with chronic obstructive pulmonary disease. *Am J Respir Crit Care Med*. 2008 Apr 15;177(8):861-70.
168. Abdelmohsen K, Kuwano Y, Kim HH, et al. Posttranscriptional gene regulation by RNA-binding proteins during oxidative stress: implications for cellular senescence. *Biol Chem*. 2008 Mar;389(3):243-55.
169. Dutta J. Role of Oxidative Stress and DNA Damage/Repair in Lung Cancer. In: Chakraborti, S, Ray, B.K., Roychoudhury, S. (eds) *Handbook of Oxidative Stress in Cancer: Mechanistic Aspects*. Springer, Singapore. 2022.
170. Barnes PJ. New anti-inflammatory targets for chronic obstructive pulmonary disease. *Nat Rev Drug Discov*. 2013 Jul;12(7):543-59.
171. Barnes PJ. Oxidative stress-based therapeutics in COPD. *Redox Biol*. 2020 Jun;33:101544.
172. Osoata GO, Hanazawa T, Brindicci C, et al. Peroxynitrite elevation in exhaled breath condensate of COPD and its inhibition by fudosteine. *Chest*. 2009 Jun;135(6):1513-1520.
173. Cao H, Kelly MA, Kari F, et al. Green tea increases anti-inflammatory tristetraproline and decreases pro-inflammatory tumor necrosis factor mRNA levels in rats. *J Inflamm (Lond)*. 2007 Jan 5;4:1.
174. Rahman I. The role of oxidative stress in the pathogenesis of COPD: implications for therapy. *Treat Respir Med*. 2005;4(3):175-200.
175. Paredi P, Kharitonov SA, Leak D, et al. Exhaled ethane, a marker of lipid peroxidation, is elevated in chronic obstructive pulmonary disease. *Am J Respir Crit Care Med*. 2000 Aug;162(2 Pt 1):369-73.
176. Barnes PJ. *Oxidative Stress in Chronic Obstructive Pulmonary Disease*. *Antioxidants (Basel)*. 2022 May 13;11(5).
177. Nucera F, Bianco A, David T, et al. Treatable traits in COPD patients. *Minerva Med*. 2022 Jun;113(3):449-459.

178. Kirkham PA, Caramori G, Casolari P, et al. Oxidative stress-induced antibodies to carbonyl-modified protein correlate with severity of chronic obstructive pulmonary disease. *Am J Respir Crit Care Med.* 2011 Oct 1;184(7):796-802.
179. Caramori G, Adcock IM, Casolari P, et al. Unbalanced oxidant-induced DNA damage and repair in COPD: a link towards lung cancer. *Thorax.* 2011 Jun;66(6):521-7.
180. Meek K, Gupta S, Ramsden DA, et al. The DNA-dependent protein kinase: the director at the end. *Immunol Rev.* 2004 Aug;200:132-41.
181. Ito K, Barnes PJ. COPD as a disease of accelerated lung aging. *Chest.* 2009 Jan;135(1):173-180.
182. Mercado N, Ito K, Barnes PJ. Accelerated ageing of the lung in COPD: new concepts. *Thorax.* 2015 May;70(5):482-9.
183. Barnes PJ, Baker J, Donnelly LE. Cellular Senescence as a Mechanism and Target in Chronic Lung Diseases. *Am J Respir Crit Care Med.* 2019 Sep 1;200(5):556-564.
184. Fulop T, Larbi A, Dupuis G, et al. Immunosenescence and Inflamm-Aging As Two Sides of the Same Coin: Friends or Foes? *Front Immunol.* 2017;8:1960.
185. Yang J, Liu M, Hong D, et al. The Paradoxical Role of Cellular Senescence in Cancer. *Front Cell Dev Biol.* 2021;9:722205.
186. Laberge RM, Awad P, Campisi J, et al. Epithelial-mesenchymal transition induced by senescent fibroblasts. *Cancer Microenviron.* 2012 Apr;5(1):39-44.
187. Salvato I, Ricciardi L, Nucera F, Nigro A, Dal Col J, Monaco F, Caramori G, Stellato C. RNA-binding proteins as a molecular link between COPD and lung cancer. *COPD.* 2022. *In press.*
188. Agustí A, Hogg JC. Update on the Pathogenesis of Chronic Obstructive Pulmonary Disease. *N Engl J Med.* 2019 Sep 26;381(13):1248-1256.
189. Savale L, Chaouat A, Bastuji-Garin S, et al. Shortened telomeres in circulating leukocytes of patients with chronic obstructive pulmonary disease. *Am J Respir Crit Care Med.* 2009 Apr 1;179(7):566-71.
190. Córdoba-Lanús E, Cazorla-Rivero S, Espinoza-Jiménez A, et al. Telomere shortening and accelerated aging in COPD: findings from the BODE cohort. *Respir Res.* 2017 Apr 13;18(1):59.

191. Birch J, Anderson RK, Correia-Melo C, et al. DNA damage response at telomeres contributes to lung aging and chronic obstructive pulmonary disease. *Am J Physiol Lung Cell Mol Physiol*. 2015 Nov 15;309(10):L1124-37.
192. Nakamaru Y, Vuppusetty C, Wada H, et al. A protein deacetylase SIRT1 is a negative regulator of metalloproteinase-9. *Faseb j*. 2009 Sep;23(9):2810-9.
193. Cloonan SM, Kim K, Esteves P, et al. Mitochondrial dysfunction in lung ageing and disease. *Eur Respir Rev*. 2020 Sep 30;29(157).
194. Chen R, Zhang K, Chen H, et al. Telomerase Deficiency Causes Alveolar Stem Cell Senescence-associated Low-grade Inflammation in Lungs. *J Biol Chem*. 2015 Dec 25;290(52):30813-29.
195. Johnson SC, Rabinovitch PS, Kaeberlein M. mTOR is a key modulator of ageing and age-related disease. *Nature*. 2013 Jan 17;493(7432):338-45.
196. Liu GY, Sabatini DM. mTOR at the nexus of nutrition, growth, ageing and disease. *Nat Rev Mol Cell Biol*. 2020 Apr;21(4):183-203.
197. Houssaini A, Breau M, Kebe K, et al. mTOR pathway activation drives lung cell senescence and emphysema. *JCI Insight*. 2018 Feb 8;3(3).
198. Ricciardi L, Giurato G, Memoli D, et al. Posttranscriptional Gene Regulatory Networks in Chronic Airway Inflammatory Diseases: In silico Mapping of RNA-Binding Protein Expression in Airway Epithelium. *Front Immunol*. 2020;11:579889.
199. Herranz N, Gallage S, Mellone M, et al. mTOR regulates MAPKAPK2 translation to control the senescence-associated secretory phenotype. *Nat Cell Biol*. 2015 Sep;17(9):1205-17.
200. Graham JR, Hendershott MC, Terragni J, et al. mRNA degradation plays a significant role in the program of gene expression regulated by phosphatidylinositol 3-kinase signaling. *Mol Cell Biol*. 2010 Nov;30(22):5295-305.
201. Barnes PJ. Inflammatory mechanisms in patients with chronic obstructive pulmonary disease. *J Allergy Clin Immunol*. 2016 Jul;138(1):16-27.
202. Barnes PJ. Inflammatory endotypes in COPD. *Allergy*. 2019 Jul;74(7):1249-1256.
203. Gao W, Li L, Wang Y, et al. Bronchial epithelial cells: The key effector cells in the pathogenesis of chronic obstructive pulmonary disease? *Respirology*. 2015 Jul;20(5):722-9.

204. Russell RE, Thorley A, Culpitt SV, et al. Alveolar macrophage-mediated elastolysis: roles of matrix metalloproteinases, cysteine, and serine proteases. *Am J Physiol Lung Cell Mol Physiol*. 2002 Oct;283(4):L867-73.
205. Sapey E, Stockley JA, Greenwood H, et al. Behavioral and structural differences in migrating peripheral neutrophils from patients with chronic obstructive pulmonary disease. *Am J Respir Crit Care Med*. 2011 May 1;183(9):1176-86.
206. Grumelli S, Corry DB, Song LZ, et al. An immune basis for lung parenchymal destruction in chronic obstructive pulmonary disease and emphysema. *PLoS Med*. 2004 Oct;1(1):e8.
207. Costa C, Rufino R, Traves SL, et al. CXCR3 and CCR5 chemokines in induced sputum from patients with COPD. *Chest*. 2008 Jan;133(1):26-33.
208. Di Stefano A, Caramori G, Gnemmi I, et al. T helper type 17-related cytokine expression is increased in the bronchial mucosa of stable chronic obstructive pulmonary disease patients. *Clin Exp Immunol*. 2009 Aug;157(2):316-24.
209. Kumar M, Seeger W, Voswinckel R. Senescence-associated secretory phenotype and its possible role in chronic obstructive pulmonary disease. *Am J Respir Cell Mol Biol*. 2014 Sep;51(3):323-33.
210. Caramori G, Casolari P, Adcock I. Role of transcription factors in the pathogenesis of asthma and COPD. *Cell Commun Adhes*. 2013 Feb;20(1-2):21-40.
211. Di Stefano A, Caramori G, Oates T, et al. Increased expression of nuclear factor-kappaB in bronchial biopsies from smokers and patients with COPD. *Eur Respir J*. 2002 Sep;20(3):556-63.
212. Bucchioni E, Kharitonov SA, Allegra L, et al. High levels of interleukin-6 in the exhaled breath condensate of patients with COPD. *Respir Med*. 2003 Dec;97(12):1299-302.
213. Di Stefano A, Caramori G, Barczyk A, et al. Innate immunity but not NLRP3 inflammasome activation correlates with severity of stable COPD. *Thorax*. 2014 Jun;69(6):516-24.
214. Bradford E, Jacobson S, Varasteh J, et al. The value of blood cytokines and chemokines in assessing COPD. *Respir Res*. 2017 Oct 24;18(1):180.
215. de Boer WI, Sont JK, van Schadewijk A, et al. Monocyte chemoattractant protein 1, interleukin 8, and chronic airways inflammation in COPD. *J Pathol*. 2000 Apr;190(5):619-26.

216. Traves SL, Culpitt SV, Russell RE, et al. Increased levels of the chemokines GRO α and MCP-1 in sputum samples from patients with COPD. *Thorax*. 2002 Jul;57(7):590-5.
217. Caramori G, Di Stefano A, Casolari P, et al. Chemokines and chemokine receptors blockers as new drugs for the treatment of chronic obstructive pulmonary disease. *Curr Med Chem*. 2013;20(35):4317-49.
218. Anderson P. Post-transcriptional control of cytokine production. *Nat Immunol*. 2008 Apr;9(4):353-9.
219. Hamilton T, Novotny M, Pavicic PJ, Jr., et al. Diversity in post-transcriptional control of neutrophil chemoattractant cytokine gene expression. *Cytokine*. 2010 Oct-Nov;52(1-2):116-22.
220. Patino WD, Kang JG, Matoba S, et al. Atherosclerotic plaque macrophage transcriptional regulators are expressed in blood and modulated by tristetraprolin. *Circ Res*. 2006 May 26;98(10):1282-9.
221. Al-Haj L, Blackshear PJ, Khabar KS. Regulation of p21/CIP1/WAF-1 mediated cell-cycle arrest by RNase L and tristetraprolin, and involvement of AU-rich elements. *Nucleic Acids Res*. 2012 Sep;40(16):7739-52.
222. Chang N, Yi J, Guo G, et al. HuR uses AUF1 as a cofactor to promote p16INK4 mRNA decay. *Mol Cell Biol*. 2010 Aug;30(15):3875-86.
223. Pang L, Tian H, Chang N, et al. Loss of CARM1 is linked to reduced HuR function in replicative senescence. *BMC Mol Biol*. 2013 Jul 9;14:15.
224. Wang W, Martindale JL, Yang X, et al. Increased stability of the p16 mRNA with replicative senescence. *EMBO Rep*. 2005 Feb;6(2):158-64.
225. Zhou H, Jarujaron S, Gurley EC, et al. HIV protease inhibitors increase TNF- α and IL-6 expression in macrophages: involvement of the RNA-binding protein HuR. *Atherosclerosis*. 2007 Nov;195(1):e134-43.
226. Spooren A, Mestdagh P, Rondou P, et al. IL-1 β potently stabilizes IL-6 mRNA in human astrocytes. *Biochem Pharmacol*. 2011 Apr 15;81(8):1004-15.
227. Ouhara K, Munenaga S, Kajiya M, et al. The induced RNA-binding protein, HuR, targets 3'-UTR region of IL-6 mRNA and enhances its stabilization in periodontitis. *Clin Exp Immunol*. 2018 Jun;192(3):325-336.

228. Patil CS, Liu M, Zhao W, et al. Targeting mRNA stability arrests inflammatory bone loss. *Mol Ther*. 2008 Oct;16(10):1657-64.
229. Van Tubergen E, Vander Broek R, Lee J, et al. Tristetraprolin regulates interleukin-6, which is correlated with tumor progression in patients with head and neck squamous cell carcinoma. *Cancer*. 2011 Jun 15;117(12):2677-89.
230. Zhao W, Liu M, D'Silva NJ, et al. Tristetraprolin regulates interleukin-6 expression through p38 MAPK-dependent affinity changes with mRNA 3' untranslated region. *J Interferon Cytokine Res*. 2011 Aug;31(8):629-37.
231. Dean JL, Wait R, Mahtani KR, et al. The 3' untranslated region of tumor necrosis factor alpha mRNA is a target of the mRNA-stabilizing factor HuR. *Mol Cell Biol*. 2001 Feb;21(3):721-30.
232. Deleault KM, Skinner SJ, Brooks SA. Tristetraprolin regulates TNF TNF-alpha mRNA stability via a proteasome dependent mechanism involving the combined action of the ERK and p38 pathways. *Mol Immunol*. 2008 Jan;45(1):13-24.
233. Sadri N, Schneider RJ. *Auf1/Hnnpd*-deficient mice develop pruritic inflammatory skin disease. *J Invest Dermatol*. 2009 Mar;129(3):657-70.
234. Li M, Yang J, Liu K, et al. p16 promotes proliferation in cervical carcinoma cells through CDK6-HuR-IL1A axis. *J Cancer*. 2020;11(6):1457-1467.
235. Sneezum L, Eismayr K, Dworak H, et al. Context-Dependent IL-1 mRNA-Destabilization by TTP Prevents Dysregulation of Immune Homeostasis Under Steady State Conditions. *Front Immunol*. 2020;11:1398.
236. Chen YL, Huang YL, Lin NY, et al. Differential regulation of ARE-mediated TNFalpha and IL-1beta mRNA stability by lipopolysaccharide in RAW264.7 cells. *Biochem Biophys Res Commun*. 2006 Jul 21;346(1):160-8.
237. Fan J, Ishmael FT, Fang X, et al. Chemokine transcripts as targets of the RNA-binding protein HuR in human airway epithelium. *J Immunol*. 2011 Feb 15;186(4):2482-94.
238. Ishmael FT, Fang X, Galdiero MR, et al. Role of the RNA-binding protein tristetraprolin in glucocorticoid-mediated gene regulation. *J Immunol*. 2008 Jun 15;180(12):8342-53.
239. Hintzen C, Haan C, Tuckermann JP, et al. Oncostatin M-induced and constitutive activation of the JAK2/STAT5/CIS pathway suppresses CCL1, but not CCL7 and CCL8, chemokine expression. *J Immunol*. 2008 Nov 15;181(10):7341-9.

240. Datta S, Biswas R, Novotny M, et al. Tristetraprolin regulates CXCL1 (KC) mRNA stability. *J Immunol*. 2008 Feb 15;180(4):2545-52.
241. Qiu LQ, Lai WS, Bradbury A, et al. Tristetraprolin (TTP) coordinately regulates primary and secondary cellular responses to proinflammatory stimuli. *J Leukoc Biol*. 2015 Apr;97(4):723-36.
242. Kratochvill F, Machacek C, Vogl C, et al. Tristetraprolin-driven regulatory circuit controls quality and timing of mRNA decay in inflammation. *Mol Syst Biol*. 2011 Dec 20;7:560.
243. Wang S, Zhang J, Zhang Y, et al. Nitric oxide-p38 MAPK signaling stabilizes mRNA through AU-rich element-dependent and -independent mechanisms. *J Leukoc Biol*. 2008 Apr;83(4):982-90.
244. Hudy MH, Proud D. Cigarette smoke enhances human rhinovirus-induced CXCL8 production via HuR-mediated mRNA stabilization in human airway epithelial cells. *Respir Res*. 2013 Aug 30;14(1):88.
245. Suswam E, Li Y, Zhang X, et al. Tristetraprolin down-regulates interleukin-8 and vascular endothelial growth factor in malignant glioma cells. *Cancer Res*. 2008 Feb 1;68(3):674-82.
246. Bourcier C, Griseri P, Grépin R, et al. Constitutive ERK activity induces downregulation of tristetraprolin, a major protein controlling interleukin8/CXCL8 mRNA stability in melanoma cells. *Am J Physiol Cell Physiol*. 2011 Sep;301(3):C609-18.
247. Jimbo M, Blanco FF, Huang YH, et al. Targeting the mRNA-binding protein HuR impairs malignant characteristics of pancreatic ductal adenocarcinoma cells. *Oncotarget*. 2015 Sep 29;6(29):27312-31.
248. Liu H, Lan T, Li H, et al. Circular RNA circDLC1 inhibits MMP1-mediated liver cancer progression via interaction with HuR. *Theranostics*. 2021;11(3):1396-1411.
249. Van Tubergen EA, Banerjee R, Liu M, et al. Inactivation or loss of TTP promotes invasion in head and neck cancer via transcript stabilization and secretion of MMP9, MMP2, and IL-6. *Clin Cancer Res*. 2013 Mar 1;19(5):1169-79.
250. Chenette DM, Cadwallader AB, Antwine TL, et al. Targeted mRNA Decay by RNA Binding Protein AUF1 Regulates Adult Muscle Stem Cell Fate, Promoting Skeletal Muscle Integrity. *Cell Rep*. 2016 Aug 2;16(5):1379-1390.
251. Yiakouvaki A, Dimitriou M, Karakasiliotis I, et al. Myeloid cell expression of the RNA-binding protein HuR protects mice from pathologic inflammation and colorectal carcinogenesis. *J Clin Invest*. 2012 Jan;122(1):48-61.

252. Brennan SE, Kuwano Y, Alkharouf N, et al. The mRNA-destabilizing protein tristetraprolin is suppressed in many cancers, altering tumorigenic phenotypes and patient prognosis. *Cancer Res.* 2009 Jun 15;69(12):5168-76.
253. Fellows A, Griffin ME, Petrella BL, et al. AUF1/hnRNP D represses expression of VEGF in macrophages. *Mol Biol Cell.* 2012 Apr;23(8):1414-22.
254. Doller A, Gauer S, Sobkowiak E, et al. Angiotensin II induces renal plasminogen activator inhibitor-1 and cyclooxygenase-2 expression post-transcriptionally via activation of the mRNA-stabilizing factor human-antigen R. *Am J Pathol.* 2009 Apr;174(4):1252-63.
255. Yu H, Stasinopoulos S, Leedman P, et al. Inherent instability of plasminogen activator inhibitor type 2 mRNA is regulated by tristetraprolin. *J Biol Chem.* 2003 Apr 18;278(16):13912-8.
256. Liu S, Zhan Y, Luo J, et al. Roles of exosomes in the carcinogenesis and clinical therapy of non-small cell lung cancer. *Biomed Pharmacother.* 2019 Mar;111:338-346.
257. van Niel G, D'Angelo G, Raposo G. Shedding light on the cell biology of extracellular vesicles. *Nat Rev Mol Cell Biol.* 2018 Apr;19(4):213-228.
258. Zhang Y, Liu Y, Liu H, et al. Exosomes: biogenesis, biologic function and clinical potential. *Cell Biosci.* 2019;9:19.
259. Kulshreshtha A, Ahmad T, Agrawal A, et al. Proinflammatory role of epithelial cell-derived exosomes in allergic airway inflammation. *J Allergy Clin Immunol.* 2013 Apr;131(4):1194-203, 1203.e1-14.
260. Kesimer M, Scull M, Brighton B, et al. Characterization of exosome-like vesicles released from human tracheobronchial ciliated epithelium: a possible role in innate defense. *Faseb j.* 2009 Jun;23(6):1858-68.
261. Beninson LA, Fleshner M. Exosomes: an emerging factor in stress-induced immunomodulation. *Semin Immunol.* 2014 Oct;26(5):394-401.
262. Takasugi M, Okada R, Takahashi A, et al. Small extracellular vesicles secreted from senescent cells promote cancer cell proliferation through EphA2. *Nat Commun.* 2017 Jun 6;8:15729.
263. Pasquale EB. Eph receptors and ephrins in cancer: bidirectional signalling and beyond. *Nat Rev Cancer.* 2010 Mar;10(3):165-80.

264. Mensà E, Guescini M, Giuliani A, et al. Small extracellular vesicles deliver miR-21 and miR-217 as pro-senescence effectors to endothelial cells. *J Extracell Vesicles*. 2020;9(1):1725285.
265. Fujita Y, Araya J, Ito S, et al. Suppression of autophagy by extracellular vesicles promotes myofibroblast differentiation in COPD pathogenesis. *J Extracell Vesicles*. 2015;4:28388.
266. Tan DBA, Armitage J, Teo TH, et al. Elevated levels of circulating exosome in COPD patients are associated with systemic inflammation. *Respir Med*. 2017 Nov;132:261-264.
267. Liu Z, Yan J, Tong L, et al. The role of exosomes from BALF in lung disease. *J Cell Physiol*. 2022 Jan;237(1):161-168.
268. O'Brien K, Breyne K, Ughetto S, et al. RNA delivery by extracellular vesicles in mammalian cells and its applications. *Nat Rev Mol Cell Biol*. 2020 Oct;21(10):585-606.
269. Statello L, Maugeri M, Garre E, et al. Identification of RNA-binding proteins in exosomes capable of interacting with different types of RNA: RBP-facilitated transport of RNAs into exosomes. *PLoS One*. 2018;13(4):e0195969.
270. Vestbo J, Decramer M. Reply: Comorbidities and chronic obstructive pulmonary disease: is there a place for lung fibrosis? *Am J Respir Crit Care Med*. 2013 Dec 1;188(11):1368.
271. Szalontai K, Gémes N, Furák J, et al. Chronic Obstructive Pulmonary Disease: Epidemiology, Biomarkers, and Paving the Way to Lung Cancer. *J Clin Med*. 2021 Jun 29;10(13).
272. Stockley RA, Halpin DMG, Celli BR, et al. Chronic Obstructive Pulmonary Disease Biomarkers and Their Interpretation. *Am J Respir Crit Care Med*. 2019 May 15;199(10):1195-1204.
273. Shaw JG, Vaughan A, Dent AG, et al. Biomarkers of progression of chronic obstructive pulmonary disease (COPD). *J Thorac Dis*. 2014 Nov;6(11):1532-47.
274. Paone G, Conti V, Vestri A, et al. Analysis of sputum markers in the evaluation of lung inflammation and functional impairment in symptomatic smokers and COPD patients. *Dis Markers*. 2011;31(2):91-100.
275. Koutsokera A, Kostikas K, Nicod LP, et al. Pulmonary biomarkers in COPD exacerbations: a systematic review. *Respir Res*. 2013 Oct 21;14(1):111.
276. Kelly E, Owen CA, Pinto-Plata V, et al. The role of systemic inflammatory biomarkers to predict mortality in chronic obstructive pulmonary disease. *Expert Rev Respir Med*. 2013 Feb;7(1):57-64.

277. Walters JA, Tang JN, Poole P, et al. Pneumococcal vaccines for preventing pneumonia in chronic obstructive pulmonary disease. *Cochrane Database Syst Rev*. 2017 Jan 24;1(1):Cd001390.
278. Singh D, Mathioudakis AG, Higham A. Chronic obstructive pulmonary disease and COVID-19: interrelationships. *Curr Opin Pulm Med*. 2022 Mar 1;28(2):76-83.
279. Spruit MA, Pitta F, McAuley E, et al. Pulmonary Rehabilitation and Physical Activity in Patients with Chronic Obstructive Pulmonary Disease. *Am J Respir Crit Care Med*. 2015 Oct 15;192(8):924-33.
280. Stefan MS, Fisher KA, Lindenauer PK. Does Adherence to GOLD Recommendations Regarding Inhaler Therapy Lead to Better Patient Outcomes?: Insights from the LOTT Trial. *Chest*. 2020 Aug;158(2):437-439.
281. Nannini LJ, Lasserson TJ, Poole P. Combined corticosteroid and long-acting beta(2)-agonist in one inhaler versus long-acting beta(2)-agonists for chronic obstructive pulmonary disease. *Cochrane Database Syst Rev*. 2012 Sep 12;2012(9):Cd006829.
282. Dransfield MT, Bourbeau J, Jones PW, et al. Once-daily inhaled fluticasone furoate and vilanterol versus vilanterol only for prevention of exacerbations of COPD: two replicate double-blind, parallel-group, randomised controlled trials. *Lancet Respir Med*. 2013 May;1(3):210-23.
283. Festic E, Scanlon PD. Incident pneumonia and mortality in patients with chronic obstructive pulmonary disease. A double effect of inhaled corticosteroids? *Am J Respir Crit Care Med*. 2015 Jan 15;191(2):141-8.
284. Lo Bello F, Hansbro PM, Donovan C, et al. New drugs under development for COPD. *Expert Opin Emerg Drugs*. 2020 Dec;25(4):419-431.
285. Ricciardi L, Col JD, Casolari P, et al. Differential expression of RNA-binding proteins in bronchial epithelium of stable COPD patients. *Int J Chron Obstruct Pulmon Dis*. 2018;13:3173-3190.
286. JR B, C V, K I, et al. RNA-binding protein HuR inhibits the expression of sirtuin-1 in patients with COPD. *European Respiratory Journal*; 2017
287. Skerrett-Byrne DA, Bromfield EG, Murray HC, et al. Time-resolved proteomic profiling of cigarette smoke-induced experimental chronic obstructive pulmonary disease. *Respirology*. 2021 Oct;26(10):960-973.

288. Spurrell JC, Wiehler S, Zaheer RS, et al. Human airway epithelial cells produce IP-10 (CXCL10) in vitro and in vivo upon rhinovirus infection. *Am J Physiol Lung Cell Mol Physiol*. 2005 Jul;289(1):L85-95.
289. Navratilova Z, Novosadova E, Hagemann-Jensen M, et al. Expression Profile of Six RNA-Binding Proteins in Pulmonary Sarcoidosis. *PLoS One*. 2016;11(8):e0161669.
290. P W. Inhibition of RNA-binding proteins with small molecules. Vol. 4. *Nature Reviews Chemistry*; 2020.
291. Angelbello AJ, Chen JL, Childs-Disney JL, et al. Using Genome Sequence to Enable the Design of Medicines and Chemical Probes. *Chem Rev*. 2018 Feb 28;118(4):1599-1663.
292. Childs-Disney JL, Yang X, Gibaut QMR, et al. Targeting RNA structures with small molecules. *Nat Rev Drug Discov*. 2022 Aug 8:1-27.
293. Crooke ST, Witztum JL, Bennett CF, et al. RNA-Targeted Therapeutics. *Cell Metab*. 2018 Apr 3;27(4):714-739.
294. Li J, Matsumoto J, Bai LP, et al. A Ligand That Targets CUG Trinucleotide Repeats. *Chemistry*. 2016 Oct 10;22(42):14881-14889.
295. Mukherjee S, Błaszczyk L, Rypniewski W, et al. Structural insights into synthetic ligands targeting A-A pairs in disease-related CAG RNA repeats. *Nucleic Acids Res*. 2019 Nov 18;47(20):10906-10913.
296. Mohibi S, Chen X, Zhang J. Cancer the'RBP'eutics-RNA-binding proteins as therapeutic targets for cancer. *Pharmacol Ther*. 2019 Nov;203:107390.
297. Meisner NC, Hintersteiner M, Mueller K, et al. Identification and mechanistic characterization of low-molecular-weight inhibitors for HuR. *Nat Chem Biol*. 2007 Aug;3(8):508-15.
298. Peng W. Inhibition of RNA-binding proteins with small molecules. *Nature Reviews Chemistry*2020. p. 441–458.
299. Kondaskar A, Kondaskar S, Kumar R, et al. Novel, Broad Spectrum Anti-Cancer Agents Containing the Tricyclic 5:7:5-Fused Diimidazodiazepine Ring System. *ACS Med Chem Lett*. 2010 Dec 31;2(3):252-256.
300. Clingman CC, Deveau LM, Hay SA, et al. Allosteric inhibition of a stem cell RNA-binding protein by an intermediary metabolite. *Elife*. 2014 Jun 16;3.

301. Abdelmohsen K, Panda AC, Munk R, et al. Identification of HuR target circular RNAs uncovers suppression of PABPN1 translation by CircPABPN1. *RNA Biol.* 2017 Mar 4;14(3):361-369.
302. Raguraman R, Shanmugarama S, Mehta M, et al. Drug delivery approaches for HuR-targeted therapy for lung cancer. *Adv Drug Deliv Rev.* 2022 Jan;180:114068.
303. Amreddy N, Babu A, Panneerselvam J, et al. Chemo-biologic combinatorial drug delivery using folate receptor-targeted dendrimer nanoparticles for lung cancer treatment. *Nanomedicine.* 2018 Feb;14(2):373-384.
304. Muralidharan R, Babu A, Amreddy N, et al. Tumor-targeted Nanoparticle Delivery of HuR siRNA Inhibits Lung Tumor Growth In Vitro and In Vivo By Disrupting the Oncogenic Activity of the RNA-binding Protein HuR. *Mol Cancer Ther.* 2017 Aug;16(8):1470-1486.
305. Klyachko NL, Arzt CJ, Li SM, et al. Extracellular Vesicle-Based Therapeutics: Preclinical and Clinical Investigations. *Pharmaceutics.* 2020 Dec 1;12(12).
306. Cianferoni A, Schroeder JT, Kim J, et al. Selective inhibition of interleukin-4 gene expression in human T cells by aspirin. *Blood.* 2001 Mar 15;97(6):1742-9.
307. Yu SY, Ip MS, Li X, et al. Low-dose aspirin and incidence of lung carcinoma in patients with chronic obstructive pulmonary disease in Hong Kong: A cohort study. *PLoS Med.* 2022 Jan;19(1):e1003880.
308. Blanco FF, Preet R, Aguado A, et al. Impact of HuR inhibition by the small molecule MS-444 on colorectal cancer cell tumorigenesis. *Oncotarget.* 2016 Nov 8;7(45):74043-74058.
309. Zhou L, Gu W, Kui F, et al. The mechanism and candidate compounds of aged citrus peel (chenpi) preventing chronic obstructive pulmonary disease and its progression to lung cancer. *Food Nutr Res.* 2021;65.
310. Eggert M, Michel J, Schneider S, et al. The glucocorticoid receptor is associated with the RNA-binding nuclear matrix protein hnRNP U. *J Biol Chem.* 1997 Nov 7;272(45):28471-8.
311. Ishmael FT, Fang X, Houser KR, et al. The human glucocorticoid receptor as an RNA-binding protein: global analysis of glucocorticoid receptor-associated transcripts and identification of a target RNA motif. *J Immunol.* 2011 Jan 15;186(2):1189-98.

312. Subramaniam K, Kandasamy K, Joseph K, et al. The 3'-untranslated region length and AU-rich RNA location modulate RNA-protein interaction and translational control of β 2-adrenergic receptor mRNA. *Mol Cell Biochem.* 2011 Jun;352(1-2):125-41.
313. Blaxall BC, Port JD. Determination of mRNA stability and characterization of proteins interacting with adrenergic receptor mRNAs. *Methods Mol Biol.* 2000;126:453-65.
314. Blaxall BC, Pellett AC, Wu SC, et al. Purification and characterization of beta-adrenergic receptor mRNA-binding proteins. *J Biol Chem.* 2000 Feb 11;275(6):4290-7.

Part 2.

PhD Research plan:

***Characterization of the RNA-binding protein AUF-1
in airway epithelial inflammatory responses***

1. General Aim and Specific Study of the PhD project

The general aim of this thesis is to study the role of the RBP AUF-1 in human airway epithelium as determinant of inflammation and accelerated cellular senescence in COPD pathogenesis.

Based on our previous evidence of the selective decrease of AUF-1 in the bronchiolar epithelium of patients with stable COPD, in the specific study of the PhD project we focused on the biology of AUF-1 using the *in vitro* model of airway epithelial cell lines BEAS-2B and HSAEC.

First, using AUF-1 immunoprecipitation coupled with high-throughput sequencing, we defined epithelial AUF-1 mRNA targets and identified their binding interface. Then, we characterized the functional role of AUF-1 association on a selected sample of the newly identified regulated transcripts. Finally, we investigated the mechanisms inducing AUF-1 protein loss upon inflammatory stimulus.

All data presented in this thesis are in the final stages of preparation of an original manuscript:

Characterization of the RNA-binding protein AUF-1 in airway epithelial inflammatory responses

Ilaria Salvato, Luca Ricciardi, Annunziata Nigro, Giorgio Giurato, Domenico Memoli, Assunta Sellitto, Maria Assunta Crescenzi, Monica Vitale, Francesco Nucera, Paola Brun, Federico Caicci, Leandro Castellano, Jessica Dal Col, Ian Adcock, Gaetano Caramori, Cristiana Stellato.

1.1. Specific study

Characterization of the RNA-binding protein AUF-1 in airway epithelial inflammatory responses

Abstract

The RNA-binding protein (RBP) AU-rich element factor 1 (AUF-1) is a regulator of inflammation and cellular senescence through modulation of mRNA decay rates and translation via binding to sequences enriched within the 3'untranslated region (UTR) of targeted mRNAs. Loss of AUF-1 expression was previously documented in airway epithelium of patients with stable chronic obstructive pulmonary disease (COPD) compared to matched smoker controls, and in cytokine-and cigarette smoke-challenged human epithelial cells. By identifying AUF-1-targeted transcripts, investigating its function and the mechanism of its loss, we seeked understanding of AUF-1 role in the epithelial response contributing to inflammation and accelerated cellular senescence in COPD. RNA immunoprecipitation-sequencing (RIP-Seq) analysis identified 494 AUF-1-bound mRNAs in cytoplasmic lysates of unstimulated human airway BEAS-2B cell line, enriched in their 3'UTR for a Guanosine-Cytosine (GC)-rich binding motif. AUF-1 association to selected transcripts and to a synthetic transcript modeling the GC-rich motif was validated by biotin pulldown. Steady-state levels of AUF-1 targets evaluated by qRT-PCR were equally affected by partial or near-total loss of AUF-1 induced by cytomix and by siRNA approach, respectively; however, mRNA decay rates were differentially affected by changes in AUF-1 levels. Cytomix-induced decreased levels of AUF-1 in BEAS-2B and human small airways epithelial cells (HSAEC) associated with accelerated cell senescence readouts of lysosomal damage, cell cycle arrest and secretion of Senescence-Associated Secretory Phenotype (SASP) factors. Cytomix-induced loss of intracellular AUF-1 was mirrored in both cell types by stimulus-dependent increase into extracellular vesicles. Genome ontology revealed significant enrichment of AUF-1 targets within critical COPD-related pathways. AUF-1 targets were also identified *ex vivo* as differentially expressed genes in transcriptomic databases of HSAEC and lung tissue samples from stable COPD patients versus age/smoking history-matched control subjects, as well as within the human SASP proteome atlas. These data suggest that AUF-1 loss triggered by inflammatory stimuli can participate to the epithelial-derived inflammaging response through intracellular and exosomal-driven functions.

Introduction

RNA-binding proteins (RBPs) participate in post-transcriptional gene regulation (PTGR) mediating the processing, transport and cytoplasmic fate of mRNAs. Among their multiple tasks, RBPs regulate transcript stability and translation, largely by recognizing *cis*-elements that are mostly present on the 3'-Untranslated Region (3'-UTR) on mRNAs targets and forming ribonucleoprotein complex (mRNPs) along with other regulatory proteins and RNA species (miRNA, lncRNAs). Through context-driven interplay in levels and activation of mRNP partners, PTGR actions ultimately determine and adapt the rate of protein output in fundamental processes like cell cycle, proliferation and stress responses [1-5]. Alteration of these events, for example through changes in RNP composition favouring aberrant mRNA stabilization and/or increased translation rate, participates to development or persistence of cancer and other pathological conditions [6-10]. A crucial role of RBPs in this setting is also supported, largely by preclinical evidence, in regulation of immune and inflammatory responses. These events are finely coordinated through the rapid turnover of mRNAs of pathogenic cytokines, chemokines and other mediators. Their degradation and/or translational repression promotes the physiologic resolution of inflammatory reactions, preventing an excessive inflammatory response [11], as confirmed by preclinical evidence and animal models in which altered RBP expression and functions convey overexpressed immune and inflammatory responses [12]. Current understanding of RBP participation in the pathogenesis of human chronic inflammatory diseases is still largely incomplete, yet understanding of their role could uncover potential targeting, as in cancer. A leading cause of morbidity and mortality worldwide, chronic obstructive pulmonary disease (COPD) is a lung disease characterized by destruction of lung parenchyma leading to pulmonary emphysema, inflammation and remodeling of the peripheral and central airways (www.goldcopd.org). Hampered by the lacking of effective therapies able to reduce disease progression and a partial understanding of molecular mechanisms underlying disease pathology, COPD, which affects over 350 million people globally, with 44 million cases in Europe alone, harbours multiple pathogenic features in which RBP-mediated function could be involved.

The chronic inflammatory response present in the lungs of COPD patients is triggered, on a complex basis of genetic and epigenetic factors, by chronic exposure to environmental noxious stimuli, chiefly cigarette smoking. The increased burden in oxidative stress in the airways and in the distal lung drives DNA damage and accelerated cellular senescence, a condition characterized by cell cycle arrest along with continued metabolic activity. Persistence of these conditions trigger a cellular Senescence-Associated Secretory Phenotype (SASP), in which transcriptomic and epigenetic changes drive a secretory pattern characterized by overexpression of cytokines, chemokines, growth factors [13] that is, in fact, largely represented in the inflammatory response in COPD [14]. RBPs mediate the PTGR

of numerous SASP mediators, including cytokines like interleukin (IL)-6 and IL-1 β , chemokines like chemokine (C-X-C motif) ligand 1 (CXCL8 or IL-8) and chemokine (C-C motif) ligand 2 (CCL2), and growth factors like transforming growth factor-(TGF)- β [12,15-17] and are recognized determinants of oxidative stress-mediated response and cellular senescence [18-20].

In a previous investigation of human disease-driven RBP expression patterns, we documented a selective loss of AUF-1 expression in the airway epithelium of patients with COPD compared to control smoking subjects, a finding also reproduced *in vitro* by challenge of the airway epithelial cell line BEAS-2B with cigarette smoke extract and cytomix [21]. We further identified *in silico* a global downregulation of a curated list of 600 RBPs in two transcriptomic databases from bronchiolar epithelium of COPD patients compared to matched control smokers with normal lung function. Downregulation involved clusters of co-regulated RBPs, one of them including AUF-1, and Genome Ontology analysis indicated significant impact on pathogenic COPD pathways [22], expanding the potential relevance of RBPs beyond a single player.

AUF-1, encoded by the Heteronuclear Ribonucleoprotein D (*HNRNPD*) gene belongs to a family of ubiquitously expressed proteins, functionally described chiefly as promoting decay of mRNA targets [6,23]. Four isoforms of AUF-1 (p45^{AUF-1}, p42^{AUF-1}, p40^{AUF-1}, p37^{AUF-1}) originate from a common precursor mRNA by the alternative splicing of exons 2 and 7, which determines their different molecular weight. Particularly, p45^{AUF-1} contains the entire AUF-1 coding sequence, p40^{AUF-1} and p42^{AUF-1} contain only exon 2 and exon 7, respectively, while p37^{AUF-1} isoform lacks both exons [24]. The smaller isoforms p37^{AUF-1} and p40^{AUF-1} contain a nuclear import signal (NIS) in their C-terminal domain and shuttle efficiently between the nucleus and cytoplasm. The insertion of exon 7-encoded amino acids in p42^{AUF-1} and p45^{AUF-1} isoforms disrupt the NIS, promoting their restriction to the nucleus [25-27].

Very relevant to COPD pathogenesis, mouse models of AUF-1 knockout indicate its critical involvement in both inflammatory responses - through post-transcriptional control of cytokines, chemokines and inflammatory mediators - and in mechanisms of cell senescence. Mouse model AUF-1^{-/-} are highly susceptible to endotoxin-induced septic shock with increased mortality due to an overexpressed inflammatory response, mediated by the lack of degradation of tumor necrosis factor (TNF)- α and IL-1 β mRNA mediated by AUF-1 [28]. This knockout model also develops spontaneously an age-dependent, chronic pruritic inflammatory skin dermatitis highly resembling atopic dermatitis, characterized by enhanced dermal infiltration of inflammatory cells, reduced wound healing and elevated serum IgE levels; in these animals, AUF-1^{-/-} T cells and macrophages have increased expression of inflammatory cytokines, such as IL-2, TNF - α , and IL-1 β [29]. Moreover, AUF-1 knockout mice displayed early-onset aging with increased telomere erosion and accelerated

cellular senescence. The mechanism underlying this phenotype was found to be complex, as AUF-1 acts as transcriptional regulator of the telomere subunit TERT but also exerts post-transcriptional control by destabilizing cell-cycle checkpoint mRNAs, such as cyclin-dependent kinase inhibitors p21^{WAP/CIP1}, contrasting senescence-induced cell cycle arrest [30]. Overall, mouse models lacking AUF-1 allowed to postulate, and in some cases to identify, the role of this RBP in numerous human diseases, such as breast cancer and melanoma [16].

Recent findings highlight the role of extracellular vesicles (EVs) as mediator of intercellular communication and disease pathogenesis [31]. EVs specificity is defined by their cargo (generally they include DNA, RNA, proteins and lipids [32] that is strictly related to the state and type of donor cell, resulting in a precise message carried to the recipient cell [33]. In lung microenvironment, EVs are secreted by both structural and immune cells, but the major producers are bronchial epithelial cells [34].

In COPD patients, EVs are involved in inflammatory responses, airway remodelling [35] and their release could be a mechanism to spread cellular senescence [36]. To this end, a large proteomic analysis of SASP profiles in different human cell types indicated that this secretory pattern is enriched for protein markers of human aging [37]. Recent evidence indicate that RBPs are present in EVs and could mediate target mRNAs and miRNA transferring into EVs [38,39]. RBPs role in EVs in the context of lung disease, like COPD, has never been explored.

Identification of a selective loss of AUF-1 in bronchiolar epithelium of stable COPD subjects prompted the present investigation on the identity of AUF-1 mRNA targets in airway epithelium and the relevance of AUF-1-dependent regulation in this context, along with the mechanism of decreased AUF-1 levels.

AUF-1-associated transcripts were identified by RNA immunoprecipitation and sequencing (RIP-Seq), validated to confirm AUF-1 association and to investigate the effect of AUF-1 loss on their expression profile and stability. To characterize accelerated aging and SASP induced by cytomix and test the role of AUF-1 in this process, we analysed beta-galactosidase expression, cell cycle markers and the release of SASP factors, as readouts of replicative/oxidative stress-induced senescence. Investigation of mechanisms mediating cytomix-induced AUF-1 loss led to identification of cytokine-induced transfer of AUF-1 into EVs released by airway epithelial cells. Collectively, the study points at AUF-1 stimulus-induced intracellular loss as a novel determinant of airway epithelial cell responses in inflammation and accelerated cellular aging, as well as to exosomal AUF-1, potentially spreading inflammation and senescence acting as cargo for bound transcripts to exosomes.

Material and Methods

Cell culture and treatment protocols. The SV40-immortalized human bronchial epithelial cell line BEAS-2B (ATCC) was cultured in DMEM/Ham's F12 (EuroClone) supplemented with 5% heat-inactivated FBS (EuroClone), 2 mM L-glutamine (Lonza), penicillin (100 U/ml), streptomycin (100 mg/ml) (Lonza) and 0.2% fungizone (EuroClone) [40]. Human small airway epithelial cells (HSAEC; PCS-301-010, ATCC) were cultured in Airway Epithelial Cell Basal Medium (PCS-300-030, ATCC) supplemented with Bronchial Epithelial Growth Kit (PCS-300-040, ATCC). Both cell lines were incubated at 37°C, 5% CO₂. For cell challenge protocols, cells were kept in medium only or stimulated using cytomix (10 nM each rHuIL-1 β , TNF α , IFN- γ , GoldBio) for 48 hours.

For exogenous changes in AUF-1 levels, BEAS-2B cells were transfected when reaching 50%–60% confluency using the nonliposomal cationic vehicle FuGENE HD (Promega) according to manufacturer's instructions: for AUF-1 silencing using 100 nM AUF-1 siRNA (5'-AAGAUC CUAUCACAGGGCGATdTdT-3') [41] or a scrambled control siRNA (5'-GAGUCAACCUUAUGAUACUdTdT-3'); after 48 hours, cells were exposed to cytomix or medium for additional 48 hours prior to cell harvesting.

For mRNA stability assay, resting and cytomix-treated cells were either harvested at 48 hours as time 0, for analysis of steady state levels or after 1, 2 and 4 hours of culture with the transcriptional inhibitor actinomycin D (3 μ g/ml ActD, Sigma).

In all experiments, cells were harvested using trypsin/EDTA (Lonza), counted and viability was verified with the Trypan Blue exclusion test (EuroClone). Cell viability was \geq 90% at harvest in all conditions.

For proteasome inhibition, BEAS-2B cells were treated with proteasome inhibitor MG-132 (Sigma) at the concentration of 10 μ M for 6 hours. After, the cell supernatant was replaced with fresh medium and the cells were harvested after 24, 30 and 48 hours.

RNA immunoprecipitation and sequencing (RIP-Seq) assay. RNA immunoprecipitation (RIP) is an antibody (Ab)-based technique developed to study the interaction between an RBP and its endogenous targets [42,43]. After generating cytosolic cell extracts under conditions that preserved the integrity of RNP complexes, the RBP of interest is immunoprecipitated with an RBP-specific Ab (and an isotype-matched, non-specific Ab as control) together with its associated RNA species. After RNA purification, bound transcripts (mRNAs and non-coding RNAs) are identified through sequencing.

Cytosolic fractions were collected after lysing BEAS-2B cells (10⁸ cells/conditions) with polysome lysis buffer, as described [42]. The buffer components were: 10 mM HEPES pH 7.0, 100 mM KCl,

5 mM MgCl₂, 0.5% NP40, 1 mM DTT, 100 U/ml RNase out, 400 μM Vanadyl-Ribonucleoside Complex, 1X Protease Inhibitors. An aliquot of cytosolic extract (10% of total) was taken as Input. For IP with anti-AUF-1 Ab (HPA004911, *Atlas Antibodies*), 2 mg of cytosolic extract were incubated at 4 °C overnight with 4 μg of antibody. For control IP, IgG isotype (02-6102, *Thermo Fisher Scientific*) was used at the same conditions. Then, 100 μl of pre-blocked magnetic beads (*Dynabeads, Thermofisher*) were added and the incubation was continued at 4 °C for 4 h.

Total RNA pools bound to AUF-1/control Ab were extracted adding TriFast reagent (*EuroClone*) directly to the washed beads, following the manufacturer's instructions. The size distribution of each RNA sample was assessed by running a 1 μl aliquot on an Agilent High Sensitivity RNA chip using an Agilent Technologies 2100 Bioanalyzer (*Agilent Technologies*). The concentration of each RNA sample was determined by using a Quant-IT RNA Assay Kit-High Sensitivity and a Qubit Fluorometer (*Life Technologies*).

Total RNA was used for the preparation of the sequencing library. Library preparation was performed as described [44]. Briefly, 1 μg of RNA Input and 300 ng of AUF-1- and Ctrl Ab-IP RNA were used as the starting material for sequencing library preparation from three independent experiments. Indexed triplicate libraries were prepared with a TruSeq Stranded Total RNA (*Illumina Inc.*). The quality of the libraries was evaluated by 2100 Bioanalyzer (*Agilent*) and Qubit dsDNA HS Assay Kit (*Thermo Fisher Scientific*). Libraries were sequenced at a concentration of 3 pM/lane (paired-end, 2 × 75 cycles) on a NextSeq 500 (*Illumina Inc.*).

Bioinformatic analysis was performed as described in Tarallo et al. [44]. In details, the quality of the sequenced reads was assessed by evaluating several factors, such as the quality score, the presence of k-mers, the balance of the GC percentage, using FastQC software Cutadapt software was used to remove the adapter sequences using default parameters. The Human transcriptome and genome (assembly hg38) was used as a reference for the alignment, which was performed using STAR version 2.7 (default parameters) [45].

RIP-Seq data analysis. Feature-count was used with default parameter to compute gene-level read counts [46]. Only the genes whose read count was ≥ 10 in at least one samples were considered for the further analysis. The R bioconductor package DESeq2 was used to test the differential expression of genes from RIP-Seq data, when compared to control. RNAs showing Enrichment Factor (EF) ≥ 1.5 and False Discovery Rate (FDR) ≤ 0.05 computed according to Benjamini–Hochberg were considered for further analysis. Transcript per million (TPM) was computed using RSEM [47]. Scatter plot and box plot were elaborated with R version 3.6.2 (<https://www.r-project.org/>).

Prediction of binding motifs. The p45^{AUF-1} sequence from NCBI was used for analysis with CatRAPID algorithm [48]. The list of coding and non-coding targets of AUF-1 protein was filtered considering a Discriminative Power (DP) ≥ 0.75 . Enrichment ratios for every transcript in each of RIP-Seq experiments were log transformed. Graphics visualization was elaborated with R version 3.6.2 (available at: <https://www.r-project.org/>). Prediction of binding motifs for AUF-1 were identified on 3'UTR sequences of experimental targets with Sequence & Structure Motif enrichment Analysis for Ranked RNA data generated from *in vivo* binding experiments (SMARTIV) [49,50], setting standard setting and Multiple Expectation maximizations for Motif Elicitation (MEME version 5.4.1), a position weight matrix-based tool for motif identification, using the following parameters: number of repetitions, any; minimum width for each motif: 5; maximum width for each motif: 35; and maximum number of motifs to be found: 20. Motifs with p-value ≤ 0.05 according to minimum hypergeometric statistical approach (mmHG) were considered significant.

Genome Ontology and pathway analyses. Gene Ontology (GO) was performed with Ingenuity Pathway Analysis (IPA) software [51]. Heatmaps and Pearson correlation matrices for correlated expression changes were generated using tMEV. GOPlot was used to visualize the Circos plot [52].

RNA extraction, cDNA synthesis and qRT-PCR. Total RNA was extracted using TriFast reagent (*EuroClone*) and reverse transcription was prepared using LunaScript® RT SuperMix Kit (*New England Biolabs*) following the manufacturer's protocol. Template complementary DNA (cDNA) was subjected to quantitative real-time PCR (qRT-PCR) with the FluoCycle II SYBR Master Mix (*Euroclone*) according to the manufacturer's protocol. Primers were published or designed with Primer-BLAST software (<https://www.ncbi.nlm.nih.gov/tools/primer-blast/>) and are listed in **Table 1**. Reactions were run in duplicate on a LightCycler 480 II (*Roche*), using the following setup: 5 minutes, 95°C; 15 seconds at 95°C, 45 cycles; 15 seconds, 60°C. Target expression was normalized to GAPDH by the cycle threshold (Ct) method and expressed using the $2^{-\Delta\Delta Ct}$ calculation as fold over control.

Table 1. Primers used for qPCR and biotin pulldown.

Primer	Sequence (5'-3')	
DDX17	Forward	GGATGTCTGCATGGAAAGTG
	Reverse	TCAGATCATCACAGCGTCTC
EGR1	Forward	CTTCAACCCTCAGGCGGACA
	Reverse	GGAAAAGCGGCCAGTATAGGT
FOXP4	Forward	CCAGGATGTTCGCCTATTTCG
	Reverse	TTTGCGGTCTCCGCTTCTGAT

GAPDH	Forward	TGCACCACCAACTGCTTAGC
	Reverse	GGCATGGACTGTGGTCATGAG
GLIS2	Forward	GGAGAACCTGAAGATCCACAACC
	Reverse	GCGTGTGCTTAAAGCGGTCACT
HDAC2	Forward	GCTATTCCAGAAGATGCTGTTC
	Reverse	GTTGCTGAGCTGTTCTGATTTG
IL-6	Forward	GTAGCCGCCCCACACAGA
	Reverse	CATGTCTCCTTTCTCAGGGCTG
MUC1	Forward	CTTTCTCCTGCTGCTGCTCCT
	Reverse	AGCCGAAGTCTCCTTTTCTCCA
TGF-β1	Forward	TACCTGAACCCGTGTTGCTCTC
	Reverse	GTTGCTGAGGTATCGCCAGGAA
CyclinD1-3'UTR	Forward (T7)	GTGAATTGTAATACGACTCACTATAGGGGCTGTTTACAATACC TCATGC
	Reverse	TGTGAGCTGGCTTCATTGAG
DDX17-3'UTR A	Forward (T7)	GTGAATTGTAATACGACTCACTATAGGGTCACGTAAATGAAACC ACTCAAG
	Reverse	TTCACAGATGGTCCCCAGTT
DDX17-3'UTR B	Forward (T7)	GTGAATTGTAATACGACTCACTATAGGGCATCTCAGCATCTGGG TGGAA
	Reverse	GAACCCCTCAGAAACCATCC
DDX17-3'UTR C	Forward (T7)	GTGAATTGTAATACGACTCACTATAGGGGCCTGAATGCTTGCTC ATCTG
	Reverse	ACAAGATGATGGTATCAAAGGACA
EGR1-3'UTR	Forward (T7)	GTGAATTGTAATACGACTCACTATAGGGAAGGGAAAGGGGAAA GAAAGG
	Reverse	TACACCACATATCCCATGGGCA
FoxP4-3'UTR A	Forward (T7)	GTGAATTGTAATACGACTCACTATAGGGAAGACAGGGACCTGG AGGAG
	Reverse	GGCGACAAAGGAAAAAGCCA
FoxP4-3'UTR B	Forward (T7)	GTGAATTGTAATACGACTCACTATAGGGCCGGAAGCAAAAACC AAAAC
	Reverse	TGTTTAAGCGTGGAAGGGACA
FoxP4-3'UTR C	Forward (T7)	GTGAATTGTAATACGACTCACTATAGGGAGTGGATGGAATGAG CAGCC
	Reverse	CCCCTGCTCCCCAAATACAC
FoxP4-3'UTR D	Forward (T7)	GTGAATTGTAATACGACTCACTATAGGGTTCTGGACACTCCCTC CTTGA
	Reverse	CCATTGTCCACAGATTACATGCAG
GLIS2-3'UTR A	Forward (T7)	GTGAATTGTAATACGACTCACTATAGGGTGGTGAAGTGGAGCCCA TCCT
	Reverse	GGAAGCAACGTGTCATGGGT
GLIS2-3'UTR B	Forward (T7)	GTGAATTGTAATACGACTCACTATAGGGAGTGCTGTGTTGGGAG CTTT
	Reverse	TTCTCTCCCATGGAGGAAT
HDAC2-3'UTR A	Forward (T7)	GTGAATTGTAATACGACTCACTATAGGGCCTGAATTTGACAGTC TCACCA
	Reverse	GCACATCTTAGTAGCAGGAGT
HDAC2-3'UTR B	Forward (T7)	GTGAATTGTAATACGACTCACTATAGGGCACTCAGAGCTTACAC TCAGAG
	Reverse	CAGTTGTTGTCCCAATTCCAC
HDAC2-3'UTR C	Forward (T7)	GTGGAATTGGGACAACAAC

	Reverse	GTGAATTGTAATACGACTCACTATAGGGCTGAGGCACAGAGGT TAGTAAT
HDAC2-3'UTR D	Forward (T7)	GTGAATTGTAATACGACTCACTATAGGGCCCTCAGTTGCTTCAT CATT
	Reverse	CACTGGCTGCAAAATGGGTC
HDAC2-3'UTR E	Forward (T7)	GTGAATTGTAATACGACTCACTATAGGGGACCCATTTTGCAGCC AGTG
	Reverse	ACGCATCTCAAGGCCAGAAA
HDAC2-3'UTR F	Forward (T7)	GTGAATTGTAATACGACTCACTATAGGGTTTCTGGCCTTGAGAT GCGT
	Reverse	GCCAGTATCCTTGGGGGA
IL-6-3'UTR	Forward (T7)	GTGAATTGTAATACGACTCACTATAGGGGCTCTTCGGCAAATGT AGCA
	Reverse	GTTAGCCATTTATTTGAGGTAAGCC
MUC1-3'UTR isoform 1	Forward (T7)	GTGAATTGTAATACGACTCACTATAGGGCCAACCTGTAGGGGCA CGTC
	Reverse	GCAGTGGGAGACCACGTTTT
MUC1-3'UTR isoform 2	Forward (T7)	GTGAATTGTAATACGACTCACTATAGGGCTATGTGCCCCCTAGC AGTA
	Reverse	CAGTGGGAGACCACGTTTTATT
PDL1-3'UTR	Forward (T7)	GTGAATTGTAATACGACTCACTATAGGGTGTGCATGGAGAGGA AGACC
	Reverse	TGGCTCCCAGAATTACCAAG
TGF- β 1-3'UTR	Forward (T7)	GTGAATTGTAATACGACTCACTATAGGGTGTCCAACATGATCGT GCG
	Reverse	TTGACCTCCCAGGATCAAGTGA
Motif	Forward (T7)	GTGAATTGTAATACGACTCACTATAGGGCCTGTAATCTCAGCCT CCTGGGAGGCTGAGA
	Reverse	TCTCAGCCTCCCAGGAGGCTGAGATTACAGGCCCTATAGTGAGT CGTATTACAATTCAC

Protein extraction and Western blot. For total protein extraction, cells were directly lysed in a buffer containing 50 mM Tris/HCl at pH 7.5, 150 mM NaCl, 2 mM EDTA, 2 mM EGTA, 25 mM NaF, 25 mM β -glycerolphosphate, 0.1 mM Na₃VO₄, 0.1 mM PMSF, 0.2% Triton X-100, 0.3% Nonidet P40, and a cocktail of protease inhibitors (100 X, *EuroClone*). After incubation on ice for 30 min, the lysate was centrifuged at 13,000 rpm for 15 min at 4°C. A total of 15 μ g of protein per well was separated by 4–15% sodium dodecyl sulfate-polyacrylamide gel electrophoresis and transferred to nitrocellulose membranes. Membranes were then blocked with 5% milk-TBST buffer (TBS plus 0.1% Tween-20) for 1 h at room temperature and incubated with primary antibodies anti-AUF-1 [HPA004911, *Atlas*], anti- β -tubulin [9F3, *Cell Signaling Technology*], anti-CD9 [10626D, *Invitrogen*], anti-CD63 [10628D, *Invitrogen*], anti-phospho-Rb [9308, *Cell Signaling Technology*], anti-p21 [2947, *Cell Signaling Technology*], anti-p53 [sc-126, *Santa Cruz*], anti-phospho-p53 [9286, *Cell Signaling Technology*], anti- β -actin [3700, *Cell Signaling Technology*], anti-HuR [sc-5261, *Santa Cruz*], anti-TTP [ab83579, *abcam*]) overnight at 4°C, washed with TBST buffer three times, and incubated with corresponding horseradish peroxidase-conjugated secondary antibodies at room

temperature for 45 min. Signals were detected by the “Pierce ECL Western Blotting Substrate” method (*Thermo Fisher Scientific*) and analyzed by the ImageLab software, using the Chemidoc image acquisition and analysis tool (*BioRad*).

Biotin pulldown assay. Biotinylated 3'UTRs were generated by PCR of BEAS-2B RNA by using specific primers (**Table 1**). Long 3'UTRs were fragmented in adjacent sequences to allow correct *in vitro* transcription and biotinylation. PCR products were purified from agarose gels and used as templates for the synthesis of biotinylated RNAs by using the MAXIscript™ T7 Kit (AM1312, *Invitrogen*) and Biotin-11-cytidine-5'-triphosphate (ENZ-42818, *Enzolife*). Unstimulated BEAS-2B cells were lysed with polysomal extraction buffer (100 mM KCl, 100 mM KCL, 100 mM KCL, 0.5% NP-40, 1X protease inhibitor) to obtain cytoplasmic fraction. 500 µg of cytosolic lysate were incubated with 1 µg of biotinylated transcripts for 30 minutes and, then, ribonucleoprotein complexes were isolated with streptavidin-conjugated Dynabeads (11205D, *Invitrogen*). The presence of AUF-1 in the pulldown material was verified by Western blot analysis [53].

Cellular senescence assays. Cells were cultured in submerged condition with medium only, cytomix for 48 hours or etoposide (6 µM) for 24 hour, used as positive control for senescence. After treatment, the culture medium was replaced with no further stimulation and cells were cultured at 37°C for additional 5 days. Cellular senescence was then detected by flowcytometric analysis of beta-D-galactopyranoside, a fluorogenic beta-galactosidase substrate, using Cell Meter™ Cellular Senescence Activity Assay Kit (23005, *AAT Bioquest*) according to manufacturer's protocol. Fluorescence was detected with BD FACSVerser™ flow cytometer (*BD Biosciences*), using FITC channel, and the data were analysed using the BD FACSuite™ software.

Analysis of SASP cytokines. BEAS-2B and HSAEC supernatant were screened for inflammatory cytokines associated to SASP (IL-1β, MCP-1, IL-6, IL-8) using the bead-based immunoassay LEGENDplex™ (740809, *Biolegend*), following manufacturer's protocol. Briefly, cell supernatants were incubated for 2 hours with two sets of specific anti-cytokine antibodies-conjugated beads, differentiated by size and internal fluorescence intensities, followed by 1-hour incubation with a detection antibody. After 30 minutes' incubation of the mix with streptavidin-conjugated phycoerythrin, the fluorescent signal intensity, which is proportional to the amount of bound analytes, was detected using BD FACSVerser™ flow cytometer (*BD Biosciences*) and data were analyzed with the LEGENDplex Data Analysis Software.

Extracellular vesicles (EVs) isolation. BEAS-2B and HSAEC cells were cultured with EVs-depleted medium, obtained by overnight centrifugation of each culture medium at 100,000 g. Cell-derived EVs were isolated from culture media of unstimulated and cytomix-stimulated cells by differential centrifugation, following an established protocol [54]. Briefly, cell supernatants were centrifuged at 300 g for 10 minutes to pellet cells, then at 2000 g for 10 minutes to pellet dead cells and at 10 000 g for 30 minutes to eliminate cell debris. Finally, the supernatants were ultracentrifuged at 100 000 g for 70 minutes using Beckman Coulter's Optima XE-100 Ultracentrifuge with SW 32.1 swinging-rotor. EVs pellet was resuspended in 50 μ l of PBS.

Dynamic light scattering (DLS) analysis. DLS analyses the velocity distribution of particle movement caused by Brownian motion by measuring fluctuations of scattered light intensity. Then, the particle size is calculated size via the Stokes-Einstein equation. For DLS measurements, 10 μ L of EVs were diluted in 990 μ L of water to obtain a concentration within the recommended measurement range and then transferred to a tube for size measurement using Nano ZS Malvern Zeta Sizer (model 1000HSa, UK) at 25°C, equipped with a He-Ne laser of 633 nm and detector angle of 173°C. The analyses were performed in three independent technical replicates for each sample. EVs size was expressed as mean \pm Standard Deviation (SD).

Transmission electron microscopy (TEM). One drop of sample solution (about 25 μ l) was placed on 400 mesh holey film grid; after staining with 2% uranyl acetate (for 2 minutes) the sample was observed with a Tecnai G2 (*FEI*) transmission electron microscope operating at 100 kV. Images were captured with a Veleta (*Olympus Soft Imaging System*) digital camera.

For monolayer cells samples, cells seeded were washed in 1x HBSS and fixed in 2.5% glutaraldehyde (*Sigma-Aldrich*) in 0.1M HEPES buffer pH 7.4 for 1 h at 4 °C. After 3 water washes, samples were dehydrated in a graded ethanol series and embedded in an epoxy resin (*Sigma-Aldrich*). Ultrathin sections (60-70 nm) were obtained with an Ultratome V (*LKB*) ultramicrotome, counterstained with uranyl acetate and lead citrate and viewed with a Tecnai G2 (*FEI*) transmission electron microscope operating at 100 kV. Images were captured with a Veleta (*Olympus Soft Imaging System*) digital camera.

Immunogold labeling. A drop of sample solution (about 25 μ l) was placed on a 400 mesh holey film grid for 2-3 minutes. Subsequently they were incubated with blocking solution (0.5% bovine serum albumin (BSA), in PBS for 30 minutes at room temperature. Immediately the grids were incubated at 4° C, for 30 minutes at room temperature with a primary antibody anti-HNRNPD (HPA004911 *Atlas*)

diluted 1:40 in blocking solution and then proceeded with 3 washes with PBS (5 minutes each). The grids were then incubated with a IgG Gold II secondary antibody anti-rabbit coupled to gold particles (5nm) (G3779 *Sigma Aldrich*) for 30 minutes at room temperature. After washing in PBS (3X) and in the water (2X), the grids were counterstained with uranyl acetate and lead citrate and viewed with a Tecnai G2 (FEI) transmission electron microscope operating at 100 kV. Images were captured with a Veleta (*Olympus Soft Imaging System*) digital camera.

Study population providing lung biopsy samples for RNA Sequencing

Bronchial rings and peripheral lung samples were obtained from subjects recruited from the Respiratory Unit of the University Hospital of Messina, Italy, among patients undergoing lung resection for peripheral lung carcinoma (**Table 2**). Smokers with mild-to-moderate stable COPD (n=7) were compared with age- and smoke history-matched smokers with normal lung function (NLF) (n=5). Diagnosis of COPD was defined according to international guidelines as the presence of post-bronchodilator forced expiratory volume in 1 s (FEV₁)/forced vital capacity (FVC) ratio <70% or the presence of cough and sputum production for at least 3 months in each of two consecutive years [55]. All patients were in stable condition at the time of the surgery and had not suffered acute exacerbations or upper respiratory tract infections in the preceding two months. None had received glucocorticoids or antibiotics within the month preceding surgery, or inhaled bronchodilators within the previous 48 h. Patients had no history of asthma or other allergic diseases. All former smokers had stopped smoking for more than one year. Each patient was subjected to medical history, physical examination, chest radiography, electrocardiogram, routine blood tests, and pulmonary function tests during the week prior to surgery. Pulmonary function tests (Biomedin Spirometer, Padova, Italy) were performed as previously described [56] according to published guidelines. The study was approved by the local Ethics Committees of the University Hospitals of Messina and participating patients and control subjects signed the approved informed consent forms.

Table 2. Characteristics of subjects for RNA-sequencing on the formalin-fixed/paraffin-embedded (FF/PE) peripheral lung tissue.

Groups	n.	Age (years)	M/F	Ex/current smokers	Pack-years	Chronic bronchitis	FEV ₁ (% predicted)	FEV ₁ /FVC%
COPD patients	7	71 ±4	11/1	10/2	57±32	1	74±20#	60±9*
Smokers with normal lung function	5	70 ±8	11/1	10/2	49±39	2	96±14	76±4

Abbreviations: COPD, chronic obstructive pulmonary disease; M, male; F, female; FEV₁, forced expiratory volume in one second; FVC, forced vital capacity. For COPD and control smoker subjects, FEV₁% predicted and FEV₁/FVC% are

post-bronchodilator values. Data expressed as mean±SD. Statistical analysis: t test * $p < 0.0001$, significantly different from control smokers with normal lung function; t test # $p < 0.05$, significantly different from control smokers with normal lung function.

RNA-seq of human lung biopsies. For gene expression analysis libraries were prepared with the Lexogen QuantSeq 3' mRNA-Seq Library Prep Kit (FWD) for Illumina (cat. no. 015.96), as per manufacturer's instructions. The modified protocol for FFPE samples was used and RNA input was 250ng. qPCR was performed to find the optimal cycle number for the endpoint PCR, using the PCR Add-on Kit for Illumina (cat. no. 020.96) to quantify cDNA before final library amplification. Library pooling was performed by BGI and NGS was run on their DNBSEQ platform (BGI Genomics, HK) with PE100 reads. Read count was performed on the BlueBee platform using standard settings for the Quantseq 3' kit (www.lexogen.bluebee.com). Differential expression analysis was performed using DESeq2 package from the Bioconductor (<https://bioconductor.org/packages/release/bioc/html/DESeq2.html>). Heatmaps were generated using tMEV tools v4_9_0.45 (Howe et al. Cancer Research ,2010; Saeed et al. BioTechniques 2003).

Statistical analysis. Data from Western blot densitometry and qRT-PCR were analyzed using Student's paired *t*-test. For cellular senescence activity assays ANOVA test with FDR post hoc multiple comparison analysis was performed. A probability $p \leq 0.05$ was considered significant. Statistical analysis was performed using GraphPad Prism 5 (*GraphPad Software Inc.*). For RIP-seq data statistical analysis, $FDR \leq 0.05$ computed according to Benjamini–Hochberg were considered for further analysis.

Gene Set Variation Analysis (GSVA). This statistical method evaluates variations in underlying mechanisms between groups [57] and was used to compute the Enrichment Score (ES) of the AUF-1 RIP-seq gene set in all subjects included in the database GSE5058 [58]. The analysis was performed according to described parameters [59]. In particular, gene signature was considered significantly differentially expressed in presence of differences in ESs ($dES \geq 0.2$ between the groups and p -value $< .05$).

Results

Identification of AUF-1-associated transcripts in BEAS-2B cells by RIP-Seq analysis.

Cytosolic extracts of unstimulated BEAS-2B cells (n=3) were isolated and subjected to RIP. AUF-1- and IgG control-associated RNAs were immunoprecipitated (IP AUF-1, IP IgG), along with a No-Ab IP to evaluate potential non-specific interactions during IP procedure. Input samples for each condition were also collected for the sequencing analysis. Western Blot analysis of the protein fraction (**Figure 1A**) revealed a high level of enrichment in IP AUF-1 compared to IP IgG, No-Ab IP and unbound fractions controls. Immunoprecipitated RNAs were fragmented and converted to cDNA after adaptor ligations, and then sequenced on an *Illumina* platform. An average of 27466311, 36765708 and 25288124 reads were obtained from the Input, AUF-1 IP and IgG IP libraries, respectively. Despite differences in total read numbers due to the low amount of Input cDNA, the IPs consistently yielded many more mappable reads than did the controls. Principal Component Analysis (PCA) (**Figure 1B**) indicated that one of the biological replicates was discordant respect to the other two samples; therefore, two of the three original experiments were considered for further analysis. After normalization, a total of 12,727 transcripts were expressed in the cell line in Input samples. Enrichment analysis was set with EF ratio vs Input at ≥ 1.5 and FDR ≤ 0.05 . To visualize the enrichment data, each sequenced transcript in the IP sample versus the Input samples were plotted. The scatter plot was constructed using the log-transformed and normalized read numbers (**Figure 1C**).

With the described cutoff, 1078 transcripts resulted as significantly immunoprecipitated in AUF-1 IP vs Input and 1149 transcripts in IgG IP vs Input samples. Subsequently, the two datasets were crossed and overlapping targets with IgG IP vs Input transcripts were excluded. As result, 494 AUF-1 IP-targets were identified and considered for further analysis (**Figure 2A**). **Table 3** lists the transcripts for the top twenty AUF-1-bound transcripts by enrichment value (full list in **Table 4** at the end of the manuscript). For these selected targets, the average of reads enrichment was significantly higher in AUF-1 IP compared to the Input and to IgG IP (median normalized reads: 1024, 583 and 762 in AUF-1 IP, Input and IgG IP samples, respectively) (**Figure 2B**).

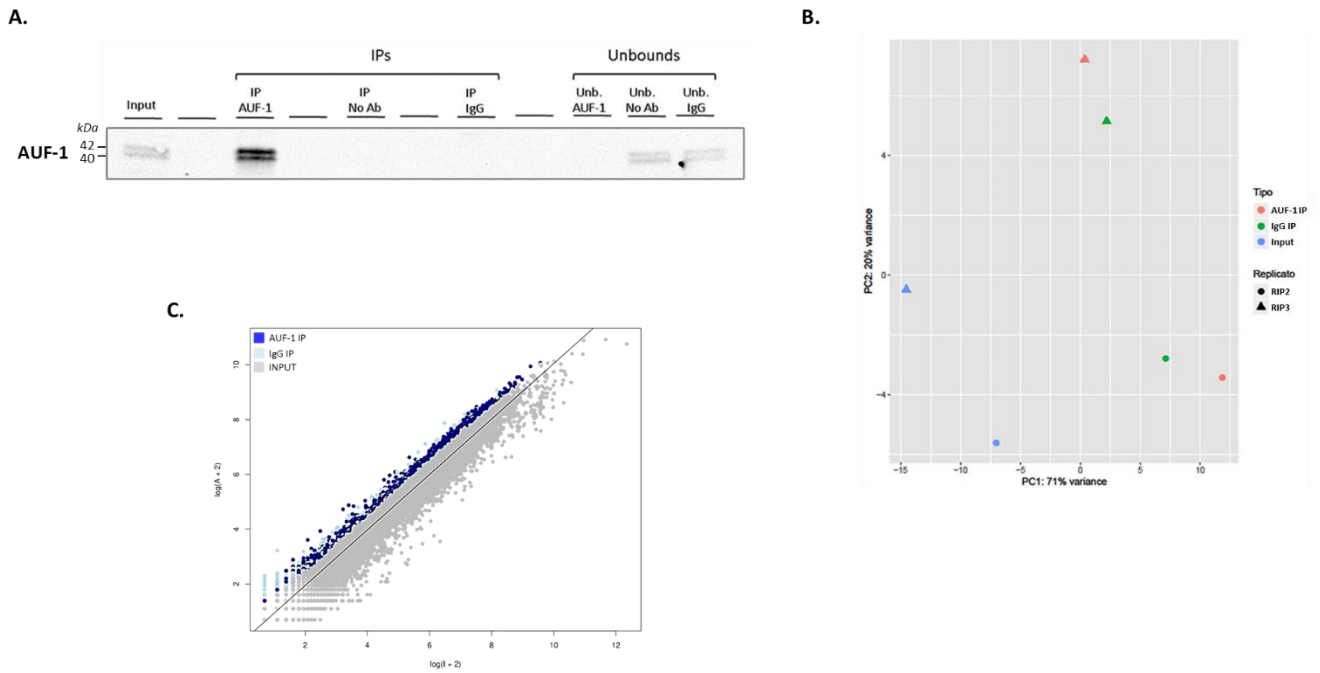


Figure 1. RIP-Seq analysis performed in unstimulated BEAS-2B cells.

A. Representative Western Blot analysis (n=3) showing selective AUF-1 IP compared to controls. The Input samples (Input) were incubated with both AUF-1 and IgG antibodies (AUF-1 IP and IgG IP, respectively) and then immunoprecipitated with magnetic beads. An additional antibody-free control sample (no Ab) was performed. **B.** Principal component analysis (PCA) based on gene enrichment profile after sequencing, considering the two biological replicates of the AUF-1 IP, IgG IP and Input samples. The two principal components (PC) variables are shown on the two axes of the graph. **C.** Scatter plot of RIP-Seq data. Read counts for AUF-1 IP, IgG and Input controls were normalized and log-transformed. Dark blue and light blue dots represent enriched AUF-1 IP and IgG targets ($EF \geq 1.5$ and $FDR \leq 0.05$), respectively. Gray dots represent background (Input). Axes represent \log_2 read count in Input (X) and AUF-1 IP (Y).

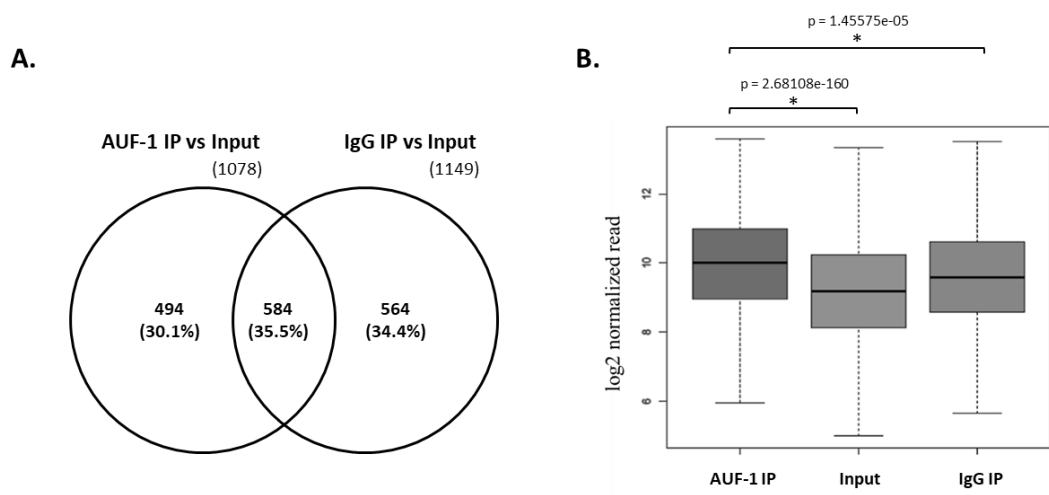


Figure 2. Transcripts associated with AUF-1 in unstimulated BEAS-2B cells identified by RIP-Seq.

A. Venn diagram showing exclusive and overlapping targets between AUF-1 IP- and IgG-IP-enriched transcripts vs Input ($EF \geq 1.5$ and $FDR \leq 0.05$). **B.** Boxplot showing the enrichment of the 494 AUF-1 transcript targets in Input, AUF-1 IP and IgG IP samples. The average enrichment of the two biological replicates for each condition have been considered. Y axis represents the \log_2 of the normalized read count. * $p \leq 0.05$ (Student's t-test).

Table 3. Top twenty AUF-1 target genes according to highest fold enrichment (AUF-1 IP vs Input) in RIP-Seq experiments. Full list (n=494) in Table 4. FE = Fold Enrichment, FDR = False Discovery Rate.

Gene symbol	Full Name	FE	FDR	Main Functions	References
PRR36	Proline Rich 36	5,73	0,020203	Unknown function	[60]
GLIS2	GLIS Family Zinc Finger 2	4,95	0,00745	Transcription factor	[61,62]
ZNF385A	Zinc Finger Protein 385A	4,4	5,15E-05	Zinc finger protein	[63]
TCF7L1	Transcription Factor 7 Like 1	4,14	0,003217	Wnt signaling pathway	[64,65]
PIANP	PILR Alpha Associated Neural Protein	3,52	0,000871	Ligand for the paired immunoglobulin-like type 2 receptor alpha	[66]
MBD6	Methyl-CpG Binding Domain Protein 6	3,42	2,49E-09	Binds to heterochromatin	[67]
MUC1	Mucin 1, Cell Surface Associated	3,37	1,81E-06	Binds to oligosaccharides by the extracellular domain	[68,69]
FOXP4	Forkhead Box P4	3,27	7,46E-05	Trascriptor factor	[70]
KDM6B	Lysine Demethylase 6B	3,2	0,000139	Lysine-specific demethylase	[71,72]
FBRSL1	Fibrosin Like 1	3,09	0,000336	Unknown function	[73]
C1orf226	Chromosome 1 Open Reading Frame 226	2,86	0,039358	Unknown function	[74]
AP001972.5	AP001972.5	2,84	0,032884	Unknown function	
STX1B	Syntaxin 1B	2,83	0,012534	Mediator of calcium-dependent synaptic vesicle release	[75]
CRTC1	CREB regulated transcription coactivator 1	2,73	0,001314	Co-activator of the transcription factor CREB	[76,77]

AL513165.1	AL513165.1	2,66	0,034496	Unknown function	
ATXN2L	Ataxin 2 Like	2,6	1,37E-08	Regulator of stress granules	[78]
RNF44	Ring Finger Protein 44	2,6	0,000146	E3 ligase	[79]
IL17RD	Interleukin-17 Receptor D	2,58	0,026678	Orphan receptor member of the IL-17R family	[80,81]
KIAA1522	KIAA1522	2,58	1,23E-08	Unknown function	[82]
HIVEP3	Human Immunodeficiency Virus Type 1 Enhancer-Binding Protein 3	2,47	0,000702	Transcription factor	[83,84]

Identification of predicted binding motifs in AUF-1-associated transcripts; AUF-1 association to 3'UTR regions of selected transcripts by biotin pull-down.

The interaction of AUF-1 with its target mRNAs has been shown to be mediated predominantly by motifs located in the 3'UTR of the transcripts [16,41,85]. Therefore, we focused our analysis of enriched elements to the 3'UTR of the AUF-1-bound targets. We screened the 494 epithelial AUF-1 targets for the occurrence of 3'UTR motifs using the SMARTIV tool. **Figure 3A** shows 4 core motifs with k-mer length of 5 and 6, compatible with the pentameric sequence previously recognized by AUF-1 [41]. Within the experimental dataset 12 enriched gapped k-mer motifs were identified, mostly comprising Guanosine-Cytosine (GC) nucleotides, which had the highest frequency of hits over the entire SMARTIV database (**Figure 3B**).

We have also searched for an extended 30-mer core motif using a MEME Suite tool. As shown in **Figure 4A** and **4B**, the majority of experimental AUF-1 epithelial targets shared a GC-rich motif.

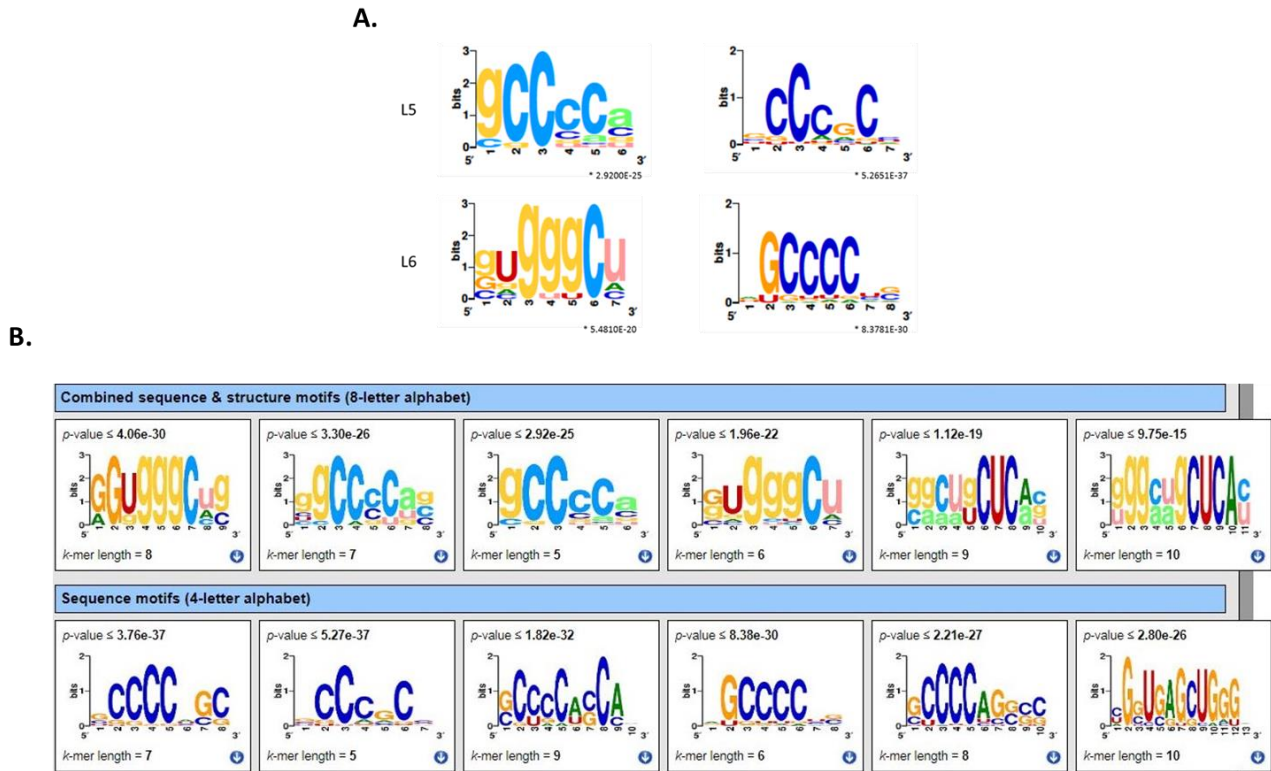


Figure 3. Identification of predicted binding motifs in AUF-1-associated transcripts.

A. *k*-mer length 5 (L5) and 6 (L6) graphic logo generated by SMARTIV tool (see Methods) representing the probability matrix of the AUF-1 motif, showing the relative frequency of each nucleotide for each position within the motif sequence. The motif is originated from the 3'UTR sequences of the exclusive $n=494$ AUF-1 transcripts (see Figure 1C) obtained from the RIP-Seq study. Upper and lower case alphabets show the secondary structure prediction (A,G,C,U for unpaired nucleotides and a,g,c,u for paired nucleotides). * p -value ≤ 0.05 [according to minimum hypergeometric statistical approach (mmHG)]. **B.** 12 enriched gapped *k*-mer motifs generated by SMARTIV tool (see Methods) representing the probability matrix of the AUF-1 motif, showing the relative frequency of each nucleotide for each position within the motif sequence. The motif is originated from the 3'UTR regions of the experimental data set ($n=494$ AUF-1 transcripts) obtained from the RIP-Seq study. Upper and lower case alphabets show the secondary structure prediction (A,G,C,U for unpaired nucleotides and a,g,c,u for paired nucleotides). * p -value ≤ 0.05 [according to minimum hypergeometric statistical approach (mmHG)].

HDAC2	Histone deacetylase 2	1.7	A, D
IL-6	Interleukin-6	as control	Full length

IL-6 mRNA was included in its 3'UTR sequence, being an important mediator of SASP known to be regulated by AUF-1 [13,26,29], as well as a biotinylated sequence representative of the newly identified GC-rich motif, comprising the nucleotides with highest frequency. The 3'UTR of Cyclin D1, a known target of AUF-1 [86] and a beads-only sample and a non-AUF-1 target sequence (PD-L1 coding sequence) were included as positive and negative controls, respectively. Western blot analysis (**Figure 5**) revealed the presence of AUF-1 in the starting lysate (Input) and in the pulldown fractions obtained with biotinylated 3'UTR sequences of all experimental transcripts. In particular, AUF-1 was detected in the pulldown fraction obtained with full-length 3'UTRs (EGR1, TGF- β 1, isoform 1 of MUC1 and IL-6) and specific segments for other transcripts, whose 3'UTR was too long for synthesis of a single biotin-labelled molecule: segment A and, more abundantly, with segment D of HDAC2 3'UTR, segment A of FoxP4-3'UTR, all segment of DDX17-3'UTR, segment B of GLIS2-3'UTR. Importantly, AUF-1 was detected in association with the sequence modelled on the motif shown in Figure 4A. These results support the data obtained from RIP-Seq analysis, confirming the association of AUF-1 to the 3'UTR of the selected transcripts, pointing in some cases to specific regions of 3'UTRs.

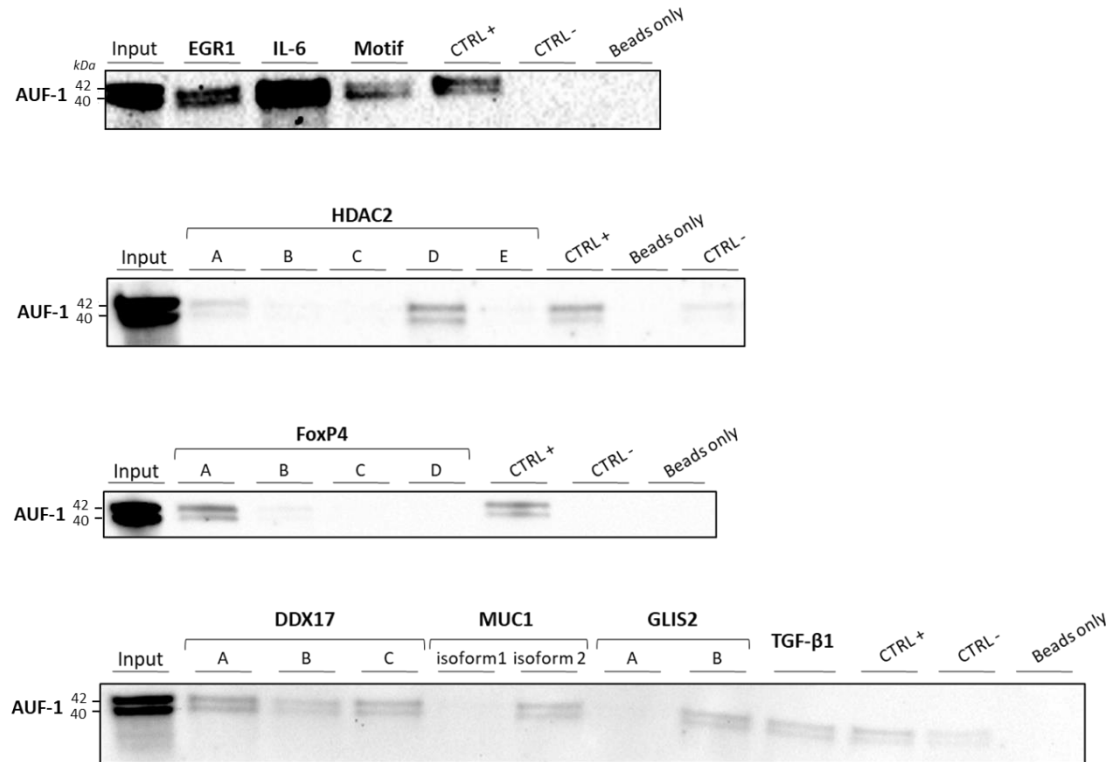


Figure 5. AUF-1 association to 3'UTR regions of selected transcripts by biotin pull-down.

Representative immunoblots (n=2) of AUF-1 detection by RNA biotin pulldown in BEAS-2B cytoplasmic lysates using biotinylated 3'UTR probes for the indicated AUF-1 targets, listed in the table along their enrichment factor (EF). Capital letters (from A to E) represent biotinylated fragments of adjacent sequences used for long 3'UTRs; “CTRL+”, positive control (Cyclin D1 3'UTR) “CTRL-”, negative control (PD-L1 coding sequence).

Role of AUF-1 on steady state and stability of selected transcripts in BEAS-2B cells.

We previously documented that cytomix- and CSE-induced loss of AUF-1 in BEAS-2B occurred along with changes in expression levels of many established AUF-1-regulated cytokines and chemokines and this modulation was replicated in condition of greater AUF-1 loss induced by siRNA [21]. We hypothesized that loss of AUF-1 occurring upon cytomix stimulation might reflect in changes in mRNA stability of its targets. We therefore evaluated steady-state levels and mRNA decay rates of selected experimental targets displaying different enrichment values from RIP-Seq analysis (GLIS2, MUC1, FOXP4, CRTCL1, TGF-β1, EGR1, DDX17, DHX36, HDAC2, IGF1R), according to levels of AUF-1 in resting BEAS-2B cells (basal AUF-1 levels), cytomix-stimulated (lower AUF-1 levels compared to basal) and cytomix-stimulated AUF-1 siRNA-transfected (near-complete AUF-1 loss) (**Figure 6**).

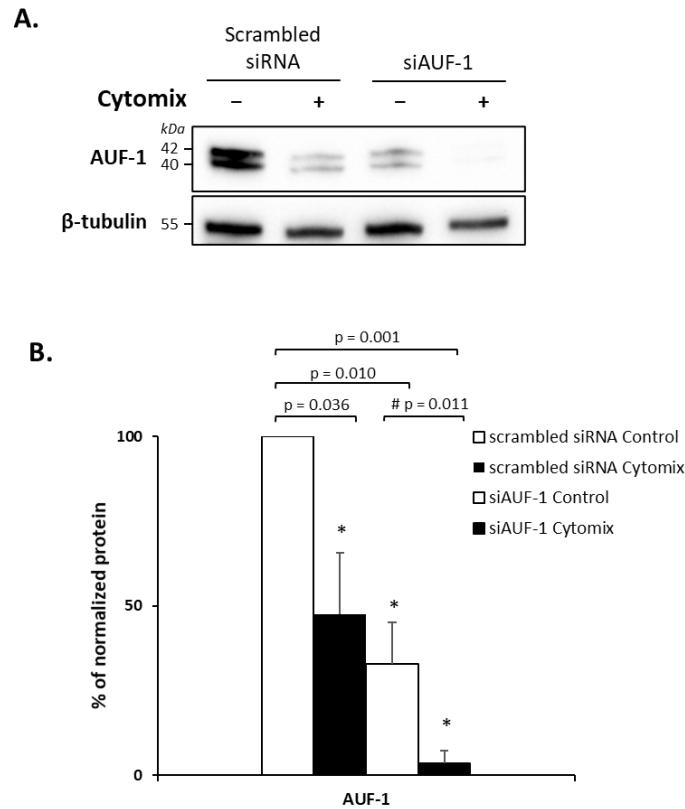


Figure 6. AUF-1 silencing and cytomix stimulation in BEAS-2B cells.

A-B. Representative immunoblot (**A**) and densitometric analysis (**B**) of AUF-1 levels after transfection with scrambled/AUF-1 siRNA (48 hours) and subsequent culture (48 hours) with cytomix or medium control (mean \pm SEM of $n=3$). β -tubulin detected as loading and normalization control. * $p<0,05$ compared to the scrambled-transfected medium control, # $p<0,05$ compared to AUF-1-siRNA (siAUF-1) control.

As also previously observed [21] in BEAS-2B cells transfected with scrambled siRNA the cytomix stimulation significantly decreased AUF-1 protein level (53.1%). Upon AUF-1 silencing, AUF-1 protein levels in resting and cytomix-treated cells were reduced by 67% and by 96.6%, respectively, compared to scrambled siRNA-transfected, unstimulated cells.

Interestingly, silencing of AUF-1 did not affect steady-state mRNA target levels in unstimulated condition while in cytomix-treated cells it reproduced, with no further enhancement, the stimulus-induced changes detected in scrambled siRNA-transfected cells (**Figure 7**), as previously observed for other known AUF-targeted cytokines and chemokines [21].

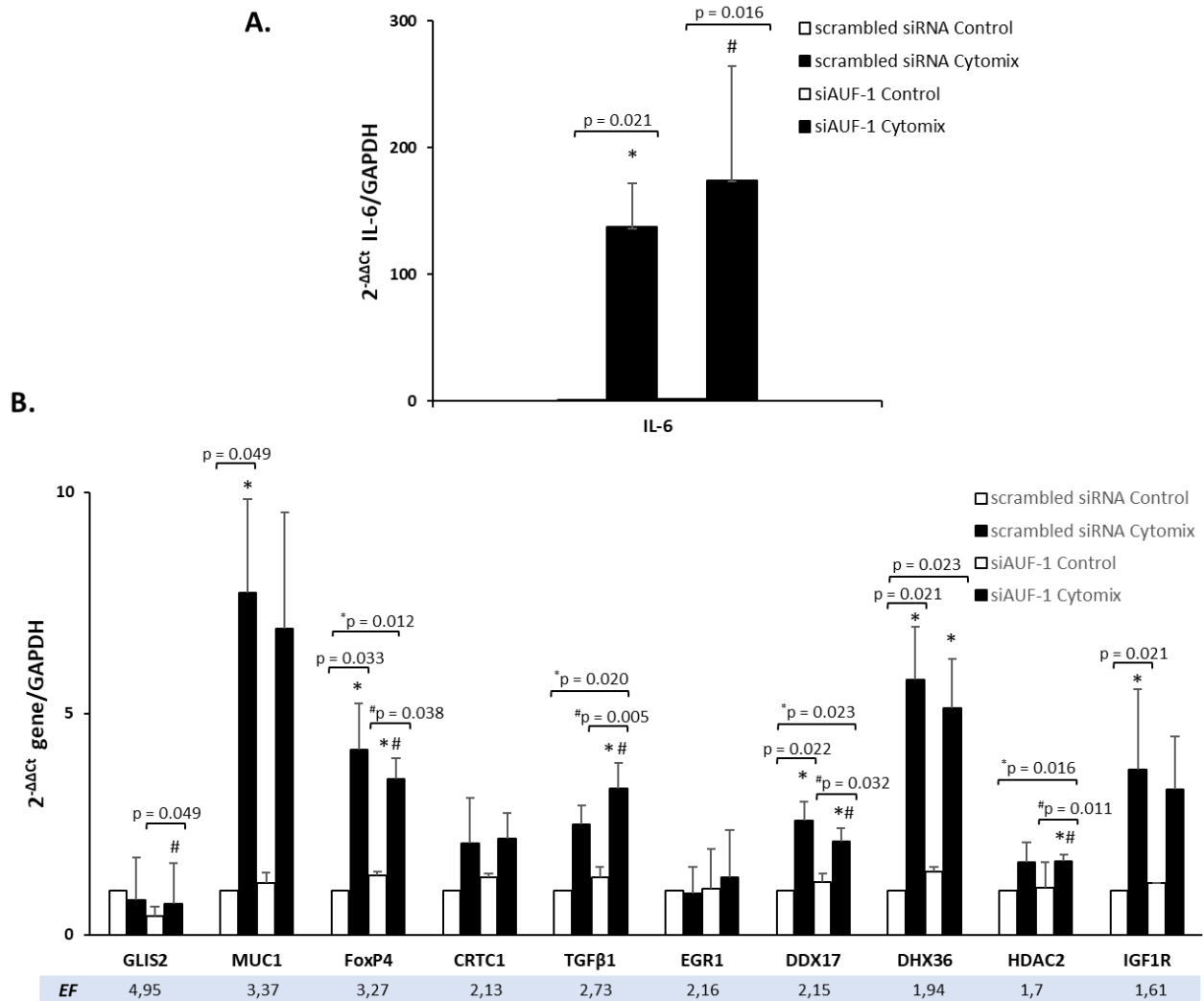


Figure 7. Analysis of AUF-1 target mRNA steady state according to changes in AUF-1 intracellular levels. A. qRT-PCR analysis of steady-state mRNA expression of IL-6, as known AUF-1-regulated gene **B.** qRT-PCR analysis of steady-state mRNA expression of indicated AUF-1 targets, listed in decreasing EF. * $p < 0,05$ cytomix compared to the scrambled-transfected medium control, # $p < 0,05$ compared to AUF-1-siRNA (siAUF-1) control.

Evaluation of mRNA decay by actinomycin D assay indicated for most transcripts – namely, MUC-1, FOXP4, CRTCl, TGF- β 1, DDX17, DHX36, HDAC2, IGF1R – a slow rate of mRNA decay in resting cells with half-lives > 4 hours, without changes induced by cytomix treatment regardless of AUF-1 levels (**Figure 8-9-10**). As expected, IL-6 mRNA steady state was significantly increased by cytomix along with the stability of the mRNA (**Figure 7A-8A**) (half-life: 0.4 hr in unstimulated cells versus >4 hr in cytomix-treated cells). In AUF-1-silenced cells, IL-6 mRNA stabilization was already detectable at the earliest timepoint (1 hr after ActD treatment), with 96% of mRNA compared to 55% present at that time in scrambled-transfected cells.

For GLIS2 mRNA, decay rate in unstimulated cells was slower than IL-6 (half life: 3 hr) and cytomix treatment did increase mRNA stability, with significantly higher expression at 2 and 4 hr after ActD (74% and 60% in cytomix-treated, half life: >4 hr versus 56% and 39% compared to time 0 in unstimulated cells), but no further stabilization in AUF-1-silenced cells.

The EGR-1 mRNA showed a yet different pattern according to increasing loss of AUF-1: in scrambled siRNA-transfected cells, similar to IL-6 mRNA, a rapid mRNA decay rate (half life: 0.3 hr) was found in unstimulated cells (basal AUF-1 levels) with evident mRNA stabilization upon cytomix treatment (half life: 2 hours). Interestingly, in AUF-1 silenced cells EGR-1 mRNA decay rate reverted to a faster rate at all three timepoints in both control (8%, 8% and 3% in AUF-1siRNA-treated cells, half life: < 0.5 hr; versus 16%, 15% and 5% in scrambled siRNA compared to time 0) and stimulated cells (39%, 30% and 14% in AUF-1siRNA-treated cells, half life: 0.5 hr versus 64%, 63% and 30% in scrambled siRNA compared to time 0), though such difference with the scrambled-transfected cells was statistically non-significant due to data variability.

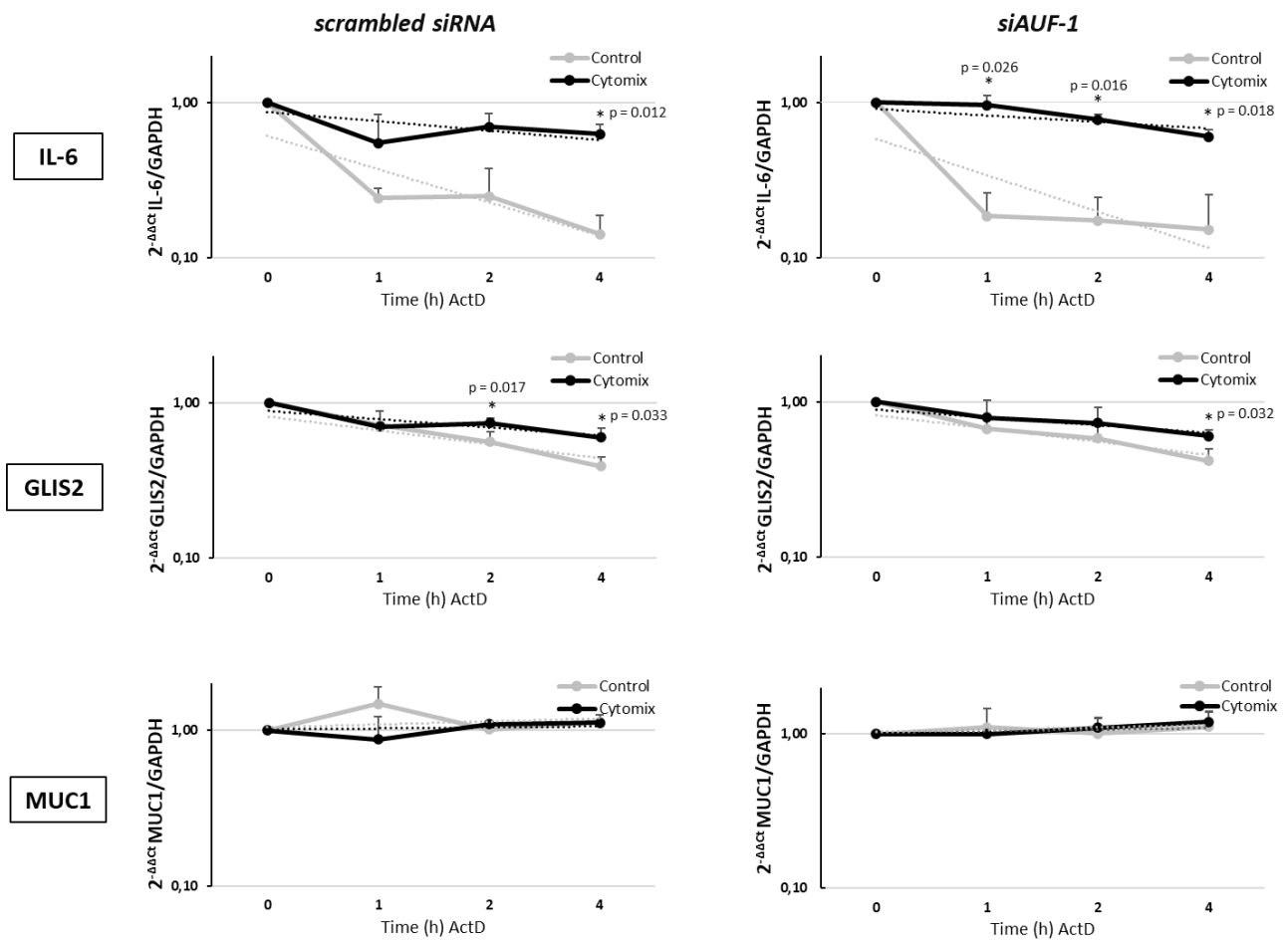


Figure 8. Analysis of AUF-1 target mRNA decay according to changes in AUF-1 intracellular levels.

qRT-PCR analysis (mean \pm SEM of $n=3$) of mRNA decay rate of IL-6, as known AUF-1-regulated gene, and AUF-1 targets GLIS2 and EGR-1 upon treatment with actinomycin D (ActD) for indicated times, initiated after 48hr of cytomix treatment (Time 0). Target mRNA expression levels were normalized to housekeeping mRNA (GAPDH) and expressed for each timepoint as fold change over time 0, as $2^{-\Delta\Delta C_t}$. * $p < 0,05$ cytomix value versus corresponding unstimulated (CTRL) value at each datapoint.

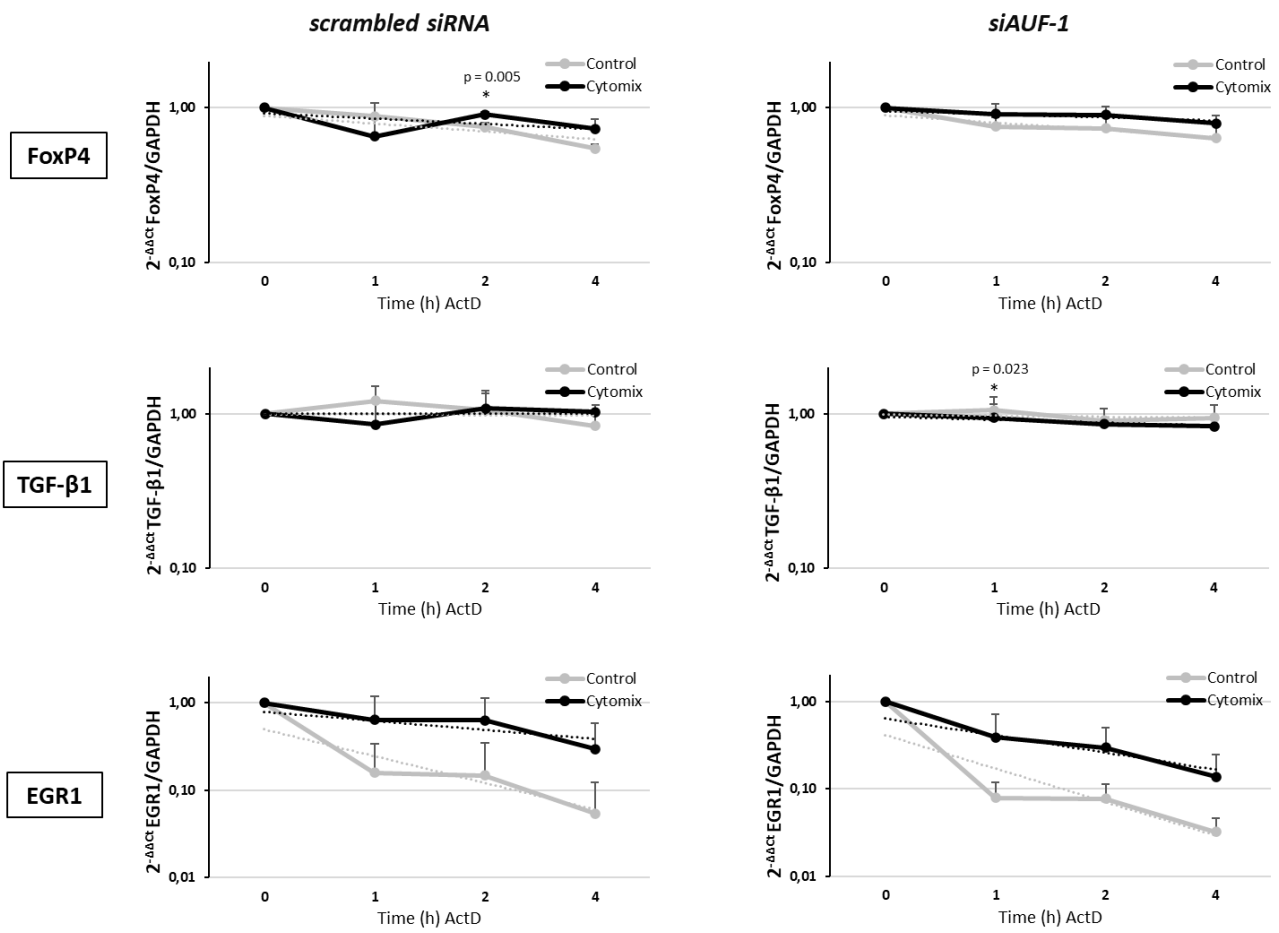


Figure 9. Analysis of AUF-1 target mRNA decay according to changes in AUF-1 intracellular levels.

qRT-PCR analysis (mean \pm SEM of n=3) of mRNA decay rate of FoxP4, TGF-β1 and EGR1 upon treatment with actinomycin D (ActD) for indicated times, initiated after 48hr of cytomix treatment (Time 0). Target mRNA expression levels were normalized to housekeeping mRNA (GAPDH) and expressed for each timepoint as fold change over time 0, as $2^{-\Delta\Delta C_t}$. *p<0,05 cytomix value versus corresponding unstimulated (CTRL) value at each datapoint.

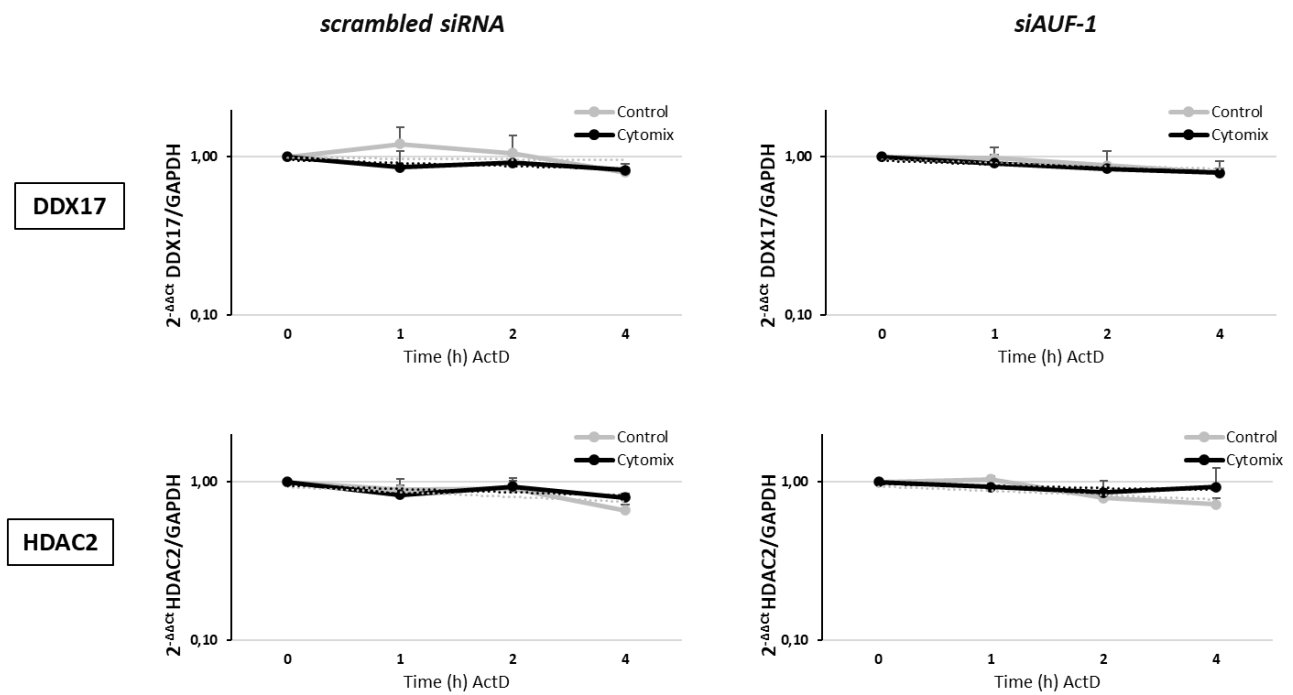


Figure 10. Analysis of AUF-1 target mRNA decay according to changes in AUF-1 intracellular levels. qRT-PCR analysis (mean \pm SEM of n=3) of mRNA decay rate of DDX17 and HDAC2 upon treatment with actinomycin D (ActD) for indicated times, initiated after 48hr of cytomix treatment (Time 0). Target mRNA expression levels were normalized to housekeeping mRNA (GAPDH) and expressed for each timepoint as fold change over time 0, as $2^{-\Delta\Delta C_t}$. *p<0,05 cytomix value versus corresponding unstimulated (CTRL) value at each datapoint.

Analysis of cellular senescence induced by cytomix in BEAS-2B and primary human small airway epithelial cells (HSAEC).

AUF-1 knockout mouse models indicate that its loss favors not only overexpressed cytokine response, but also promotes cellular senescence through multiple mechanisms, lending a strong rationale for pathogenic relevance of AUF-1 loss in COPD. We therefore investigated whether conditions of AUF-1 loss modelled by cytomix stimulation impacted readouts of cellular senescence. We extended this study to HSAEC, in which we confirmed a selective decrease in AUF-1 protein levels by cytomix treatment without concurrent changes in mRNA levels, or in the expression of other two relevant RBPs, TTP and HuR (**Figure 11**) as shown in BEAS-2B [21].

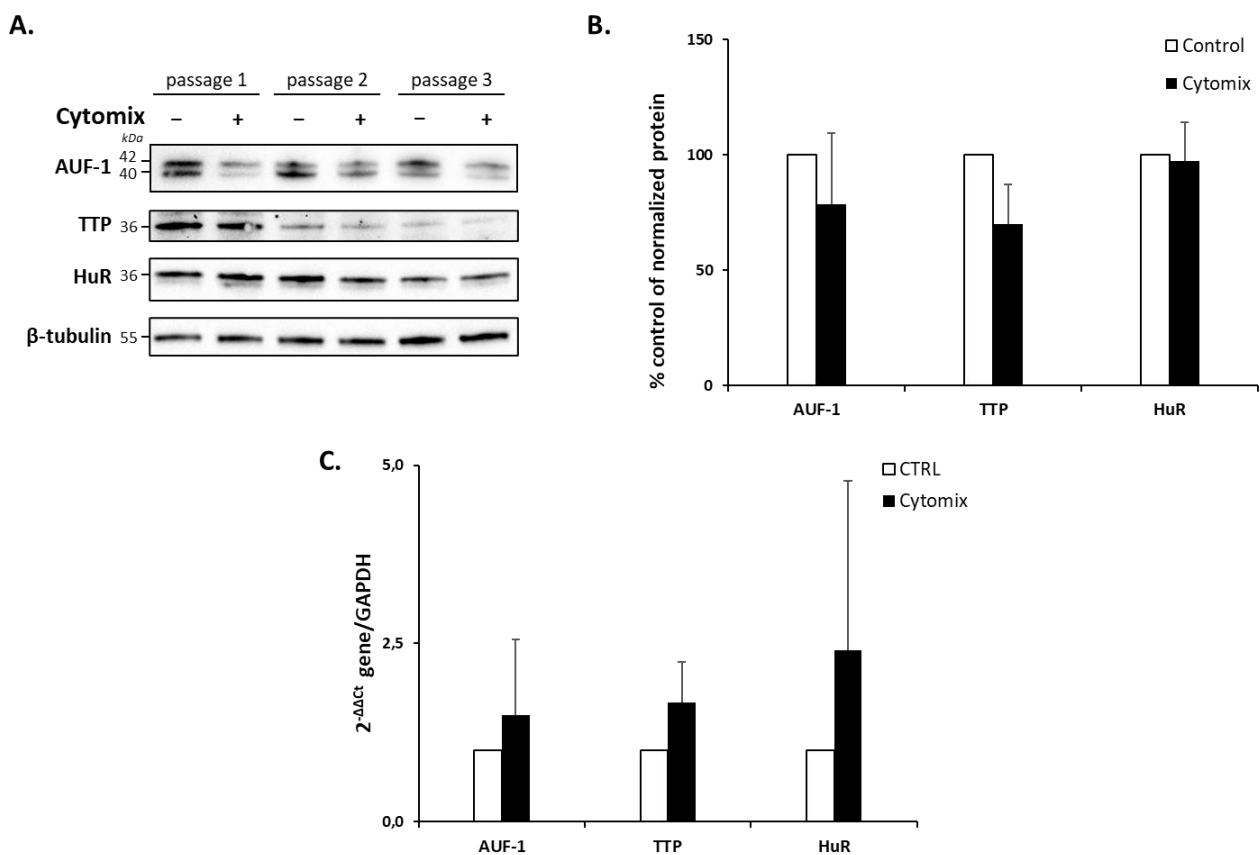


Figure 11. Modulation of RNA-binding proteins expression in HSAEC upon cytomix stimulation.

A-B. Representative immunoblots (**A**) and densitometric analysis (**B**) of AUF-1, TTP and HuR in whole cell lysate of HSEAC stimulated with cytomix for 48 hours (mean \pm SEM of $n=3$). β -tubulin as loading control. **C.** qRT-PCR analysis of AUF-1, TTP and HuR mRNA in HSEAC stimulated with cytomix for 48 hours (mean \pm SEM of $n=3$). mRNA levels were normalized to housekeeping mRNA levels (GAPDH) and expressed as fold change $2^{-\Delta\Delta Ct}$.

Both cell types were stimulated with cytomix for 48 hours or with low-dose etoposide (6 μ M) as trigger control for senescence [87,88] for 24 hours. At the end of this period, considered as experimental time 0, culture medium was replaced without adding any stimulus and cells were further incubated at 37°C for 5 days (time 5). Importantly, at time 5 the levels of AUF-1 protein detected by Western blot remained significantly lower than in unstimulated controls and comparable to those present after 48 hrs of stimulation, at time 0 (71.3 and 79.9 % inhibition of control at time 0 and 5, respectively). (**Figure 12A-B**). The same cells were subjected by immunoblot analysis to detection of several markers of senescence. In particular, the described treatment time-dependently decreased levels of phospho-Retinoblastoma protein (43.9 and 59.6% inhibition of control at time 0 and 5, respectively, with statistically significance at time 5) and consistently increased levels of the cyclin-dependent kinase (CDK) inhibitor p21 (563.4 and 280.1% of control at time 0 and 5, respectively) and of phospho-p53 and p53 ratio (2618 and 1306% of control at time 0 and 5, respectively), suggesting that cytomix-pretreated cells, while expressing low levels of AUF-1, underwent to cell cycle arrest, similar to etoposide-treated cells (**Figure 12A-B**). Concurrently, qRT-PCR showed a significant decrease of mRNA levels of AUF-1 (42% inhibition over unstimulated control) after 5 days of cytomix treatment, in contrast to unchanged mRNA levels determined after 48 hr of the treatment (**Figure 12C**).

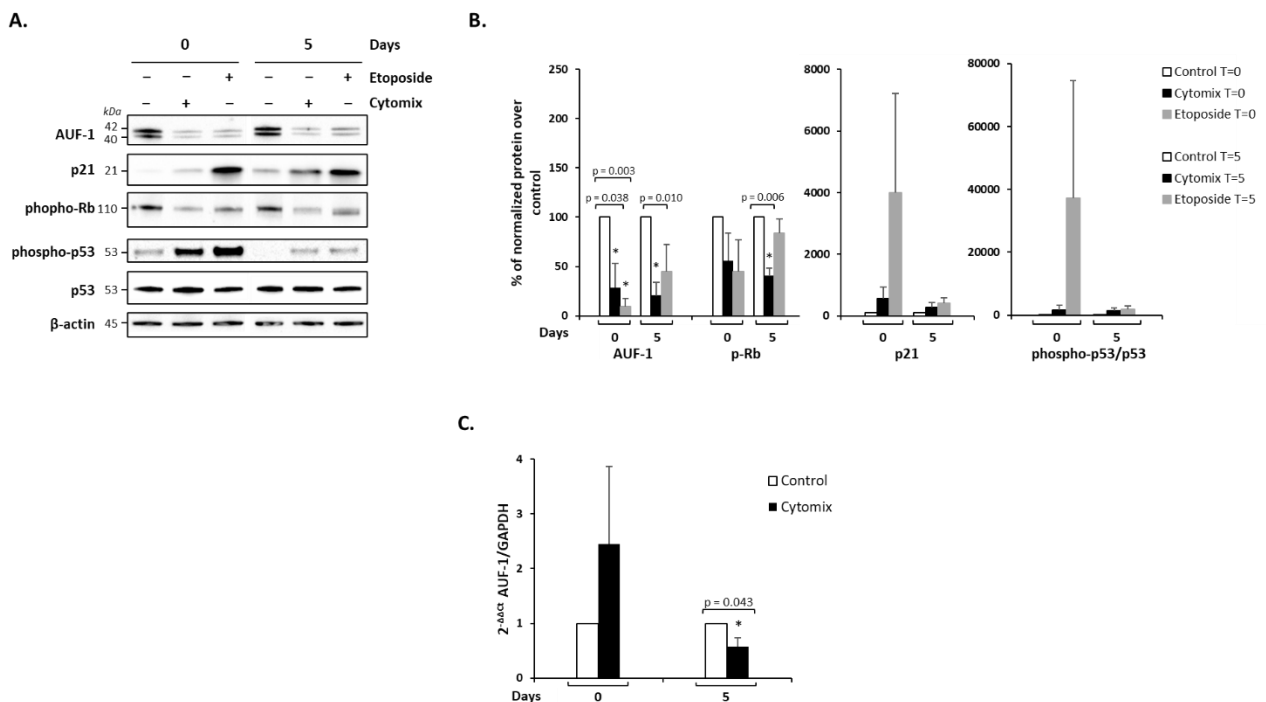


Figure 12. AUF-1 loss and cellular senescence readout (cell cycle arrest) in BEAS-2B upon cytomix stimulation. A-B. Representative immunoblots (A) and densitometric analysis (B) of AUF-1, phospho-retinoblastoma (p-Rb) protein, p21, p53 and phospho-p53 after prolonged cell culture for senescence assays.

BEAS-2B cell lysates were harvested after 48 hr in resting or cytomix treatment conditions, or 24 hr etoposide treatment (6 μ M, as control inducer of senescence) (as Time 0 days) and after additional 5 days of unstimulated culture in same conditions (Time 5). β -actin as loading control (mean \pm SEM of n=3). * p <0,05 compared to corresponding medium control. **C.** qRT-PCR analysis of AUF-1 mRNA from BEAS-2B cells evaluated as described in A (mean \pm SEM of n=3). mRNA levels were normalized to housekeeping mRNA levels (GAPDH) and expressed as fold change over unstimulated cells as $2^{-\Delta\Delta C_t}$.

We further performed in both cell types a senescence-associated β -galactosidase (SA- β -gal) assay, as detection of β -galactosidase (β -gal) reflects an increase in lysosomal mass during replicative senescence. Cellular senescence was assessed by flowcytometric detection of β -D-galactopyranoside, a fluorogenic β -gal substrate. Treatment with cytomix induced a consistent and significant increase in β -gal activity compared to that of unstimulated cells in both cell types (to a maximum of 26.4% increase at 5 days for BEAS-2B and 23.6% increase at 5 days for HSAEC, $p \leq 0.05$ compared to controls) (**Figure 13**), also in this case in agreement with the sustained effect of control etoposide treatment.

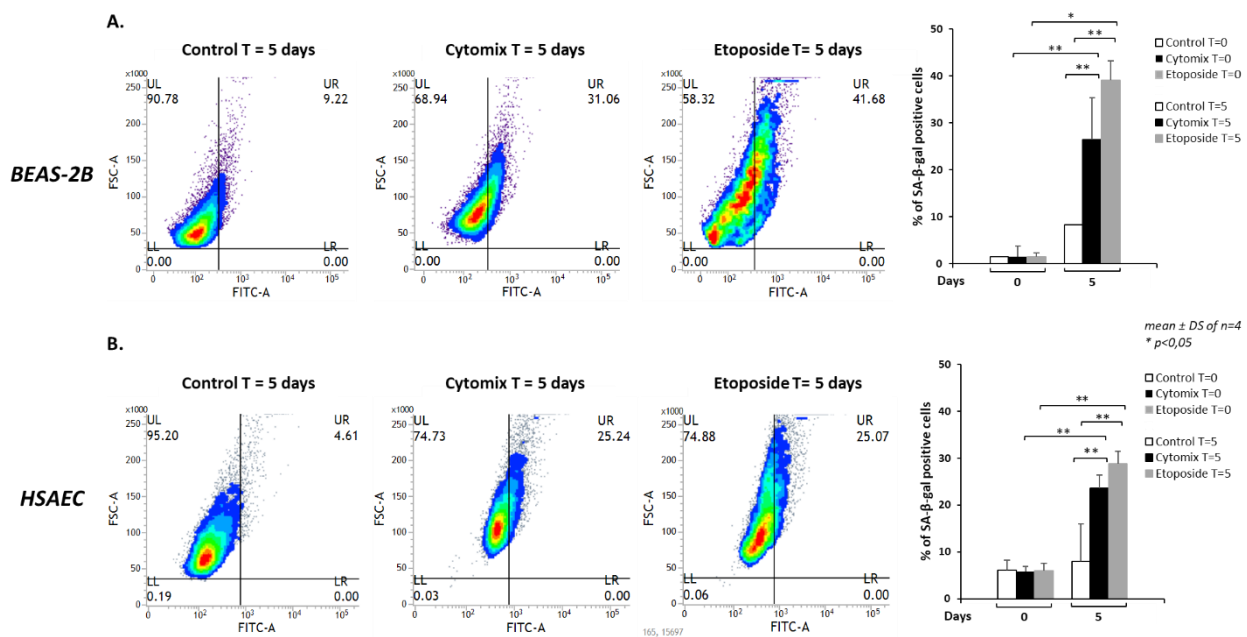


Figure 13. AUF-1 loss and cellular senescence readout (senescence-associated β -galactosidase) in BEAS-2B and HSAEC upon cytomix stimulation.

A-B. Representative contour plots (n=3) of SA- β -gal activity (**A**) in BEAS-2B cells (upper panels) and HSAEC cells (lower panels) and relative mean MFI (**B**) upon cytomix stimulation for 48 hours or etoposide for 24 hours. After treatment, the culture medium was replaced with no further stimulation and cells were incubated at 37°C for 5 days.

Lastly, we evaluated in the cell culture supernatants the expression of SASP-related inflammatory mediators IL-1 β , CCL2 (MCP-1), IL-6 and IL-8 [13] using the LEGENDplex immunoassay. In BEAS-2B cells, cytomix stimulation induced a robust and prolonged upregulation of IL-1 β , IL-6 and IL-8, that became statistically significant for the latter two at time 5, of greater magnitude than the one induced by etoposide and with little CCL2 modulation; interestingly, in HSAEC the increase for IL-6 and IL-8 was smaller and not sustained at time 5, while IL-1 β and CCL2 levels remained elevated up to 5 days from the initial stimulation (**Figure 14**).

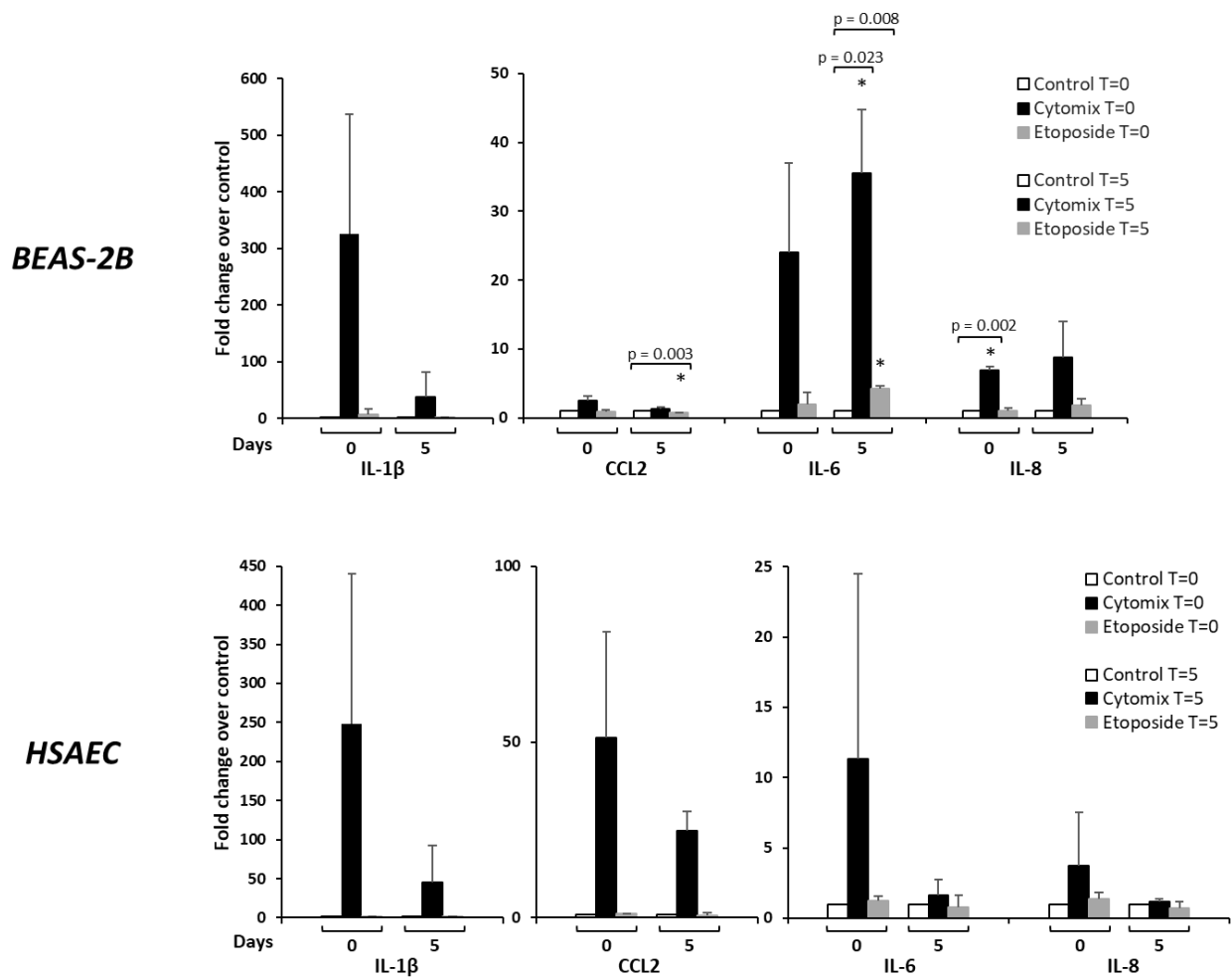


Figure 14. AUF-1 loss and cellular senescence readout (SASP cytokines) in BEAS-2B and HSAEC upon cytomix stimulation.

Detection of SASP cytokines in BEAS-2B (upper panel, mean \pm SEM of n=3) and HSAEC (lower panel, mean \pm SEM of n=2) supernatants upon indicated conditions. Cytokines levels are represented as fold change of mean fluorescence intensity over values in control cell supernatants.

*p<0,05 vs corresponding control.

Cytomix-induced enrichment of AUF-1 in extracellular vesicles.

Given that AUF-1 mRNA expression was unchanged upon cytomix stimulation for 48 hours in BEAS-2B [21] and in HSAEC (**Figure 11C-12C**), we subsequently verified if that protein loss was due to cytomix-induced protein degradation through proteasome complex.

BEAS-2B cells were pre-treated with the proteasome inhibitor MG-132 at the concentration of 10 μ M for 6 hours. After, the cell supernatant was replaced with fresh medium and the cells were harvested after 24, 30 and 48 hours in order to verify the persistence of proteasome inhibition. Western blot analysis revealed that AUF-1 levels were still decreased when the proteasome machinery was inhibited, as indicated by the accumulation of ubiquitinated proteins (**Figure 15**).

However, it was hard to combine the proteasome inhibition with the prolonged time of cytomix stimulation (48 hours), since at that time MG-132 has no more effect. Therefore, it remains to be determined the role of proteasome degradation in cytomix-induced loss of AUF-1.

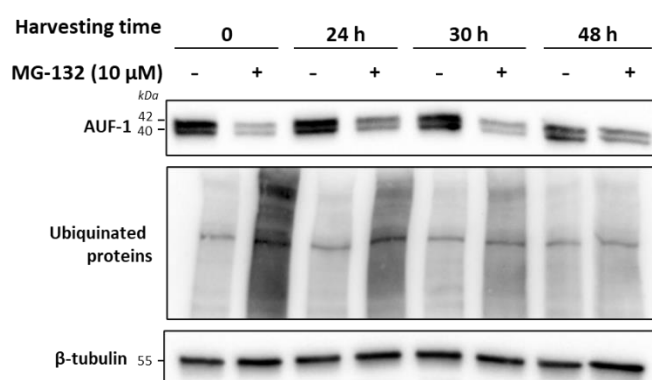


Figure 15. Proteasome inhibition in unstimulated BEAS-2B cells. Immunoblot of unstimulated BEAS2b cells pre-treated for 6 hours with proteasome inhibitor MG-132 (10 μ M) and then harvested after indicated time. β -tubulin as loading control.

Subsequently, given the rising interest on intercellular communication processes, we focused our attention on EVs release, given the possible involvement of RBPs as chaperon for mRNAs delivery [38,39]. EVs from normal and cytomix-treated BEAS-2B cells were isolated by differential centrifugation and characterized by immunoblot, DLS and TEM. Western blot analysis (n=3) revealed that along with the decrease of intracellular AUF-1 levels, cytomix induced a specular increase in secreted protein, detected in EVs fraction, both in BEAS-2B and HSAEC (**Figure 16**). CD63 and CD9 were detected as markers for EVs.

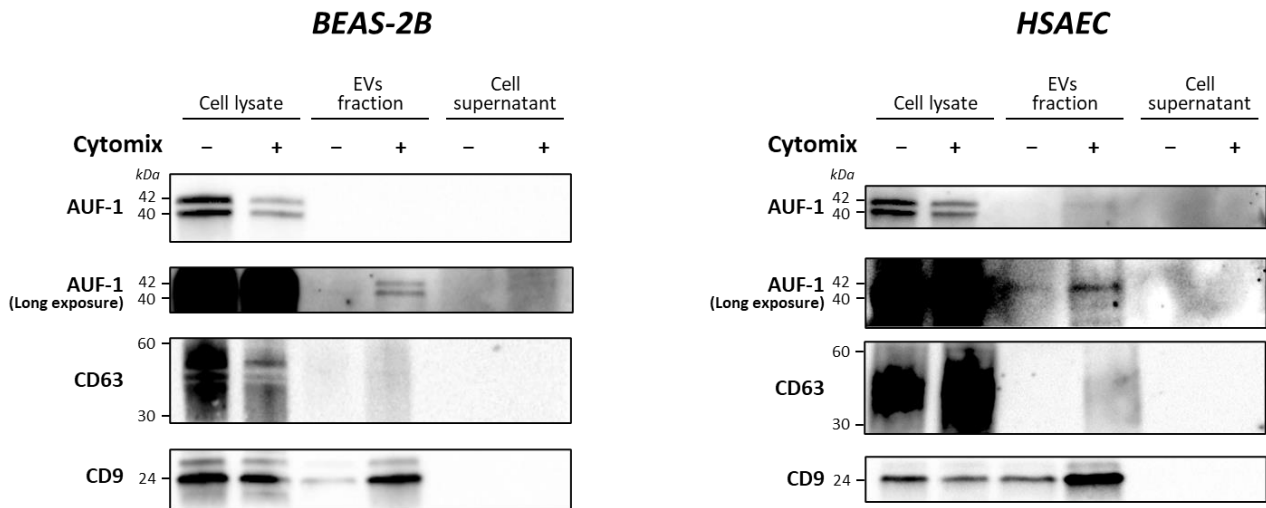


Figure 16. Detection of AUF-1 in extracellular vesicles (EVs) from cytomix-stimulated BEAS-2B and HSAEC. Representative immunoblots of AUF-1 in whole cell lysate, EVs fraction and remaining supernatant (as EV isolation control) obtained by differential centrifugation of culture media of BEAS-2B (left panel) and primary HSAEC cells (right panel) in the indicated conditions, showing cytomix-induced changes in AUF-1 cellular and extracellular detection. CD63 and CD9 were used as markers for EVs. (n=3).

Cell supernatant of EVs pellet, obtained after ultracentrifugation, was loaded to verify the correct isolation of EVs. DLS analysis showed that, both in basal conditions and upon cytomix stimulation, BEAS-2B cells release EVs population with an average size of 226,6 nm and 307,1 nm, respectively. DLS analysis of HSAEC supernatants from unstimulated and cytomix-treated cells showed a similar range of particle size (average size of 293,3 nm and 366,8 nm, respectively), with both EVs populations showing heterogeneity in size (**Figure 17**).

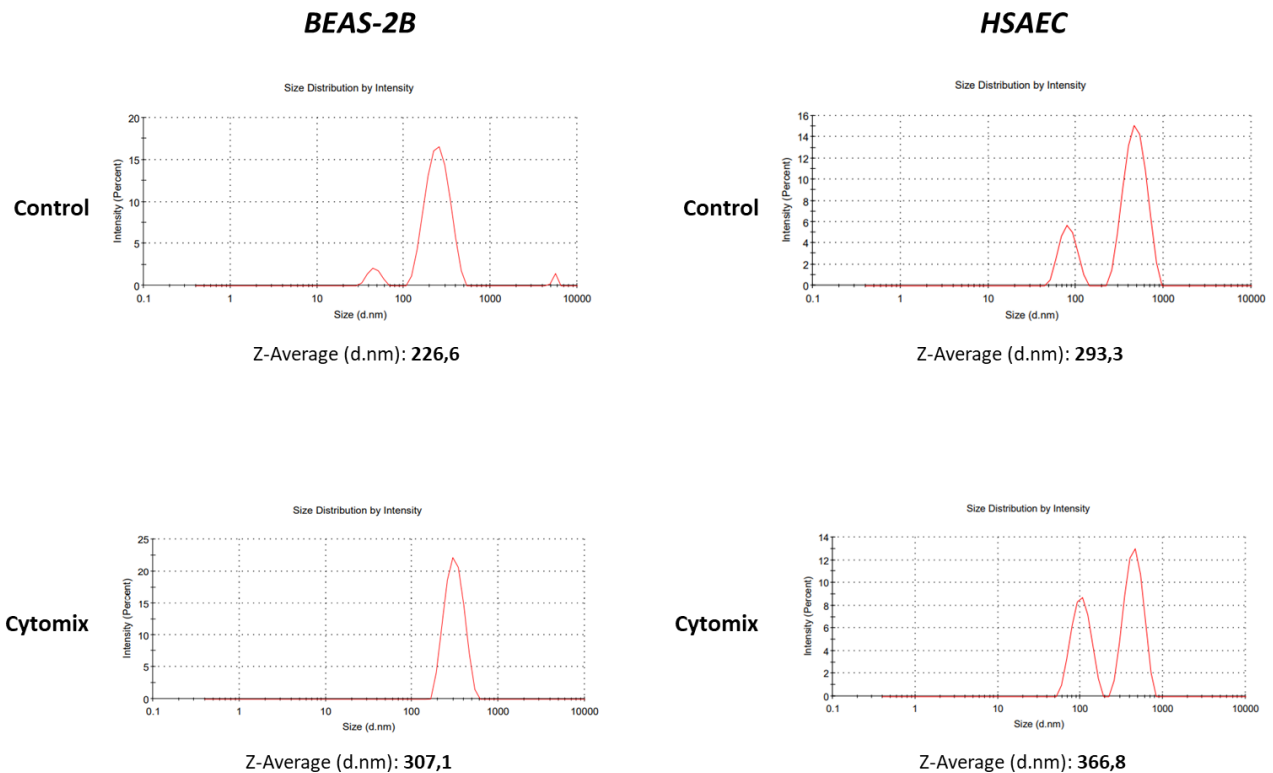
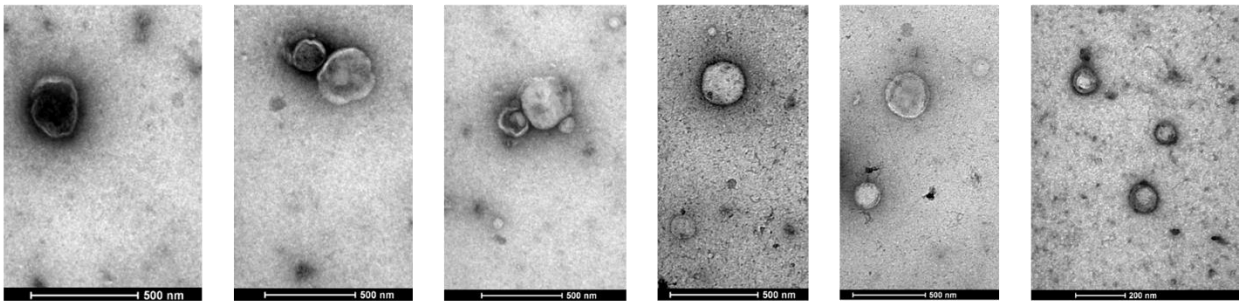


Figure 17. Detection of AUF-1 in extracellular vesicles (EVs) from cytomix-stimulated BEAS-2B and HSAEC. Dynamic light scattering (DLS) analysis showing the average size of EVs isolated from resting and cytomix-treated BEAS-2B (left panels) and HSAEC (right panels).

Further EV analysis by TEM in BEAS-2B cells (**Figure 18**) revealed EVs of spherical shape surrounded by a bilayer with a mean average diameter of 116.73 nm in unstimulated sample and 117 nm in cytomix-treated sample. Findings of smaller size in TEM measurement compared to DLS for EVs have been previously documented [89]. TEM analysis of BEAS-2B cell monolayers whose supernatants was used for EV analysis showed an enrichment of membrane protrusions suggesting of budding vesicles in cytomix-stimulated cells, suggesting that the cells are actively releasing EVs (**Figure 19**). Moreover, immunogold labeling with anti-AUF-1 antibody revealed some positive signals within EVs, suggesting a specific localization of AUF-1 in this extracellular compartment, in agreement to western blot results (**Figure 20**).

A.



B.

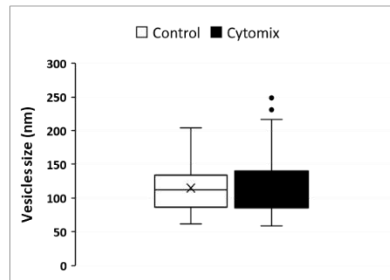


Figure 18. Detection of AUF-1 in extracellular vesicles (EVs) from cytomix-stimulated BEAS-2B

A-B. Representative transmission electron microscopy (TEM) images of EVs isolated from BEAS-2B cells and graph of mean \pm SD EVs size. The scale bars are reported in each photograph.

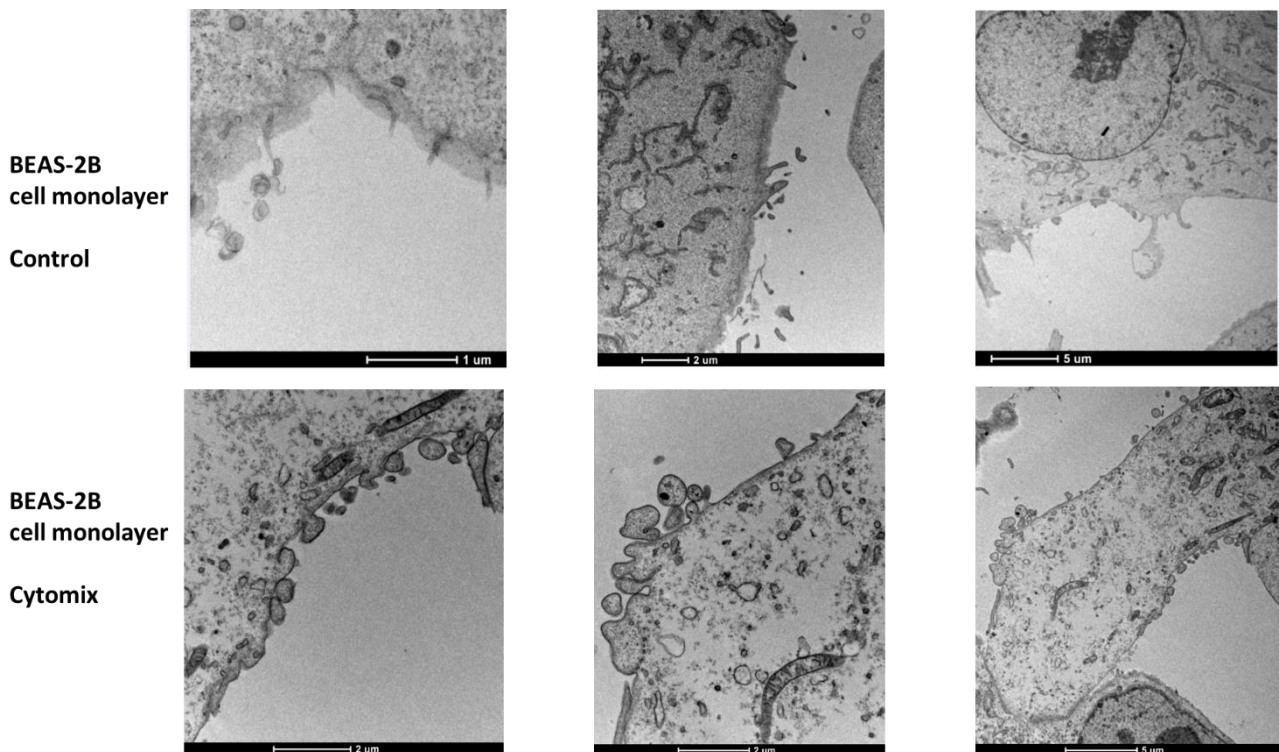


Figure 19. Cytomix-induced morphological changes in BEAS-2B cell monolayers by TEM.

Representative TEM images of BEAS-2B cells monolayer in basal condition (upper panels) and upon cytomix stimulation (lower panels). The scale bars are reported in each photograph.

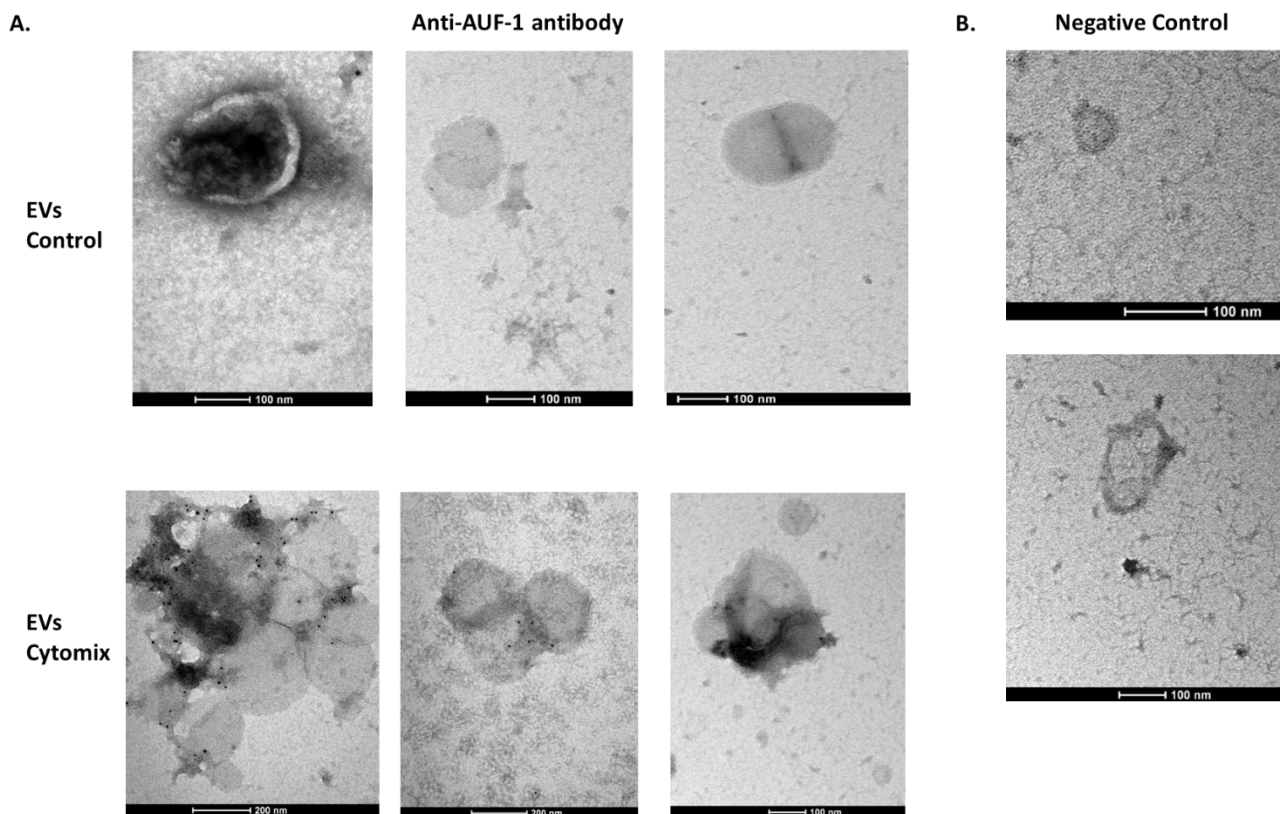


Figure 20. AUF-1 detection by immunogold labelling of BEAS-2B-derived EVs.

A. Immunogold labelling for AUF-1 in EVs derived from BEAS-2B cells in basal condition (upper panels) and upon cytomix stimulation (lower panels). **B.** The panels show the negative control (isotype matched Ab) for immunogold staining. The scale bars are reported in each photograph.

Gene Ontology analysis of AUF-1-bound epithelial transcript pool.

Target gene list (n=494) was subjected to computational analysis to map the main biological pathways putatively impacted by AUF-1 regulation. Gene Ontology analysis showed several Canonical Pathways (CPs) involving the recognized AUF-1 regulated genes of clear relevance for COPD (**Figure 21A**; **Table 6** and full list in **Table 7** at the end of the manuscript). Furthermore, AUF-1 targets were validated in a SASP database of secreted proteins and exosomal cargo-associated SASP factors (www.SASPAAtlas.com) originating from primary renal cortical epithelial cells and human lung fibroblasts, in which senescence was induced by X-irradiation (IR) and inducible RAS overexpression (RAS) [Basisty et al. *PloS Biol.* 2020]. In this setting, we identified 26 AUF-1 targets as secreted by IR-induced senescent epithelial cells vs control, 10 of which reaching significant increase ($\log_2(\text{SEN}/\text{CT}) \geq 0.58$) (**Figure 21B**). Importantly, 7 AUF-1 targets were also modulated in exosome SASP of IR-induced senescent fibroblasts ($\log_2(\text{SEN}/\text{CT}) \geq |0.58|$).

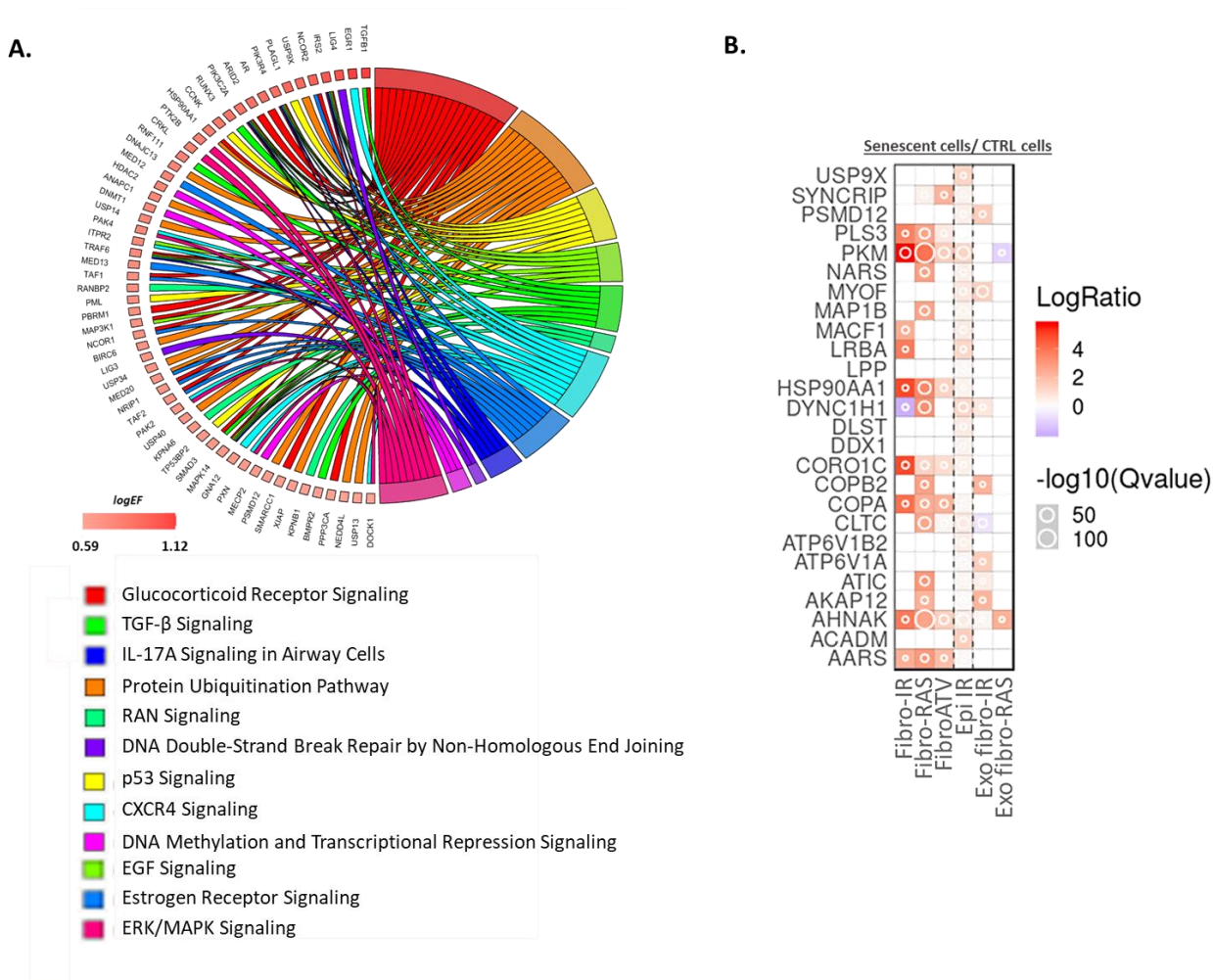


Figure 21. Gene Ontology analysis of AUF-1-bound transcripts: impact on canonical pathways and SASP proteome. **A.** Gene's log₂EF are presented in Circos plot, showing the association between selected AUF-1 targeted transcripts and the indicated canonical pathways. The colored arks connect a gene to pathways. The thickness of the arks correlates to the number of differentially enriched genes belonging to that pathway. Data derived from the list of statistically over-represented (p -value ≤ 0.05) pathways are selected among relevant COPD processes (see Table 2 and S2). **B.** Heatmap of Protein Secretomes-Ratio (Senescent cells/Control cells) of 26 AUF-1-associated transcripts identified as soluble, released protein or as exosomal cargo (Exo) in SASP secretome database (www.saspatlas.com) from senescent primary renal cortical epithelial cells induced by X-irradiation (Epi IR), and relative expression in primary human lung fibroblasts treated with IR or alternative SASP inducers such as inducible RAS overexpression (RAS) or atazanavir treatment (ATV). * FDR-corrected q -value ≤ 0.05 .

Table 6. Selected list of significant Canonical Pathways (CPs) of AUF-1 targets obtained by Ingenuity Pathway Analysis (IPA). Full list in Table 7.

Ingenuity Canonical Pathways	p-value	Ratio	Molecules
RANK Signaling in Osteoclasts	8,31764E-05	9,62E-02	TRAF6,MAP3K9,MAPK14,PIK3C2A,PTK2B,MAP3K1,IRS2,PIK3R4,XIAP,PPP3CA
Glucocorticoid Receptor Signaling	0,000234423	5,43E-02	PBRM1, PIK3C2A, SMAD3, MAP3K1, ARID2, PIK3R4, TRAF6, TAF1, AR, MAPK14, TGFB1, HSP90AA1, IRS2, NCOR1, NCOR2,SMARCC1, NRIP1, TAF2, PPP3CA
PPAR α /RXR α Activation	0,000245471	6,88E-02	CAND1,TRAF6,MAPK14,TGFB1,SMAD3,HSP90AA1,NCOA6,BMPR2,NR2C2,NCOR1,BCL3,NCOR2,MED12
Protein Ubiquitination Pathway	0,002344229	5,17E-02	USP14,MED20,USP9X,BIRC6,DNAJC13,ANAPC1,XIAP,TRAF6,USP13,PSMD12,HSP90AA1,USP40,NEDD4L,USP34
p53 Signaling	0,003090295	7,08E-02	MAPK14,PIK3C2A,PLAGL1,CCNK,IRS2,PIK3R4,PML,TP53BP2
EGF Signaling	0,003981072	8,57E-02	MAPK14,PIK3C2A,ITPR2,MAP3K1,IRS2,PIK3R4
TGF- β Signaling	0,004677351	7,29E-02	TRAF6,RUNX3,MAPK14,RNF111,TGFB1,SMAD3,BMPR2
RAN Signaling	0,005370318	1,76E-01	KPNB1,RANBP2,KPNA6
CXCR4 Signaling	0,006456542	5,46E-02	DOCK1,PXN,PAK4,PIK3C2A,ITPR2,GNA12,EGR1,PAK2,IRS2,PIK3R4
Estrogen Receptor Signaling	0,009772372	5,84E-02	MED13,TAF1,MED20,NCOR1,NCOR2,NRIP1,MED12,TAF2
Role of NFAT in Cardiac Hypertrophy	0,011220185	4,8E-02	MAPK14,HDAC2,PIK3C2A,CAMK1D,ITPR2,TGFB1,MAP3K1,IGF1R,IRS2,PIK3R4,PPP3CA
SAPK/JNK Signaling	0,012302688	6,09E-02	MAP3K9,PIK3C2A,CRKL,GNA12,MAP3K1,IRS2,PIK3R4
Role of Osteoblasts, Osteoclasts and Chondrocytes in Rheumatoid Arthritis	0,013803843	4,66E-02	TRAF6,MAPK14,PIK3C2A,PTK2B,TGFB1,BMPR2,IRS2,TCF7L1,PIK3R4,XIAP,PPP3CA
Osteoarthritis Pathway	0,016982437	4,72E-02	SIK3,FN1,GLIS2,GLI3,TGFB1,SMAD3,CTNNA1,BMPR2,RBPJ,TCF7L1
TNFR1 Signaling	0,022387211	0,08	PAK4,PAK2,MAP3K1,XIAP
B Cell Receptor Signaling	0,027542287	4,57E-02	MAP3K9,MAPK14,PIK3C2A,PTK2B,EGR1,MAP3K1,IRS2,PIK3R4,PPP3CA
IL-17A Signaling in Airway Cells	0,029512092	6,25E-02	TRAF6,MAPK14,PIK3C2A,IRS2,PIK3R4
CD40 Signaling	0,030902954	6,17E-02	TRAF6,MAPK14,PIK3C2A,IRS2,PIK3R4
CCR3 Signaling in Eosinophils	0,032359366	0,05	PAK4,MAPK14,PIK3C2A,ITPR2,PAK2,IRS2,PIK3R4
DNA Double-Strand Break Repair by Non-Homologous End Joining	0,035481339	1,43E-01	LIG4,LIG3
DNA Methylation and Transcriptional Repression Signaling	0,036307805	8,82E-02	MECP2,HDAC2,DNMT1

ERK/MAPK Signaling	0,037153523	4,33E-02	DOCK1,PXN,PAK4,PIK3C2A,PTK2B,CRKL,PAK2,IRS2,PIK3R4
Nitric Oxide Signaling in the Cardiovascular System	0,03801894	5,22E-02	PIK3C2A,ITPR2,HSP90AA1,IRS2,PIK3R4,PDE1C
IL-23 Signaling Pathway	0,040738028	6,67E-02	RUNX1,PIK3C2A,IRS2,PIK3R4
Choline Degradation I	0,042657952	0,5	ALDH7A1
Cardiac Hypertrophy Signaling	0,048977882	3,94E-02	MAP3K9,MAPK14,PIK3C2A,TGFB1,GNAN12,MAP3K1,IGF1R,IRS2,PIK3R4,PPP3CA

Expression of AUF-1-associated transcripts in primary small airway epithelial transcriptome and lung biopsy databases of COPD patients versus control subjects.

Disease-related changes in AUF-1 targeted transcripts were searched in a public microarray database from small airway epithelium obtained by bronchial brushings of stable COPD patients, smokers and non-smokers both with NLF (GEO ID: GSE5058) (**Figure 22**). Out of 494 AUF-1 targets, 150 (30%) were expressed as DEG in COPD patients vs. smokers with NLF ($FC \geq |1.5|$, $FDR \leq 0.05$), with the large majority (102 of them, 66% of DEG, 66 with $FC \leq -2$) resulting downregulated, with decreasing changes in non-smokers and healthy controls (**Figure 22A, Table 8** at the end of the manuscript). Genes whose relative probes showed discordant FC values (up- and down-regulated) were not included in the total gene count. Expression of the experimental AUF-1 targets was also searched in a newly generated database of RNA sequencing from whole lung biopsies of stable moderate-to severe COPD patients and age- and smoking history-matched smoker subjects with NLF (**Table 2**). Fifty-two (10%) AUF-1 targets were expressed as DEG and also in this case the majority (41 of them, 79%) were significantly downregulated ($\log_2FC \leq -0.40$) (**Figure 22, Table 9**). Crossing of the two AUF-1 target DEG lists identified 24 common transcripts, also in this case largely downregulated.

We further probed the transcriptomic profiles of GSE5058 by applying GSEA analysis to calculate the enrichment score of AUF-1-RNA targets characterized by an $EF \geq 2$ and $FDR \leq 0.05$ ($n=73$). This gene signature was found to be significantly enriched in COPD patients compared to smokers with NLF (difference of ES (dES) = 0.20; $p\text{-value} < 0.05$) (**Figure 22B**).

Central arrow down: Venn diagram showing overlap of AUF-1 IP DEG datasets and heatmap showing relative expression of n=24 shared AUF-1 targets. **B.** Gene signatures identified by GSVA in GSE5058 datasets. Boxplot showing the enrichment score (ES) of the AUF-1 transcript targets (EF \geq 2 and FDR \leq 0.05) in Non- Smokers (NS), Smokers (S) and Chronic obstructive pulmonary disease (COPD) patients. **p-value* \leq 0.05(Student's t-test).

Table 9. AUF-1 targets from RIP-Seq identified as DEG in RNAseq analysis of lung biopsies from COPD vs matched smoker controls (Figure 21).

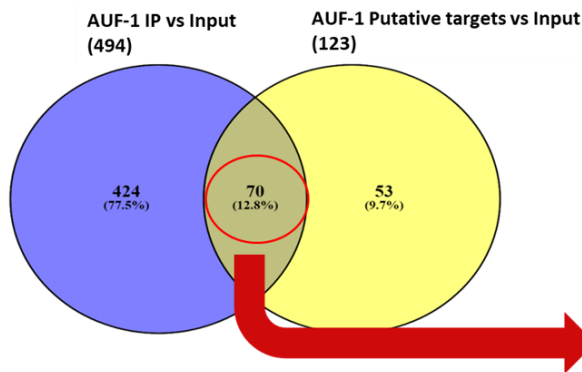
hgnc_symbol	ensembl_gene_id	Entrez gene_id	baseMean	log2FoldChange	lfcSE	stat	pvalue	padj
PTK2B	ENSG00000120899	2185	396.0882	1.52	0.261798	5.797319	6.74E-09	7.62E-06
SF3A2	ENSG00000104897	8175	73.79135	1.28	0.262028	4.9039	9.40E-07	0.000227
IRS2	ENSG00000185950	8660	452.0256	1.08	0.214528	5.05681	4.26E-07	0.000136
PER1	ENSG00000179094	5187	408.6825	0.91	0.295455	3.09459	0.001971	0.034843
GRINA	ENSG00000178719	2907	305.7394	0.86	0.275986	3.114607	0.001842	0.033724
CRYBG1	ENSG00000112297	202	149.2555	0.75	0.223963	3.367845	0.000758	0.018993
CPSF7	ENSG00000149532	79869	144.137	0.75	0.184255	4.07881	4.53E-05	0.002941
CORO1C	ENSG00000110880	23603	182.7091	0.73	0.252345	2.91104	0.003602	0.048691
SELENO N	ENSG00000162430	57190	104.0103	0.73	0.231076	3.162768	0.001563	0.030312
TRIM13	ENSG00000204977	10206	100.0442	0.60	0.197568	3.046343	0.002316	0.038002
SF1	ENSG00000168066	7536	356.7719	0.50	0.16285	3.083675	0.002045	0.03569
PBRM1	ENSG00000163939	55193	207.7532	-0.45	0.146572	-3.04898	0.002296	0.037977
SON	ENSG00000159140	6651	767.3564	-0.57	0.155555	-3.65121	0.000261	0.009887
KPNB1	ENSG00000108424	3837	380.6281	-0.58	0.190597	-3.0594	0.002218	0.037449
BMPR2	ENSG00000204217	659	354.92	-0.62	0.207531	-2.98079	0.002875	0.042681
MYO6	ENSG00000196586	4646	240.1765	-0.66	0.1734	-3.78205	0.000156	0.00681
TRIP12	ENSG00000153827	9320	247.407	-0.66	0.217495	-3.0333	0.002419	0.039
DHX36	ENSG00000174953	170506	160.1471	-0.68	0.233418	-2.92636	0.003429	0.047147
SMC3	ENSG00000108055	9126	135.904	-0.70	0.215952	-3.25658	0.001128	0.024646
SMC1A	ENSG00000072501	8243	218.3076	-0.71	0.168738	-4.22021	2.44E-05	0.001903
FBXO11	ENSG00000138081	80204	90.73085	-0.78	0.215722	-3.63061	0.000283	0.010434
ASXL2	ENSG00000143970	55252	65.1955	-0.81	0.225346	-3.58398	0.000338	0.011887
RANBP2	ENSG00000153201	5903	120.36	-0.82	0.22954	-3.57238	0.000354	0.012144
EIF4G3	ENSG00000075151	8672	115.454	-0.82	0.251236	-3.26873	0.00108	0.024059
CEBPZ	ENSG00000115816	10153	97.73255	-0.83	0.213576	-3.86863	0.000109	0.005592
UBR3	ENSG00000144357	130507	45.26861	-0.84	0.272804	-3.09168	0.00199	0.034957
SETX	ENSG00000107290	23064	265.1972	-0.86	0.166474	-5.13655	2.80E-07	0.000102
CHD1	ENSG00000153922	1105	212.3894	-0.86	0.290132	-2.96632	0.003014	0.04378
BPTF	ENSG00000171634	2186	531.0232	-0.86	0.206082	-4.17669	2.96E-05	0.002206
PSMD12	ENSG00000197170	5718	124.4738	-0.86	0.2513	-3.43894	0.000584	0.016298
LPP	ENSG00000145012	4026	412.0042	-0.87	0.204457	-4.24004	2.23E-05	0.0018

KIAA1109	ENSG00000138688	84162	240.6623	-0.89	0.24761	-3.57435	0.000351	0.012087
DDHD1	ENSG00000100523	80821	88.86231	-0.90	0.250807	-3.57719	0.000347	0.01206
MACF1	ENSG00000127603	23499	2201.619	-0.93	0.236038	-3.92415	8.70E-05	0.004613
DNMT1	ENSG00000130816	1786	139.8132	-0.93	0.184844	-5.02291	5.09E-07	0.000154
FRMD4B	ENSG00000114541	23150	174.164	-0.94	0.232992	-4.0224	5.76E-05	0.003506
ICE1	ENSG00000164151	23379	88.46696	-0.94	0.211827	-4.4537	8.44E-06	0.000955
PDS5B	ENSG00000083642	23047	106.4105	-0.95	0.192756	-4.91084	9.07E-07	0.000224
MTR	ENSG00000116984	4548	117.4341	-0.99	0.203255	-4.87876	1.07E-06	0.000253
TET3	ENSG00000187605	200424	22.10637	-1.00	0.320757	-3.1131	0.001851	0.033845
DMXL1	ENSG00000172869	1657	68.78459	-1.02	0.291393	-3.4864	0.00049	0.014716
NEU3	ENSG00000162139	10825	28.47665	-1.03	0.339304	-3.04736	0.002309	0.037987
TRIM5	ENSG00000132256	85363	35.78818	-1.04	0.352397	-2.94466	0.003233	0.045375
ERC1	ENSG00000082805	23085	124.4265	-1.04	0.193759	-5.36804	7.96E-08	4.58E-05
LEMD3	ENSG00000174106	23592	50.46957	-1.07	0.260014	-4.11646	3.85E-05	0.002597
MKI67	ENSG00000148773	4288	21.00531	-1.14	0.387295	-2.95523	0.003124	0.04447
DNAJC13	ENSG00000138246	23317	60.04671	-1.19	0.224584	-5.31574	1.06E-07	5.83E-05
CRYBG3	ENSG00000080200	131544	81.82177	-1.32	0.225379	-5.87238	4.30E-09	7.42E-06
EGR1	ENSG00000120738	1958	2022.615	-1.34	0.332313	-4.02393	5.72E-05	0.003506
DOCK7	ENSG00000116641	85440	17.04528	-1.41	0.397187	-3.54986	0.000385	0.012546
SAMD9L	ENSG00000177409	219285	98.68918	-1.42	0.401584	-3.53722	0.000404	0.012961
DOCK1	ENSG00000150760	1793	77.0781	-1.46	0.260014	-5.60119	2.13E-08	1.71E-05

***In silico* validation of AUF-1 targeted transcripts.**

Full length p45^{AUF-1} protein sequence (containing all exons) was submitted to target search through CatRAPID tool. Through this computational analysis we identified a list of 3367 coding genes as AUF-1 targets. Of these, 123 were expressed in our Input dataset with a TPM cutoff ≥ 0.5 in a least one biological replicate and shown a DP ≥ 0.75 computed by catRAPID tool. Of these computationally derived targets, 70 were shared with the RIP-Seq experimental dataset (**Figure 23, Table 10** at the end of the manuscript). Among these genes, some transcripts of particular interest have emerged, such as HDAC2, a deacetylase critically involved in the suppression of inflammatory gene transcription .

A.



B.

- | | | |
|-----------|------------|------------|
| 1. MUC1 | 26.SF3B3 | 51.MED20 |
| 2. KDM6B | 27.CORO1C | 52.UBXN7 |
| 3. SORBS3 | 28.RBMXL1 | 53.NIPBL |
| 4. MLXIP | 29.SMNDCC1 | 54.PEG10 |
| 5. DDX17 | 30.NUP214 | 55.MKI67 |
| 6. SMC1A | 31.PACS1 | 56.PRR14L |
| 7. TMED7 | 32.HDAC2 | 57.RREB1 |
| 8. VPS37C | 33.ANAPC1 | 58.ATXN1L |
| 9. RAP2C | 34.COL5A2 | 59.ZNF587 |
| 10.SRRM2 | 35.PRDM11 | 60.FRMD6 |
| 11.MYOF | 36.WNK1 | 61.PSMD12 |
| 12.NCOR2 | 37.GRINA | 62.TNRC6B |
| 13.VPS41 | 38.PAPSS1 | 63.APBB2 |
| 14.ZFH4 | 39.SDCBP | 64.FAM208B |
| 15.COPB2 | 40.ZNF462 | 65.HLCS |
| 16.PREP | 41.AHNAK | 66.SF1 |
| 17.ATIC | 42.DOCK9 | 67.ARF3 |
| 18.CNOT1 | 43.ALDH7A1 | 68.KPNB1 |
| 19.LMNB1 | 44.DCAF7 | 69.LPIN2 |
| 20.POGZ | 45.EIF4A3 | 70.XIAP |
| 21.SUCLA2 | 46.SCAF11 | |
| 22.TRIP12 | 47.PBRM1 | |
| 23.DDX3X | 48.ATP6V1A | |
| 24.NEK9 | 49.MACF1 | |
| 25.MPLKIP | 50.LPP | |

Figure 23. *In silico* validation of AUF-1 targets identified by RIP-Seq through the catRAPID tool.

A. Venn diagram showing the crossing of AUF-1 IP dataset from RIP-Seq (blue) and putative AUF-1 targets obtained from catRAPID prediction (yellow). **B.** List of transcripts shared by the two lists (Table 10).

Discussion

In human disease, we previously reported selective loss of AUF-1 in bronchiolar epithelium of patients with stable moderate disease, which was reproducible *in vitro* in cytokine- and cigarette smoke-stimulated airway epithelial cells [21]. A putative role of AUF-1 in chronic inflammation and accelerated aging characteristic of COPD was also strongly supported by several overlapping phenotypic features of the mouse AUF-1 knockout, such as overexpressed cytokine response to LPS-induced inflammation, spontaneous accelerated cellular senescence, accelerated age-related muscle wasting due to MMP9 upregulation, altered B cell maturation [16,28,29]. In COPD, bronchiolar epithelium displays overexpressed inflammatory responses and features of accelerated aging [13,90,91]. On this collective evidence, we further investigated the potential role of AUF-1 in airway epithelial responses and probed the mechanisms and functional effect of its downregulation.

We identified through RIP-Seq analysis 494 transcripts associated to AUF-1 in cytoplasmic lysates from unstimulated BEAS-2B cells. Given the potential limitation of the RIP-seq approach, we sought validation of the association to AUF-1 of a group of epithelial mRNAs, selected by significant enrichment of different amplitude, by biotin pulldown. This approach confirmed the interaction of AUF-1 to the 3'UTR of the selected transcripts, and in some case to specific regions, regardless the fold enrichment. Further validation of transcript association was obtained *in silico* through a search for predicted target mRNAs based on AUF-1 protein structure using the CATRapid search engine. Of the 123 putative targets identified *in silico*, 70 (56%) were included in the RIP-Seq experimental epithelial dataset.

Increased resolution of methods investigating RNP interfaces have expanded the knowledge on binding motifs by which RBP coordinate multiple transcripts. AUF-1 has been primarily defined for its high-affinity binding to the adenylate/urydylate-rich elements (ARE) [6,24,92]. Yoon et al. subsequently described AUF-1 binding to GU- and U-rich regions located in the intronic regions and 3'UTR of targeted transcripts identified in HEK293 cells through PAR-CLIP analysis, a high-resolution method for identification of RBP binding sequences, using isoform-specific overexpressing systems [41]. Our analysis reveals a predominant GC-rich signature in the 3'UTR of targets associating to the endogenous levels of AUF-1 in unstimulated airway epithelial cells, which we further validated by biotin pulldown using a representative synthetic GC-rich motif. As for the more characterized ARE elements, GC-rich elements are conserved in coding and non-coding regions of mammalian mRNAs. They have been identified in transcripts associated with the RBPs nucleolin, PCBP1 [Poly(RC) Binding Protein 1] and UPF and regulate target mRNA stability, decay, and translational efficiency [93,94].

Our *ex vivo* findings of AUF-1 loss of expression in stable COPD state vs controls along with *in vitro* evidence of its cytokine- and smoke-induced downregulation led us to consider that decreased AUF-1 levels coexisted with an epithelial expression profile characterized by inflammation, increased oxidative stress response and accelerated aging. To this end we previously documented, along with the loss of AUF-1 expression, a significant representation of established AUF-1-regulated transcripts as differentially expressed genes (DEG) in a transcriptomic database of bronchiolar epithelial cell from COPD patients versus control smokers, (GEO ID: GSE5058) [Ricciardi et al Int J Chron Obstruct Pulmon Dis 2018]. In the current study we identified in the GSE5058 database about 30% the AUF-1 targets identified by RIP-seq as DEGs in COPD patients vs control smokers and non-smokers; similarly, transcriptomic analysis of lung parenchyma from stable COPD versus matched smoker controls identified as DEG 10% of AUF-1 targets, a quote that was also largely overlapping with the targets identified in the bronchiolar epithelium database. In both analyses, the majority of AUF-1 targets showing as DEG were downregulated in COPD, which goes against a main role of AUF-1 as promoting mRNA decay, given its loss in this condition. Therefore, we aimed at comparing the mRNA steady-state and stability of AUF-1 validated targets in resting BEAS-2B cells (with basal AUF-1 levels) to cytokine-treated cells (with decreased AUF-1 levels) to cells carrying siRNA-mediated AUF-1 silencing (near-total loss of AUF-1). For all transcripts, cytomix effect on steady state was highly similar between the latter two conditions, yet it affected target mRNA decay differently. We compared the mRNA decay patterns of the experimental targets to that of IL-6, which is an ARE-bearing gene whose mRNA decay is accelerated by AUF-1 binding [26,29]. As expected, IL-6 mRNA steady state was highly increased by cytomix along with mRNA stability, and near-complete loss of AUF-1 by siRNA led to an even more rapid mRNA stabilization. In the same settings, the validated epithelial mRNA targets displayed instead different steady-state and decay patterns. Upon cytomix stimulation some targets increased (FoxP4, TGF β 1, DDX17) or did not change (HDAC2) their steady state levels but displayed a highly stable mRNA at baseline, which was not modified by AUF-1 loss, ruling against a role as positive regulator of mRNA stability and shifting a putative function towards translational control.

The two AUF-1-targeted transcription factors, GLIS2 and EGR1 showed different behaviours according to AUF-1 cellular levels. Both had no changes in mRNA steady state levels upon cytomix treatment but displayed a stimulus-induced increase in mRNA half-life, thus inferring a role of AUF-1 levels in regulating their baseline mRNA decay. However, while for IL-6 mRNA the larger mRNA stabilization occurred in cells with near-total loss of AUF-1, stabilization of GLIS2 mRNA did not further increase in this condition. EGR-1 mRNA showed at baseline a very short half-life and, similar to IL-6 and GLIS2 mRNAs, a strong mRNA stabilization occurred upon decreased AUF-1 levels seen

along cytomix treatment. Unexpectedly, this effect was largely reverted with treatment in cells with near-total AUF-1 loss through silencing. Overall, AUF-1 functional outcomes on mRNA target levels appear to be heterogeneous and, at least in part, dependent on relative amounts of AUF-1 available. Indeed, phenotypic changes related to disease were observable already in heterozygous AUF-1 knockout mice [16,28,29]. The functional analysis of AUF-1 association on targets identified by PAR-CLIP revealed a diversified repertoire as well, with subsets of targets regulated through accelerated decay and other subsets regulated instead through a positive effect on mRNA stability or translation [41]. This is also likely related to subcellular distribution and activation state of other RBPs and miRNAs that share binding ability with AUF-1 motifs, such as HuR [41] and could contextually associate with AUF-1 targets in conditions of decreased, or absent, AUF-1.

The novel finding of EGR1 among most enriched among AUF-1 targets could be of specific relevance. EGR1 is a major transcription factor, induced by different cellular stressors as an immediate-early response gene, regulating the expression of multiple genes involved in fundamental cell processes [95]. Increased levels of EGR1 were detected in late-stage lung emphysema [96] and in COPD transcriptomic analysis of lung samples from GOLD-2 stage COPD patients versus GOLD-0 smokers, with expression localized on small airways and alveolar epithelium by immunofluorescence [97]. EGR1 has a key role in regulating autophagy associated to cigarette smoke [98]. Moreover, the G allele of the Egr-1 gene polymorphism was associated with an increased risk of developing COPD [99]. Primary human fibroblast exposed to cigarette smoke extract (CSE) showed EGR1-dependent increased release of MMP2 [97] and IL-8: in this case, activation of EGR1 by CSE increases intracellular levels and secretion of heat shock protein (HSP)-70, which stimulates cells as feedback to produce IL-8 [100]. Importantly, HSP70 is a known partner of AUF-1 together with HSP27, in the assembly of ribonucleoprotein complex denominated ASTRC (ARE-BP and signal transduction regulated complex), responsible for the recruitment of mRNA degradation machinery to bound transcripts [28,101]. At large, the newly found AUF-1 targets in airway epithelium are enriched in intracellular and signaling molecules, likely also due to their detection in unstimulated cells. The evidence supporting relevance for COPD-related pathogenesis are striking, as already in the top twenty pathways identified with high statistical value are listed signaling pathways related to DNA damage, accelerated aging, inflammation, COPD comorbidities (for example RANK, p53, EGF, TGF- β , CXCR4 Signaling, SAPK, ERK/MAPK).

Increasing evidence indicate a key role of stress-induced epithelial senescence in COPD, IPF and lung cancer [102]. A relevant finding further supporting the role of AUF-1 in this context is the persistent decrease of its protein levels, maintained 5 days after the stimulation with cytomix and etoposide in both BEAS-2B and primary epithelial cells, associated to indices of increased lysosomal

damage and cell cycle arrest, together with the persistence of pro-inflammatory cytokines that characterize SASP acquired by senescent cells. *In vitro* and *in vivo* models of CSE exposure indicate that airway epithelial cells undergo accelerated senescence upon exposure [103] and we previously demonstrated loss of AUF-1 upon CSE exposure in BEAS-2B cells [21]. The novel finding of cytomix-triggered accelerated aging *in vitro*, to levels highly superimposable to those induced by etoposide, strongly suggests that the concurrent loss of AUF-1 is contributing to cytokine-induced cellular aging, supporting in human lung disease the role of this RBP in inflammatory and aging responses revealed by the AUF-1 knockout mice model. This evidence expands to AUF-1 targets in the SASP secretome: established targets and COPD determinants such as IL-1 β [28], IL-6 [26], IL-8 [104] but also the newly identified targets that we found to be listed among members of the complex SASP secretome [37]. These results could help understanding the role of AUF-1 expression in bronchiolar epithelium as a factor coordinately regulating cell cycle-, DNA damage- and SASP-related responses, whose loss in oxidative stress-driven context as COPD may therefore critically contribute to the complex inflammaging response through mechanisms yet to be uncovered, likely also related to its extracellular transfer in exosomes. Loss of RBPs is a relevant feature in aging: the loss of the RBP HuR related to replicative senescence, in cell lines and aged tissue has been long established, with multiple mechanisms involved [105,106]. Recent studies are increasingly reported loss of other RBPs in *in vitro* and mouse models of cellular senescence, such as HuD [107], fragile X-related protein 1 (FXR1) [108], Cold shock domain containing E1 (CSDE1)/upstream of N-Ras (UNR) [109].

Increasing knowledge on lung homeostatic and pathological processes uncovers the role of EVs as regulator of important biological processes, including [110]. EVs are a group of membraned vesicles characterized by different size and origin. Microvesicles are the larger size class of EVs with a diameter of 50-500 nm and they are generated by budding of the plasma membrane. Exosomes are smaller EVs of 50–150 nm size originated in the lumen of multivesicular endosomes (MVEs) as intraluminal vesicles (ILVs) and secreted during the fusion of MVEs with the cell surface [31]. AUF-1 detection into EVs opens multiple hypothesis of its function. AUF-1 may be shuttled in EVs as a stimulus-specific process to preserve RNP-bound RNA targets and spread inflammation to other organs. It can also be secreted in airway fluid and potentially affect macrophage function. Identifying AUF-1 partners in EVs, both as target mRNAs but also associated RBPs, could be predictive of how AUF-1 could impact biological processes in recipient cells and it can be harnessed to develop new therapeutic strategies.

The complex mechanisms underlying AUF-1 function not only rely on features of target binding, but extend to interactions with other RNA (miRNAs, lncRNA) and protein components of RNP complex as well as to posttranslational modifications [24] leaving much uncharted fields to be further evaluated to our investigation, which is the first describing AUF-1 function in a model of human chronic inflammatory lung disease. Our study has been shaped primarily upon the *ex vivo* finding of a diminished bronchiolar expression of AUF-1 in stable COPD disease. This is a challenging experimental system to interrogate *in vitro* and created several boundaries for interpretation of our results. The AUF-1 targets have been identified in unstimulated conditions with basal AUF-1 levels and may not represent fully those affected by AUF-1 regulation upon exposure to chronic pathogenic conditions. More in-depth analysis of AUF-1 isoform-specific targets may reveal further levels of regulatory complexity and specific functions. Moreover, the cytomix-induced migration of AUF-1 in extracellular vesicles has limited the use of overexpression models as phenotype rescue strategy and further extends the need for analysis of AUF-1 function in COPD to its extracellular component. To this end, stable AUF-1 knockout epithelial cell lines will provide an important tool to understand AUF-1 role in both intra-and extracellular compartments.

RBPs have been recently targeted in lung cancer to antagonize overexpression of pathogenic molecules under their control, as for HuR [111,112]. So far, their pathogenic role and targeting in COPD is lagging, despite this condition being a major risk factor for lung cancer development. Identification of a global downregulation of RBPs in epithelial COPD transcriptomic databases [22] and of the protein TTP as a relevant target in a mouse smoke-induced model of COPD [] have been recently identified, warranting further studies in this field. Discovery of disease-associated RBP profiles and their regulatory influence may identify novel molecules and mechanisms useful as biomarkers for phenotypic traits and for other smoking-related diseases with increased lung cancer risk as idiopathic lung fibrosis [13,113]; furthermore, specific RBP signatures may coordinately control pathogenic pathways or altered response to treatment related to SASP, and therefore may be extended to COPD comorbidities and to other chronic diseases characterized by inflammaging as heart disease, diabetes, obesity. In these instances, molecular resolution of RBP-transcript interface could reveal elements targetable for therapeutics.

Appendix

Generation of BEAS-2B-AUF-1 knockout clones. To perform genome editing, two guide sequences targeting AUF-1 gene, (gRNA F1: CACCGACCGGGGGCGGAACCGCGTC; gRNA R1: AAACGACGCGGTTCCGCCCGGTC; gRNA F2: CACCGCGTCTGGAGGCACCGAAGG; gRNA R2: AAACCCTTCGGTGCCTCCAGACGCC) were designed in the first exon of the gene, in order to target all AUF-1 isoforms, based on high target specificity and low number of off-target sites, as determined using the online CRISPRdirect tool available at <http://crispr.dbcls.jp/>. Complementary oligonucleotides containing cloning overhangs were synthesized at ThermoFisher, annealed, and the obtained double stranded oligonucleotide was cloned into the pSpCas9(BB)-2A-GFP (PX458) plasmid, which was obtained from Addgene. Plasmids were then transfected into BEAS-2B cells using FuGENE® HD Transfection Reagent (*Promega*) following the manufacturer's instructions. Two days after transfection, GFP-positive BEAS-2B cells were sorted using FacsARIA III (*Beckton Dickinson*) and plated as single clones in 96-well plates. Clones were cultured for 2–3 weeks and analyzed for successful AUF-1- knockout by western blotting. Validated AUF-1- knockout clones were then amplified and stored.

Generation of BEAS-2B cells knockout for AUF-1.

To gain insight into the biological effects of AUF-1 protein, we generated a CRISPR/Cas9 AUF-1 knockout model in BEAS-2B cell line (see Methods). After sgRNA/Cas9 plasmid transfection (**Figure 24A**), several clones (generated with two independent sgRNAs targeting AUF-1 exons 1) were identified, and validated by immunoblotting to completely lack AUF-1 protein (**Figure 24B**). This model will be used for future experiments for the validation of AUF-1 function.

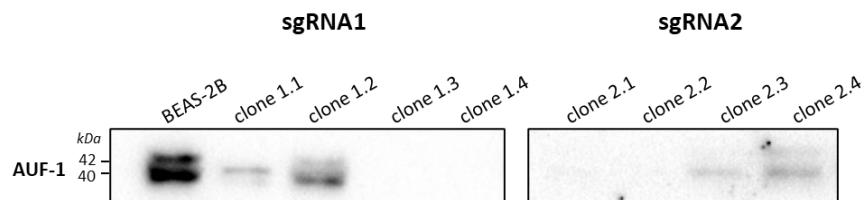


Figure 24. BEAS-2B AUF-1-knockout cells. Representative immunoblots of AUF-1 expression in BEAS-2B cells and AUF-1 clones generated using gRNA1 and gRNA2.

2. Final considerations: Study limitations and Future direction

2.1. Study limitations

In this thesis we investigated the potential role of AUF-1 in airway epithelial responses and probed the mechanisms and functional effect of its downregulation which is the finding that we observed in human COPD [21].

The limits of the study performed pertain both to the general approach as well as to specific problems encountered along the use of experimental procedures: as we aimed at integrating different laboratory techniques and bioinformatic tools, we often found ourselves facing problems that concerned both specific protocols at the bench as well as aspects of the *in silico* analysis.

- The identification of AUF-1 targets in unstimulated conditions with basal AUF-1 levels may not represent fully those affected by AUF-1 regulation upon exposure to chronic pathogenic conditions.
- The discrepancy in PCA analysis among the three biological replicates of immunoprecipitation experiments in BEAS-2B cells may be due to the use of cells of different passages, or by the different lot of anti-AUF-1 antibody used. The use of bioinformatic tools capable of removing the batch effect may be considered.
- The incomplete silencing of the AUF-1 protein we achieved should be overcome through the development of cells with stable loss of AUF-1 gene. To this end, we have applied the CRISPR-Cas9 technique to develop airway epithelial knockout cell line, as shown in our preliminary data (see appendix). This cellular model will be used to gain a deeper characterization of AUF-1-related transcriptomic changes and its epithelial functions, and will provide an important tool to understand AUF-1 role in both intra- and extracellular compartments.
- The use of overexpression models as phenotype rescue strategy will be planned in order to validate AUF-1 silencing results. However, this is a complex model. First of all, we will need to overexpress all four AUF-1 isoforms and evaluate their contribution on both their overlapping and specific targets [41]. Importantly, AUF-1 overexpression does not necessarily counterpose the phenotype obtained in condition of AUF-1 loss. In fact, transgenic mice overexpressing p37^{AUF-1} isoform develop spontaneous soft tissue sarcomas, along with the increase of multiple cancer-associated mRNAs, although it is the isoform most associated with increased decay of ARE-mRNAs [114]. In light of these considerations and given the importance of AUF-1 migration into EVs, a more important and interesting approach may be to block EVs release.

2.2. Future direction

Studies on the biology of the RBPs regulating the fate of protein-coding RNAs, both at basic level and increasingly in translational settings, indicate the powerful impact of these regulatory factors in

coordinating the expression of multiple genes participating to a disease process. On these basis, our general aim is to study the role of the RBP AUF-1 in human airway epithelium as determinant of inflammation and accelerated cellular senescence in COPD pathogenesis.

Much of this aim is still being tested by work in progress, and the discussed limitations we encountered so far are contributing to improve the design of our upcoming studies and shape future directions.

- In the short term, *in vitro* studies will address validation of AUF-1-bound targets followed by functional characterization of AUF-1 regulation using phenotype rescue cellular models.
- AUF-1-dependent changes on mRNA target stability and translation could be investigated through a Luciferase reporter system using constructs bearing the 3'UTR of pulldown-validated AUF-1 targets and known AUF-1-regulated SASP factors (IL-6, CXCL8, CCL2) in resting/cytomix-treated cells with normal or ablated AUF-1 levels.
- The study of AUF-1-containing EVs will be significantly expanded. The transcriptomic analysis of EVs isolated from resting and cytomix-treated airway cells could be used to search for AUF-1 motifs to identify AUF-1 target delivered into EVs. More challenging and fascinating is the characterization of EVs isolated from COPD patients and their effect on phagocytic activity of activity on neighbouring epithelial cells, macrophages and other infiltrating immune cells.

Overall, validation of AUF-1 associated targets and characterization of functional outcomes will allow to study how altered post-transcriptional processes shape epithelial cell phenotype, how they contribute to disease or altered response to treatment. Interestingly, AUF-1 detection into EVs opens multiple hypothesis of its function, including the possibility to develop new therapeutic strategies. More in general, the identification of RBP profiles may identify novel molecules and mechanisms useful as biomarkers for phenotypic traits and for other smoking-related diseases. Furthermore, specific RBP signatures may control pathogenic pathways related to SASP, and therefore may be extended to COPD comorbidities and to other chronic diseases characterized by the same features. It is our hope that on the long term, preclinical evidences may be translated to clinical research on COPD and conceptually transferable to other chronic inflammatory lung diseases, according to the concept of translational medicine “from the bench to the bedside”.

Table 4. Full list of experimental targets of the RIP-Seq (n=494). EF = Enrichment Factor, FDR = False Discovery Rate.

GENE SYMBOL	EF	FDR	GENE SYMBOL	EF	FDR	GENE SYMBOL	EF	FDR
PRR36	5,73	0,020203	DIO2	1,77	0,007614	PDE1C	1,6	0,010379
GLIS2	4,95	0,00745	DOCK4	1,77	0,017798	PKM	1,6	0,028566
ZNF385A	4,4	5,15E-05	ERC1	1,77	0,009031	QSER1	1,6	0,032528
TCF7L1	4,14	0,003217	ERF	1,77	0,013416	UBXN7	1,6	0,009406
PIANP	3,52	0,000871	MCM10	1,77	0,026995	ZNF281	1,6	0,043779
MBD6	3,42	2,49E-09	MTR	1,77	0,007964	ABL2	1,59	0,011266
MUC1	3,37	1,81E-06	NOL11	1,77	0,044104	C2CD3	1,59	0,029498
FOXP4	3,27	7,46E-05	POLR1A	1,77	0,028233	CLASP1	1,59	0,023914
KDM6B	3,2	0,000139	POM121	1,77	0,006086	FN1	1,59	0,031621
FBRS1	3,09	0,000336	TRERF1	1,77	0,005063	ICE1	1,59	0,025196
C1orf226	2,86	0,039358	TRPS1	1,77	0,02826	LRPPRC	1,59	0,048861
AP001972.5	2,84	0,032884	TSPYL1	1,77	0,001935	NIPBL	1,59	0,029242
STX1B	2,83	0,012534	YTHDC2	1,77	0,045855	NRIP1	1,59	0,015232
CRTC1	2,73	0,001314	ARFGEF3	1,76	0,025196	PAK2	1,59	0,010016
AL513165.1	2,66	0,034496	CSTF2T	1,76	0,020999	PHF20	1,59	0,023516
ATXN2L	2,6	1,37E-08	DDX1	1,76	0,029098	RGP1	1,59	0,017329
RNF44	2,6	0,000146	DMXL1	1,76	0,003715	TAF2	1,59	0,047451
IL17RD	2,58	0,026678	FASTKD2	1,76	0,042233	UBR4	1,59	0,010492
KIAA1522	2,58	1,23E-08	TRIP12	1,76	0,00196	ADAT1	1,58	0,037967
HIVEP3	2,47	0,000702	WDR47	1,76	0,024643	GLI3	1,58	0,034866
RNF165	2,46	0,026659	ACADM	1,75	0,010333	GNA12	1,58	0,037128
MNT	2,45	0,000654	ATG2B	1,75	0,003324	KPNA6	1,58	0,043402
BICRA	2,43	0,011555	BAG3	1,75	0,019395	MAP1B	1,58	0,025353
SYNPO	2,43	8,11E-07	DDX3X	1,75	0,018266	MAPK14	1,58	0,030753
RIN3	2,42	0,005946	ERCC6L	1,75	0,028489	NEU3	1,58	0,041545
ZBTB7A	2,42	0,001117	HSP90AA1	1,75	0,023752	PAN3	1,58	0,020557
AL158212.3	2,38	0,020718	MINPP1	1,75	0,042958	PEG10	1,58	0,017043
ZFHX2	2,37	0,04323	NEK9	1,75	0,015949	RFX7	1,58	0,022644
AL365181.3	2,3	0,004542	SYT16	1,75	0,044134	SIPA1L2	1,58	0,046799
ZNF697	2,3	0,043455	TOP2B	1,75	0,007066	SMAD3	1,58	0,014242
SORBS3	2,29	0,000841	WDR36	1,75	0,04438	THUMPD1	1,58	0,038338
AKAP12	2,27	0,000177	COPA	1,74	0,041701	TP53BP2	1,58	0,037967
LINC01963	2,25	0,011995	DHX40	1,74	0,019459	USP40	1,58	0,043165
ZNF555	2,25	0,002913	DMXL2	1,74	0,021561	BHLHE40	1,57	0,04742
PPP1R13L	2,24	0,000906	DOP1A	1,74	0,037632	CRYBG1	1,57	0,026855
NFIX	2,19	0,000846	EPG5	1,74	0,016524	MIEF1	1,57	0,032281
CREB3L1	2,18	0,038525	GIT2	1,74	0,013925	MKI67	1,57	0,021889
TGFB1	2,16	0,003603	KLHL24	1,74	0,013386	PAFAH1B1	1,57	0,011198
EGR1	2,15	0,00016	MPLKIP	1,74	0,024103	PJA2	1,57	0,04553
FRMD4B	2,15	0,047394	POLR3A	1,74	0,017697	PRR14L	1,57	0,01896

MLXIP	2,15	0,002861	PTK2B	1,74	0,037832	RAB11FIP1	1,57	0,020592
PER1	2,15	0,00825	SF3B3	1,74	0,027771	RREB1	1,57	0,042637
GENE_SYMBOL	EF	FDR	GENE_SYMBOL	EF	FDR	GENE_SYMBOL	EF	FDR
AC037459.3	2,14	0,032596	URB1	1,74	0,01869	STXBP1	1,57	0,02617
CRNKL1	2,14	0,005231	ADGRL1	1,73	0,023475	SYNCRIP	1,57	0,048277
DDX17	2,13	6,31E-06	BEND3	1,73	0,039406	TMPO	1,57	0,020991
RERE	2,13	2,14E-05	CORO1C	1,73	0,003582	AAK1	1,56	0,030407
AC012513.3	2,12	0,037906	CRKL	1,73	0,002197	ATXN1L	1,56	0,039925
CPNE8	2,11	0,019199	EED	1,73	0,028789	DICER1	1,56	0,026375
SMC1A	2,09	0,000554	FBXO11	1,73	0,017493	GBF1	1,56	0,039763
UBR5	2,09	1,57E-05	GCH1	1,73	0,020541	GJA1	1,56	0,043402
FAM98B	2,07	0,002364	IREB2	1,73	0,004428	PCNX1	1,56	0,024485
SF3A2	2,07	0,004451	PAICS	1,73	0,002123	PXN	1,56	0,023271
CAMTA2	2,06	0,004478	RBMXL1	1,73	0,012451	ZNF587	1,56	0,035882
NFATC2IP	2,06	4,41E-05	RNF111	1,73	0,039845	ANKRD17	1,55	0,049895
SVEP1	2,06	0,010826	SMNDC1	1,73	0,014471	ARHGEF7	1,55	0,045818
WDR3	2,06	0,007161	CHD1	1,72	0,022644	FRMD6	1,55	0,019485
ZXDA	2,06	0,033232	FAM222B	1,72	0,033972	MECP2	1,55	0,045722
CDC42EP1	2,05	0,003648	MAMLD1	1,72	0,020665	PSMD12	1,55	0,035743
POLR1B	2,05	0,001552	NPEPPS	1,72	0,012968	RBPJ	1,55	0,028668
SCARNA7	2,05	0,001451	NUP214	1,72	0,032662	TFCP2	1,55	0,046532
TMEM178B	2,05	0,017907	PACS1	1,72	0,0035	TNRC6B	1,55	0,026788
LIG4	2,04	0,012687	PLS3	1,72	0,027236	TUBGCP4	1,55	0,042235
NPTXR	2,03	0,016856	PTPN14	1,72	0,001692	APBB2	1,54	0,020718
YLPM1	2,03	0,0003	AP1G1	1,71	0,005593	CAND1	1,54	0,049007
FAM120C	2,02	0,013125	CPSF7	1,71	0,004825	FAM208B	1,54	0,02591
IRS2	2,01	0,003319	DNAJC13	1,71	0,011256	HIF1AN	1,54	0,021424
BCL3	2	0,016054	MED12	1,71	0,00733	HLCS	1,54	0,045645
DAGLA	2	0,017176	MIB1	1,71	0,003195	NSD3	1,54	0,023881
RAB14	2	0,000195	NHLRC2	1,71	0,013803	SF1	1,54	0,020991
SUPT16H	2	0,009683	RAB3B	1,71	0,001753	ARF3	1,53	0,024611
TMED7	2	0,001526	RALGAPB	1,71	0,012032	ARHGAP21	1,53	0,030715
ZMIZ2	2	0,003344	RAPH1	1,71	0,002963	HPS3	1,53	0,035819
ZNF888	2	0,027102	STK35	1,71	0,008742	KMT2A	1,53	0,035849
CBX5	1,99	6,46E-05	ZBTB10	1,71	0,016877	KPNB1	1,53	0,037058
SAMD9L	1,99	0,019229	DNMBP	1,7	0,030715	LPIN2	1,53	0,035849
VPS37C	1,99	0,01312	DOCK5	1,7	0,002992	NR2C2	1,53	0,036826
ZNF221	1,99	0,033232	GPATCH8	1,7	0,020406	PSME4	1,53	0,023595
COL12A1	1,98	0,002492	HDAC2	1,7	0,017493	SMARCC1	1,53	0,043732
HNRNPH2	1,98	0,009816	PDCD4	1,7	0,019496	SWAP70	1,53	0,029709
MARCKS	1,98	0,00108	WDR11	1,7	0,026166	TNKS2	1,53	0,028566
NECTIN1	1,98	0,003359	ABCD3	1,69	0,013297	VPS26A	1,53	0,049267
SMC3	1,98	0,006401	ANAPC1	1,69	0,011066	XIAP	1,53	0,038949
SMG8	1,98	0,005702	COL5A2	1,69	0,026243	ZNF609	1,53	0,025731

SON	1,98	0,000719	DYNC1H1	1,69	0,011245	BMPR2	1,52	0,044307
HSD17B4	1,97	0,012356	FAM160A1	1,69	0,030753	GLG1	1,52	0,049989
RAP2C	1,97	0,001002	HEATR6	1,69	0,031621	MICAL2	1,52	0,023687
TET3	1,97	0,00108	KIAA1109	1,69	0,013803	PPP3CA	1,52	0,029034
GENE_SYMBOL	EF	FDR	GENE_SYMBOL	EF	FDR	GENE_SYMBOL	EF	FDR
BRD4	1,96	0,001236	SAMD4B	1,69	0,012752	BPTF	1,51	0,03306
POM121C	1,96	0,000586	VIRMA	1,69	0,024321	NEDD4L	1,51	0,037268
SRRM2	1,96	8,29E-05	ATP6V1B2	1,68	0,024643	PUM2	1,51	0,031876
TOP1	1,96	0,007066	CTNNA1	1,68	0,037269	RBM12	1,51	0,048281
AL031587.5	1,95	0,011276	DDX46	1,68	0,033733	USP13	1,51	0,032808
EPN1	1,95	0,005678	DNMT1	1,68	0,045856	VPS13D	1,51	0,044307
MAST4	1,95	0,04438	FBXO38	1,68	0,046632	DOCK1	1,5	0,032698
MYOF	1,95	0,001451	GLCCI1	1,68	0,021442	PDPR	1,5	0,045776
DHX36	1,94	0,009784	MAST3	1,68	0,022542			
NCOR2	1,94	0,01749	MYO6	1,68	0,045818			
SLFN11	1,93	0,002032	NF1	1,68	0,006862			
TMEM8B	1,93	0,030496	SRGAP1	1,68	0,014568			
ACTR6	1,92	0,038294	TEAD3	1,68	0,023595			
FOXJ2	1,92	0,001315	TUG1	1,68	0,010064			
NATD1	1,92	0,007202	USP14	1,68	0,026166			
NUP160	1,92	0,024106	WNK1	1,68	0,003319			
PSAT1	1,92	0,004771	BLMH	1,67	0,011218			
VPS41	1,92	0,002647	GRINA	1,67	0,014701			
ZFHX4	1,92	0,000304	ITPR2	1,67	0,037847			
ADAMTSL4	1,91	0,015213	MYO1E	1,67	0,044752			
EIF5B	1,91	0,013755	NOL9	1,67	0,023025			
ELFN2	1,91	0,022742	NT5DC3	1,67	0,00686			
TRIP4	1,91	0,028566	PAK4	1,67	0,044413			
CCDC120	1,9	0,048041	PAPSS1	1,67	0,048926			
DCAF1	1,9	0,007427	PIKFYVE	1,67	0,007311			
LEMD3	1,9	0,007714	RAP1GAP2	1,67	0,028754			
MCCC2	1,9	0,009406	TRAF6	1,67	0,029498			
USP9X	1,9	0,000813	ZNF148	1,67	0,006623			
BRWD3	1,89	0,001032	APOBEC3C	1,66	0,023025			
COL4A6	1,89	0,048614	APOOL	1,66	0,030843			
DDX20	1,89	0,024583	ATXN1	1,66	0,017697			
EFTUD2	1,89	0,018566	CYB5RL	1,66	0,04387			
MYO5A	1,89	0,000363	DDHD1	1,66	0,018784			
PLAGL1	1,89	0,007338	EIF4G3	1,66	0,005624			
SART3	1,89	0,004504	LRBA	1,66	0,010908			
GRAMD1B	1,88	0,012766	MAP3K9	1,66	0,031094			
SF3B4	1,88	0,004953	MAVS	1,66	0,027521			
TRIM13	1,88	0,00447	MED13	1,66	0,004775			
CEBPZ	1,87	0,006399	N4BP2	1,66	0,044454			

CLTC	1,87	0,004478	SDCBP	1,66	0,011202
COPB2	1,87	0,018715	TCEAL9	1,66	0,016357
GEMIN5	1,87	0,027269	TRIM14	1,66	0,014761
NKRF	1,87	0,016649	ZNF462	1,66	0,006012
PLAGL2	1,87	0,002967	AHNAK	1,65	0,004293
AR	1,86	0,009351	DOCK9	1,65	0,009985
GTF3C1	1,86	0,012556	MTHFR	1,65	0,043674
GENE_SYMBOL	EF	FDR	GENE_SYMBOL	EF	FDR
KLHL28	1,86	0,024761	NARS	1,65	0,049028
MTHFD1	1,86	0,022111	NIF3L1	1,65	0,026166
NCAPD3	1,86	0,007964	PDS5B	1,65	0,017191
NPRL3	1,86	0,011963	PFKFB2	1,65	0,048243
PIK3R4	1,86	0,020724	PHIP	1,65	0,037967
WDR7	1,86	0,013386	RANBP6	1,65	0,04022
AASDH	1,85	0,042012	RBM15	1,65	0,026375
ANKFY1	1,85	0,00301	SRP54	1,65	0,049409
CHD9	1,85	0,001472	TBL1X	1,65	0,026678
CTPS1	1,85	0,007537	TULP3	1,65	0,036366
DLST	1,85	0,001575	ZFP36L2	1,65	0,042908
FBXO30	1,85	0,004943	ALDH7A1	1,64	0,014021
MDGA1	1,85	0,043779	CBLL1	1,64	0,048504
TRIM5	1,85	0,018156	CCDC82	1,64	0,043851
ZNF607	1,85	0,025731	DCAF7	1,64	0,010168
AARS	1,84	0,011116	EIF4A3	1,64	0,034914
ARID2	1,84	0,002333	FAM168A	1,64	0,006668
HNRNPM	1,84	0,010043	KIF24	1,64	0,028489
MMP24OS	1,84	0,005863	MDN1	1,64	0,041353
NEURL1B	1,84	0,002201	PML	1,64	0,023736
PREP	1,84	0,005009	PRMT6	1,64	0,048848
PRICKLE2	1,84	0,005593	RANBP2	1,64	0,019229
PROSER3	1,84	0,011712	SCAF11	1,64	0,031544
AC004943.2	1,83	0,043402	SETX	1,64	0,018609
FAM160B1	1,83	0,003045	TAF1	1,64	0,01499
FIGN	1,83	0,005163	TANC2	1,64	0,004497
SEC24D	1,83	0,01381	ZBED5	1,64	0,045056
THRA	1,83	0,009064	MPHOSPH8	1,63	0,042752
ATIC	1,82	0,011266	MYNN	1,63	0,048625
CAMK1D	1,82	0,009148	PALLD	1,63	0,00675
CNOT1	1,82	0,000347	PBRM1	1,63	0,014761
IBA57	1,82	0,040616	SBNO1	1,63	0,013508
KBTBD7	1,82	0,040506	SEMA3A	1,63	0,026078
RECQL	1,82	0,030015	ZNF765	1,63	0,033282
RNF20	1,82	0,030753	ZNF845	1,63	0,045805
RPAP3	1,82	0,020991	ZSWIM6	1,63	0,012968

VAPB	1,82	0,000414	ATP6V1A	1,62	0,042774
ZNF219	1,82	0,035867	ERCC6	1,62	0,028489
CRYBG3	1,81	0,019199	MAP3K1	1,62	0,024063
LMNB1	1,81	0,00929	METTL16	1,62	0,01558
NACC2	1,81	0,009609	MPP5	1,62	0,019258
PIK3C2A	1,81	0,005266	NCOR1	1,62	0,02023
RUNX3	1,81	0,032767	SELENON	1,62	0,016313
ZBTB21	1,81	0,004685	SIK3	1,62	0,019111
BMS1	1,8	0,033384	SPATA13	1,62	0,049615
DLD	1,8	0,012046	SRPRA	1,62	0,022284
GENE_SYMBOL	EF	FDR	GENE_SYMBOL	EF	FDR
PLRG1	1,8	0,033329	BIRC6	1,61	0,028575
POGZ	1,8	0,001353	HELLS	1,61	0,031652
ZNF106	1,8	0,000631	IGF1R	1,61	0,016693
ZNF551	1,8	0,021424	LIG3	1,61	0,032138
AMIGO2	1,79	0,027058	MACF1	1,61	0,014615
ASXL2	1,79	0,002797	MAT2A	1,61	0,038683
DENND4C	1,79	0,015438	NCOA6	1,61	0,016198
MYORG	1,79	0,042896	PDP1	1,61	0,026678
NHS	1,79	0,034874	RTCB	1,61	0,042896
TSC22D4	1,79	0,024377	RUNX1	1,61	0,021062
CCNK	1,78	0,018413	SPRED2	1,61	0,0298
DOCK7	1,78	0,042714	TSC22D2	1,61	0,020438
G3BP2	1,78	0,002332	USP34	1,61	0,009784
SEC23IP	1,78	0,037567	DDX21	1,6	0,043779
SUCLA2	1,78	0,015724	FTO	1,6	0,049895
TOPORS	1,78	0,014124	LPP	1,6	0,013544
UBR3	1,78	0,016497	MED20	1,6	0,032051
WDFY3	1,78	0,001371	NAV2	1,6	0,027014

For tables 5 and 6 see the text.

Table 7. Complete list of significant Canonical Pathways (CPs) of AUF-1 targets obtained by Ingenuity Pathway Analysis (IPA).

Ingenuity Canonical Pathways	p-value	Ratio	Molecules
TR/RXR Activation	6,0256E-05	0,1	RAB3B,PIK3C2A,NCOA6,IRS2,THRA,BCL3,NCOR1,NCOR2,PIK3R4,DIO2
Paxillin Signaling	7,76247E-05	8,87E-02	DOCK1,PXN,PAK4,MAPK14,PIK3C2A,PTK2B,ARHGEF7,PAK2,IRS2,PIK3R4,GIT2
RANK Signaling in Osteoclasts	8,31764E-05	9,62E-02	TRAF6,MAP3K9,MAPK14,PIK3C2A,PTK2B,MAP3K1,IRS2,PIK3R4,XIAP,PPP3CA
Glucocorticoid Receptor Signaling	0,000234423	5,43E-02	PBRM1,PIK3C2A,SMAD3,MAP3K1,ARID2,PIK3R4,TRAF6,TAF1,AR,MAPK14,TGFB1,HSP90AA1,IRS2,NCOR1,NCOR2,SMARCC1,NRIP1,TAF2,PPP3CA
PPAR α /RXR α Activation	0,000245471	6,88E-02	CAND1,TRAF6,MAPK14,TGFB1,SMAD3,HSP90AA1,NCOA6,BMP2,NR2C2,NCOR1,BCL3,NCOR2,MED12
FAK Signaling	0,000630957	8,18E-02	DOCK1,PXN,PAK4,PIK3C2A,ARHGEF7,PAK2,IRS2,PIK3R4,GIT2
Folate Transformations I	0,000758578	3,33E-01	MTHFR,MTR,MTHFD1
Germ Cell-Sertoli Cell Junction Signaling	0,000812831	6,38E-02	MAP3K9,PXN,PAK4,EPN1,MAPK14,PIK3C2A,TGFB1,PAK2,MAP3K1,CTNNA1,IRS2,PIK3R4
RAR Activation	0,000891251	6,32E-02	PBRM1,MAPK14,TGFB1,SMAD3,MAP3K1,SOBBS3,ARID2,NCOR1,NCOR2,SMARCC1,NRIP1,PML
Inosine-5'-phosphate Biosynthesis II	0,001380384	6,67E-01	PAICS,ATIC
Protein Ubiquitination Pathway	0,002344229	5,17E-02	USP14,MED20,USP9X,BIRC6,DNAJC13,ANAPC1,XIAP,TRAF6,USP13,PSMD12,HSP90AA1,USP40,NEDD4L,USP34
Renin-Angiotensin Signaling	0,002398833	6,77E-02	PAK4,MAPK14,PIK3C2A,PTK2B,ITPR2,PAK2,MAP3K1,IRS2,PIK3R4
Mitotic Roles of Polo-Like Kinase	0,002951209	9,09E-02	SMC3,TGFB1,WEE1,HSP90AA1,ANAPC1,SMC1A
PAK Signaling	0,002951209	7,14E-02	PXN,PAK4,PTK2B,PIK3C2A,ARHGEF7,PAK2,IRS2,PIK3R4
p53 Signaling	0,003090295	7,08E-02	MAPK14,PIK3C2A,PLAGL1,CCNK,IRS2,PIK3R4,PML,TP53BP2
EGF Signaling	0,003981072	8,57E-02	MAPK14,PIK3C2A,ITPR2,MAP3K1,IRS2,PIK3R4
2-ketoglutarate Dehydrogenase Complex	0,004466836	0,4	DLST,DLSD
Lysine Degradation II	0,004466836	0,4	AASDH,ALDH7A1
Lysine Degradation V	0,004466836	0,4	AASDH,ALDH7A1
TGF- β Signaling	0,004677351	7,29E-02	TRAF6,RUNX3,MAPK14,RNF111,TGFB1,SMAD3,BMP2
RAN Signaling	0,005370318	1,76E-01	KPNB1,RANBP2,KPNA6
HGF Signaling	0,005495409	6,45E-02	DOCK1,MAP3K9,PXN,PIK3C2A,CRKL,MAP3K1,IRS2,PIK3R4
Clathrin-mediated Endocytosis Signaling	0,005623413	5,29E-02	MYO6,EPN1,PIK3C2A,USP9X,CLTC,AAK1,IRS2,PIK3R4,AP1G1,MYO1E,PPP3CA
Rac Signaling	0,006309573	6,3E-02	PAK4,PTK2B,PIK3C2A,MAP3K1,PAK2,PIKFYVE,IRS2,PIK3R4

CXCR4 Signaling	0,006456542	5,46E-02	DOCK1,PXN,PAK4,PIK3C2A,ITPR2,GNA12,EGR1,PAK2,IRS2,PIK3R4
Estrogen Receptor Signaling	0,009772372	5,84E-02	MED13,TAF1,MED20,NCOR1,NCOR2,NRIP1,MED12,TAF2
Role of NFAT in Cardiac Hypertrophy	0,011220185	4,8E-02	MAPK14,HDAC2,PIK3C2A,CAMK1D,ITPR2,TGFB1,MAP3K1,IGF1R,IRS2,PIK3R4,PPP3CA
Integrin Signaling	0,011220185	4,8E-02	DOCK1,PXN,PAK4,PIK3C2A,ARF3,ARHGEF7,CRKL,PAK2,PIKFYVE,IRS2,PIK3R4
Synaptogenesis Signaling Pathway	0,012022644	4,28E-02	MARCKS,STXBP1,MAPK14,PIK3C2A,STX1B,CRKL,ARHGEF7,MAP1B,NECTIN1,IRS2,PAFAH1B1,PIK3R4,SYT16,GRINA
SAPK/JNK Signaling	0,012302688	6,09E-02	MAP3K9,PIK3C2A,CRKL,GNA12,MAP3K1,IRS2,PIK3R4
GNRH Signaling	0,012882496	5,2E-02	MAP3K9,PXN,PAK4,MAPK14,PTK2B,ITPR2,EGR1,PAK2,MAP3K1
Chronic Myeloid Leukemia Signaling	0,012882496	6,03E-02	PIK3C2A,HDAC2,TGFB1,SMAD3,CRKL,IRS2,PIK3R4
Actin Cytoskeleton Signaling	0,012882496	4,7E-02	DOCK1,PXN,PAK4,FN1,PIK3C2A,ARHGEF7,CRKL,GNA12,PAK2,IRS2,PIK3R4
Mouse Embryonic Stem Cell Pluripotency	0,013489629	5,98E-02	MAPK14,PIK3C2A,BMP2,IRS2,TCF7L1,PIK3R4,XIAP
Role of Osteoblasts, Osteoclasts and Chondrocytes in Rheumatoid Arthritis	0,013803843	4,66E-02	TRAF6,MAPK14,PIK3C2A,PTK2B,TGFB1,BMP2,IRS2,TCF7L1,PIK3R4,XIAP,PPP3CA
TCA Cycle II (Eukaryotic)	0,014454398	1,25E-01	SUCLA2,DLST,DLD
FGF Signaling	0,014454398	6,52E-02	MAPK14,PIK3C2A,CRKL,MAP3K1,IRS2,PIK3R4
Leucine Degradation I	0,015135612	2,22E-01	ACADM,MCCC2
Renal Cell Carcinoma Signaling	0,015135612	6,45E-02	PAK4,PIK3C2A,TGFB1,PAK2,IRS2,PIK3R4
Reelin Signaling in Neurons	0,016218101	6,38E-02	MAP3K9,PIK3C2A,CRKL,IRS2,PAFAH1B1,PIK3R4
Osteoarthritis Pathway	0,016982437	4,72E-02	SIK3,FN1,GLIS2,GLI3,TGFB1,SMAD3,CTNNA1,BMP2,RBPJ,TCF7L1
IL-9 Signaling	0,018197009	8,51E-02	PIK3C2A,IRS2,BCL3,PIK3R4
Hereditary Breast Cancer Signaling	0,019498446	5,16E-02	PBRM1,HDAC2,PIK3C2A,WEE1,IRS2,ARID2,SMARCC1,PIK3R4
PDGF Signaling	0,021877616	5,94E-02	PIK3C2A,ABL2,CRKL,MAP3K1,IRS2,PIK3R4
Purine Nucleotides De Novo Biosynthesis II	0,022387211	1,82E-01	PAICS,ATIC
TNFR1 Signaling	0,022387211	0,08	PAK4,PAK2,MAP3K1,XIAP
Acute Myeloid Leukemia Signaling	0,023988329	5,83E-02	RUNX1,PIK3C2A,IRS2,TCF7L1,PML,PIK3R4
Signaling by Rho Family GTPases	0,025118864	4,25E-02	MAP3K9,PAK4,PIK3C2A,PTK2B,ARHGEF7,GNA12,PAK2,PIKFYVE,CDC42EP1,IRS2,PIK3R4
Assembly of RNA Polymerase I Complex	0,02630268	1,67E-01	POLR1A,POLR1B
Role of Tissue Factor in Cancer	0,026915348	5,19E-02	MAPK14,PTK2B,PIK3C2A,GNA12,EGR1,IRS2,PIK3R4
B Cell Receptor Signaling	0,027542287	4,57E-02	MAP3K9,MAPK14,PIK3C2A,PTK2B,EGR1,MAP3K1,IRS2,PIK3R4,PPP3CA

Molecular Mechanisms of Cancer	0,028840315	3,73E-02	PAK4,PIK3C2A,GNA12,ARHGEF7,SMAD3,CTNNA1,BMPR2,PIK3R4,XIAP,MAPK14,NF1,TGFB1,PAK2,RBPJ,IRS2
IL-17A Signaling in Airway Cells	0,029512092	6,25E-02	TRAF6,MAPK14,PIK3C2A,IRS2,PIK3R4
CD40 Signaling	0,030902954	6,17E-02	TRAF6,MAPK14,PIK3C2A,IRS2,PIK3R4
ErbB Signaling	0,030902954	5,5E-02	PAK4,MAPK14,PIK3C2A,PAK2,IRS2,PIK3R4
CCR3 Signaling in Eosinophils	0,032359366	0,05	PAK4,MAPK14,PIK3C2A,ITPR2,PAK2,IRS2,PIK3R4
Circadian Rhythm Signaling	0,033884416	9,09E-02	PER1,BHLHE40,GRINA
GM-CSF Signaling	0,035481339	5,95E-02	RUNX1,PIK3C2A,IRS2,PIK3R4,PPP3CA
Aryl Hydrocarbon Receptor Signaling	0,035481339	4,9E-02	NCOA7,NFIX,TGFB1,HSP90AA1,NCOR2,NR1P1,ALDH7A1
DNA Double-Strand Break Repair by Non-Homologous End Joining	0,035481339	1,43E-01	LIG4,LIG3
Amyotrophic Lateral Sclerosis Signaling	0,035481339	5,31E-02	PIK3C2A,IRS2,PIK3R4,XIAP,PPP3CA,GRINA
DNA Methylation and Transcriptional Repression Signaling	0,036307805	8,82E-02	MECP2,HDAC2,DNMT1
ERK/MAPK Signaling	0,037153523	4,33E-02	DOCK1,PXN,PAK4,PIK3C2A,PTK2B,CRKL,PAK2,IRS2,PIK3R4
Nitric Oxide Signaling in the Cardiovascular System	0,03801894	5,22E-02	PIK3C2A,ITPR2,HSP90AA1,IRS2,PIK3R4,PDE1C
Gα12/13 Signaling	0,038904514	4,79E-02	PXN,PTK2B,PIK3C2A,GNA12,MAP3K1,IRS2,PIK3R4
Human Embryonic Stem Cell Pluripotency	0,040738028	4,76E-02	PIK3C2A,TGFB1,SMAD3,BMPR2,IRS2,TCF7L1,PIK3R4
IL-23 Signaling Pathway	0,040738028	6,67E-02	RUNX1,PIK3C2A,IRS2,PIK3R4
Neuropathic Pain Signaling In Dorsal Horn Neurons	0,040738028	5,13E-02	CAMK1D,PIK3C2A,ITPR2,IRS2,PIK3R4,GRINA
Choline Degradation I	0,042657952	0,5	ALDH7A1
Sulfate Activation for Sulfonation	0,042657952	0,5	PAPSS1
Angiopoietin Signaling	0,043651583	5,62E-02	PAK4,PIK3C2A,PAK2,IRS2,PIK3R4
Estrogen-Dependent Breast Cancer Signaling	0,044668359	5,56E-02	PIK3C2A,IGF1R,IRS2,PIK3R4,HSD17B4
Superpathway of Methionine Degradation	0,044668359	8,11E-02	DLD,MAT2A,MTR
Cardiac Hypertrophy Signaling	0,048977882	3,94E-02	MAP3K9,MAPK14,PIK3C2A,TGFB1,GNA12,MAP3K1,IGF1R,IRS2,PIK3R4,PPP3CA

Table 8. AUF1 targets from RIP-Seq identified as DEG in GSE5058 database (Figure 21).

Gene Name Probe ID	Gene Name	FC S vs NS	FC COPD vs NS	FC COPD vs S	FDR S vs NS	FDR COPD vs NS	FDR COPD vs S
AAK1_205434_s_at	AAK1	-1.17	2.03	2.37	0.469897	0.021086	0.032392
AASDH_235435_at	AASDH	-1	-3.38	-3.38	0.440533	0.001294	0.039932
ABCD3_1554878_a_at	ABCD3	1.26	-3.38	-4.25	0.306527	0.003054	0.03357
ADAMTSL4_226071_at	ADAM TSL4	1.3	4.58	3.52	0.302344	0.006052	0.028377
ALDH7A1_213591_a_t	ALDH7 A1	-1.15	2.21	2.53	0.434129	0.002874	0.01685
ANKRD17_225852_a_t	ANKR D17	1.16	-2.19	-2.54	0.426806	0.006507	0.015434
APOOL_213289_at	APOOL	1.04	-2.08	-2.16	0.395676	0.00708	0.021562
ARF3_200734_s_at	ARF3	-1.24	1.72	2.14	0.420739	0.030535	0.028699
ATG2B_226684_at	ATG2B	1.14	-1.8	-2.05	0.440552	0.011771	0.031026
ATP6V1A_201971_s_at	ATP6V 1A	1.41	-1.56	-2.2	0.130562	0.040144	0.02084
BPTF_209271_at	BPTF	1.02	-2.08	-2.11	0.46733	0.029573	0.023045
CCDC82_223300_s_a_t	CCDC8 2	1.25	-3.73	-4.67	0.290011	0.011508	0.022287
CHD1_204258_at	CHD1	1.07	-2.28	-2.45	0.425096	0.013281	0.015718
CLASP1_240757_at	CLASP 1	1.04	-3.84	-3.99	0.349083	0.122587	0.044096
CNOT1_1554052_at	CNOT1	1.15	-2.07	-2.39	0.422792	0.022938	0.046065
CREB3L1_213059_at	CREB3 L1	1.01	2.2	2.18	0.341422	0.002041	0.02538
DDX17_230180_at	DDX17	1.17	-13.61	-15.92	0.383776	0.000387	0.047352
DDX3X_212515_s_at	DDX3X	1.23	-2.09	-2.58	0.403669	0.041865	0.037017
DHX36_223138_s_at	DHX36	1.08	-2.58	-2.79	0.483939	0.001143	0.021094
DHX36_223139_s_at	DHX36	-1.07	-5.31	-4.96	0.407713	0.000859	0.011513
DHX40_222574_s_at	DHX40	1.18	-1.84	-2.17	0.294556	0.008248	0.025778
DOCK1_241708_at	DOCK1	1.42	3.14	2.21	0.248063	0.000427	0.021124
DOCK4_1558691_a_at	DOCK4	1.85	-2.16	-3.99	0.108956	0.108664	0.02247
EIF5B_201024_x_at	EIF5B	1.02	-2.58	-2.62	0.439861	0.013002	0.029949
FBXO30_242007_at	FBXO3 0	1.38	-1.86	-2.57	0.215344	0.057107	0.031788
FBXO38_219608_s_a_t	FBXO3 8	1.27	-2.32	-2.95	0.489286	0.011969	0.023259
FIGN_238964_at	FIGN	1.13	3.42	3.03	0.430784	0.002166	0.02247
GLCCI1_1560316_s_at	GLCCI1	1.14	-2.26	-2.57	0.417569	0.031549	0.044182
GPATCH8_212487_a_t	GPATC H8	-1.52	-6.8	-4.49	0.138867	1.9E-05	0.038277
IBA57_231983_at	IBA57	-1.33	2.46	3.28	0.249237	0.052393	0.015333
IL17RD_229263_at	IL17RD	1.51	3.64	2.4	0.482597	0.04187	0.049587
KIAA1109_216294_s_at	KIAA11 09	1.33	-2.61	-3.48	0.20908	0.032229	0.038093

KLHL24_221986_s_at	KLHL24	1.23	-2.5	-3.07	0.415935	0.001575	0.046051
KLHL28_228328_at	KLHL28	1.08	-2.28	-2.47	0.494939	0.022483	0.032057
KMT2A_212076_at	KMT2A	1.51	-1.38	-2.08	0.366656	0.049826	0.023025
LIG4_206235_at	LIG4	1.34	-3.38	-4.53	0.368653	0.007339	0.021218
LPP_214902_x_at	LPP	1.15	3.72	3.24	0.394337	0.006533	0.030139
MACF1_208633_s_at	MACF1	1.23	-1.98	-2.43	0.271967	0.006087	0.024916
MACF1_215222_x_at	MACF1	1.13	-2.05	-2.33	0.306527	0.009828	0.040816
MAP1B_214577_at	MAP1B	1.7	-1.78	-3.02	0.150117	0.025256	0.037591
MAST4_40016_g_at	MAST4	-1.11	1.81	2	0.36285	0.034997	0.026658
MAT2A_200769_s_at	MAT2A	-1.04	-2.85	-2.75	0.469037	0.027406	0.045077
MIB1_224720_at	MIB1	1.03	-2.13	-2.19	0.392678	0.036959	0.031553
MIB1_224726_at	MIB1	1.17	-2.5	-2.93	0.382171	0.038152	0.049578
MNT_204206_at	MNT	-1.08	2.02	2.19	0.417361	0.000195	0.012342
MPHOSPH8_225041_at	MPHOSPH8	1.02	-2.32	-2.37	0.497609	0.001795	0.021585
MPP5_219321_at	MPP5	1.25	-1.61	-2.02	0.272737	0.052324	0.044082
MYO6_203215_s_at	MYO6	1.29	-4.49	-5.79	0.475466	0.001185	0.034392
MYO6_210480_s_at	MYO6	1.07	-2.34	-2.52	0.467418	0.002177	0.042972
NAV2_222599_s_at	NAV2	1.76	4.36	2.48	0.03297	0.00012	0.035452
NEK9_214738_s_at	NEK9	1.37	-4.27	-5.83	0.462558	0.002099	0.039716
NFIX_227400_at	NFIX	-1.59	1.4	2.24	0.212993	0.339383	0.039185
NIPBL_207108_s_at	NIPBL	1.26	-3.22	-4.06	0.306829	0.009912	0.01765
NIPBL_213918_s_at	NIPBL	1.18	-1.9	-2.24	0.411864	0.017114	0.042183
NIPBL_242352_at	NIPBL	1.09	-2.76	-3	0.354387	0.008901	0.030065
PAFAH1B1_200813_s_at	PAFAH1B1	1.06	-1.97	-2.08	0.390348	0.00272	0.021585
PAFAH1B1_211547_s_at	PAFAH1B1	1.11	-2.43	-2.69	0.349264	0.011298	0.03472
PBRM1_224152_s_at	PBRM1	1.52	-4.58	-6.94	0.258331	0.013385	0.021562
PDP1_218273_s_at	PDP1	1.23	-2.45	-3.01	0.316797	0.014357	0.03987
PEG10_212092_at	PEG10	-1.45	-5.32	-3.66	0.192581	0.002426	0.036816
PHIP_244811_at	PHIP	1.17	-3.1	-3.64	0.447478	0.007906	0.025977
PIK3C2A_1553694_at	PIK3C2A	1.33	-2.72	-3.62	0.261245	0.009931	0.028677
PIK3C2A_226094_at	PIK3C2A	1.22	-1.79	-2.18	0.221601	0.069455	0.02617
PKM_213700_s_at	PKM	-1.15	2.02	2.32	0.414636	0.01697	0.023045
PML_211012_s_at	PML	-1.96	1.41	2.75	0.054697	0.193539	0.015959
POLR3A_231763_at	POLR3A	-1.03	2.15	2.22	0.429949	0.003455	0.025678
PSMD12_202353_s_at	PSMD12	-1.15	-2.6	-2.27	0.22525	0.009828	0.04135
PTPN14_242321_at	PTPN14	1.04	2.53	2.44	0.359104	0.003942	0.022577
QSER1_229982_at	QSER1	1.05	-3.51	-3.68	0.411361	0.000748	0.046065
RANBP2_201711_x_at	RANBP2	1.57	-2.64	-4.15	0.248063	0.001892	0.033242

RANBP2_201712_s_at	RANBP2	1.11	-1.93	-2.15	0.391851	0.022487	0.022129
RPAP3_1557984_s_at	RPAP3	1.23	-2.98	-3.67	0.47592	0.009286	0.027228
SART3_209127_s_at	SART3	1.38	-3.75	-5.18	0.448871	0.003597	0.028107
SCAF11_209376_x_at	SCAF11	1.13	-12.7	-14.4	0.409218	3.86E-05	0.026344
SCAF11_213850_s_at	SCAF11	1.26	-4.84	-6.11	0.394189	0.0001	0.03215
SEC23IP_216392_s_at	SEC23IP	1.26	-1.98	-2.49	0.242411	0.002837	0.015747
SETX_201965_s_at	SETX	1.3	-1.56	-2.02	0.204946	0.027311	0.030127
SF3A2_209381_x_at	SF3A2	-1.15	2.05	2.35	0.461391	0.01213	0.022581
SMARCC1_201072_s_at	SMARCC1	1.98	-3.68	-7.28	0.217396	0.010509	0.038469
SMARCC1_201073_s_at	SMARCC1	1.14	-1.87	-2.13	0.410596	0.024456	0.015434
SMC3_209257_s_at	SMC3	1.73	-15.76	-27.21	0.284797	0.003181	0.038615
SON_201085_s_at	SON	-1.03	-2.56	-2.49	0.499061	0.003234	0.044315
SPATA13_1557470_at	SPATA13	1.21	-6.54	-7.93	0.47783	0.04039	0.041628
SRRM2_208610_s_at	SRRM2	-1.2	-4.28	-3.57	0.29185	0.005391	0.019718
SYNCRIP_209024_s_at	SYNCRIP	1.68	-2.16	-3.64	0.139935	0.001091	0.019507
TFCP2_207627_s_at	TFCP2	1.22	-1.83	-2.23	0.208759	0.002788	0.013395
TNKS2_222562_s_at	TNKS2	1.18	-2.83	-3.33	0.388121	0.000512	0.029335
TNKS2_222563_s_at	TNKS2	1.33	-3.34	-4.44	0.219443	0.015904	0.036618
TOP1_208900_s_at	TOP1	1.24	-3.31	-4.11	0.409758	0.001103	0.038938
TOPORS_204071_s_at	TOPORS	-1.09	-2.57	-2.35	0.436596	0.018467	0.026884
TRPS1_224218_s_at	TRPS1	1.37	-1.47	-2	0.14553	0.059401	0.015233
TSC22D2_240557_at	TSC22D2	1.37	-1.75	-2.39	0.34754	0.181367	0.048724
TSC22D4_1554501_at	TSC22D4	-1.18	1.69	2	0.328236	0.053432	0.027344
TUG1_212337_at	TUG1	1.06	-2.26	-2.39	0.478324	0.00011	0.022844
USP34_212065_s_at	USP34	1.26	-2.83	-3.57	0.320041	0.00106	0.039308
USP34_215013_s_at	USP34	1.16	-3.11	-3.59	0.468635	0.03508	0.049295
USP34_242647_at	USP34	1.73	-6.8	-11.77	0.288597	0.039172	0.033316
YTHDC2_1568680_s_at	YTHDC2	1.49	-2.24	-3.34	0.20568	0.001661	0.045361
ZBTB10_219312_s_at	ZBTB10	-1.18	-2.69	-2.28	0.401266	0.011927	0.027027
ZFP36L2_201369_s_at	ZFP36L2	-1.09	2.08	2.27	0.313641	0.037188	0.027057
ZNF148_203319_s_at	ZNF148	1.24	-2.69	-3.34	0.35783	0.012998	0.027824

For table 9 see the text.

Table 10. Common AUF-1 targets identified by RIP-Seq and by catRAPID tool.

Transcript_name	Gene_id	Z.score	Discriminative_Power	Interaction_Strength	EF_AUF1	FDR
ALDH7A1-006	ENSG00000164904.15	3.75	1	1	1.64	0.014021
PSMD12-004	ENSG00000197170.9	3.45	1	1	1.55	0.035743
RBMXL1-002	ENSG00000213516.9	4.57	1	1	1.73	0.012451
DOCK9-002	ENSG00000088387.17	1.73	0.99	0.99	1.65	0.009985
FAM208B-008	ENSG00000108021.19	1.53	0.99	0.99	1.54	0.02591
SCAF11-005	ENSG00000139218.17	1.5	0.99	0.97	1.64	0.031544
ALDH7A1-013	ENSG00000164904.15	1.15	0.98	0.97	1.64	0.014021
COL5A2-002	ENSG00000204262.11	1.28	0.98	0.99	1.69	0.026243
EIF4A3-009	ENSG00000141543.9	1.26	0.98	0.99	1.64	0.034914
MPLKIP-001	ENSG00000168303.6	1.46	0.98	0.99	1.74	0.024103
PRDM11-004	ENSG00000019485.12	1.43	0.98	0.99	1.69	0.03023
SMNDC1-002	ENSG00000119953.12	1.19	0.98	0.98	1.73	0.014471
ANAPC1-008	ENSG00000153107.11	1	0.97	0.98	1.69	0.011066
FAM208B-006	ENSG00000108021.19	1.12	0.97	0.99	1.54	0.02591
HDAC2-014	ENSG00000196591.11	1.1	0.97	0.99	1.7	0.017493
NEK9-006	ENSG00000119638.12	0.94	0.97	0.97	1.75	0.015949
PEG10-004	ENSG00000242265.5	1.06	0.97	0.98	1.58	0.017043
PREP-002	ENSG00000085377.13	1.07	0.97	0.97	1.84	0.005009
RAP2C-003	ENSG00000123728.9	0.96	0.97	0.98	1.97	0.001002
SF1-011	ENSG00000168066.20	0.97	0.97	0.96	1.54	0.020991
SORBS3-024	ENSG00000120896.13	0.95	0.97	0.97	2.29	0.000841
SORBS3-013	ENSG00000120896.13	0.92	0.97	0.98	2.29	0.000841
UBXN7-002	ENSG00000163960.11	1.08	0.97	0.97	1.6	0.009406
CORO1C-018	ENSG00000110880.10	0.85	0.96	0.96	1.73	0.003582
KPNB1-006	ENSG00000108424.9	0.79	0.96	0.96	1.53	0.037058
LPIN2-002	ENSG00000101577.9	0.85	0.96	0.96	1.53	0.035849
MKI67-004	ENSG00000148773.12	0.8	0.96	0.95	1.57	0.021889
NCOR2-009	ENSG00000196498.13	0.82	0.96	0.96	1.94	0.01749
XIAP-001	ENSG00000101966.12	0.84	0.96	0.97	1.53	0.038949
ZNF587-004	ENSG00000198466.11	0.85	0.96	0.98	1.56	0.035882
DCAF7-004	ENSG00000136485.14	0.76	0.95	0.95	1.64	0.010168
LMNB1-004	ENSG00000113368.11	0.76	0.95	0.96	1.81	0.00929
MYOF-001	ENSG00000138119.16	0.76	0.95	0.92	1.95	0.001451
PAPSS1-006	ENSG00000138801.8	0.76	0.95	0.92	1.67	0.048926
MUC1-018	ENSG00000185499.16	0.67	0.94	0.93	3.37	1.81E-06
PBRM1-013	ENSG00000163939.18	0.66	0.94	0.93	1.63	0.014761
SF3B3-014	ENSG00000189091.12	0.68	0.94	0.93	1.74	0.027771
ARF3-012	ENSG00000134287.9	0.64	0.93	0.95	1.53	0.024611
SF1-012	ENSG00000168066.20	0.61	0.92	0.93	1.54	0.020991
VPS41-010	ENSG00000006715.15	0.6	0.92	0.92	1.92	0.002647
APBB2-018	ENSG00000163697.16	0.55	0.91	0.87	1.54	0.020718
ATIC-016	ENSG00000138363.14	0.52	0.91	0.91	1.82	0.011266

CORO1C-017	ENSG00000110880.10	0.53	0.91	0.92	1.73	0.003582
LMNB1-006	ENSG00000113368.11	0.53	0.91	0.91	1.81	0.00929
LPP-004	ENSG00000145012.12	0.56	0.91	0.88	1.6	0.013544
MACF1-025	ENSG00000127603.23	0.56	0.91	0.9	1.61	0.014615
RREB1-011	ENSG00000124782.19	0.54	0.91	0.87	1.57	0.042637
SRRM2-028	ENSG00000167978.16	0.56	0.91	0.95	1.96	8.29E-05
VPS37C-003	ENSG00000167987.10	0.54	0.91	0.91	1.99	0.01312
DDX17-007	ENSG00000100201.19	0.48	0.89	0.87	2.13	6.31E-06
AHNAK-001	ENSG00000124942.13	0.45	0.88	0.84	1.65	0.004293
NIPBL-003	ENSG00000164190.16	0.47	0.88	0.89	1.59	0.029242
SF3B3-018	ENSG00000189091.12	0.47	0.88	0.9	1.74	0.027771
ATXN1L-003	ENSG00000224470.7	0.44	0.87	0.95	1.56	0.039925
CORO1C-014	ENSG00000110880.10	0.42	0.85	0.8	1.73	0.003582
HLCS-004	ENSG00000159267.14	0.41	0.85	0.85	1.54	0.045645
TMED7-004	ENSG00000134970.13	0.41	0.85	0.89	2	0.001526
TNRC6B-004	ENSG00000100354.20	0.41	0.85	0.94	1.55	0.026788
GRINA-011	ENSG00000178719.16	0.39	0.84	0.79	1.67	0.014701
GRINA-009	ENSG00000178719.16	0.39	0.84	0.87	1.67	0.014701
PACS1-006	ENSG00000175115.11	0.39	0.84	0.87	1.72	0.0035
SMC1A-002	ENSG00000072501.17	0.39	0.84	0.79	2.09	0.000554
COPB2-005	ENSG00000184432.9	0.34	0.83	0.77	1.87	0.018715
KDM6B-005	ENSG00000132510.10	0.34	0.83	0.97	3.2	0.000139
POGZ-018	ENSG00000143442.21	0.34	0.83	0.86	1.8	0.001353
ZFHX4-008	ENSG00000091656.15	0.35	0.83	0.8	1.92	0.000304
ATP6V1A-005	ENSG00000114573.9	0.32	0.81	0.82	1.62	0.042774
CNOT1-009	ENSG00000125107.16	0.33	0.81	0.85	1.82	0.000347
DDX3X-003	ENSG00000215301.9	0.32	0.81	0.84	1.75	0.018266
SDCBP-013	ENSG00000137575.11	0.31	0.81	0.84	1.66	0.011202
SUCLA2-010	ENSG00000136143.14	0.32	0.81	0.77	1.78	0.015724
WNK1-016	ENSG00000060237.16	0.32	0.81	0.79	1.68	0.003319
ZNF462-010	ENSG00000148143.12	0.34	0.81	0.87	1.66	0.006012
CNOT1-023	ENSG00000125107.16	0.29	0.8	0.83	1.82	0.000347
DOCK9-012	ENSG00000088387.17	0.3	0.8	0.75	1.65	0.009985
PRR14L-007	ENSG00000183530.13	0.29	0.8	0.77	1.57	0.01896
TRIP12-009	ENSG00000153827.13	0.31	0.8	0.79	1.76	0.00196
MED20-007	ENSG00000124641.14	0.26	0.79	0.82	1.6	0.032051
FRMD6-012	ENSG00000139926.15	0.24	0.77	0.82	1.55	0.019485
PBRM1-018	ENSG00000163939.18	0.24	0.77	0.83	1.63	0.014761
SRRM2-029	ENSG00000167978.16	0.23	0.77	0.77	1.96	8.29E-05
MLXIP-006	ENSG00000175727.13	0.21	0.76	0.83	2.15	0.002861
NUP214-006	ENSG00000126883.16	0.23	0.76	0.8	1.72	0.032662
SF3B3-008	ENSG00000189091.12	0.22	0.76	0.78	1.74	0.027771
SORBS3-006	ENSG00000120896.13	0.23	0.76	0.8	2.29	0.000841

References part 2

1. Barreau C, Paillard L, Osborne HB. AU-rich elements and associated factors: are there unifying principles? *Nucleic Acids Res.* 2005;33(22):7138-50.
2. Glisovic T, Bachorik JL, Yong J, et al. RNA-binding proteins and post-transcriptional gene regulation. *FEBS Lett.* 2008 Jun 18;582(14):1977-86.
3. Ray D, Kazan H, Cook KB, et al. A compendium of RNA-binding motifs for decoding gene regulation. *Nature.* 2013 Jul 11;499(7457):172-7.
4. Corley M, Burns MC, Yeo GW. How RNA-Binding Proteins Interact with RNA: Molecules and Mechanisms. *Mol Cell.* 2020 Apr 2;78(1):9-29.
5. Coppin L, Leclerc J, Vincent A, et al. Messenger RNA Life-Cycle in Cancer Cells: Emerging Role of Conventional and Non-Conventional RNA-Binding Proteins? *Int J Mol Sci.* 2018 Feb 25;19(3).
6. White EJ, Brewer G, Wilson GM. Post-transcriptional control of gene expression by AUF1: mechanisms, physiological targets, and regulation. *Biochim Biophys Acta.* 2013 Jun-Jul;1829(6-7):680-8.
7. Iadevaia V, Gerber AP. Combinatorial Control of mRNA Fates by RNA-Binding Proteins and Non-Coding RNAs. *Biomolecules.* 2015 Sep 24;5(4):2207-22.
8. Luo NA, Qu YQ, Yang GD, et al. Post-transcriptional up-regulation of PDGF-C by HuR in advanced and stressed breast cancer. *Int J Mol Sci.* 2014 Nov 6;15(11):20306-20.
9. Wang H, Ding N, Guo J, et al. Dysregulation of TTP and HuR plays an important role in cancers. *Tumour Biol.* 2016 Nov;37(11):14451-14461.
10. Barton M, Meyer MR. HuR-ry Up: How Hydrogen Sulfide Protects Against Atherosclerosis. *Circulation.* 2019 Jan 2;139(1):115-118.
11. Stumpo DJ, Lai WS, Blackshear PJ. Inflammation: cytokines and RNA-based regulation. *Wiley Interdiscip Rev RNA.* 2010 Jul-Aug;1(1):60-80.
12. Anderson P. Post-transcriptional control of cytokine production. *Nat Immunol.* 2008 Apr;9(4):353-9.
13. Barnes PJ, Baker J, Donnelly LE. Cellular Senescence as a Mechanism and Target in Chronic Lung Diseases. *Am J Respir Crit Care Med.* 2019 Sep 1;200(5):556-564.

14. Kumar M, Seeger W, Voswinckel R. Senescence-associated secretory phenotype and its possible role in chronic obstructive pulmonary disease. *Am J Respir Cell Mol Biol*. 2014 Sep;51(3):323-33.
15. Hamilton T, Novotny M, Pavicic PJ, Jr., et al. Diversity in post-transcriptional control of neutrophil chemoattractant cytokine gene expression. *Cytokine*. 2010 Oct-Nov;52(1-2):116-22.
16. Moore AE, Chenette DM, Larkin LC, et al. Physiological networks and disease functions of RNA-binding protein AUF1. *Wiley Interdiscip Rev RNA*. 2014 Jul-Aug;5(4):549-64.
17. Stoecklin G, Tenenbaum SA, Mayo T, et al. Genome-wide analysis identifies interleukin-10 mRNA as target of tristetraprolin. *J Biol Chem*. 2008 Apr 25;283(17):11689-99.
18. Abdelmohsen K, Kuwano Y, Kim HH, et al. Posttranscriptional gene regulation by RNA-binding proteins during oxidative stress: implications for cellular senescence. *Biol Chem*. 2008 Mar;389(3):243-55.
19. Wang W. Regulatory RNA-binding proteins in senescence. *Ageing Res Rev*. 2012 Sep;11(4):485-90.
20. Harley J, Clarke BE, Patani R. The Interplay of RNA Binding Proteins, Oxidative Stress and Mitochondrial Dysfunction in ALS. *Antioxidants (Basel)*. 2021 Apr 2;10(4).
21. Ricciardi L, Col JD, Casolari P, et al. Differential expression of RNA-binding proteins in bronchial epithelium of stable COPD patients. *Int J Chron Obstruct Pulmon Dis*. 2018;13:3173-3190.
22. Ricciardi L, Giurato G, Memoli D, et al. Posttranscriptional Gene Regulatory Networks in Chronic Airway Inflammatory Diseases: In silico Mapping of RNA-Binding Protein Expression in Airway Epithelium. *Front Immunol*. 2020;11:579889.
23. Sarkar B, Xi Q, He C, et al. Selective degradation of AU-rich mRNAs promoted by the p37 AUF1 protein isoform. *Mol Cell Biol*. 2003 Sep;23(18):6685-93.
24. White EJ, Matsangos AE, Wilson GM. AUF1 regulation of coding and noncoding RNA. *Wiley Interdiscip Rev RNA*. 2017 Mar;8(2).
25. Ing NH, Massuto DA, Jaeger LA. Estradiol up-regulates AUF1p45 binding to stabilizing regions within the 3'-untranslated region of estrogen receptor alpha mRNA. *J Biol Chem*. 2008 Jan 18;283(3):1764-1772.

26. Paschoud S, Dogar AM, Kuntz C, et al. Destabilization of interleukin-6 mRNA requires a putative RNA stem-loop structure, an AU-rich element, and the RNA-binding protein AUF1. *Mol Cell Biol.* 2006 Nov;26(22):8228-41.
27. Xu N, Chen CY, Shyu AB. Versatile role for hnRNP D isoforms in the differential regulation of cytoplasmic mRNA turnover. *Mol Cell Biol.* 2001 Oct;21(20):6960-71.
28. Lu JY, Sadri N, Schneider RJ. Endotoxic shock in AUF1 knockout mice mediated by failure to degrade proinflammatory cytokine mRNAs. *Genes Dev.* 2006 Nov 15;20(22):3174-84.
29. Sadri N, Schneider RJ. AUF1/HnRNP D-deficient mice develop pruritic inflammatory skin disease. *J Invest Dermatol.* 2009 Mar;129(3):657-70.
30. Pont AR, Sadri N, Hsiao SJ, et al. mRNA decay factor AUF1 maintains normal aging, telomere maintenance, and suppression of senescence by activation of telomerase transcription. *Mol Cell.* 2012 Jul 13;47(1):5-15.
31. van Niel G, D'Angelo G, Raposo G. Shedding light on the cell biology of extracellular vesicles. *Nat Rev Mol Cell Biol.* 2018 Apr;19(4):213-228.
32. Zaborowski MP, Balaj L, Breakefield XO, et al. Extracellular Vesicles: Composition, Biological Relevance, and Methods of Study. *Bioscience.* 2015 Aug 1;65(8):783-797.
33. Trappe A, Donnelly SC, McNally P, et al. Role of extracellular vesicles in chronic lung disease. *Thorax.* 2021 Oct;76(10):1047-1056.
34. Wahlund CJE, Eklund A, Grunewald J, et al. Pulmonary Extracellular Vesicles as Mediators of Local and Systemic Inflammation. *Front Cell Dev Biol.* 2017;5:39.
35. Fujita Y, Araya J, Ito S, et al. Suppression of autophagy by extracellular vesicles promotes myofibroblast differentiation in COPD pathogenesis. *J Extracell Vesicles.* 2015;4:28388.
36. Kadota T, Fujita Y, Yoshioka Y, et al. Emerging role of extracellular vesicles as a senescence-associated secretory phenotype: Insights into the pathophysiology of lung diseases. *Mol Aspects Med.* 2018 Apr;60:92-103.
37. Basisty N, Kale A, Jeon OH, et al. A proteomic atlas of senescence-associated secretomes for aging biomarker development. *PLoS Biol.* 2020 Jan;18(1):e3000599.
38. O'Brien K, Breyne K, Ughetto S, et al. RNA delivery by extracellular vesicles in mammalian cells and its applications. *Nat Rev Mol Cell Biol.* 2020 Oct;21(10):585-606.

39. Statello L, Maugeri M, Garre E, et al. Identification of RNA-binding proteins in exosomes capable of interacting with different types of RNA: RBP-facilitated transport of RNAs into exosomes. *PLoS One*. 2018;13(4):e0195969.
40. Fan J, Ishmael FT, Fang X, et al. Chemokine transcripts as targets of the RNA-binding protein HuR in human airway epithelium. *J Immunol*. 2011 Feb 15;186(4):2482-94.
41. Yoon JH, De S, Srikantan S, et al. PAR-CLIP analysis uncovers AUF1 impact on target RNA fate and genome integrity. *Nat Commun*. 2014 Nov 4;5:5248.
42. Keene JD. RNA regulons: coordination of post-transcriptional events. *Nat Rev Genet*. 2007 Jul;8(7):533-43.
43. Gagliardi M, Matarazzo MR. RIP: RNA Immunoprecipitation. *Methods Mol Biol*. 2016;1480:73-86.
44. Tarallo R, Giurato G, Bruno G, et al. The nuclear receptor ER β engages AGO2 in regulation of gene transcription, RNA splicing and RISC loading. *Genome Biol*. 2017 Oct 6;18(1):189.
45. Dobin A, Davis CA, Schlesinger F, et al. STAR: ultrafast universal RNA-seq aligner. *Bioinformatics*. 2013 Jan 1;29(1):15-21.
46. Liao Y, Smyth GK, Shi W. featureCounts: an efficient general purpose program for assigning sequence reads to genomic features. *Bioinformatics*. 2014 Apr 1;30(7):923-30.
47. Li B, Dewey CN. RSEM: accurate transcript quantification from RNA-Seq data with or without a reference genome. *BMC Bioinformatics*. 2011 Aug 4;12:323.
48. Agostini F, Zanzoni A, Klus P, et al. catRAPID omics: a web server for large-scale prediction of protein-RNA interactions. *Bioinformatics*. 2013 Nov 15;29(22):2928-30.
49. Polishchuk M, Paz I, Kohen R, et al. A combined sequence and structure based method for discovering enriched motifs in RNA from in vivo binding data. *Methods*. 2017 Apr 15;118-119:73-81.
50. Polishchuk M, Paz I, Yakhini Z, et al. SMARTIV: combined sequence and structure de-novo motif discovery for in-vivo RNA binding data. *Nucleic Acids Res*. 2018 Jul 2;46(W1):W221-w228.
51. Kramer A, Stathopoulos V, Girolami M, et al. MCMC_CLIB-an advanced MCMC sampling package for ODE models. *Bioinformatics*. 2014 Oct 15;30(20):2991-2.

52. Subramanian A, Tamayo P, Mootha VK, et al. Gene set enrichment analysis: a knowledge-based approach for interpreting genome-wide expression profiles. *Proc Natl Acad Sci U S A*. 2005 Oct 25;102(43):15545-50.
53. Panda AC, Martindale JL, Gorospe M. Affinity Pulldown of Biotinylated RNA for Detection of Protein-RNA Complexes. *Bio Protoc*. 2016 Dec 20;6(24).
54. Théry C, Ostrowski M, Segura E. Membrane vesicles as conveyors of immune responses. *Nat Rev Immunol*. 2009 Aug;9(8):581-93.
55. Kirkham PA, Caramori G, Casolari P, et al. Oxidative stress-induced antibodies to carbonyl-modified protein correlate with severity of chronic obstructive pulmonary disease. *Am J Respir Crit Care Med*. 2011 Oct 1;184(7):796-802.
56. Marwick JA, Caramori G, Casolari P, et al. A role for phosphoinositol 3-kinase delta in the impairment of glucocorticoid responsiveness in patients with chronic obstructive pulmonary disease. *J Allergy Clin Immunol*. 2010 May;125(5):1146-53.
57. Hänzelmann S, Castelo R, Guinney J. GSEA: gene set variation analysis for microarray and RNA-seq data. *BMC Bioinformatics*. 2013 Jan 16;14:7.
58. Carolan BJ, Heguy A, Harvey BG, et al. Up-regulation of expression of the ubiquitin carboxyl-terminal hydrolase L1 gene in human airway epithelium of cigarette smokers. *Cancer Res*. 2006 Nov 15;66(22):10729-40.
59. Hekking PP, Loza MJ, Pavlidis S, et al. Pathway discovery using transcriptomic profiles in adult-onset severe asthma. *J Allergy Clin Immunol*. 2018 Apr;141(4):1280-1290.
60. <https://www.genecards.org/cgi-bin/carddisp.pl?gene=PRR36>, PG-GPPPAa.
61. Attanasio M, Uhlenhaut NH, Sousa VH, et al. Loss of GLIS2 causes nephronophthisis in humans and mice by increased apoptosis and fibrosis. *Nat Genet*. 2007 Aug;39(8):1018-24.
62. Jetten AM. GLIS1-3 transcription factors: critical roles in the regulation of multiple physiological processes and diseases. *Cell Mol Life Sci*. 2018 Oct;75(19):3473-3494.
63. ZAGZAPZAAAa hwgoc-bcpgZA.
64. Murphy M, Chatterjee SS, Jain S, et al. TCF7L1 Modulates Colorectal Cancer Growth by Inhibiting Expression of the Tumor-Suppressor Gene EPHB3. *Sci Rep*. 2016 Jun 23;6:28299.

65. Sierra RA, Hoverter NP, Ramirez RN, et al. TCF7L1 suppresses primitive streak gene expression to support human embryonic stem cell pluripotency. *Development*. 2018 Feb 23;145(4).
66. Kogure A, Shiratori I, Wang J, et al. PANP is a novel O-glycosylated PILR α ligand expressed in neural tissues. *Biochem Biophys Res Commun*. 2011 Feb 18;405(3):428-33.
67. <https://www.genecards.org/cgi-bin/carddisp.pl?gene=MBD6>, MGMPMAAa.
68. Milara J, Díaz-Platas L, Contreras S, et al. MUC1 deficiency mediates corticosteroid resistance in chronic obstructive pulmonary disease. *Respir Res*. 2018 Nov 20;19(1):226.
69. Nath S, Mukherjee P. MUC1: a multifaceted oncoprotein with a key role in cancer progression. *Trends Mol Med*. 2014 Jun;20(6):332-42.
70. Kim JH, Hwang J, Jung JH, et al. Molecular networks of FOXP family: dual biologic functions, interplay with other molecules and clinical implications in cancer progression. *Mol Cancer*. 2019 Dec 9;18(1):180.
71. Wijayatunge R, Liu F, Shpargel KB, et al. The histone demethylase Kdm6b regulates a mature gene expression program in differentiating cerebellar granule neurons. *Mol Cell Neurosci*. 2018 Mar;87:4-17.
72. Burchfield JS, Li Q, Wang HY, et al. JMJD3 as an epigenetic regulator in development and disease. *Int J Biochem Cell Biol*. 2015 Oct;67:148-57.
73. <https://www.genecards.org/cgi-bin/carddisp.pl?gene=FBRSL1>, FGFPFAAa.
74. <https://www.genecards.org/cgi-bin/carddisp.pl?gene=C1orf226&keywords=C1orf226>.
75. Südhof TC. Neurotransmitter release: the last millisecond in the life of a synaptic vesicle. *Neuron*. 2013 Oct 30;80(3):675-90.
76. Altarejos JY, Montminy M. CREB and the CRTC co-activators: sensors for hormonal and metabolic signals. *Nat Rev Mol Cell Biol*. 2011 Mar;12(3):141-51.
77. Parra-Damas A, Rubió-Ferrarons L, Shen J, et al. CRTC1 mediates preferential transcription at neuronal activity-regulated CRE/TATA promoters. *Sci Rep*. 2017 Dec 21;7(1):18004.
78. Kaehler C, Isensee J, Nonhoff U, et al. Ataxin-2-like is a regulator of stress granules and processing bodies. *PLoS One*. 2012;7(11):e50134.
79. Li YY, Wu C, Shah SS, et al. Degradation of AMPK- α 1 sensitizes BRAF inhibitor-resistant melanoma cells to arginine deprivation. *Mol Oncol*. 2017 Dec;11(12):1806-1825.

80. Mellett M, Atzei P, Horgan A, et al. Orphan receptor IL-17RD tunes IL-17A signalling and is required for neutrophilia. *Nat Commun.* 2012;3:1119.
81. Rong Z, Wang A, Li Z, et al. IL-17RD (Sef or IL-17RLM) interacts with IL-17 receptor and mediates IL-17 signaling. *Cell Res.* 2009 Feb;19(2):208-15.
82. <https://www.genecards.org/cgi-bin/carddisp.pl?gene=KIAA1522&keywords=KIAA1522>.
83. Allen CE, Mak CH, Wu LC. The kappa B transcriptional enhancer motif and signal sequences of V(D)J recombination are targets for the zinc finger protein HIVEP3/KRC: a site selection amplification binding study. *BMC Immunol.* 2002 Aug 22;3:10.
84. Jones DC, Wein MN, Oukka M, et al. Regulation of adult bone mass by the zinc finger adapter protein Schnurri-3. *Science.* 2006 May 26;312(5777):1223-7.
85. Wagner BJ, DeMaria CT, Sun Y, et al. Structure and genomic organization of the human AUF1 gene: alternative pre-mRNA splicing generates four protein isoforms. *Genomics.* 1998 Mar 1;48(2):195-202.
86. Lal A, Mazan-Mamczarz K, Kawai T, et al. Concurrent versus individual binding of HuR and AUF1 to common labile target mRNAs. *Embo j.* 2004 Aug 4;23(15):3092-102.
87. Tamamori-Adachi M, Koga A, Susa T, et al. DNA damage response induced by Etoposide promotes steroidogenesis via GADD45A in cultured adrenal cells. *Sci Rep.* 2018 Jun 25;8(1):9636.
88. Puca AA, Lopardo V, Montella F, et al. The Longevity-Associated Variant of BPIFB4 Reduces Senescence in Glioma Cells and in Patients' Lymphocytes Favoring Chemotherapy Efficacy. *Cells.* 2022 Jan 15;11(2).
89. Ito T, Sun L, Bevan MA, et al. Comparison of nanoparticle size and electrophoretic mobility measurements using a carbon-nanotube-based coulter counter, dynamic light scattering, transmission electron microscopy, and phase analysis light scattering. *Langmuir.* 2004 Aug 3;20(16):6940-5.
90. Gao W, Li L, Wang Y, et al. Bronchial epithelial cells: The key effector cells in the pathogenesis of chronic obstructive pulmonary disease? *Respirology.* 2015 Jul;20(5):722-9.
91. Barnes PJ. Senescence in COPD and Its Comorbidities. *Annu Rev Physiol.* 2017 Feb 10;79:517-539.
92. Mazan-Mamczarz K, Kuwano Y, Zhan M, et al. Identification of a signature motif in target mRNAs of RNA-binding protein AUF1. *Nucleic Acids Res.* 2009 Jan;37(1):204-14.

93. Chakraborty A, Mukherjee S, Saha S, et al. Phorbol-12-myristate-13-acetate-mediated stabilization of leukemia inhibitory factor (lif) mRNA: involvement of Nucleolin and PCBP1. *Biochem J.* 2017 Jul 3;474(14):2349-2363.
94. Saha S, Chakraborty A, Bandyopadhyay SS. Stabilization of Oncostatin-M mRNA by Binding of Nucleolin to a GC-Rich Element in Its 3'UTR. *J Cell Biochem.* 2016 Apr;117(4):988-99.
95. Yan SF, Pinsky DJ, Mackman N, et al. Egr-1: is it always immediate and early? *J Clin Invest.* 2000 Mar;105(5):553-4.
96. Zhang W, Yan SD, Zhu A, et al. Expression of Egr-1 in late stage emphysema. *Am J Pathol.* 2000 Oct;157(4):1311-20.
97. Ning W, Li CJ, Kaminski N, et al. Comprehensive gene expression profiles reveal pathways related to the pathogenesis of chronic obstructive pulmonary disease. *Proc Natl Acad Sci U S A.* 2004 Oct 12;101(41):14895-900.
98. Chen ZH, Kim HP, Sciruba FC, et al. Egr-1 regulates autophagy in cigarette smoke-induced chronic obstructive pulmonary disease. *PLoS One.* 2008 Oct 2;3(10):e3316.
99. Chen CZ, Ou CY, Wang RH, et al. Association of Egr-1 and autophagy-related gene polymorphism in men with chronic obstructive pulmonary disease. *J Formos Med Assoc.* 2015 Aug;114(8):750-5.
100. Li CJ, Ning W, Matthay MA, et al. MAPK pathway mediates EGR-1-HSP70-dependent cigarette smoke-induced chemokine production. *Am J Physiol Lung Cell Mol Physiol.* 2007 May;292(5):L1297-303.
101. Sinsimer KS, Gratacós FM, Knapinska AM, et al. Chaperone Hsp27, a novel subunit of AUF1 protein complexes, functions in AU-rich element-mediated mRNA decay. *Mol Cell Biol.* 2008 Sep;28(17):5223-37.
102. Hansel C, Jendrossek V, Klein D. Cellular Senescence in the Lung: The Central Role of Senescent Epithelial Cells. *Int J Mol Sci.* 2020 May 6;21(9).
103. Tsuji T, Aoshiba K, Nagai A. Cigarette smoke induces senescence in alveolar epithelial cells. *Am J Respir Cell Mol Biol.* 2004 Dec;31(6):643-9.
104. Chowdhury S, Dijkhuis A, Steiert S, et al. IL-17 attenuates degradation of ARE-mRNAs by changing the cooperation between AU-binding proteins and microRNA16. *PLoS Genet.* 2013;9(9):e1003747.

105. Wang W, Furneaux H, Cheng H, et al. HuR regulates p21 mRNA stabilization by UV light. *Mol Cell Biol.* 2000 Feb;20(3):760-9.
106. Kawagishi H, Hashimoto M, Nakamura H, et al. HuR maintains a replicative life span by repressing the ARF tumor suppressor. *Mol Cell Biol.* 2013 May;33(10):1886-900.
107. Ryu S, Jung M, Kim C, et al. Loss of RNA binding protein HuD facilitates the production of the senescence-associated secretory phenotype. *Cell Death Dis.* 2022 Apr 11;13(4):329.
108. Majumder M, House R, Palanisamy N, et al. RNA-Binding Protein FXR1 Regulates p21 and TERC RNA to Bypass p53-Mediated Cellular Senescence in OSCC. *PLoS Genet.* 2016 Sep;12(9):e1006306.
109. Avolio R, Inglés-Ferrándiz M, Ciocia A, et al. Coordinated post-transcriptional control of oncogene-induced senescence by UNR/CSDE1. *Cell Rep.* 2022 Jan 11;38(2):110211.
110. Liu S, Zhan Y, Luo J, et al. Roles of exosomes in the carcinogenesis and clinical therapy of non-small cell lung cancer. *Biomed Pharmacother.* 2019 Mar;111:338-346.
111. Muralidharan R, Panneerselvam J, Chen A, et al. HuR-targeted nanotherapy in combination with AMD3100 suppresses CXCR4 expression, cell growth, migration and invasion in lung cancer. *Cancer Gene Ther.* 2015 Dec;22(12):581-90.
112. Hitti E, Bakheet T, Al-Souhibani N, et al. Systematic Analysis of AU-Rich Element Expression in Cancer Reveals Common Functional Clusters Regulated by Key RNA-Binding Proteins. *Cancer Res.* 2016 Jul 15;76(14):4068-80.
113. Barnes PJ, Adcock IM. Chronic obstructive pulmonary disease and lung cancer: a lethal association. *Am J Respir Crit Care Med.* Vol. 184. United States 2011. p. 866-7.
114. Fellows A, Griffin ME, Petrella BL, et al. AUF1/hnRNP D represses expression of VEGF in macrophages. *Mol Biol Cell.* 2012 Apr;23(8):1414-22.